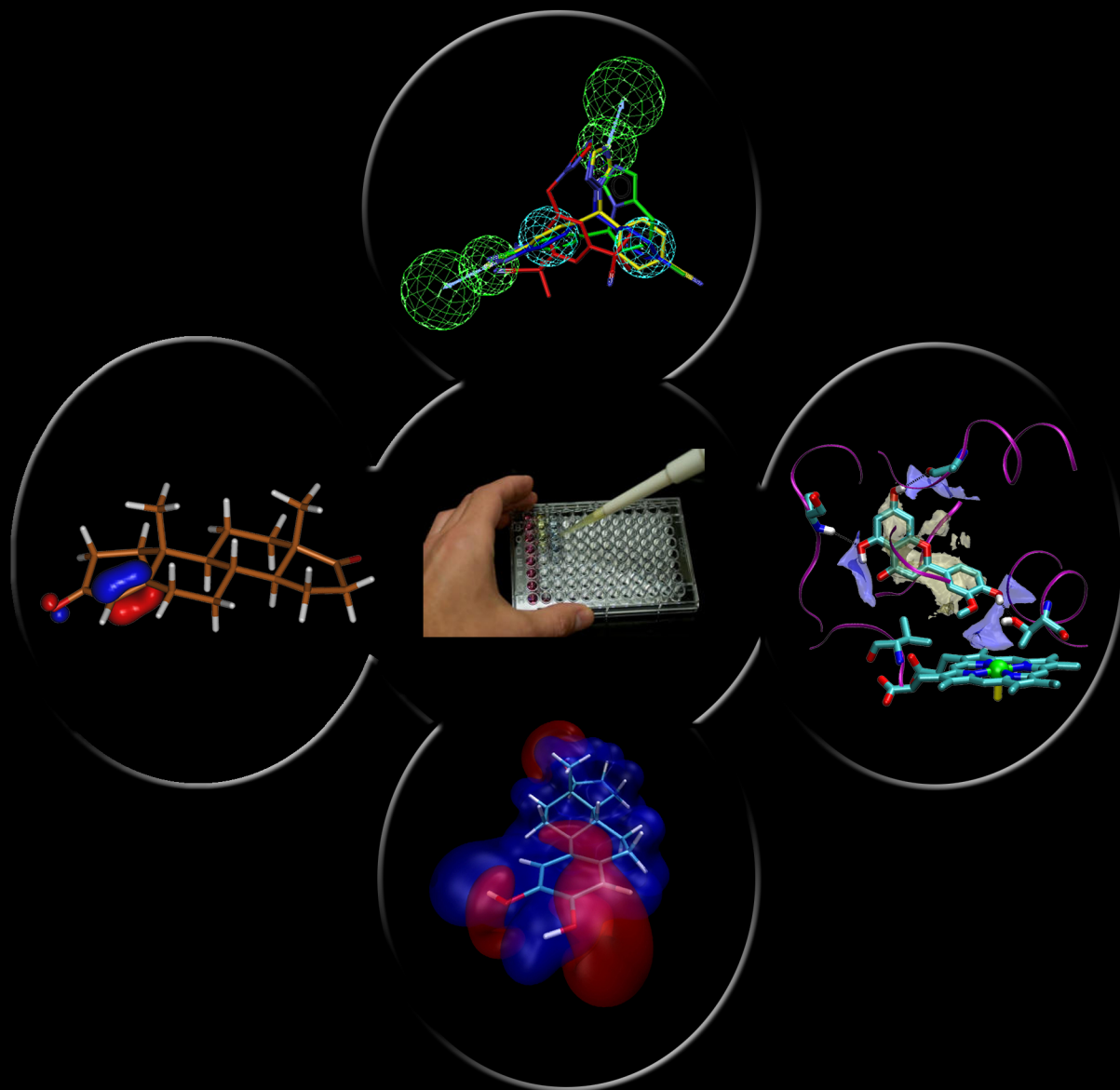


Aromatase inhibitors in breast cancer

The discovery of new compounds by computational design
and biochemical evaluation



Marco André Coelho das Neves

Faculdade de Farmácia
Universidade de Coimbra
2008

Aromatase inhibitors in breast cancer

The discovery of new compounds by computational design
and biochemical evaluation

Marco André Coelho das Neves



Faculdade de Farmácia
Universidade de Coimbra
2008

Dissertação apresentada à Faculdade de Farmácia da Universidade de
Coimbra para obtenção do grau de Doutor em Farmácia, na especialidade
de Química Farmacêutica

Trabalho desenvolvido sob orientação científica da Professora Doutora Maria Luísa Sá e Melo, no Laboratório de Química Farmacêutica da Faculdade de Farmácia da Universidade de Coimbra, e do Doutor Giorgio Colombo, no Istituto di Chimica del Riconoscimento Molecolare, CNR, Milão, Itália, em colaboração com a Professora Doutora Teresa do Carmo Pimenta Dinis Silva, no Laboratório de Bioquímica da Faculdade de Farmácia da Universidade de Coimbra.

Trabalho financiado pela Fundação para a Ciência e a Tecnologia
no âmbito do programa POCI 2010
(SFRH / BD / 17624 / 2004)



Ciência.Inovação
2010

Programa Operacional Ciência e Inovação 2010
MINISTÉRIO DA CIÊNCIA, TECNOLOGIA E ENSINO SUPERIOR



Aos meus pais e à minha irmã

Agradecimentos/Acknowledgements

À Professora Doutora Maria Luisa Sá e Melo expresso o meu profundo agradecimento pela confiança que desde cedo depositou em mim e que culminou com a realização deste trabalho. Agradeço ainda a orientação crítica e o entusiasmo que sempre mostrou por este trabalho, assim como a contribuição científica na revisão de todos os manuscritos. Foi para mim um enorme orgulho trabalhar no Laboratório de Química Farmacêutica da Faculdade de Farmácia da Universidade de Coimbra.

I thank Doctor Giorgio Colombo for accepting me at the Computational Biochemistry Group of the Istituto di Chimica del Riconoscimento Molecolare, and also for his supervision, continuous support and enthusiasm with this work. I also thank him for allowing me to work in some of his own research projects which provided me a much broader experience.

À Professora Doutora Teresa Pimenta Dinis e Silva agradeço o imenso apoio e orientação que se estendeu muito para além dos ensaios bioquímicos. Agradeço ainda a revisão crítica dos artigos e da tese de doutoramento, imprescindível para a qualidade final destes documentos. Agradeço igualmente o modo simpático e sempre bem disposto com que me recebeu no Laboratório de Bioquímica da Faculdade de Farmácia da Universidade de Coimbra.

À Professora Doutora Leonor Martins de Almeida, Directora do Laboratório de Bioquímica da Faculdade de Farmácia da Universidade de Coimbra, agradeço o caloroso acolhimento neste laboratório proporcionando todas as condições para a realização deste trabalho. Agradeço ainda o interesse que sempre demonstrou pelo mesmo, o apoio e a amizade.

I am grateful to Doctor Giacomo Carrea, president of the Istituto di Chimica del Riconoscimento Molecolare, for accepting me at this institute and also to Doctor Sergio Riva, responsible for the Milano 1 section, for his warm reception and friendship.

À Professora Doutora Maria Manuel da Cruz Silva agradeço o apoio que, desde o início, deu a este trabalho. Agradeço ainda a importante discussão de ideias e o apoio na correcção da tese de doutoramento.

Ao Professor Doutor Rodrigo Antunes da Cunha, Director do Departamento de Neurofarmacologia do Centro de Neurociências e Biologia Celular, o meu sincero agradecimento pela disponibilidade concedida na utilização da sala de radioactividade e do equipamento contador de cintilações.

Aos médicos e funcionários da Maternidade Doutor Daniel de Matos agradeço o fornecimento de amostras de placenta humana.

I thank the Drug Synthesis and Chemistry Branch, Developmental Therapeutics Program, Division of Cancer Treatment and Diagnosis of the National Cancer Institute for kindly providing the compounds screened in this study.

A todos os docentes e funcionários do Laboratório de Química Farmacêutica e do Laboratório de Bioquímica da Universidade de Coimbra, o meu agradecimento pela agradável convivência e pelo apoio técnico e científico.

Living in Milan, Italy, was for me a unique life experience. I thank all my friends there for the countless good moments we had together. I really appreciate the support and friendship of my colleagues at the Istituto di Chimica del Riconoscimento Molecolare.

Aos colegas de laboratório agradeço a amizade, o importante contributo que deram a este trabalho pela troca de ideias e a disponibilidade que sempre mostraram para me ajudar.

Aos amigos a minha gratidão por tornarem a minha vida tão rica e por, tantas vezes, me terem feito deixar de pensar no trabalho.

Agradeço à Rita por me apoiar, entender e ajudar.

À minha família agradeço o apoio incondicional nas escolhas que fiz ao longo dos últimos anos, e por terem estado sempre presentes, mesmo quando me afastei por motivos de trabalho.

À Fundação para a Ciência e a Tecnologia agradeço o apoio financeiro sob a forma de uma bolsa de doutoramento (SFRH/ BD/17624/2004).

À Fundação Calouste Gulbenkian agradeço o apoio na participação em congressos científicos internacionais.

Contents

Resumo	I
Abstract	V
List of abbreviations.....	VII
List of tables	XI
List of figures	XIII
Thesis organization	XVII
I. General introduction	1
1.1. Breast cancer	3
1.1.1. General considerations	3
1.1.2. Breast cancer treatment approaches.....	4
1.1.3. Breast tissue estrogens.....	6
1.1.3.1. Uptake from the circulation.....	7
1.1.3.2. Local production of estrogens	8
3 β -Hydroxysteroid dehydrogenase Δ^{5-4} isomerase	9
Aromatase.....	9
17 β -Hydroxysteroid dehydrogenase.....	10
Steroid sulfatase and estrogen sulfotransferase	11
1.1.4. The estrogen receptor.....	11
1.1.5. Estrogen metabolism	14
1.1.5.1. C2-Metabolites	16
1.1.5.2. C4-Metabolites	17
1.1.5.3. C16-Metabolites	17
1.1.5.4. The impact of estrogen metabolism in breast cancer carcinogenesis.....	18
1.2. Cytochrome P450 enzymes	20
1.2.1. Function, classification and nomenclature	20
1.2.2. Three-dimensional structure	23
1.2.3. Catalytic cycle	24
1.2.4. Aromatization mechanism of CYP19	26
1.2.5. Spectral properties	29
1.3. Aromatase inhibitors.....	29

1.3.1. Clinical development	29
1.3.2. Steroid aromatase inhibitors	32
1.3.2.1. Competitive inhibitors	32
1.3.2.2. Mechanism-based inactivators	34
1.3.3. Non-steroid aromatase inhibitors	35
1.3.4. Polyphenol aromatase inhibitors	38
1.3.4.1. Natural compounds	38
1.3.4.2. Synthetic derivatives	40
1.3.5. Dual inhibitors	42
1.3.5.1. Thromboxane A ₂ synthase and aromatase	42
1.3.5.2. Steroid sulfatase and aromatase	43
1.4. Biochemical evaluation of new compounds as aromatase inhibitors	44
1.4.1. The human placental microsomal assay	45
1.4.2. Comparison with other <i>in vitro</i> assays and other sources of aromatase	46
1.5. The use of computer-aided drug design in drug discovery and development	47
1.5.1. Computer-aided drug design basic principles	49
1.5.1.1. Structure optimization	49
1.5.1.2. Molecular dynamics	53
1.5.1.3. Calculation of electronic properties	53
1.5.1.4. Calculation of molecular interaction fields	54
1.5.1.5. Three-dimensional quantitative structure-activity relationships	55
1.5.1.6. Homology modelling	58
1.5.1.7. Docking	60
1.5.1.8. Pharmacophore modelling	61
1.5.1.9. Virtual screening	62
1.6. Objective of this thesis	64

II. Biochemical and computational insights into the anti-aromatase

activity of natural catechol estrogens	65
2.1. Abstract	67
2.2. Introduction	67
2.3. Results and discussion	69

2.3.1. Concentration-response study	69
2.3.2. Kinetic analysis	72
2.3.3. Electrostatic surface potential calculation	74
2.4. Conclusions	76
2.5. Materials and methods	80
2.5.1. Materials and general methods.....	80
2.5.2. Enzymatic preparation	80
2.5.3. Concentration-response study	81
2.5.4. Kinetic analysis	82
2.5.5. Electrostatic surface potential calculation details.....	82

III. Combining computational and biochemical studies for a rationale on the anti-aromatase activity of natural polyphenols

3.1. Abstract	87
3.2. Introduction.....	87
3.3. Results and discussion.....	88
3.3.1. Biochemical evaluation	88
3.3.2. 3D-QSAR with GRIND descriptors	95
3.3.3. Virtual receptor site derivation.....	100
3.3.4. Comparison with an aromatase homology model.....	102
3.3.5. Docking calculations	104
3.4. Conclusions	113
3.5. Materials and methods	116
3.5.1. Materials and general methods.....	116
3.5.2. Enzymatic preparation	117
3.5.3. Concentration-response study	117
3.5.4. Conformational search and geometry optimization.....	117
3.5.5. 3D-QSAR using ALMOND	117
3.5.6. Statistical analysis.....	118
3.5.7. Active site MIF calculations.....	118
3.5.8. Binding mode prediction.....	119

IV. Pharmacophore modelling, virtual screening and biochemical evaluation of new potent aromatase inhibitors	121
4.1. Abstract.....	123
4.2. Introduction.....	123
4.3. Results and discussion.....	125
4.3.1. 3D-pharmacophore modelling.....	125
4.3.1.1. Pharmacophore model based on non-steroid inhibitors.....	125
4.3.1.2. Pharmacophore model based on C6-substituted steroids.....	130
4.3.1.3. Pharmacophore model based on polyphenols.....	132
4.3.2. Virtual screening.....	134
4.3.2.1. Pharmacophore model based on non-steroid inhibitors.....	134
4.3.2.2. Pharmacophore model based on C6-substituted steroids.....	137
4.3.2.3. Pharmacophore model based on polyphenols.....	138
4.3.3. Biochemical evaluation.....	139
4.3.3.1. Pharmacophore model based on non-steroid inhibitors.....	140
4.3.3.2. Pharmacophore model based on C6-substituted steroids.....	141
4.3.3.3. Pharmacophore model based on polyphenols.....	145
4.3.4. Docking into the active site of an aromatase homology model.....	146
4.3.5. Stereoelectronic characterization.....	149
4.4. Conclusions.....	150
4.5. Materials and methods.....	155
4.5.1. Materials and general methods.....	155
4.5.2. Pharmacophore modelling.....	155
4.5.3. Virtual screening.....	156
4.5.4. Post-processing filtering.....	157
4.5.5. Enzymatic preparation.....	157
4.5.6. Concentration-response study.....	157
4.5.7. Kinetic analysis.....	158
4.5.8. Time-dependent inactivation assay.....	158
4.5.9. Docking calculations.....	159
4.5.10. <i>ab initio</i> calculation details.....	160
V. Concluding remarks	161

VI. Appendix	167
Appendix A. NAI-HYP2-HBA+Shape pharmacophore model validation results.	169
VII. References	175

Resumo

A exposição contínua a níveis elevados de hormonas estrogénicas está associada a um maior risco de aparecimento de cancro da mama. Neste sentido, a aromatase, uma enzima da família citocromo P450 envolvida na conversão de androgénios (testosterona e androstenodiona) em estrogénios (estradiol e estrona), é um importante alvo terapêutico para o tratamento anti-hormonal do cancro da mama em mulheres na pós-menopausa. A inibição desta enzima é possível recorrendo a compostos estruturalmente semelhantes ao substrato androstenodiona, ou através de compostos do tipo não-esteróide. Adicionalmente, diversos estudos têm sugerido que moléculas relacionadas com os produtos da reacção catalisada pela aromatase, tais como estrogénios endógenos ou polifenóis naturais, têm capacidade para se ligar ao local activo da aromatase actuando como inibidores competitivos.

Actualmente, a aplicação de técnicas informáticas no *design* assistido por computador de novos fármacos tem permitido a descoberta e optimização de compostos com potente actividade biológica. Ao longo deste trabalho, diversas técnicas de modelação molecular foram combinadas com um ensaio rápido e preciso de avaliação biológica, tendo em vista a descoberta de novos compostos inibidores da aromatase e a racionalização da sua actividade ao nível atómico.

O objectivo inicial deste trabalho consistiu em estudar a relação estrutura-actividade de novas classes de inibidores da aromatase, tais como estrogénios e seus metabolitos endógenos e compostos polifenólicos naturais. Estas moléculas foram testadas num ensaio bioquímico usando microssomas de placenta humana como fonte da aromatase, e a actividade anti-hormonal foi comparada com diversos inibidores de referência. Derivados dos estrogénios do tipo catecol e polifenóis naturais provenientes

de diversas origens e com diferentes graus de funcionalização, tais como flavonas, flavanonas, resveratrol e oleuropeína, foram identificados como potentes inibidores da aromatase. Os requisitos físico-químicos para uma ligação eficaz ao local activo da enzima foram identificados através de uma combinação de técnicas de modelação molecular, tais como cálculos de superfícies de potencial electrostático, estudos de relações quantitativas estrutura-actividade tridimensionais, mapeamento de campos de interacção molecular no local activo de um modelo de homologia da enzima e estudos de *docking* enzima-ligando. Da análise dos resultados obtidos, foi proposto um modelo virtual para o local activo de ligação a polifenóis naturais e foram apresentadas novas regras de relação estrutura-actividade, úteis para o *design* racional de derivados de síntese. Para além disso, este estudo permitiu discutir um possível envolvimento dos catecois estrogénios num mecanismo de controlo da aromatase, assim como possíveis implicações clínicas para o desenvolvimento de cancro da mama em mulheres na pós-menopausa.

Os resultados destes estudos motivaram o desenvolvimento de uma estratégia de *screening* virtual para a descoberta de novos inibidores potentes da aromatase, com base na estrutura de inibidores conhecidos. Na ausência de uma estrutura cristalográfica de alta resolução da enzima, obtida por difracção de raios-X, o elevado número de inibidores potentes da aromatase descritos na literatura, em combinação com um conjunto de inibidores identificados na parte inicial deste estudo, constituíram uma base científica consistente para os estudos de *screening* virtual de moléculas. Três modelos de farmacóforos foram desenvolvidos tendo por base características físico-químicas comuns a diferentes conjuntos de inibidores da aromatase, nomeadamente compostos do tipo não esteróide contendo azóis, compostos do tipo esteróide e polifenóis naturais. O volume e a forma destas moléculas, assim como a informação acerca do modo como se ligam ao local activo da aromatase, foram igualmente incluídos nestes

modelos. Trinta e seis compostos promissores foram identificados numa vasta livraria *virtual* de moléculas pertencente ao “Nacional Cancer Institute” e testados *in vitro*. Os resultados obtidos permitiram identificar novos inibidores da aromatase de elevada potência, activos em concentrações nanomolares, comparáveis a inibidores da aromatase de segunda e terceira geração. Estas moléculas foram identificadas como inibidores competitivos, tendo uma delas provocado também inactivação irreversível da enzima dependente do mecanismo de catálise.

Em conclusão, os resultados obtidos neste trabalho fornecem novos dados para a discussão do papel do metabolismo dos estrogénios no cancro da mama, identificam novos compostos com elevada actividade anti-aromatase e evidenciam a importância do uso combinado de técnicas computacionais e ensaios de avaliação biológica no processo de descoberta de novos inibidores da aromatase.

Abstract

Continuous exposure to high levels of endogenous estrogens is associated with increased risks of developing breast cancer. In this sense, aromatase, the cytochrome P450 enzyme involved in the conversion of androgens, testosterone and androstenedione, into estrogens, estradiol and estrone, is an important target for the endocrine treatment of breast cancer in postmenopausal women. Aromatase inhibition is achieved either with compounds structurally related to the androstenedione substrate or with non-steroid inhibitors. Moreover, increasing evidence suggests that compounds mimicking the products of catalysis, such as endogenous estrogens as well as natural polyphenols, are able to bind into the aromatase active site as competitive inhibitors.

Computer-assisted drug design refers to the application of informatics on the discovery and optimization of biologically active compounds. In this work we took advantage of several molecular modelling tools, combined with a fast and accurate biochemical evaluation assay, to the discovery and rational at an atomic level, of the anti-aromatase properties of new molecules.

The first objective of this study was to explore the structure-activity relationships of emerging new classes of aromatase inhibitors such as estrogens and their endogenous metabolites, and natural polyphenols. The compounds were tested on a biochemical assay with aromatase extracted from human term placenta and their activities compared to that of reference compounds. Catechol estrogens as well as polyphenols from several natural sources and variable degree of functionalization, including flavones, flavanones, resveratrol and oleuropein, were found to be strong aromatase inhibitors. The physicochemical determinants for their productive binding to the active site of the enzyme were characterized through a combination of

molecular modelling techniques, such as electrostatic surface potential calculations, three-dimensional quantitative structure-activity relationships, molecular interaction field mapping at the active site of a homology model of the enzyme, and docking experiments. A virtual receptor site for the binding of natural polyphenols was proposed and new structure-activity rules, useful to the rational design of synthetic derivatives were derived. Moreover, the involvement of catechol estrogens in a control mechanism of estrogen production was discussed, along with the clinical implications to breast cancer development in postmenopausal women.

The results of these preliminary studies motivated a ligand-based virtual screening strategy for new potent compounds. In the absence of a high resolution X-ray structure of the enzyme, the vast information on strong aromatase inhibitors reported in the literature, combined with some of the most active polyphenols identified in this study, provided a good starting point. Three pharmacophore models were built based on the common physicochemical features of distinct sets of aromatase inhibitors, namely,azole non-steroid, steroid and polyphenol compounds. Molecular shape and information about their active site binding mode was also included in the models. Thirty six promising compounds were extracted from the large National Cancer Institute database and tested experimentally. New potent aromatase inhibitors were identified, active at very low nanomolar concentrations, comparable to second and third generation reference compounds. These molecules are competitive inhibitors and one of them was identified as a mechanism-based inactivator.

In summary, the results of this work provided new data on the role of catechol estrogens in breast cancer and identified new potent aromatase inhibitors, highlighting the importance of a combined use of computational studies and biochemical assays for the discovery of new aromatase inhibitors.

List of abbreviations

17 β -HSD	17 β -hydroxysteroid dehydrogenase
2-MeOE ₂	2-methoxyestradiol
2-OHE ₂	2-hydroxyestradiol
3 β -HSD	3 β -hydroxysteroid dehydrogenase Δ^{5-4} isomerase
3D-QSAR	three-dimensional quantitative structure-activity relationships
ADIOL	androst-5-ene-3 β ,17 β -diol
ADMET	absorption, distribution, metabolism, excretion and toxicity
AI	aromatase inhibitor
AIDS	acquired immunodeficiency syndrome
CADD	computer-aided drug design
COMT	catechol-O-methyltransferase
CYP	cytochrome P450 enzyme
CYP19	aromatase
DASI	dual aromatase and sulfatase inhibitor
DHEA	dehydroepiandrosterone
DMSO	dimethyl sulfoxide
DRY	hydrophobic probe
E ₁	estrone
E ₁ S	estrone sulfate
E ₂	estradiol
E ₃	16 α -hydroxyestradiol
EBE	estimated binding energy
ER	estrogen receptor
ERE	DNA estrogen response element
ESP	electrostatic surface potential
EST	estrogen sulfotransferase
FAD	flavin-adenine dinucleotide
FFD	fractional factorial design
FMN	flavin mononucleotide
GB/SA	generalized Born equation/surface area continuum solvation
GRIND	grid independent descriptor

HBA	hydrogen bond acceptor
HBD	hydrogen bond donor
HF	Hartree–Fock
HOMO	highest occupied molecular orbital
HTS	high-throughput screening
HYD	hydrophobic group
HYP	hypothesis
IC ₅₀	half-maximal inhibitory concentration
K_d	dissociation constant for the receptor-ligand complex
K_i	dissociation constant for the enzyme-inhibitor complex
K_i	inactivation constant
k_{inact}	maximal inactivation rate
K_m	Michaelis-Menten constant
k_{obs}	apparent inactivation rate constant
logP	octanol/water partition coefficient
LOO	leave-one-out cross validation
LSC	liquid scintillation counting
LUMO	lowest unoccupied molecular orbital
MACC2	maximum auto and cross covariance transformation
MIF	molecular interaction field
MM	molecular mechanics
MMFF	Merck molecular force field
NADH	nicotinamide adenine dinucleotide
NADPH	nicotinamide adenine dinucleotide phosphate
NAI	azol non-steroid aromatase inhibitor
NCI	National Cancer Institute
NMR	nuclear magnetic resonance
PAI	polyphenol aromatase inhibitor
PDB	protein data bank
PLS	partial least squares
PSA	polar surface area
q^2	cross-validated correlation coefficient
QM	quantum mechanics
r^2	correlation coefficient

VIII

RG	random groups
RMSD	root mean square deviation
SAI	steroid aromatase inhibitor
SAR	structure-activity relationships
SDEP	standard deviation of errors of prediction
SEM	standard error of the mean
SERM	selective estrogen receptor modulator
STS	steroid sulfatase
SUMM	systematic unbounded multiple minimum
$t_{1/2}$	half-life
TIP	shape probe
TxA ₂ S	thromboxane A ₂ synthase
USP	United States pharmacopeia
V_{\max}	maximum velocity of catalysis
VS	virtual screening

List of tables

Table 2.1. <i>In vitro</i> aromatase inhibition by estradiol, estrone and derivatives	71
Table 2.2. Kinetic constants, relative inhibitory potency and type of aromatase inhibition by 2-OHE ₂ (2.6).....	73
Table 3.1. Estimated binding energie and aromatase inhibitory activities of flavones 3.1-3.12	90
Table 3.2. Estimated binding energies and aromatase inhibitory activities of flavanones 3.13-3.17	92
Table 3.3. Estimated binding energies and aromatase inhibitory activities of cyanidin and malvidin-3-O-glucoside	93
Table 3.4. Estimated binding energies and aromatase inhibitory activities of coumarins 3.20-3.23	94
Table 3.5. Estimated binding energies and aromatase inhibitory activities of <i>trans</i> -resveratrol and oleuropein	95
Table 3.6. Cross-validation of the PLS 3D-QSAR regression model	97
Table 3.7. Relevant variables with high impact on the GRIND PLS model with three latent variables.....	99
Table 4.1. Screening results on a literature database with non-steroid AIs	130
Table 4.2. NCI database screening results.....	135
Table 4.3. Aromatase inhibitory activity of the selected NCI hits based on the NAI-HYP2-HBA+Shape pharmacophore model	140
Table 4.4. Aromatase inhibitory activity of the selected NCI hits based on the SAI-HYP1+Shape pharmacophore model.	142
Table 4.5. Enzyme kinetic parameters for compounds 4.28 and 4.34 , based on a kinetic and time-dependent inactivation procedure.....	143

Table 4.6. Aromatase inhibitory activity of the selected NCI hits based on the PAI-HYP+Shape pharmacophore model.....	146
--	-----

List of figures

Figure 1.1. Enzymes involved in production and transformation of estrogens in the human breast cells	8
Figure 1.2. Estrogen receptor activation by ligand-dependent and ligand-independent mechanisms	13
Figure 1.3. Schematic representation of the ER structure	13
Figure 1.4. Schematic representation of the main metabolic pathways of estradiol hydroxylation and O-methylation	15
Figure 1.5. Oxidative and conjugative metabolism of estrogens.....	16
Figure 1.6. Metabolic redox cycling and generation of depurinating adducts by 4-OHE ₂	19
Figure 1.7. 2D and 3D representation of a heme prosthetic group linked to a cysteine residue.....	21
Figure 1.8. Schematic representation of class I and class II cytochrome P450 multienzymatic systems	22
Figure 1.9. Catalytic cycle of cytochrome P450 enzymes.....	25
Figure 1.10. Aromatization mechanism of androstenedione into estrone by the human aromatase enzyme.....	27
Figure 1.11. Oxygen rebound mechanism involved in two initial hydroxylations catalyzed by aromatase	27
Figure 1.12. Proposed mechanism for the third oxidative step of the aromatase enzyme	28
Figure 1.13. Classification of the main aromatase inhibitors.....	31
Figure 1.14. Examples of steroid aromatase inhibitors	33

Figure 1.15. Examples of non-steroid aromatase inhibitors	37
Figure 1.16. Examples of natural polyphenol aromatase inhibitors	40
Figure 1.17. Examples of polyphenol synthetic derivatives with improved anti-aromatase potency	41
Figure 1.18. Examples of dual aromatase-steroid sulfatase inhibitors	44
Figure 1.19. Basis of the radiometric assay used to measure the aromatase activity	45
Figure 1.20. Drug discovery and development workflow	48
Figure 1.21. Schematic representation of the main energy contributions to a molecular mechanics force field	50
Figure 1.22. Schematic representation of a one-dimensional energy surface	52
Figure 1.23. Hydrophobic and hydrogen bond donor MIFs calculated for flavone and represented at a negative energy level.....	54
Figure 1.24. Schematic representation of a LOO cross-validation study with 4 compounds	57
Figure 1.25. 3D Structure of CYP1A2 and CYP2C9.....	59
Figure 2.1. Schematic representation of estrogen conversion paths	70
Figure 2.2. 2-Methoxyestradiol-3-methyl ether (2.12)	71
Figure 2.3. Concentration-response curves obtained with 4-OHE ₁ (2.7), 2-OHE ₂ ,3Me (2.11), 2-MeOE ₂ ,3Me (2.12) and 16 α -OHE ₁ (2.3) tested as AIs	72
Figure 2.4. Lineweaver-Burk plot of the inhibition of human placental aromatase by 2-OHE ₂ (2.6)	73
Figure 2.5. Electrostatic surface potential of E ₂ (2.1), E ₃ (2.4), 2-OHE ₂ (2.6), 4-OHE ₂ (2.8), 2-MeOE ₂ (2.9) and 2-MeOE ₂ ,3Me (2.12) mapped on the 0.02 e/A ³ electron density isocontour	75

Figure 2.6. Electrostatic surface potential of E ₂ (2.1), E ₃ (2.4), 2-OHE ₂ (2.6), 4-OHE ₂ (2.8), 2-MeOE ₂ (2.9) and 2-MeOE ₂ ,3Me (2.12) at isosurface values of V= 0.025 eV and V= -0.025 eV	76
Figure 3.1. Concentration-response curves of compounds 3.14 and 3.12	89
Figure 3.2. Superimposition of the global minimum-energy conformation found for flavone 3.12 and flavanone 3.17	92
Figure 3.3. Plot of the predicted versus experimental pIC ₅₀ from the optimal PLS model with three latent variables (q ² _{LOO} =0.85)	97
Figure 3.4. PLS coefficients plot of the GRIND variables used in the model	98
Figure 3.5. MACC2 interaction energy product and graphical representation of the three most relevant GRIND variables with direct impact obtained with 5,7,4'-trihydroxy-3'-methoxyflavone and flavone.....	101
Figure 3.6. Virtual receptor site obtained when the most relevant descriptors with direct impact on the biological activity are coded into pharmacophoric regions around the strongest flavone tested	103
Figure 3.7. MIF isosurfaces obtained with the probe DRY and OH on the homology model of the aromatase active site	105
Figure 3.8. Docked pose of 5,7,4'-trihydroxy-3'-methoxyflavone	107
Figure 3.9. Structural transformations of anthocyanins in acidic aqueous solution	108
Figure 3.10. Docked pose of the malvidin-3-O-glucoside	109
Figure 3.11. Docked pose of oleuropein and <i>trans</i> -resveratrol	110
Figure 3.12. Predicted superimposition of 5,7,4'-trihydroxy-3'-methoxyflavone and oleuropein in the active site of the aromatase model.....	111
Figure 3.13. Docked pose of the 6,7-dihydroxycoumarin.....	112

Figure 3.14. Predicted superimposition of 5,7,4'-trihydroxy-3'-methoxyflavone and <i>trans</i> -resveratrol in the active site of the aromatase model.....	112
Figure 4.1. A) Training set of azole non-steroid AIs used for the common-features pharmacophore model generation. B) Common-features pharmacophore model of azole non-steroid AIs	127
Figure 4.2. C5-N-HBA and C6-N-HBA fragment/function pharmacophore features	128
Figure 4.3. A) Training set of C6-substituted steroid AIs used for the common-features pharmacophore model generation. B) Common-features pharmacophore model of C6-substituted steroid AIs	132
Figure 4.4. A) Polyphenol AIs used for the pharmacophore model generation and validation. B) Pharmacophore model of polyphenol AIs	133
Figure 4.5. NCI hits selected based on the NAI-HYP2-HBA+Shape pharmacophore model.....	136
Figure 4.6. NCI hits selected based on the SAI-HYP1+Shape pharmacophore model.	138
Figure 4.7. NCI hits selected based on the PAI-HYP+Shape pharmacophore model.	139
Figure 4.8. Time- and concentration-dependent inactivation of human placental aromatase by compound 4.29 in the presence of NADPH	144
Figure 4.9. Effect of androstenedione (A), NADPH (B) and L-cysteine (C) on the time-dependent inactivation of aromatase by compound 4.29	145
Figure 4.10. Docked poses of compounds 4.7 , 4.8 and 4.15 into the binding site of an aromatase homology model.....	148
Figure 4.11. A) Superimposition of the minimized structures of androstenedione and B-nor-androstenedione at the <i>ab initio</i> HF/6-31G** level. B) Electrostatic surface potential, HOMO and LUMO valence orbitals derived for androstenedione and B-nor-androstenedione	150

Thesis organization

The present thesis consists of seven chapters, including a general introduction, computational and experimental results divided into three chapters, conclusion remarks, appendix and a final chapter with supporting references.

The general introduction provides the basic background for the work described. This chapter starts with a brief description of the breast cancer disease and therapeutic options available. The importance of an anti-hormonal treatment with aromatase inhibitors is introduced and the involvement of estrogens in the pathology is discussed, along with their mechanisms of production, binding to the receptor and metabolism. Functional, structural and catalytic aspects of cytochrome P450 enzymes are reviewed with particular attention given to the aromatization mechanism. Several generations and classes of aromatase inhibitors are presented. Finally, the biochemical assay used to screen new anti-aromatase candidates is discussed, as well as some basic principles of computer-assisted drug design.

The second chapter reports results on the biochemical evaluation of the main estradiol and estrone metabolites as aromatase inhibitors. The interaction of these compounds with the enzyme is discussed based on electrostatic surface potential calculations. A possible physiological role for these compounds and their potential for lead optimization are presented.

In the third chapter results from a biochemical and computational study with natural polyphenols from different natural sources are described. A virtual receptor site model is proposed for the interaction between the polyphenols and the enzyme aromatase. Structure-activity rules are extracted for the design of new aromatase inhibitors.

The fourth chapter presents the results of a virtual screening strategy for the discovery of new aromatase inhibitors based on the structures of known molecules. Three models are presented, each one derived from a different class of aromatase inhibitors. The experimental validation of this approach led to new potent aromatase inhibitors.

Chapters two, three and four include an abstract, a brief introduction, results and discussion, conclusions and a section with the materials and methods used.

Chapter five states the major conclusions drawn from this work, chapter six includes an appendix with a pharmacophore model validation results and chapter seven provides the supporting references.

I

General introduction

1.1. Breast cancer

1.1.1. General considerations

Breast cancer results from an uncontrolled proliferation of abnormal cells that starts in the ducts and nodules of the breast tissues. Although initially confined to a small area (*carcinoma in situ*), breast tumors progress into invasive lesions, spreading through the lymphatic vessels into nearby lymph nodes, usually those in the axillae, above the collarbone or in the chest. Advanced breast cancer can also metastasize at distant locations via the blood and lymphatic systems. Common locations for the development of secondary tumors include brain, bones, liver and lungs. Metastasization is the major cause of mortality associated to this type of cancer.¹

Breast cancer is the most diagnosed type of cancer in Europe, accounting for 13.5% of all cases. Other common types include colorectal cancer (12.9%), lung cancer (12.1%) and prostate cancer (10.8%). Early detection due to the use of X-ray screening mammography favors treatment efficacy. Therefore, breast cancer is only the third most common cause of cancer mortality with 7.7% of all deaths, ranked immediately after lung cancer (19.7%) and colorectal cancer (12.2%).² In men, the incidence rate of breast cancer is approximately 100 times lower than in women, being the chances of survival nearly the same.³

The risk of developing breast cancer is directly related to the female sexual hormones and the number of ovulatory cycles experienced lifelong. Besides age and gender, the most important risk factors of developing the disease, other relevant variables include an early menarche or a late menopause. A personal or familiar history of breast cancer, a late or never having pregnancy, the presence of dense breast tissue on a mammography or taking high doses of estrogens are also significant risk factors. Furthermore,

breast cancer is favored by genetic mutations in the *BRCA1* and *BRCA2* genes or by medical procedures involving high doses of radiation. Lifestyle factors, such as postmenopausal obesity, are also associated with an increased incidence.⁴

1.1.2. Breast cancer treatment approaches

Besides new therapies under clinical trials, four different types of treatment are currently used for patients with breast cancer: surgery, radiotherapy, chemotherapy and anti-hormonal therapy.⁵

Most people need surgery to remove the tumor. However, the area to remove depends on the size and spread of the disease. The most conservative procedures remove the tumor but not the breast itself (lumpectomy and partial mastectomy), whereas in other cases removal of the whole breast is required (total mastectomy), together with the chest wall muscles under the breast and the lymph nodes under the arm (radical mastectomy). Even if the whole detectable tumor is removed by surgery, adjuvant therapy can be used to eliminate malignant cells that might remain undetectable. Breast cancer adjuvant therapy uses radiotherapy, chemotherapy or anti-hormonal therapy to reduce recurrence and increase the chances of survival.

Radiotherapy uses high-energy radiation to destroy cancer cells, whereas chemotherapy uses oral or intravenous drugs, usually administered in combination. Chemotherapy protocols include nitrogen mustard alkylating agents (cyclophosphamide), antimetabolites (methotrexate, 5-fluorouracil, gemcitabine and capecitabine), anthracycline antibiotics (doxorubicin and epirubicin) and mitotic inhibitors (paclitaxel, docetaxel and vinorelbine). These treatments can be physically exhausting for the patient and have several side effects affecting mainly the fast-dividing cells of the body. For this reason, treatments are performed in cycles of therapy and recovery.

If the tumor is hormone sensitive, reduction of estrogen levels by ovariectomy, hypophysectomy or adrenalectomy can prevent tumor growth and spread or even cause regression of the disease. The need for these surgical procedures was reduced by the use of anti-hormonal therapy with tamoxifen or aromatase inhibitors (AIs). Anti-hormonal therapy has less side effects than chemotherapy, extending women's life and improving their quality of life.⁶

Tamoxifen is a selective estrogen receptor modulator (SERM) that blocks the growth of breast tumors by competitive antagonism with the female sexual hormones to the estrogen receptor (ER).⁷ Tamoxifen was approved by the U.S. Food and Drug Administration in 1977 as a drug for the treatment of advanced breast cancer and later, for the adjuvant treatment of early breast cancer. Although this molecule has antagonist activity in the breast tissue, partial estrogen agonist effects are observed in other tissues such as bone and endometrium. These effects can be advantageous, since they may prevent bone demineralization in postmenopausal women,^{8;9} but also detrimental, due to increased risks of uterine cancer^{10;11} and thromboembolism.¹² Furthermore, despite proven benefits to a large number of patients, resistance to this drug is a significant problem.¹³

On the other hand, aromatase inhibitors suppress estrogen levels by blocking the enzyme aromatase. Recent large scale clinical trials with postmenopausal women revealed that estrogen depletion, with potent and selective aromatase inhibitors, is a more effective and well tolerated therapeutic option against hormone-dependent breast cancer than tamoxifen.^{14;15} Third generation aromatase inhibitors are used as first-line therapy for the treatment of breast cancer in both early and advanced tumors, and ongoing studies are investigating the use of aromatase inhibitors to prevent breast cancer in postmenopausal women at increased

risk.¹⁶ Similar to tamoxifen, third generation aromatase inhibitors are orally active.

Used as monotherapy in premenopausal women, aromatase inhibitors increase gonadotropin secretion (follicle-stimulating and luteinizing hormones) due to decreased feedback over the hypothalamus and pituitary. Therefore, clinical application of aromatase inhibitors in premenopausal women requires concomitant administration of a gonadotropin-releasing hormone agonist.¹⁷ Moreover, used for short periods, aromatase inhibitors have been successfully employed to stimulate follicular growth and to induce ovulation in women with low fertility.¹⁸

1.1.3. Breast tissue estrogens

Estrogens are important for the normal development and growth of the human body. Besides their involvement in sexual differentiation, control of the reproductive cycle and pregnancy, they are implicated in many non reproductive functions. For instance, in the cardiovascular system, estrogens have protective effects either directly through the interaction with the blood vessels or indirectly through the plasma lipoprotein metabolism.¹⁹ In the bone, estrogens regulate the normal mineralization, controlling the balance between bone formation and bone resorption.²⁰ In the central nervous system, several neuroendocrine functions have been attributed to estrogens, namely neuroprotection against Alzheimer's disease and schizophrenia.²¹

However, prolonged exposure to high concentrations of estrogens might have detrimental effects. Breast and uterus tissues are highly sensitive to the mitogenic effects of estrogens, and excessive cell proliferation can lead to replication errors and to an increased risk of breast and endometrial cancers.²² More than a century ago, Beatson reported the importance of endocrine control in breast cancer, describing three cases of patients with

advanced breast cancer treated by bilateral ovariectomy, the surgical removal of the ovaries, leading to regression of the disease.²³ Beatson's observations were the basis of the current anti-hormonal treatment of breast cancer.

About 70-80% of breast cancers express hormone receptors that are responsive to the mitogenic effects of estrogens. If the primary tumor expresses these receptors, more than 80% of the lymph node metastases and about 70% of distant metastases retain this property. ER positive (ER+) tumors tend to grow slower and better differentiated than ER negative (ER-) tumors. Therefore, the ER+ status is associated with a better overall prognosis and is an important indicator of potential response to endocrine therapy.^{24;25}

After the menopause, a dramatic fall of about 90% is observed in the plasma estradiol (E₂) levels. However, breast tissues sustain the local E₂ concentrations at nearly the same levels found in premenopausal women, suggesting local estrogen synthesis or a mechanism of active uptake from the circulation. Moreover, the dominant estrogen in the plasma is estrone sulfate (E₁S), an inactive derivative, whereas E₂ is the most abundant estrogen in breast cancer tissue of postmenopausal women.²⁶

1.1.3.1. Uptake from the circulation

Even at very low estrogen plasma concentrations, estrogen receptor rich tissues like breast, are able to concentrate these hormones due to the high binding affinity of E₂ to the ER (K_d= 0.35×10⁻¹² M).²⁷ These plasma/tissue gradients explain, at least partially, the high concentration of estrogens found in the breast tissues of postmenopausal women.

1.1.3.2. Local production of estrogens

Breast tissue has all the enzymatic machinery to produce and store estrogens from dehydroepiandrosterone (DHEA). The most important enzymes involved are the 3 β -hydroxysteroid dehydrogenase Δ^{5-4} isomerase (3 β -HSD), the aromatase, the 17 β -hydroxysteroid dehydrogenase (17 β -HSD), the steroid sulfatase (STS) and the estrogen sulfotransferase (EST, **Figure 1.1**). These enzymes modulate the hormonal environment within breast tissue, controlling proliferation of both normal and breast cancer cells.²⁸

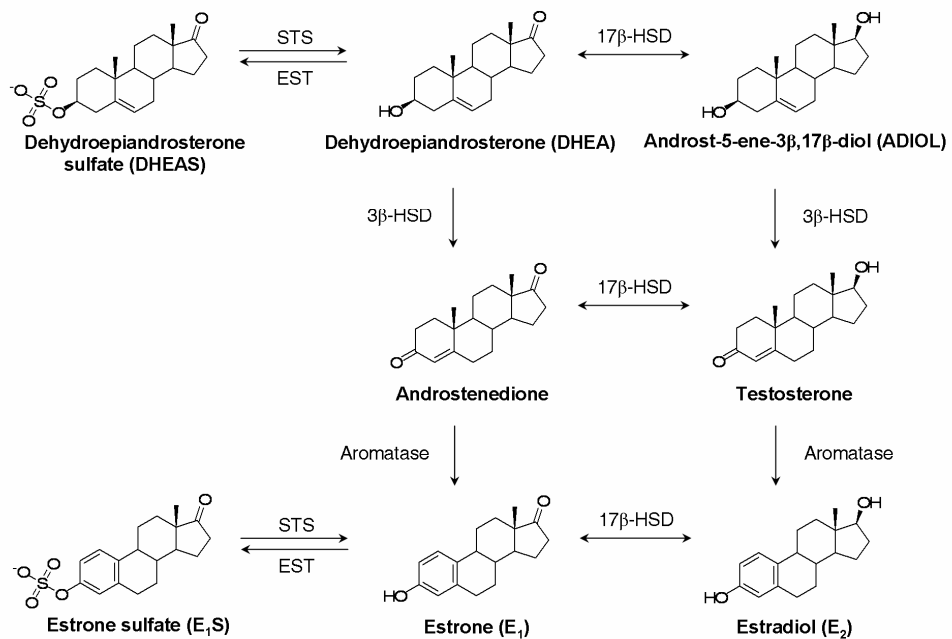


Figure 1.1. Enzymes involved in production and transformation of estrogens in the human breast cells. This figure was adapted from literature.²⁸

3 β -Hydroxysteroid dehydrogenase Δ^{5-4} isomerase

The 3 β -HSD performs a sequential 3 β -hydroxy dehydrogenation and a Δ^5 to Δ^4 isomerization of the steroid precursors, thus catalyzing the formation of the A-ring enone system from 3 β -hydroxy- Δ^5 steroids. This enzyme is essential for the biosynthesis of all steroid classes, such as glucocorticoids, mineralocorticoids, estrogens, androgens and progestagens. Type I 3 β -HSD isoenzyme is predominantly expressed in the placenta and peripheral tissues, such as skin, liver and mammary glands, whereas the type II isoenzyme is expressed in the adrenal gland and gonads.²⁹ Induction of the 3 β -HSD increases the production of androstenedione and testosterone, which are known to have antiproliferative effects in breast cancer cells.³⁰ Furthermore, 3 β -HSD converts androst-5-ene-3 β ,17 β -diol (ADIOL), a steroid with estrogenic activity due to high affinity for the ER,³¹ into testosterone. However, because aromatase is also expressed in breast cells, the androgens produced by 3 β -HSD are converted into estrone and estradiol, as described in further detail in the section below. Therefore, 3 β -HSD modulates the balance between estrogenic and androgenic responses and the final proliferative or antiproliferative effect depends on the local aromatase activity.

Aromatase

Aromatase (CYP19) is an enzyme of the cytochrome P450 superfamily that catalyzes the final and rate-limiting step of the conversion of androgens, testosterone and androstenedione, into estrogens, estradiol and estrone, respectively.

Aromatase is highly expressed in the ovaries of premenopausal women, controlled by cyclic gonadotropin stimulation and in the placenta of pregnant women.³² Other tissues, including adipose tissue,³³ liver,³⁴ muscle,³⁵ brain³⁶ and breast tissue,³⁷ have also the ability to express aromatase. After

menopause, estrogen production arrives exclusively from peripheral sources, mainly the muscle and subcutaneous fat, through aromatization of androgens derived from the adrenals and ovaries.^{33;35} Although the aromatase activity in muscle and fat is lower than in placenta and ovary, the large amount of these tissues in the body results in significant estrogen production. Furthermore, even with the mean plasma estradiol levels falling after the menopause, the concentration of estradiol in breast tissues is significantly higher, mainly due to the local aromatase activity.³⁸

17 β -Hydroxysteroid dehydrogenase

The 17 β -HSD catalyzes stereospecific redox reactions at the position C17 of steroids such as androgens and estrogens. This enzyme converts less active hormones, DHEA, E₁ and androstenedione into more potent ones, ADIOL, E₂ and testosterone, respectively, and vice-versa. Therefore, 17 β -HSD play a fundamental role in the hormonal regulation, controlling the intracellular availability of steroids to the nuclear receptors.³⁹

Distinct subtypes of 17 β -HSD have been identified. The type 1 is the major isoenzyme involved in the conversion of estrone into estradiol in the human breast tissue,⁴⁰ whereas 17 β -HSD type 2 catalyzes the reverse oxidative reaction as well as the conversion of testosterone into androstenedione.⁴¹ Both the subtypes are expressed in normal breast tissue of premenopausal women where the oxidative activity seems to be dominant.⁴² On the other hand, up-regulation of 17 β -HSD type 1 was shown in both primary breast cancer cells and metastatic tissues, being associated with a less favorable prognosis of the disease.^{43;44} On this basis, selective inhibitors of the type 1 isoenzyme could be a new potential approach to block estradiol biosynthesis in the gonads and in target tissues. Inhibitors based on this rationale have been developed for the treatment of hormone-dependent breast cancer.⁴⁵

Steroid sulfatase and estrogen sulfotransferase

After estrone production via the aromatase pathway, much of this steroid is rapidly sulfated into estrone sulfate in a reaction catalyzed by estrogen sulfotransferase, an enzyme that is found mainly in tissues such as that of the reproductive tract, breast, skin, brain, bone and blood. On the other hand, the enzyme that hydrolyses estrogen-sulfate back into free estrogen is the steroid sulfatase, which is more widely distributed in the body.^{46;47} Sulfation of estrogens renders them more hydrophilic and unable to bind the ER. Therefore, given that E₁S is the major circulating form of estrogen in the plasma, with levels 10 to 20 times higher than those of E₁ or E₂, and with a considerably longer half-life ($t_{1/2}$ =10 to 12 hours) when compared to the unconjugated estrogens ($t_{1/2}$ =20 to 30 minutes),^{48;49} it is assumed that E₁S acts as a reservoir of active estrogen, via reaction catalyzed by STS, protecting peripheral tissues from excessive estrogenic stimulation. Furthermore, STS also catalyzes the hydrolysis of dehydroepiandrosterone sulfate (DHEAS) to the unconjugated form, DHEA.²⁸

In conclusion, both STS and EST regulate the *in situ* production of estrogens in human breast cells and have prognostic significance in breast carcinomas. The EST activity was found to be inversely correlated with the tumor size and significantly associated with an improved prognosis.⁴⁷

1.1.4. The estrogen receptor

The predominant biological effects of estradiol are mediated by two members of a large family of nuclear receptors, the ER α and the ER β .⁵⁰ While the ER α is the predominant subtype in uterus,⁵¹ ER β is highly expressed in other tissues, such as breast,⁵² prostate,⁵³ testis,⁵⁴ bone,⁵⁵ immune system,⁵⁶ cardiovascular system⁵⁷ and central nervous system.⁵⁸ The proliferative actions of estradiol, mediated via the ER α , can be opposed by the ER β in several tissues.⁵⁰ Because of these anti-proliferative effects,

the role of ER β as a tumor suppressor in several types of cancer was proposed, including those of breast, ovary, colon and prostate.⁵⁹ ER β has been reported to be expressed at high levels in normal breast and, frequently, to be lost during multi-stage oncogenesis.⁶⁰ Consistent with these findings, *in vitro* studies have demonstrated growth inhibition when ER β is expressed in ER α -positive breast cancer cells.⁶¹⁻⁶³

Emerging evidence suggests that ERs are activated by multiple pathways.⁶⁴ The classical, ligand-dependent, mechanism of E₂ action states that ligand binding induces conformational changes to the ER, promoting dimerization and high affinity binding to specific DNA estrogen response elements (EREs). Depending on the cell type and promoter context, the DNA-bound receptor causes either up- or down-regulation of the gene transcription and subsequent tissue responses (**Figure 1.2**). Alternatively, ligand independent mechanisms of ER activation have been described. For example, activation of kinases by growth factor signaling leads to phosphorylation and thus activation of ERs.^{65;66} This cross-talk between signaling pathways might explain the hormone-independent growth of some tumors and the clinical resistance to anti-hormonal therapy.^{67;68}

Other important players in the activation of estrogen receptors are the coregulators, proteins recruited by ERs to activate (coactivators) or to repress (corepressors) ER transcription.^{69;70} Therefore, estrogen receptor effects are tripartite, involving the receptor itself, the ligands and the coregulator proteins recruited.

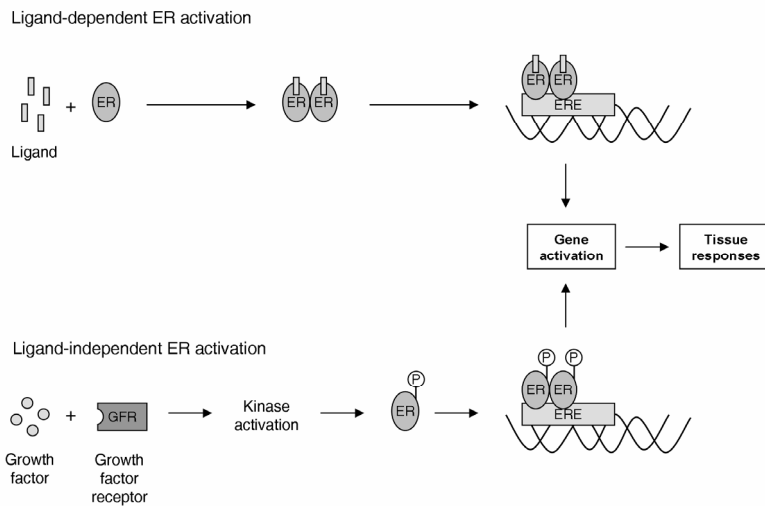


Figure 1.2. Estrogen receptor activation by ligand-dependent and ligand-independent mechanisms. This figure was adapted from literature.⁶⁴

Estrogen receptors share six common functional domains labeled A to F (**Figure 1.3**): an N-terminal region involved in interactions with coregulators (A/B domain); a DNA-binding domain (C); a hinge domain involved in dimerization and binding to heat shock protein HSP90 (D), a ligand-binding domain (E) and a C-terminal domain which contributes to the transactivation of the receptor (F).⁷¹



Figure 1.3. Schematic representation of the ER structure. The percentage of homology between ER α and ER β is shown. This figure was adapted from literature.⁷¹

The DNA-binding domain is the most conserved region with 97% homology between ER α and ER β . Less conserved domains include the ligand-binding domain, with 60% homology, and the A/B/F domains, which are highly

variable in sequence and length, with only about 18% homology. Therefore, ER α and ER β can be activated by distinct ligands and interact with different coregulator proteins, which explains the distinct effects on the transcription of genes.⁷¹

Besides E₂ and E₁, other compounds including natural diet polyphenols, and synthetic drugs, are also able to bind ERs.⁷² Whereas pure agonists, such as E₂, are active in all cell and coregulator contexts, selective estrogen receptor modulators have mixed agonist/antagonist activities depending on the ligand-induced conformational changes of the ER, the receptor isoform, the coregulatory proteins of the target tissues and the promoter sequences of the DNA. Both agonist and antagonist compounds bind to the same internal cavity of the ER ligand-binding domain, however, antagonists sterically prevent the receptor to adopt the agonist conformation, which prevents recruitment of coactivators.⁷³ Ideal SERMs retain the beneficial effects of estrogen in tissues like brain, bone and cardiovascular system, but lack the mitogenic and carcinogenic action in the breast and uterus.⁷⁴

1.1.5. Estrogen metabolism

Estrogens are metabolized by oxidative (phase I) and conjugative (phase II) pathways. Cytochrome P450 enzymes, involved in oxidative metabolism, produce mostly A-ring metabolites, by 2- and 4-hydroxylation, or D-ring metabolites by 16 α -hydroxylation (**Figure 1.4**).⁷⁵ In addition, other oxidative metabolites are produced in relatively small quantities by 6 α -, 7 α -, 12 β -, 15 α -, 15 β - and 16 β -hydroxylation.⁷⁶ Although the liver has the highest metabolic rate of oxidative metabolism, similar pathways were also identified in extrahepatic locations such as the breast tissue,^{77;78} uterus,^{79;80} placenta,⁸¹ kidney^{82;83} and brain.⁸⁴

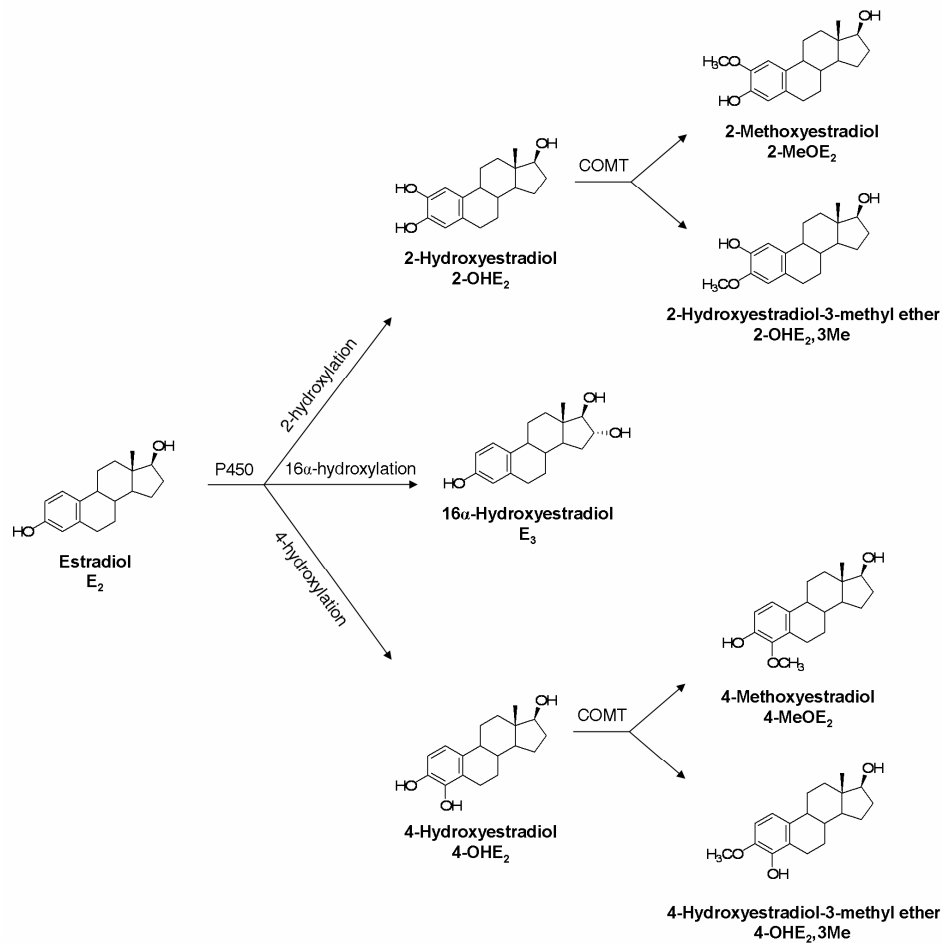


Figure 1.4. Schematic representation of the main metabolic pathways of estradiol hydroxylation and O-methylation. Estrone metabolism follows similar paths (structures not shown). Modified from literature.⁷⁵

Catechol-O-methyltransferase (COMT) converts catechol estrogens into their 2-methoxy and 4-methoxyestrogen derivatives. This enzyme is present in large amounts in the liver and kidney, but also in the uterine endometrium, mammary gland and many other tissues.^{85;86} Other phase II enzymes, such as glucuronosyltransferase (GT), sulfotransferase (ST), estrogen acyltransferase (EAT) and glutathione S-transferase (GST), convert hydroxylated metabolites to their glucuronide, sulfate, fatty acid and

glutathione conjugates, respectively (**Figure 1.5**). These more soluble metabolites are found in large amounts in the urine.⁷⁵

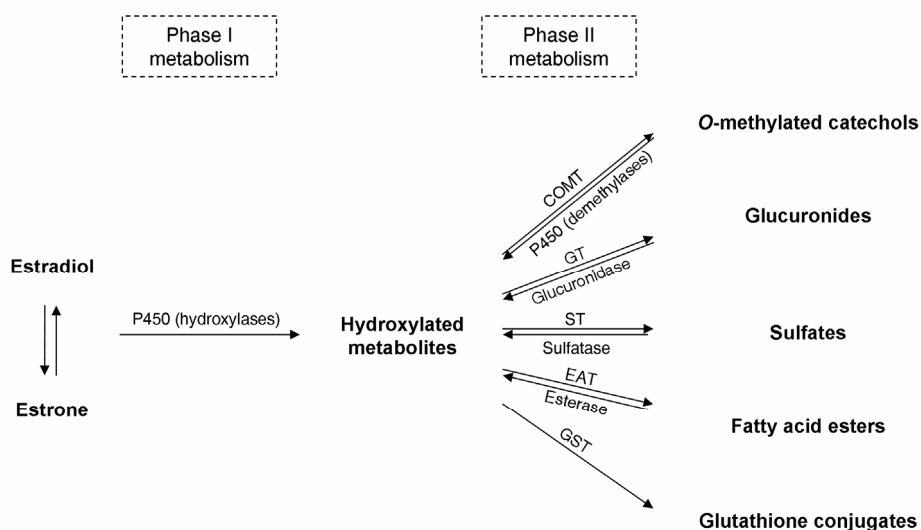


Figure 1.5. Oxidative (phase I) and conjugative (phase II) metabolism of estrogens. Modified from literature.⁷⁵

Initially considered inactive, estradiol metabolites have gained interest in recent years due to the discovery of potent pro and anticarcinogenic activities and to the elucidation of their potential to bind to the ER and to have estrogenic activity.⁸⁷ In this sense, understanding the biological properties of these compounds is extremely important, in order to assess their involvement in control mechanisms of tumor growth.

1.1.5.1. C2-Metabolites

The 2-hydroxylation of estrogens into catechol derivatives, 2-hydroxyestradiol (2-OHE₂) and 2-hydroxyestrone (2-OHE₁), is the major metabolic pathway in liver (ratio 2-OHE₂ to 4-OHE₂ of ~6:1),⁷⁶ producing compounds that bind to the classical ER with much weaker estrogenic activity than the parent hormones.⁸⁸⁻⁹⁰ Furthermore, 2-OHE₁ was found to

have potent antiestrogenic activity able to suppress the growth and proliferation of hormone-dependent human breast cancer cells.⁹¹ Several P450 isoforms contribute to the 2-hydroxylation of estrogens. In the breast, CYP1A1, CYP1A2 and CYP3A4 are the main metabolizing enzymes.⁹²⁻⁹⁴

Due to the fast activity of COMT, 2- and 4-methoxyestrogens are more abundant in the human plasma and urine than the parent catechols. These compounds have little or no binding affinity to the ER when compared to estradiol, and are deprived of its estrogenic effects. Furthermore, 2-methoxyestradiol (2-MeOE₂) exerts unique biological effects that are not associated with the ER, such as antiangiogenic, cytotoxic and antiproliferative activities in several tumor types.^{95;96} These findings led to the clinical evaluation of 2-MeOE₂ in phase I and phase II trials for the treatment of multiple types of cancer^{97;98} and to the development of several derivatives with improved potency and bioavailability.⁹⁹⁻¹⁰¹

1.1.5.2. C4-Metabolites

The 4-hydroxylation of estradiol into 4-OHE₂ is a significant hydroxylation pathway in several reproductive tissues.^{77;80} 4-OHE₂ exhibits estrogenic activity similar to that observed with estradiol and binds to the ER with a slow dissociation rate.^{90;102} The extensive mitogenic stimulation in breast tissue may play a role in both initiating and promoting breast carcinogenesis, which is corroborated by the higher levels of 4-OHE₂ found in breast tumor tissues as compared to normal breast tissues.⁷⁷ CYP1B1 is the main enzyme involved in the 4-hydroxylation of estrogens.¹⁰³

1.1.5.3. C16-Metabolites

In a similar manner to the 4-hydroxyl metabolites, 16 α -hydroxyl estrogens such as 16 α -hydroxyestradiol (E₃) retain very strong hormonal potency by

binding extensively and irreversibly to the ER¹⁰⁴ and were suggested to increase the risk of developing breast cancer.^{105;106}

Therefore, despite the oxidative and conjugative metabolism, estrogen derivatives carry out several biological activities beyond the estrogenic effects of estradiol.

1.1.5.4. The impact of estrogen metabolism in breast cancer carcinogenesis

Although estradiol and estrone are extensively hydroxylated in the liver, the concentration of unconjugated metabolites in the systemic circulation is low, which is due to rapid conjugative metabolism followed by urinary excretion.^{107;108}

If conjugation reactions are insufficient, both 2- and 4-catechol estrogens can undergo catalytic oxidation by the enzyme peroxidase, with generation of 2,3- and 3,4-semiquinones and the corresponding quinones (**Figure 1.6**).¹⁰⁹ Redox cycling, via reduction of estrogen quinones into semiquinones, catalyzed by cytochrome P450 reductase and subsequent oxidation back to estrogen quinones, produces the superoxide radical ($O_2^{\cdot-}$) which promptly dismutates in the presence of superoxide dismutase (SOD) and forms hydrogen peroxide (H_2O_2). This compound is extremely dangerous to the cell and, if not transformed into other less reactive substances, it can be easily converted into the hydroxyl radical (HO^{\cdot}), via the Fenton reaction (reaction with Fe^{2+}). The hydroxyl radical is one of the most problematic free radicals, able to damage biological macromolecules such as DNA, proteins and lipids.

Furthermore, estrogen quinones are very reactive electrophilic intermediates and may bind to DNA. Apurinic sites are formed through binding to adenine and guanine purines, followed by release of the

depurinating adducts such as 4-OHE₂-1-N3Ade and 4-OHE₂-1-N7Gua (Figure 1.6).^{109;110} This mechanism has been pointed out to explain the carcinogenic activity of estrogens. Error-prone base excision repair of the damage may lead to mutations that initiate breast and other types of cancer. Interestingly, *in vivo* studies have demonstrated that 2-OHE₂ does not induce tumors, in contrast to 4-OHE₂ which is a potent carcinogen.¹¹¹ Since 2-OHE₂ and 4-OHE₂ have similar redox potentials and can both undergo metabolic redox cycling *in vitro*, with generation of reactive species,¹¹² it is difficult to explain their different carcinogenic activities. One of the reasons might be related to the stronger reactivity of estrogen 3,4-quinones than estrogen 2,3-quinones with DNA to form depurinating adducts.¹¹³

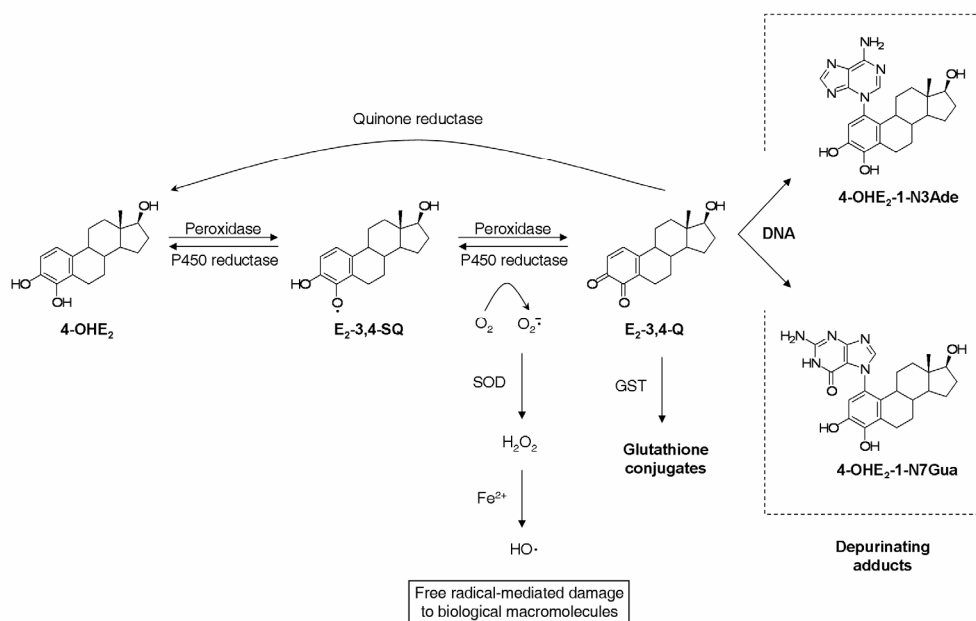


Figure 1.6. Metabolic redox cycling and generation of depurinating adducts by 4-OHE₂, 2-OHE₂, 4-OHE₁ and 2-OHE₁ catechol estrogens follow similar paths (structures not shown). This figure was adapted from literature.¹¹⁰

On the other hand, methoxy estrogens are unable to undergo redox cycling and therefore do not form depurinating adducts.¹¹² Furthermore,

2-methoxyestradiol has antiproliferative properties⁹⁵ and this may account for the lower carcinogenicity observed *in vivo* for 2-hydroxyderivatives.

The reactivity of quinones with DNA can be prevented by conjugation with glutathione, catalyzed by glutathione S-transferase, or by reduction to the original catechols by quinone reductase.^{77;114}

1.2. Cytochrome P450 enzymes

1.2.1. Function, classification and nomenclature

The cytochrome P450 (CYP) is a large family of heme-containing enzymes found in all forms of life, including eukaryotic organisms like animals, plants and fungi, and also some prokaryotes. There are more than 7000 different sequences identified to date, divided into more than 866 different P450 families, and this number continues to increase.¹¹⁵ All members share a common Fe^{III} protoporphyrin-IX center, covalently linked to the apoprotein by the sulfur atom of a cysteine residue (**Figure 1.7**). The octahedral heme iron is coordinated to four pyrrole nitrogen atoms and two additional non-porphyrin ligands in axial positions, namely, the thiolate ligand and either a water molecule or a hydroxyl group from an adjacent amino acid. Contrarily to the strong Fe-S bond, the sixth ligand binds with poor affinity, and might be displaced upon substrate binding. The protein chain of each individual P450 varies both in terms of molecular weight (45 - 60 kDa) and amino acid sequence. This accounts for the differences in substrate specificity and mechanism of reaction.

High levels of CYPs are expressed in the liver. However, several extrahepatic tissues such as the small intestine, lungs, brain and skin, have also significant activities.¹¹⁶

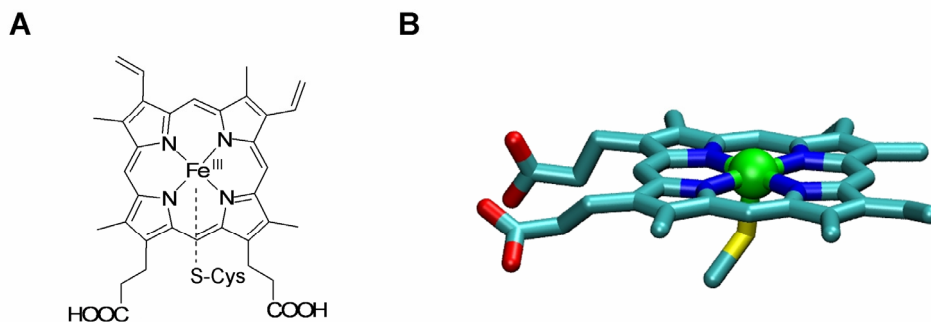
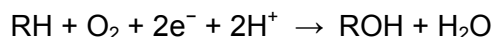


Figure 1.7. 2D (A) and 3D (B) representation of a heme prosthetic group linked to a cysteine residue. This figure was created using the program VMD.¹¹⁷

Molecular oxygen itself reacts very slowly with organic molecules at low temperature due to spin-forbiddance and high energy barriers.¹¹⁸ Therefore, living systems use enzymes such as P450s to convert dioxygen into more reactive species. Since only one of the oxygens from molecular oxygen is inserted into the substrate, these enzymes are called monooxygenases. The second oxygen is reduced into a water molecule, using two electrons provided by NADH or NADPH:



Therefore, P450 enzymes have a key role in oxidative transformations of endogenous (fatty acids, steroids, prostaglandins) and exogenous compounds (drugs and environmental chemicals).¹¹⁹ A large number of reactions such as hydroxylation, epoxidation, aromatic oxidation, *N*- and *S*-oxidation, *N*- and *O*-dealkylation, and aromatization reactions are performed by P450 enzymes.¹²⁰

Cytochrome P450 enzymes are complex multienzymatic systems composed by a P450 domain associated to an auxiliary, electron-transfer reductase system. Depending on the reductase domain, two different classes of enzymes exist. Class I P450s, found in mammalian mitochondrial

membranes and most of bacteria cytoplasm, are three component systems, comprising a flavin-adenine dinucleotide (FAD)-containing reductase, a small iron-sulfur protein (ferredoxin, Fe_2S_2) and the P450 domain. In these systems, the electrons are derived from NADH or NADPH and are transferred from the reductase to the P450 domain via ferredoxin. Class II enzymes are mammalian P450s located in the endoplasmic reticulum, with only two components, both membrane bound, a FAD- and flavin mononucleotide (FMN)-containing NADPH-dependent reductase, and the P450 domain (**Figure 1.8**).¹²¹ Class II enzymes are anchored to the membrane bilayer by the N-terminal segment of the P450 domain, with the C-terminus exposed to the cytosolic compartment, from which the catalytic center is accessible. Another anchoring point to the membrane bilayer is located at the NADPH-dependent cytochrome P450 reductase which has an intramembrane segment with high hydrophobicity and two flanking hydrophilic regions located in the cytoplasm, containing the FAD and the FMN coenzymes.¹²²⁻¹²⁴

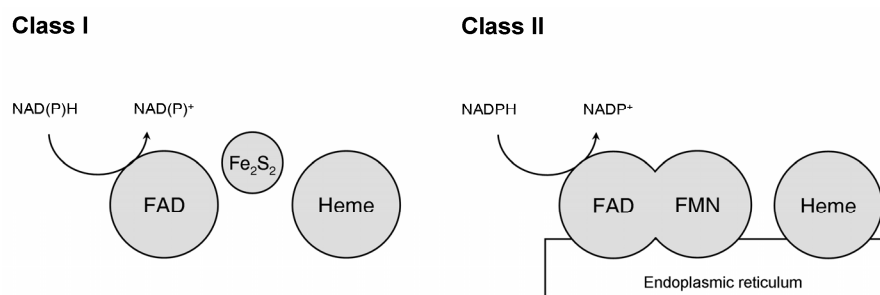


Figure 1.8. Schematic representation of class I and class II cytochrome P450 multienzymatic systems.

It is believed that the whole cytochrome P450 superfamily diverged from a single ancestral gene.¹²⁵ Therefore, individual proteins are classified in families and subfamilies based on criteria of homology. P450 sequences which share more than 40% of amino acid sequence identity are placed

within the same family, whereas those with more than 55% sequence identity are placed within the same subfamily.¹²⁶

The nomenclature of cytochrome P450 enzymes was originally organized according to their physiological function. For example, P450_{SCC} is the enzyme that catalyzes the oxidative cleavage of the side chain of cholesterol to pregnenolone. With the increasing number of P450 identified, a standardized system of nomenclature was adopted to assign individual enzymes into families and subfamilies. According to the new nomenclature rules, the root for all cytochrome P450 names is CYP, followed by a number indicating the family and a letter indicating the subfamily. Individual members within subfamilies are numbered consecutively as they are reported to the nomenclature committee. On the basis of this nomenclature, the first P450 named was CYP1A1. A more detailed description of the nomenclature system adopted for CYPs can be found elsewhere.^{115;126}

1.2.2. Three-dimensional structure

The first 3D structure of a cytochrome P450 enzyme, the bacterial P450_{cam}, was reported in 1985 by Poulos and co-workers.¹²⁷ Other bacterial P450s such as P450_{BM-3},¹²⁸ P450_{terp}¹²⁹ and P450_{eryF}¹³⁰ appeared in the literature in the following years.

Contrarily to the prokaryotic P450s which are found soluble in the cytoplasm, mammalian enzymes are bound to the endoplasmic reticulum membrane, which makes them more difficult to crystallize. One of the main achievements in this field was the structure determination of the first class II enzyme, the CYP2C5 from rabbit,¹³¹ published in 2000, followed by other mammalian, e.g. CYP2B4,¹³² and human P450s, including CYPs 1A2,¹³³ 2A6,¹³⁴ 2A13,¹³⁵ 2C8,¹³⁶ 2C9,¹³⁷ 2D6,¹³⁸ and 3A4.¹³⁹ Crystallization and structure determination of mammalian P450s was possible with the truncation of the membrane-bound N-terminal domain, which forms a trans-

membrane helix, and in some cases, with small mutations preventing protein self-aggregation without interfering with the catalytic activity and substrate specificity.

Although sequence identity between members of different P450 families is low (typically within 10-30%), all 3D structures solved to date share common structural elements and an overall characteristic topology.^{140;141} P450 enzymes have 12 helices and loops labeled from A to L. The B-C and F-G helices are involved in substrate access and specificity, and the heme group is located between helices I and L. In addition, a few β -sheets are present in the P450 structures.¹²⁰ Furthermore, the heme-binding core is highly conserved, both in terms of root mean square deviation (RMSD) and sequence identity.

1.2.3. Catalytic cycle

Besides topological information, 3D elucidation of cytochrome P450 enzymes provided a better understanding of the catalytic cycle of these monooxygenases. The Fe^{III} center of the substrate-free enzyme equilibrates between two spin conditions, the low-spin state, $S=1/2$, in which the five 3d electrons are maximally paired, and the high-spin state, $S=5/2$, in which the five 3d electrons are maximally unpaired. The low-spin state (**A, Figure 1.9**) is favored in the absence of a substrate when the sixth position of the octahedron is occupied by a water molecule or a hydroxyl group from an active site residue. In the presence of a substrate, the axial sixth ligand is displaced from the active site of the enzyme and the spin equilibrium of the Fe^{III} center is shifted toward the high-spin state (**B, Figure 1.9**). Therefore, substrate binding is entropy-driven, due to the release of water molecules from the hydrophobic binding pocket of the P450 enzyme. In its high-spin state, the heme iron has larger ionic radius than in the low-spin state, being displaced from the plane of the heme central cavity. This modification

induces a change in the redox potential of the iron, from -360 mV to -175 mV, which facilitates the first reduction of the ferric center. The first electron is transferred from the NADPH (redox potential -320 mV) by the reductase domain (redox potential -270 mV), initiating the catalytic cycle of the cytochrome.¹⁴²

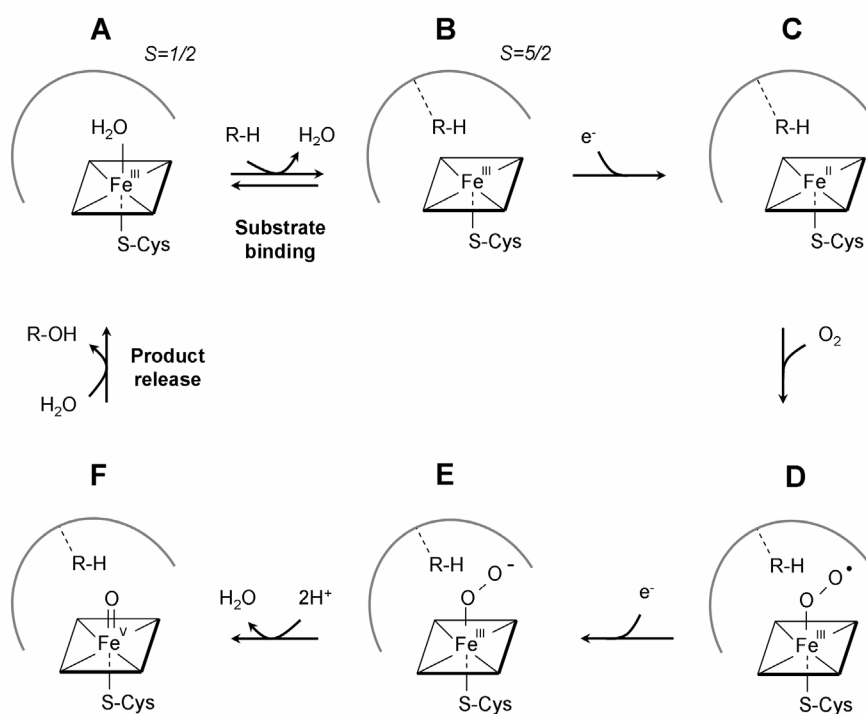


Figure 1.9. Catalytic cycle of cytochrome P450 enzymes. This figure was adapted from literature.¹²⁰

The high spin ferrous iron(II) (**C, Figure 1.9**) has high affinity for diatomic gases and reacts with triplet dioxygen to produce a low spin hexacoordinate iron(III)-dioxygen adduct (**D, Figure 1.9**) using one electron from the iron(II) center and another from the oxygen pair.

The second reduction uses one reducing equivalent from NADPH or NADH, depending on the CYP involved, and is the rate-limiting step of the catalytic cycle. A negatively charged iron(III)-peroxo complex is formed (**E, Figure 1.9**) which is probably quickly protonated to generate an iron(III)-hydroperoxo complex (structure not shown).

Monoxygenase reactions involve transfer of an activated oxygen atom to the substrate, splitting the reduced oxygen. Irreversible heterolytic cleavage of the peroxide dioxygen occurs with the two electrons remaining with the distal oxygen which, in turn, protonates to yield a water molecule. The remaining oxygen linked to the CYP complex is an iron(V)-oxene, a neutral electrophilic atom with 6 electrons in its outer layer (**F, Figure 1.9**). In the final step, the oxene is transferred to the substrate compound, regenerating the native hexacoordinate state of the cytochrome P450.^{120;125;143}

1.2.4. Aromatization mechanism of CYP19

Aromatase, a cytochrome P450-dependent enzyme, catalyzes the aromatization reaction of the A-ring of androgens into estrogens. Androstenedione is the preferred substrate.¹⁴⁴ The reaction involves three consecutive oxidative steps on the same substrate before releasing the product of catalysis outside the active site, i.e. two hydroxylations at the 19-methyl group and a final oxidative decarbonylation of the 19-aldehyde intermediate. Each reaction consumes a single mole of molecular oxygen and NADPH (**Figure 1.10**).

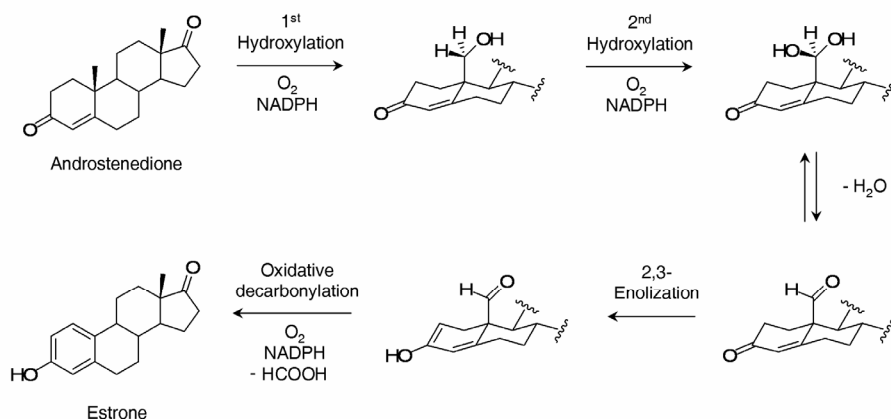


Figure 1.10. Aromatization mechanism of androstenedione into estrone by the human aromatase enzyme. This figure was adapted from literature.¹⁴⁵

Hydroxylations at the 19-methyl proceed via the oxygen rebound mechanism. Homolytic cleavage of a carbon-hydrogen bond mediated by the iron(V)-oxene (**F**, **Figure 1.9**) removes a hydrogen radical from the 19-methyl and leaves a free radical centered at C19. Collapse of the iron(IV)-hydroxyl produces the monohydroxylated androgen and returns the enzyme to its ferric state, ready to enter a second catalytic cycle (**Figure 1.11**).¹²⁰ The second hydroxylation involves stereospecific removal of the 19-*pro-R* hydrogen yielding a 19-*gem*-diol androgen which may dehydrate to the 19-aldehyde.

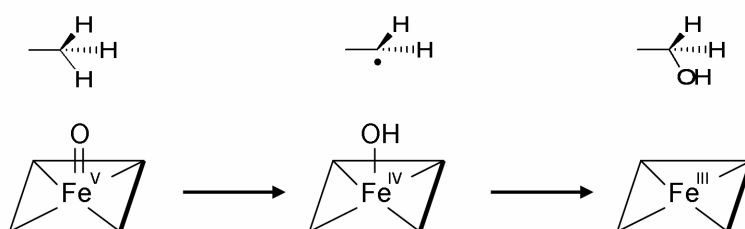


Figure 1.11. Oxygen rebound mechanism involved in two initial hydroxylations catalyzed by aromatase. Modified from literature.¹⁴³

2,3-Enolization was suggested to take place before, or simultaneously, the third oxidative step.¹⁴⁶ Aromatase homology structure prediction and substrate docking experiments, pointed a selective acid-base mechanism of catalysis for this step. Due to its proximity to the substrate, Asp 309 may be involved in the stereospecific abstraction of the androstenedione 2 β -hydrogen, whereas Lys 473 or His 475 are possible candidates for proton donation to the 3-ketone.¹⁴⁷

The final step of the aromatase catalytic cycle is the oxidative cleavage of the C10-C19 bond with aromatization of the ring A and release of the 19-methyl as formic acid. Although the mechanism of this third step remains to be completely elucidated, the hypothesis of a nucleophilic attack of the iron(III)-peroxide (**E**, **Figure 1.9**) to the 19-aldehyde is well accepted in the literature.^{148;149} It was suggested that the resulting peroxo hemiacetal fragmentizes with removal of the 1 β -hydrogen by the proximal oxygen, resulting in aromatization of the ring A and release of formic acid (**Figure 1.12**).

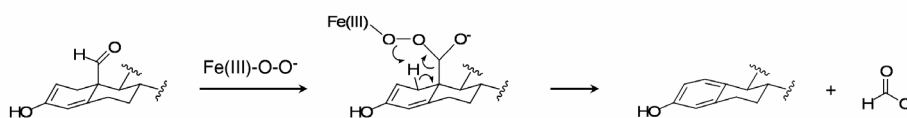


Figure 1.12. Proposed mechanism for the third oxidative step of the aromatase enzyme. This figure was adapted from literature.¹⁴⁵

Recently, a new mechanism for the third oxidative step of the aromatization reaction was proposed based on quantum chemistry calculations. According to this new hypothesis, the iron(V)-oxene (**F**, **Figure 1.9**) removes the 1 β -hydrogen atom, initiating the aromatization and deformylation cascade.¹⁴⁵

1.2.5. Spectral properties

Cytochrome P450 enzymes have unique absorbance spectra due to the heme group, a strong chromophore bound to an axial sulfur of a cysteine residue. Carbon monoxide binding to the reduced enzyme produces an absorption peak at approximately 450 nm (Soret peak), which originated the term P450.^{150;151} This peak might be shifted by the chemical environment around the heme, the oxidation number of the iron, the spin state and the binding of ligands.

The maximum absorption peak for the low-spin, hexacoordinated state, is found at 416-419 nm, whereas that for the high-spin, pentacoordinated state, is 390-416 nm. Therefore, substrate binding to microsomal cytochrome P450s, including aromatase, can be monitored by assessing the difference spectrum of the enzyme in its free- and substrate-bound states. Binding of a ligand to the active site displaces the axial water molecule and shifts the iron from a low- to a high-spin state. This induces a type I difference spectrum characterized by a shift in the Soret band maximum from about 30 nm (displacement from 420 nm to 390 nm). In contrast, binding of substrates with electronegative atoms such as nitrogen, sulphur and oxygen included in aromatic heterocyclic rings, induces a type II difference spectrum with a maximum of absorbance at 425-435 nm and a depression at 390-405 nm, indicative of water displacement from the sixth position followed by a stronger substrate coordination to the heme iron.^{125;149}

1.3. Aromatase inhibitors

1.3.1. Clinical development

Aromatase is a very attractive target for the endocrine treatment of estrogen-dependent diseases. In this sense, attention has been focused on the discovery of aromatase inhibitors, able to decrease the circulating levels

of estrogens and control the progression of hormone sensitive breast cancer in postmenopausal women.

Aromatase inhibitors were developed after the recognition that aminoglutethimide, a nonselective inhibitor of critical enzymes in the steroidogenesis, including aromatase, was an effective drug to control hormone sensitive breast cancer.^{152;153} Marketed in the late seventies, aminoglutethimide (Cytadren[®], Novartis) was the first aromatase inhibitor introduced in the clinic. However, reports of adrenocortical insufficiency and several other side effects such as nausea and rashes, led to its withdrawal from the market.

The design of inhibitors for a single member of the cytochrome P450 superfamily represented a very challenging task. In spite of this hurdle, compounds targeting aromatase more specifically were developed, with higher affinity for the target enzyme and fewer side effects than aminoglutethimide.^{6;14;15} These inhibitors can be divided into generations according to their chronological order of clinical development, i.e. second and third generation aromatase inhibitors as shown in **Figure 1.13**.

Second generation aromatase inhibitors were developed during the eighties, including formestane (Lentaron[®], Novartis) and fadrozole (Afema[®], Novartis), both with improved clinical efficacy. However, formestane had the disadvantage of being rapidly inactivated by hepatic glucuronidation, therefore requiring intramuscular injection, and fadrozole caused aldosterone suppression, which limited its use at high doses.¹⁵⁴⁻¹⁵⁶

Third generation compounds were developed in the early nineties, including anastrozole (Arimidex[®], AstraZeneca), letrozole (Femara[®], Novartis), vorozole (Rivizor[®], Johnson & Johnson) and exemestane (Aromasin[®], Pfizer). Preclinical studies showed more than three orders of magnitude increased potency compared to aminoglutethimide and almost complete

specificity at clinical doses,¹⁵⁷ with little effect on the cortisol and aldosterone levels.^{158;159} Furthermore, these new compounds are orally active and have extensive half-lives allowing a daily single-dose regimen.

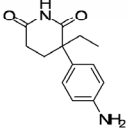
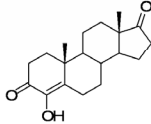
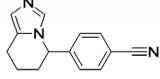
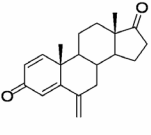
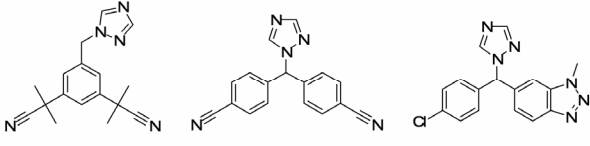
	Type 1 (Steroid inactivators)	Type 2 (Non-steroid competitive inhibitors)
First generation		 Aminoglutethimide
Second generation	 Formestane	 Fadrozole
Third generation	 Exemestane	 Anastrozole Letrozole Vorozole

Figure 1.13. Classification of the main aromatase inhibitors.

Aromatase inhibitors can be further classified as type 1 or type 2 compounds, according to their mechanism of action (**Figure 1.13**). Type 1 inhibitors, such as formestane and exemestane, are androstenedione analogs which bind to the active site of the enzyme as competitive inhibitors. Conversion into reactive intermediates upon catalysis causes mechanism-based inactivation of the enzyme, i.e. time- and concentration-dependent loss of enzymatic activity. Type 2 inhibitors such as fadrozole, anastrozole, letrozole and vorozole, are non-steroid compounds and bind strong but reversibly to the heme group of the enzyme. Spectroscopic studies identified a type II difference spectrum upon inhibitor binding,

revealing coordination between a nitrogen-containing aromatic heterocycle and the heme iron.¹⁴⁹

1.3.2. Steroid aromatase inhibitors

1.3.2.1. Competitive inhibitors

The initial development of aromatase inhibitors was focused on the basic androstenedione scaffold substituted at several positions. Most of these molecules are competitive inhibitors that bind to the same active site cavity as the natural substrates, decreasing the amount of estrogens formed. Initial structure-activity relationships on competitive aromatase inhibitors highlighted the importance of planarity at the A/B ring junction, carbonyls at positions C3 and C17, and unsaturation in the steroid nucleus, namely with 4-ene, 1,4-diene, 4,6-diene and 1,4,6-triene functions.¹⁶⁰

Later on, Numazawa reported that 3-deoxyandrostenedione is a potent aromatase inhibitor.¹⁶¹ Therefore, the C3 carbonyl does not play a critical role in the binding, suggesting that 3-deoxy steroids might have an alternative binding mode.¹⁶²⁻¹⁶⁴

The steroid ring A accepts only slight structural modifications, like the incorporation of small hydrophobic groups at C1 or small hydrophilic groups at C4, such as in 1-methyl-androsta-1,4-diene-3,17-dione (atamestane, **Figure 1.14**) and 4-hydroxy-androst-4-ene-3,17-dione (formestane, **Figure 1.13**), both compounds with *in vitro* and *in vivo* efficacy.^{165;166} On the other hand, bulky substituents at ring B positions C6 and C7 provided potent aromatase inhibitors such as 6 β -ethyl-androsta-1,4-diene-3,17-dione (6 β -ethyl-ADD, **Figure 1.14**) and 7 α -(4'-amino)phenylthio-andost-4-ene-3,17-dione (7 α -APTA, **Figure 1.14**), supporting the presence of hydrophobic pockets at the aromatase active site, a small one at the β -face of the C6 region and a larger one at the α -face of the C6-C7 region.¹⁶⁷⁻¹⁷³ As these

pockets have limited accessible volume, the length and shape of the substitution is of critical importance to the anti-aromatase activity.

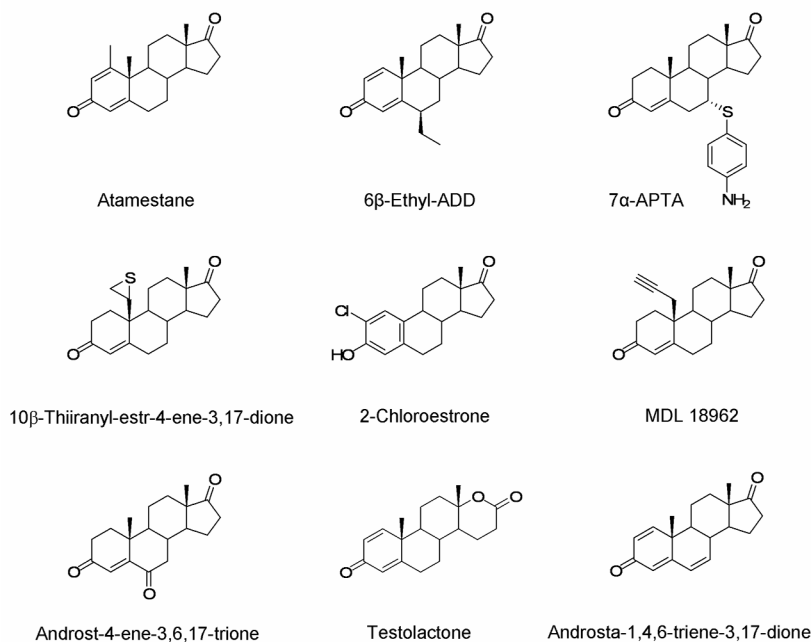


Figure 1.14. Examples of steroid aromatase inhibitors.

The C19 methyl group of androstenedione is another position that has received particular attention to the design of potent aromatase inhibitors. Being the oxidation site, the introduction of oxygen, sulphur or nitrogen heteroatoms at this position leads to strong noncovalent binding to the heme iron of aromatase, as corroborated by spectroscopic studies. Some of the most potent AIs developed based on this approach include androstenedione analogs with thiirane (10β-thiiranyl-estr-4-ene-3,17-dione, **Figure 1.14**), oxirane, thiol and amino functionalities at C19.¹⁷⁴⁻¹⁷⁷

An alternative strategy to the design of aromatase inhibitors relied on mimicking the final products of the aromatization reaction. Shimizu *et al.* showed that natural estrogens are able to bind to the active site of human placental aromatase as competitive inhibitors.¹⁴⁴ This finding led to the

discovery of a new class of aromatase inhibitors based on the estradiol and estrone scaffolds, with potent aromatase inhibitors such as 2-chloroestrone (**Figure 1.14**).¹⁷⁸

1.3.2.2. Mechanism-based inactivators

Besides mimicking the substrate, some steroid inhibitors are converted into reactive intermediates by the enzyme, able to cause time-dependent inactivation (mechanism-based inhibitors). The activation step is triggered during a normal catalytic process and depends on the presence of the coenzyme, NADPH. Typically, a reactive electrophilic intermediate is formed and immediately reacts with a nucleophilic residue within the active site.¹⁶⁰

Although mechanism-based inactivation is relatively unusual in enzymatic reactions, it is frequently observed in cytochrome P450 enzymes, due to the reactivity of the oxygenated species generated.¹⁷⁹ Mechanism-based inactivators have superior selectivity compared to reversible inhibitors because both the initial compound and the final activated species must bind to the active site. Furthermore, an additional nucleophilic residue must be properly located in order to react with the activated compound. Once bound, the compound remains permanently linked to the enzyme and no longer available to interact with non-target proteins. These properties were explored to the design of compounds with potential clinical advantages, namely improved potency and selectivity.¹⁸⁰

The first compound designed as mechanism-based aromatase inhibitor, with both *in vivo* and *in vitro* activities, was 10 β -(2-propynyl)-estr-4-ene-3,17-dione (MDL18962, **Figure 1.14**).^{181;182} Furthermore, many steroids initially prepared as competitive inhibitors, such as formestane, were found to cause mechanism-based inactivation.^{166;183} Biochemical studies with radiolabeled inhibitors, confirmed covalent and irreversible binding to the enzyme. However, the exact nature of the covalent bonds, the active site

residues involved and the chemical structures of the activated compounds remain to be elucidated.¹⁸⁴ Strong electrophilic species, such as epoxide, oxirene and Michael acceptor groups have been suggested as reactive intermediates.^{182;185;186}

Similar properties were demonstrated for androstenedione derivatives with additional conjugated double bonds, such as androst-4-ene-3,6,17-trione¹⁸⁷ (**Figure 1.14**) or compounds with additional unsaturations at the A and B rings, either 1,4-diene or 1,4,6-triene functions. The most relevant compound among these is 6-methylen-androsta-1,4-diene-3,17-dione (exemestane, **Figure 1.13**),^{188;189} a third generation aromatase inhibitor. Other compounds, such as testolactone,^{190;191} androsta-1,4,6-triene-3,17-dione¹⁸⁷ and 7-substituted derivatives,^{192;193} are also able to inactivate the enzyme (**Figure 1.14**). The double bond between C1 and C2 is crucial for the mechanism-based activation of these compounds, which was hypothesized to evolve the last oxidation step of the aromatase catalytic cycle.¹⁹⁴

1.3.3. Non-steroid aromatase inhibitors

The non-steroid class of aromatase inhibitors comprises structurally different compounds that are able to bind the aromatase active site through coordination with the heme iron.¹⁹⁵ The main advantage over steroid inhibitors is the lack of androgenic effects and the complete absence of substrate activity on the aromatase enzyme. However, because of the CYP19 similarity with other essential cytochrome P450 enzymes involved in the biosynthesis of glucocorticoids and mineralocorticoids, such as cytochrome P450_{SCC} (CYP11A1), 17 α -hydroxylase/C17,20-lyase (CYP17) and steroid 18-hydroxylase (CYP11B2), lack of selectivity over distinct P450 enzymes results in significant toxicity.¹⁹⁶⁻¹⁹⁸ Third generation aromatase inhibitors (**Figure 1.13**) are several orders of magnitude more active than

aminoglutethimide, creating almost complete deprivation of estrogens at low doses, with almost no effect on the biosynthesis of other steroids such as aldosterone, progesterone and corticosterone.

The strongest interaction of type 2, non-steroid inhibitors, with aromatase is a coordinative bond between the lone pair of an aromatic heterocyclic nitrogen atom and the heme iron of the enzyme.¹⁹⁹ Although imidazole or triazole rings have been widely used, other electron rich heterocycles might be accepted as the sixth coordinating moiety, including six-membered rings such as pyridines (tetralin, indolizone and benzofuran derivatives represented in **Figure 1.15**) and pyrimidines (aniline derivative, **Figure 1.15**). Extremely important is the way in which the heterocycle is attached to the rest of the molecular framework. Direct attachment to the coordinating nitrogen or at an adjacent position, leads to loss of the anti-aromatase activity, unless one additional nitrogen is present. Furthermore, reduction of the coordinating nitrogen leads to inactive compounds, possibly because it is a sp² rather than a sp³ hybridized nitrogen orbital which most effectively interacts with the heme iron. Compounds with more than one nitrogen-containing heterocycle were also found to be strong aromatase inhibitors.²⁰⁰

Another important feature is the hydrophobic nature of the molecular scaffolds of non-steroid aromatase inhibitors, measured by a positive value of octanol/water partition coefficient (logP), which is required due to the predominant presence of amino acids with apolar side chains in the aromatase active site.²⁰¹ Potent non-steroid aromatase inhibitors were developed by optimization of leads with structurally different scaffolds, including fluorenes,²⁰² quinolines,²⁰³ tetralins,²⁰⁴ indolizones,^{205;206} indoles,²⁰⁷⁻²¹¹ benzofurans,²¹²⁻²¹⁴ biphenyls,²¹⁵ biphenyl-alkyls,²¹⁶ N-benzylanilines^{217;218} and xanthenes²¹⁹ (**Figure 1.15**).

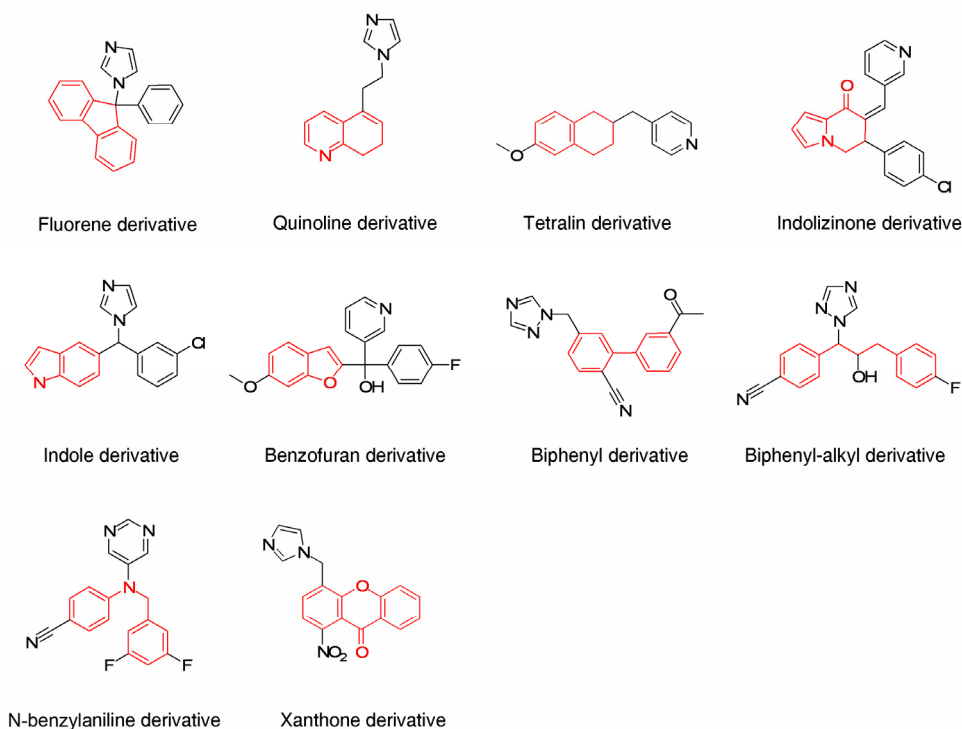


Figure 1.15. Examples of non-steroid aromatase inhibitors. The structural scaffold of each compound class is colored in red.

Whereas higher potency among non-steroid aromatase inhibitors has been achieved through strong coordinative and hydrophobic interactions, selectivity between different cytochrome P450s has explored the presence of at least one hydrogen bonding residue within the aromatase active site. Site-directed mutagenesis experiments showed that Ser 478 is located within the binding pocket of the enzyme, playing an active role in the catalysis mechanism and binding of aromatase inhibitors.²²⁰ This finding was further corroborated by homology modelling and docking experiments, highlighting the importance of a hydrogen bond acceptor group for selective aromatase inhibition.^{140;215} Additional evidence came from a molecular modelling study comparing the three-dimensional structures of steroid and non-steroid anti-aromatase compounds.¹⁹⁹ Based on the results of this study, the steroid site of hydroxylation, the 19-methyl, overlaps with the

heterocyclic moiety of non-steroid aromatase inhibitors and the hydrophobic moieties of both compound classes overlap well. Furthermore, a hydrogen bond acceptor group found in several non-steroid inhibitors mimics the C17-carbonyl function at the androstenedione D ring. This agrees with structure-activity studies with 3-deoxy steroids, showing that the presence of a carbonyl at C3 is not essential for the anti-aromatase activity.¹⁶²⁻¹⁶⁴

1.3.4. Polyphenol aromatase inhibitors

1.3.4.1. Natural compounds

Polyphenols are a large group of plant natural products characterized by the presence of at least one phenol unit. These compounds are plant secondary metabolites, occurring either isolated or as oligomers. Conjugation with sugars, carboxylic acids, amines, lipids and other compounds is also very common.²²¹

Flavonoids, the most abundant and well studied polyphenols in nature, are found in many food sources including fruits, vegetables and grains. The large number of compounds identified to date arises mostly from multiple combinations of hydroxyl and methoxyl substitutions. These molecules share a common phenylchromane heterocycle and are classified based on modifications of this scaffold. Flavans have an unchanged 2-phenylchromane skeleton whereas in flavanols one additional hydroxyl at C3 is present. An oxo group linked to C4 is found in flavanones (phenyl linked at C2) and isoflavanones (phenyl linked at C3). Flavones, flavonols and isoflavones have a double bond between C2 and C3 of the ring C. In anthocyanidines, an additional double bond is found in ring C, instead of the oxo group. Finally, chalcones are bicyclic compounds with an open B ring.²²²

Other classes of phenolic compounds include coumarins, found in fruits and green tea, and stilbenes, like resveratrol, one of the main components of red wine. Oleuropein, the major polyphenolic constituent of olive oil, is another structurally different phenolic compound.²²³ These compounds have demonstrated a host of biological activities, displaying excellent antioxidant,^{224;225} antitumor,^{226;227} antiviral,²²⁸ antimicrobial²²⁹ and anti-atherogenic^{230;231} properties.

The interest of studying polyphenols in breast cancer was stimulated by the hypothesis that these compounds are responsible for the lower incidence of the disease in women from several Asian countries where consumption of polyphenol rich products is very high.^{232;233} Due to their structural similarity to endogenous estrogens, compounds of this class, including isoflavones, flavones, lignans and coumestans, are able to bind to both ER α and ER β .⁷² However, it was found that some compounds, such as 5,7,4'-trihydroxyisoflavone (genistein), 5,7,4'-trihydroxyflavone (apigenin) and 3,5,7,4'-tetrahydroxyflavone (kaempferol), have higher binding affinity for ER β than for ER α .²³⁴ The molecular basis for ER β selectivity by phytoestrogens involves their capacity to induce changes at the surface of the receptor, improving the affinity for coactivators.²³⁵ Therefore, these compounds can act as natural selective estrogen modulators by triggering ER β -mediated transcription pathways which have been found to mediate antiproliferative effects in breast.⁵⁰ This might explain the beneficial cancer protective effects of some compounds of this class in breast.²³⁶

Furthermore, polyphenols have been recognized as aromatase inhibitors with moderate to strong potency.²³⁷ Compounds with significant anti-aromatase activity include flavans,²³⁸ flavones,²³⁹⁻²⁴³ flavanones,²⁴⁴⁻²⁴⁶ isoflavones,^{241;247} isoflavanones,²³⁹ flavonols,^{248;249} chalcones,²⁵⁰ flavanols (catechins and theaflavins),²⁵¹⁻²⁵³ coumestans,^{241;254} and lignans^{238;254;255} (**Figure 1.16**).

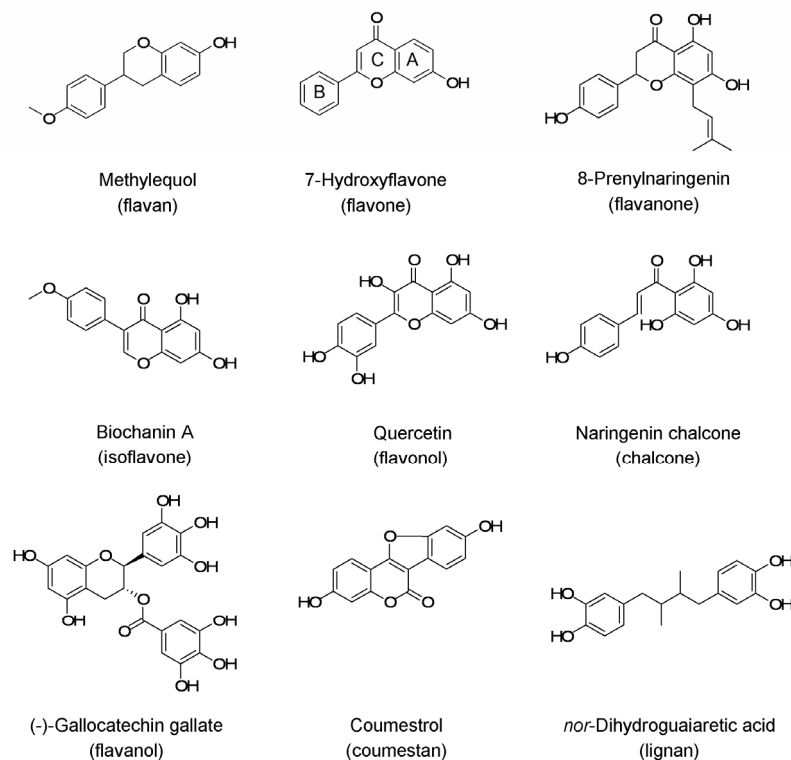


Figure 1.16. Examples of natural polyphenol aromatase inhibitors.

Kinetic analysis identified a competitive mechanism of aromatase inhibition for this type of compounds. This was further corroborated by spectroscopic studies.^{237,238} Furthermore, based on data from site-directed mutagenesis experiments and docking, a binding mode for flavones was proposed, in which the A, B and C rings of flavonoids mimic the D, A and C rings of steroids, respectively.²⁵⁶

1.3.4.2. Synthetic derivatives

The use of natural compounds as starting leads represents an attractive strategy for the discovery of new anti-hormonal drugs for the treatment of breast cancer, based on the aromatase inhibition mechanism. The small and rigid phenylchromane flavonoid nucleus is a good template for

combinatorial libraries due to the multiples sites for chemical substitution. Several examples of synthetic flavonoid derivatives have already been documented. α -Naphthoflavone and derivatives are potent aromatase inhibitors, with *in vitro* activity at least two orders of magnitude stronger than flavone (**Figure 1.17**).^{237;257} Derivatization of flavones²⁵⁸ and isoflavones^{259;260} with imidazole, triazole and pyridinyl moieties, markedly increased the anti-aromatase potency of the starting leads due to strong coordination between the nitrogen-containing heterocycle and the aromatase heme iron, confirmed by a type II difference spectrum (**Figure 1.17**). Furthermore, new aromatase inhibitors were developed based on pyridinyl-substituted flavanones²⁶¹ and imidazolyl- or triazolyl-substituted flavans (**Figure 1.17**).²⁶²⁻²⁶⁴ Most of these compounds are active at low nanomolar concentrations.

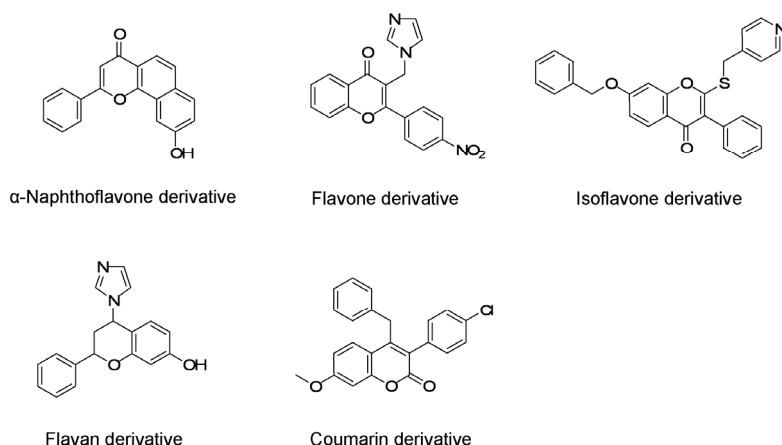


Figure 1.17. Examples of polyphenol synthetic derivatives with improved anti-aromatase potency.

In another study, coumarin derivatives were selected on the basis of geometric similarities to the substrate of the enzyme, and tested for their ability to block estrogen biosynthesis. Improved anti-aromatase potency compared to more simple coumarins was achieved with the introduction of

hydrophobic moieties at positions 3 and 4. The authors rationalized that the coumarin ring mimics the A and B rings of androstenedione, whereas a 3-(4'-chlorophenyl) group mimics the D ring of the androgen and a 4-benzyl aligns very closely with the C19-methyl (**Figure 1.17**).²⁶⁵

1.3.5. Dual inhibitors

Breast cancer is a complex disease with multiple interdependent molecular abnormalities. Therefore, simultaneous modulation of several relevant targets can provide superior therapeutic efficacy compared to the more conventional single-target therapy. The biological complexity can be addressed with the use of drug combinations or, alternatively, with multifunctional drugs, i.e. single compounds able to interfere with multiple pathways. Although currently available drugs are inherently multiple acting, the design of multi-target selective drugs is a recent trend in medicinal chemistry.²⁶⁶

1.3.5.1. Thromboxane A₂ synthase and aromatase

Thromboxane A₂ synthase (TxA₂S) is a P450 enzyme involved in the arachidonic acid pathway, responsible for the conversion of prostaglandin H₂ into thromboxane A₂, a potent vasoconstrictor and inducer of platelet aggregation.²⁶⁷ Significant TxA₂S overexpression was found in several types of tumors, including those of bladder, colorectal, prostate and breast. Recent studies confirmed that thromboxane A₂ has a critical role in promoting tumor angiogenesis and metastasis, correlating negatively with the patient survival.²⁶⁸⁻²⁷⁰ Therefore, TxA₂S is a promising target for the prophylaxis of tumor metastases. Indeed, selective TxA₂S inhibitors are able to suppress growth and reduce migration of tumor cells²⁷¹ and combined with chemotherapeutic agents, were found to increase the treatment response.²⁷²

Breast cancer treatment and prevention of metastases with the use of dual aromatase and thromboxane A₂ synthase inhibitors may have clinical advantages over the currently available, single target, anti-aromatase therapies. The design of dual inhibitors explored a common heme iron and some degree of homology between the active site of both enzymes. Imidazol-substituted quinolines like the compound depicted in **Figure 1.15** are among the most potent and selective dual inhibitors identified to date.²⁰³

1.3.5.2. Steroid sulfatase and aromatase

Hydrolysis of estrone sulfate into estrone by steroid sulfatase is the main source of active estrogens in hormone-dependent breast tumors.²⁷³ This suggests that inhibition of STS results in reduction of the estrogen levels, thus controlling the progression of the disease.

Structurally diverse STS inhibitors were developed during the past decade, ranging from steroid compounds, such as estrone-3-sulfamate, to non-steroids, such as tricyclic coumarin sulfamates.²⁷⁴⁻²⁷⁶ Potent irreversible inhibitors of the enzyme share a common phenol sulfamate ester which is believed to be transferred to an essential amino acid residue within the active site of steroid sulfatase. Additional hydrophobic interactions stabilize the enzyme-inhibitor complex. Clinical trials confirmed that steroid sulfatase inhibitors represent a promising new endocrine therapy for the treatment of postmenopausal women with hormone-dependent breast cancer.^{277,278}

Simultaneous inhibition of both aromatase and steroid sulfatase is expected to provide a more effective estrogen deprivation than through a single target inhibition. While the administration of two separate inhibitors is an obvious choice for providing a combined endocrine therapy, an alternative approach is to design a dual aromatase and sulfatase inhibitor (DASI) that will block both enzymes as a single agent. One of the strategies for designing DASIs relied on the incorporation of a phenol sulfamate moiety into the scaffold of

potent and selective non-steroid AIs such as letrozole, anastrozole and YM511, a strong aromatase inhibitor which progressed into phase II clinical trials.²¹⁷ These compounds display potent STS inhibition whilst preserving the high level of anti-aromatase activity (**Figure 1.18**).²⁷⁹⁻²⁸²

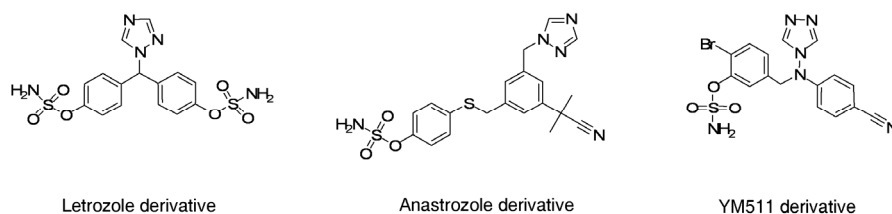


Figure 1.18. Examples of dual aromatase-steroid sulfatase inhibitors.

An alternative approach to design DASIs relied on 3-sulfamoylated derivatives of known aromatase inhibitors with the estrogenic steroid scaffold.¹⁷⁸ Although some of these new compounds are very strong STS inhibitors, the anti-aromatase potency identified was low.²⁸³

1.4. Biochemical evaluation of new compounds as aromatase inhibitors

Optimization of new lead molecules in terms of target potency and selectivity is an iterative process of design and synthesis of structurally related compounds, followed by biochemical evaluation. *In vitro* assays are used at this early stage of the drug-discovery pipeline, with the main goal of developing structure-activity relationships and understanding the structural determinants for strong affinity target binding. Subsequent steps aiming for an optimization of membrane permeability, oral bioavailability, pharmacokinetics and toxicological properties, are inherently more complex, requiring cellular and *in vivo* activity measurements.²⁸⁴

In this context, the development of methods to measure the aromatase activity has been critical to the discovery and optimization of new aromatase inhibitors.

1.4.1. The human placental microsomal assay

The human placental microsomal assay is a highly sensitive radiometric technique to perform fast screening of new anti-aromatase candidates. During pregnancy, human placenta expresses high levels of active aromatase, being therefore an excellent source of inexpensive enzyme.³² The basis of this method is that aromatization of [1β - ^3H]-androstenedione into estrone involves stereospecific removal of the 1β -hydrogen (**Figure 1.19**).¹²⁰ Therefore, aromatase activity is evaluated, after incubation for a designed time, by measuring in the aqueous phase the amount of tritium released from the substrate and incorporated into a water molecule, after rigorous extractions with organic solvents and/or dextran-coated charcoal. Analysis of the amount of tritiated water produced is performed by liquid scintillation counting (LSC).²⁸⁵ This method is one of the most used to measure the aromatase activity, *in vitro*, because of its reliability, reproducibility and straightforward use.

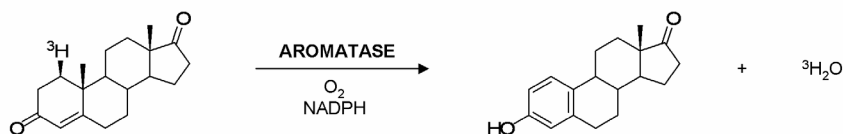


Figure 1.19. Basis of the radiometric assay used to measure the aromatase activity.

The human placental microsomal fraction is composed of smooth endoplasmic reticulum membranes which, besides aromatase, have other steroid metabolizing enzymes such as 17β -hydroxysteroid dehydrogenase.²⁸⁶ One limitation of this source of biological material arises

from possible interaction of the tested compounds with these enzymes, which may cause indirect changes in the activity measured. Variation in the aromatase levels per microsomal protein content, among placental tissues from different sources, is another variable to be controlled. Furthermore, the human placental microsomal assay is unable to detect if the compounds induce or suppress expression of the aromatase enzyme within the cell.

1.4.2. Comparison with other *in vitro* assays and other sources of aromatase

The radiometric assay previously described can also be used with other sources of aromatase including ovarian microsomes and isolated cells from human breast and ovaries.^{287,288} Other common sources of aromatase include human JEG-3 and JAR choriocarcinoma cell lines isolated from cytotrophoblasts from malignant placental tissues.²⁸⁹ Cell culture assays are sensitive to the effects on aromatase expression and provide additional information about membrane permeation.²⁹⁰ However, cytotoxicity from the test compounds, as well as possible compound metabolism and other transformations that may occur within intact cells, may limit the use of these methods.

Another widely used assay is the product isolation technique, which consists in the incubation of a ³H or ¹⁴C radiolabeled substrate such as androstenedione or testosterone, followed by isolation and measurement of the radiolabeled estrogen product formed.^{35,291} The procedure for this method is similar to the radiometric assay but involves separation of the radiolabeled product from the substrate, using a chromatography technique. Variations of this assay use unlabeled substrate, or endogenous substrate (*in vivo* studies), and other methods for measurement, including mass spectrometry,²⁹² radioimmunoassays²⁹³ and enzyme-linked immunoassays.²⁹⁴

Human recombinant microsomes with recombinant aromatase are an alternative source of enzyme.²⁹⁵ Moreover, semi-automated high-throughput screening methods, avoiding the need of radiolabeled substrates, were also developed. For example, dibenzylfluorescein is dealkylated by aromatase to form a fluorescein ester.²⁹⁶ Following hydrolysis with base, this product can be quantified by fluorescence spectroscopy, thereby allowing measurement of the enzyme activity.²⁹⁷

In vivo evaluation of the anti-aromatase potency and antitumor efficacy of new aromatase inhibitors was out of the scope of this thesis and will not be discussed in this document. A good description of such models can be found elsewhere.²⁸⁴

1.5. The use of computer-aided drug design in drug discovery and development

Identifying small-molecule modulators of the protein function, converting these into lead series and progressing the entire pre-clinical and clinical pipeline into a new drug for a particular disease is an extremely and increasingly difficult challenge.²⁹⁸ On average, it takes between 10 to 15 years to bring a new prescription drug to the market, and despite the fact that research and development costs increase every year, typically with several hundred million euros spent with each new chemical entity, the average number of new drugs released has been decreasing over the last decade.^{299,300} One of the main reasons for this is that regulatory authorities are becoming more restrictive, demanding for highly effective and safe drugs. In many areas such as with antibiotics, drug designers are working on fourth and fifth generation therapeutic agents. Therefore efficacy and safety alone are not sufficient. New drugs have to present substantial benefits over previous treatments already in the market.³⁰¹

This challenge has been faced with an increased use of computer science within the traditional drug design campaigns to improve the quality of the results.³⁰²⁻³⁰⁴ Biologists, chemists and pharmacologists use computer models in all stages of drug design and development, from the early identification of disease related genes to the interpretation of clinical trial data. At the early stages of drug discovery, virtual screening (VS) is an important tool to identify the most promising compounds to test. Structure-based drug design plays a crucial role in improving the complementarity between the ligand and the protein target by studying the nature of the complex. As biological activities are measured for related compounds in a series, computer-aided drug design (CADD) can also be used to build statistical models. Understanding the chemical and physical properties of a compound that are essential for target binding, and using this information to guide future synthesis efforts, is crucial for lead optimization. Additional studies to understand and predict the pharmacokinetic and toxicological properties of compounds are another area in which CADD helps ensure that compounds with good biological activities can be optimized into compounds that will be good drugs (**Figure 1.20**).³⁰⁴



Figure 1.20. Drug discovery and development workflow. CADD is important at lead discovery, lead optimization and, increasingly, in pre-clinical phases.

Among an increasing number of compounds designed based on a rational computer-assisted drug design, dorzolamide (Trusopt[®] from Merck, a carbonic anhydrase inhibitor for glaucoma treatment),³⁰⁵ zanamivir (Relenza[®] from GlaxoSmithKline, a neuraminidase inhibitor for influenzavirus treatment),³⁰⁶ lopinavir (Kaletra[®] from Abbott, a protease

inhibitor for HIV treatment)³⁰⁷ and imatinib (Gleevec[®] from Novartis, a tyrosine kinase inhibitor for the treatment of chronic myeloid leukemia)³⁰⁸ are just some examples. These drugs were successful cases of structure-based drug design.

1.5.1. Computer-aided drug design basic principles

CADD refers to the application of informatics to the discovery, design and optimization of biologically active compounds. Some of the most commonly used techniques will be described shortly.

1.5.1.1. Structure optimization

The low energy conformations that a ligand can adopt play an important role in its activity. For example, ligand binding to a specific receptor requires the adoption of a low energy conformation which is in some way complementary to the binding pocket. This protein-bound conformation is named the bioactive conformation. Molecular mechanics (MM) and quantum mechanics (QM) are used to calculate and optimize a compound's energy. Therefore, these are very useful techniques for structure optimization.

Molecular mechanics is often used to perform initial minimizations.³⁰⁹ MM considers the atoms in a molecule as spheres connected by springs. Changes in energy due to bond stretching, angle bending, torsional energies and non-bonded interactions (electrostatic and van der Waals interactions) are calculated using parameters such as bond lengths (l), angles (θ), torsions (ω), charges (q) and Lennard-Jones parameters (the collision parameter σ and the well depth ε), which together with a set of equations are referred to as a force field.³¹⁰ A very simple molecular mechanics force field is given below and the main energy contributions illustrated in **Figure 1.21**.

$$V = \sum_{\text{bonds}} \frac{k_i}{2} (l_i - l_{i,0})^2 + \sum_{\text{angles}} \frac{k_i}{2} (\theta_i - \theta_{i,0})^2 + \sum_{\text{torsions}} \frac{V_n}{2} [1 + \cos(n\omega - \gamma)] + \sum_{\text{electrostatic}} \frac{q_i q_j}{4\pi\epsilon_0 r_{ij}} + \sum_{\text{van der Waals}} 4\epsilon_{ij} \left[\left(\frac{\sigma_{ij}}{r_{ij}} \right)^{12} - \left(\frac{\sigma_{ij}}{r_{ij}} \right)^6 \right]$$

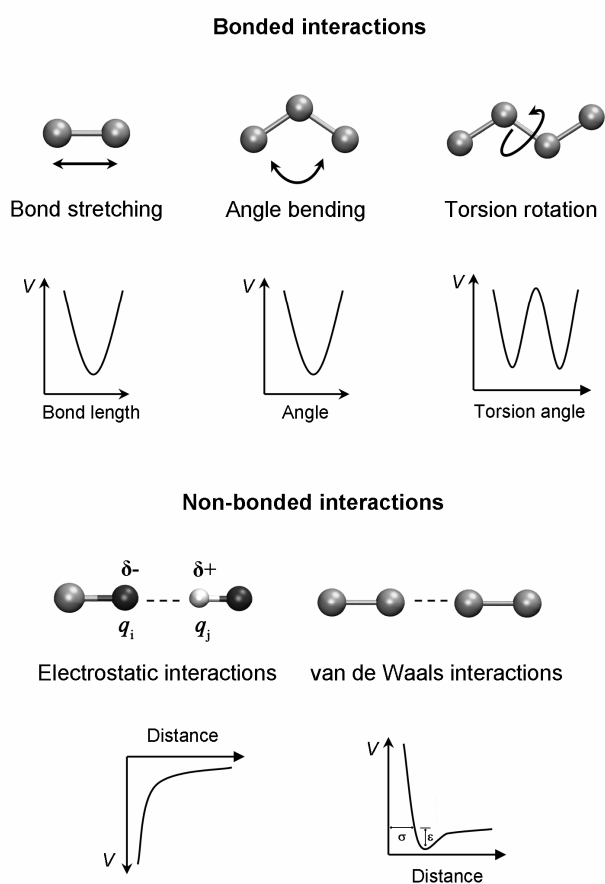


Figure 1.21. Schematic representation of the main energy contributions to a molecular mechanics force field. Variations in potential energy are illustrated. Adapted from literature.³¹⁰

Molecular mechanics calculations are fast and require limited computing time. Therefore it is the most commonly used method to optimize initial geometries into realistic compound structures. Force fields were developed

by studying different sets of molecules. Some were designed for the study of proteins, such as AMBER³¹¹ GROMOS³¹² and CHARMM,³¹³ others are better suited for small molecules, including the Molecular Merck Force Field (MMFF).³¹⁴

Energy calculations using a MM force field measure how much bond lengths, angles and torsions deviate from the “ideal” values included in the force field. Therefore, energy minimization is the process of varying bond lengths, angles and torsions in order to generate improved ligand conformations.³¹⁵ At each step the energy of the new conformation is measured and changes lowering the energy are retained for further optimization until no additional improvement is possible. This point is referred to as the nearest energy minimum.

Step-wise energy minimization of a system until no further improvement can be obtained tends to stop in a local minimum conformation rather than progressing to the global minimum as illustrated in **Figure 1.22**. The presence of an energy saddle that can not be crossed during minimization prevents finding the conformation of lowest energy, the global minimum. Therefore, conformational search is another computational tool that can be used to cross energy barriers, generating different starting conformations by stepwise bond rotation and minimizing each one of these.

Other computational tools to perform conformational analysis include molecular dynamics,^{316;317} a technique to generate conformations by simulating the time-dependent movement of the compound, and Monte Carlo simulations.³¹⁸ Monte Carlo simulations generate random conformations of the compound which, in principle, will sample all possibilities, but only if left run long enough. How long it should run depends on the number of rotatable bonds of the ligand.

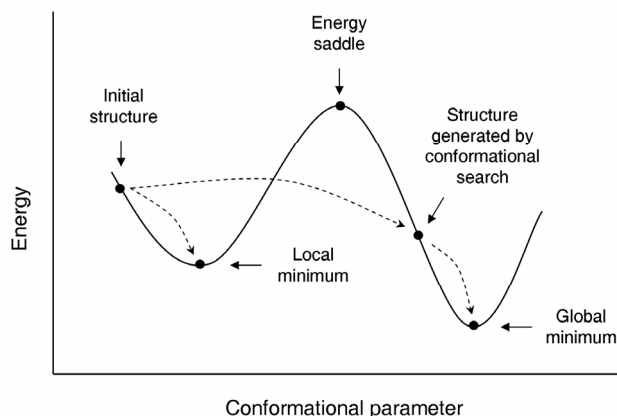


Figure 1.22. Schematic representation of a one-dimensional energy surface. Minimization methods move downhill to the nearest minimum. Energy barriers are crossed using conformational search, eventually leading the most stable molecular conformation.

In the human body, compounds exist in an aqueous environment which will influence their conformation. Therefore, energy minimization and conformational analysis can be undertaken *in vacuo*, or, more realistically, considering the interactions of the solute and the solvent.³¹⁹ More precise calculations of ligand conformations require the use of quantum mechanics, but are far more expensive in terms of computing time.³²⁰ QM calculates properties of the molecules using quantum physics to evaluate the interactions between electrons and nuclei. Quantum mechanics techniques can be divided into two main methods. The most rigorous comprises *ab initio* techniques which do not require the use of pre-defined parameters. These methods are however dependent on the selection of basis set, functions to describe the orbitals of the system. On the other hand, semi-empirical methods are faster than *ab initio* and applicable to compounds with larger molecular weight. Semi-empirical quantum chemistry methods consider only electrons in the outer shells of the atoms and use predefined parameters.³²¹

1.5.1.2. Molecular dynamics

Molecular dynamics (MD) is a computational technique in which successive configurations of a system are generated by integrating the Newton's law of motion. The result is a trajectory that describes how the positions and velocities of particles in the system vary with time.³¹⁶ MD simulations of biological macromolecules provide atomic detail on the internal motions of these systems. Constant improvements in the methodology and computational power, extended the use of molecular dynamics studies to larger systems including, for example, explicit solvent and/or membrane environment, greater conformational changes and longer time scales.³¹⁷ Drug design applications of molecular dynamics simulations include the estimation of free energies of binding,³²² prediction of target selectivity,³²³ generation of multiple conformations for flexible docking,³²⁴ development of dynamic protein-based pharmacophores,³²⁵ metabolism prediction³²⁶ and refinement of protein homology models.³²⁷

1.5.1.3. Calculation of electronic properties

Knowledge of the electrostatic surface potential (ESP) is important when studying molecular recognition by biological targets. When molecules approach each other, the initial contacts arise from long-range electrostatic forces. Therefore, ESP is a very useful tool in drug design and can be employed for the analysis and prediction of molecular interactions.³²⁸⁻³³⁰ Molecular electrostatic potentials are calculated directly from the QM wave function and are represented as the interaction energy of a positively charged proton with the charge density produced by the electrons and nuclei at any point in the space around the molecule.

QM calculations applying the molecular orbital theory to identify the most reactive positions of the compounds are useful for metabolism prediction.

Frequently, these positions correspond to the HOMO (highest occupied molecular orbital) and LUMO (lowest unoccupied molecular orbital).³³¹

1.5.1.4. Calculation of molecular interaction fields

Biological processes such as ligand-receptor binding or enzyme-substrate interaction are determined by non-covalent forces. One method to calculate the energetic conditions between molecules approaching each other is the generation of molecular interaction fields (MIF).³³² MIFs describe the interaction energy between the target molecule and chemical probes moved in a 3D grid around the target. These probes mimic the chemical properties of the binding partner. Computer graphics are able to display MIFs as 3D isoenergy contours. Those of large positive energy indicate regions from which the probe would be repelled, while those of large negative energy correspond to energetically favorable binding regions (**Figure 1.23**).

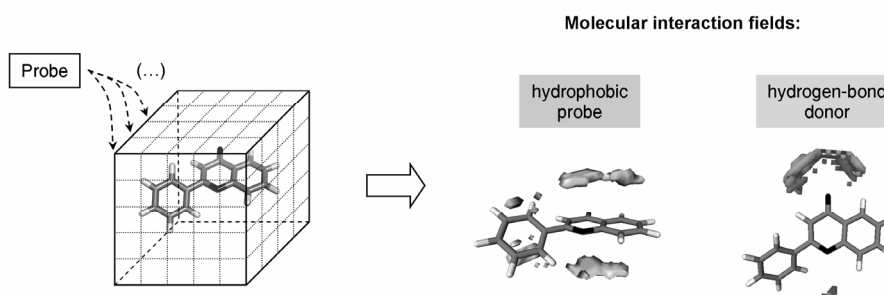


Figure 1.23. Hydrophobic and hydrogen bond donor MIFs calculated for flavone and represented at a negative energy level (favorable interactions). This figure was created using the program ALMOND.³³³

The calculation of MIFs can be applied to a wide range of molecular modelling studies.³³⁴⁻³³⁶ The strategy employed depends on the available information for ligands and macromolecular targets. If the 3D structure of a protein target is known, the MIFs can be used to locate favorable regions for the ligands. Subsequently, these regions can be taken as a starting point for

the design of new ligands for the receptor. Often, no structural information about the protein receptor is available and only ligands are known. Under such circumstances MIFs can help to generate a more or less detailed representation of the potential receptor binding site. A prerequisite for this approach is that all ligand molecules bind to the same active site with an analogous orientation.

1.5.1.5. Three-dimensional quantitative structure-activity relationships

Structure-activity relationships (SAR) are important for any medicinal chemistry project providing the direction for the next compounds to be synthesized. Accurate and descriptive SAR are used to suggest chemical modifications with better probability to provide good compounds than random. Quantitative structure-activity relationship analysis tries to statistically relate changes in the structure of a series of compounds to the experimentally measured values of biological activity. This provides a deeper understanding of the SAR and the mathematical models built can be used to predict the activity of other compounds.³³⁷

The first step of a quantitative SAR study is the selection of descriptors to describe the physical and chemical properties of the compounds in study, typically hydrophobic, steric and electrostatic measures.³³⁸ The formula generated by quantitative SAR relates multiple properties to a single biological activity:

$$\text{Biological activity} = f(\text{descriptor1, descriptor2, descriptor3, ...})$$

Three-dimensional quantitative structure-activity relationships (3D-QSAR) is a further development of this approach. It assumes that the most important properties of a molecule, when binding to a protein target, are its overall shape, electrostatic and molecular interaction fields. A lattice box is built around each compound and a probe atom is placed at each lattice point.

The interaction between the ligand and the probe is measured to define properties such as shape, hydrophobicity and hydrogen bond donor-acceptor capacity.

Superimposition of the compounds within the lattice box is the most difficult, time-consuming and subjective step in any 3D-QSAR study.³³⁹ For this reason, alignment-independent descriptors such as grid-independent descriptors (GRIND) were developed.³³⁴ GRIND descriptors identify relevant regions for the molecular recognition of the compounds in study and describe their relative position. The GRIND calculation starts with the computation of MIFs representing important non-bonded interactions found in biological targets such as hydrophobic contacts (DRY probe), hydrogen bond donation (N1 probe), hydrogen bond acceptance (O probe) and shape complementarity (TYP probe).³⁴⁰

MIFs are filtered based on the distance between node pairs and the energy levels. This procedure identifies well defined regions where relevant interactions with the macromolecular target might occur. In the next step, each individual node value is multiplied by a factor, in order to scale it within the range of 0 and 1. Then, a maximum auto and cross-covariance (MACC2) transform is applied to each pair of scaled filtered MIF nodes. The purpose of the transformation is to obtain descriptors independent of the orientation of the molecule. In practice, the scaled energy product of each pair of nodes is calculated and the values are included into a distance bin, according to the node-node separation. For each distance bin, only the highest energy product is kept. As the node pairs responsible for the highest energy product, located in each distance bin, are recorded, it is possible to trace back this information, which is useful for the chemical interpretation of the models. Taken together, the ensemble of distance bins generated for each compound defines a representative pattern of the possible compound-target interactions. In summary, the GRIND descriptors encode geometrical

relationships between the relevant sites of interaction into an orientation-independent set of variables. Although GRIND descriptors are alignment independent, they are not conformation independent.³³⁴

During a 3D-QSAR study, each compound generates a large number of variables, which are then related to the biological activity using multivariate statistical analysis with, for example, partial least squares regression (PLS).³⁴¹ As the algorithm builds the models, it systematically excludes one compound from the analysis and evaluates how well its activity is predicted. This information is used to build an improved model including the missing compound but now excluding another molecule. This cross validation method is known as leave-one-out (LOO, **Figure 1.24**).³⁴²

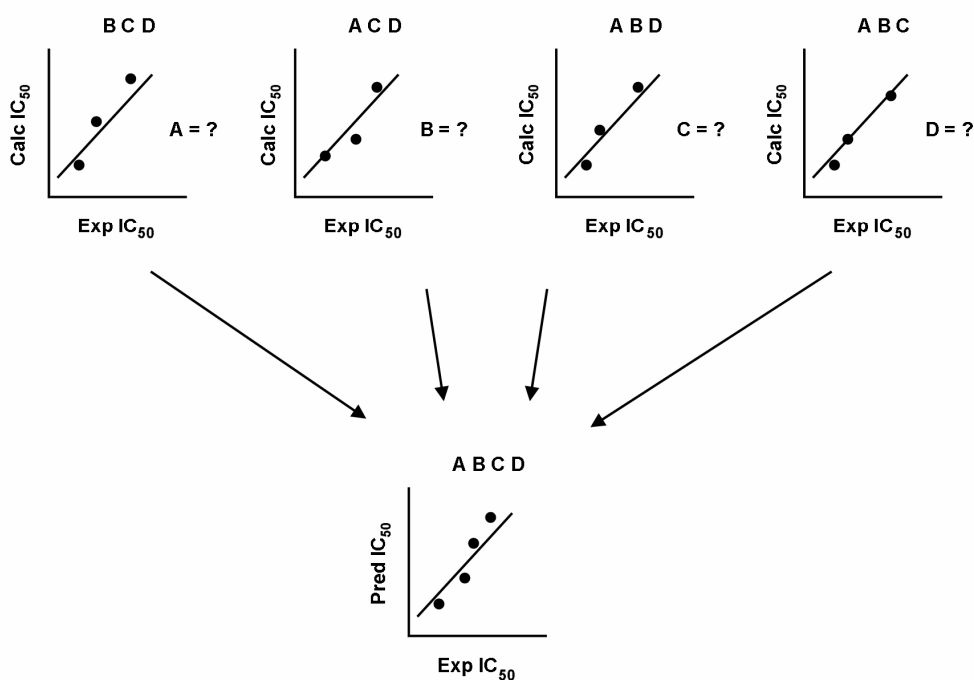


Figure 1.24. Schematic representation of a LOO cross-validation study with 4 compounds (A,B,C,D). Individual models are built, excluding one molecule at a time, and used predict the activity of the missing compound.

The statistical validation of the model is given by the r^2 (the correlation coefficient) and the q^2 (the cross-validated correlation coefficient). The r^2 is the correlation between the biological activity measured and the predicted value, using a model with all compounds. The r^2 is therefore a measure of the internal consistency of the model. The q^2 is similar to the r^2 but uses the predicted activity when the compound is not included in the model. Therefore it is used as a measure of the predictive ability of the model.

The output from 3D-QSAR calculations is a graphical representation of the beneficial and non-beneficial contributions to the field. New compounds can have their biological activities predicted by comparison of their 3D fields to the model.³³⁵

1.5.1.6. Homology modelling

Optimizing the activity of compounds by considering their direct interaction with a target, e.g. a protein, is a very attractive strategy. Protein structures are determined experimentally in two manners, by X-ray crystallography and nuclear magnetic resonance (NMR) spectroscopy. NMR spectroscopy elucidates the structures of macromolecules in solution and has been limited to the study of small proteins. Despite the growing applicability of NMR, X-ray crystallography is still the most important method to generate protein structures for structure-based drug design.³⁴³

In the absence of experimentally derived protein structures, theoretical models can be built. These models, based on homology to known crystal structures, are very useful, especially when the template protein is highly related to the modeled protein. Indeed, protein structures are better conserved than their sequences³⁴⁴ and two proteins with only about 20% of sequence similarity can still share the same 3D structure (**Figure 1.25**). However, as sequence similarity decreases, the reliability of the model is also reduced.

Homology modelling starts with a comparison of the sequence to be modeled against the sequences of available protein structures. Structures with high degree of sequence similarity are defined as templates. The next step is to align the sequence of the template protein with the sequence of the protein to be modeled. This is followed by the generation of the backbone of the protein and modelling of the side-chains, often using rotamer libraries. The model is then optimized using an molecular mechanics force-field and validated by statistical comparison of physicochemical properties from the resulting structure, to averaged values found in high-quality structures.³⁴⁵

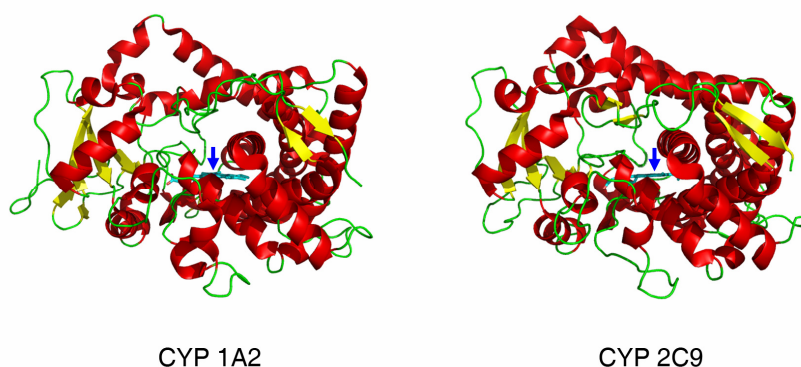


Figure 1.25. 3D Structure of CYP1A2 and CYP2C9.^{133;137} Although belonging to different families (less than 40% of amino acid sequence identity) these two P450s share the same overall structure. Heme binding pockets are identified with a blue arrow. This figure was created using the program Pymol.³⁴⁶

To date no X-ray structure of aromatase has been published in the Protein Data Bank (PDB), despite recent progresses in the 3D determination of mammalian and human cytochrome P450 enzymes.^{131;137-139} On this basis, homology models for aromatase have been built and proved to be valuable in understanding the binding determinants of several classes of inhibitors.^{140;347;348}

1.5.1.7. Docking

Molecular docking is the process of predicting if and how a ligand will bind to a protein binding pocket, followed by an estimation of how strong is the ligand binding affinity. The earliest docking approaches treated both the ligand and the protein as rigid bodies, docking compounds by rotation and translation into the binding pocket of the target. This approach was followed by semi-flexible docking in which the ligand is treated flexibly by allowing bonds to rotate. Flexible protein docking methods, which treat the protein in a flexible manner, are nowadays becoming more important.³²⁴ However, they remain too computer intensive to be used in virtual screening.

The free energy of binding (ΔG) is given by the Gibbs-Helmholtz equation, where ΔH is the enthalpy, T the temperature and ΔS the entropy:

$$\Delta G = \Delta H - T\Delta S$$

ΔG is related to the binding constant K_i by the following equation, with R corresponding to the gas constant:

$$\Delta G = -RT \ln K_i$$

A large number of scoring functions are available to predict free energies of binding for small molecules, based on the 3D structure of protein-ligand complexes. These techniques differ both in accuracy and speed. Very accurate but time-consuming techniques, such as the free energy perturbation method, can be used to predict relative binding affinities of small series of compounds.³⁴⁹ Much faster, although less accurate scoring functions, can be used to perform virtual screening of hundreds or even thousands of molecules. These scoring functions can be empirical, force field-based or knowledge-based. Empirical methods, such as ChemScore implemented in the GOLD docking software, use several terms describing important properties to the ligand binding.³⁵⁰ Force field methods such as

GOLDScore from GOLD or the GRID force field³³² used by the software GLUE,³³³ are based on the non-bonded terms of molecular mechanics force fields. Knowledge-based functions use structural information collected from high-quality X-ray structures of protein-ligand complexes.³⁵¹

As an output, docking tools rank each compound compared to the others. The values predicted by the scoring functions are able to separate the most promising compounds from those unlikely to bind the macromolecular target, although not always accurately ranking within each group.³⁵²

1.5.1.8. Pharmacophore modelling

A pharmacophore is the ensemble of steric and electronic features that is necessary to ensure the optimal supramolecular interactions with a specific biological target and to trigger (or block) its biological response.³⁵³ Using this representation is a useful way to identify new active compounds. The new molecules are most typically studied in 3D so that the pharmacophore model captures both the nature of the functional groups but also their relative orientation to each other.

Functional groups in a pharmacophore model are not usually considered at an atomic level but as broader interaction properties. The most typically used features include hydrogen bond acceptors, hydrogen bond donors, positive ionizable groups, negative ionizable groups and hydrophobic regions. Identifying the most important functional groups from which to derive a pharmacophore model can be undertaken by a ligand-based approach. A set of known active compounds are superimposed in the 3D space and the shared functional groups identified, as well as their spatial arrangement.³⁵⁴ Typically, tolerances are included for the distance values, in order to compensate for small displacements that might be allowed within the binding site. Training sets with highly active but conformationally restricted compounds avoid time-consuming and potentially misleading

superimpositions. Furthermore, in order to reproduce the bioactive conformation, pharmacophore models are usually restricted to low-energy geometries, although not necessarily an energy minimum.³⁵⁵

Pharmacophore queries can also include a measure of the required shape of the molecules, based on the shape of the compounds used to build the model, in order to improve complementarity to the biological target and avoid steric clashes. Possible adverse steric interactions are prevented with the use of excluded volume spheres, forbidden volumes that compounds cannot map. A complementary approach is the use of inclusion volume spheres selected on the basis of the shape of highly active compounds.

Using queries to search in 3D requires a method to consider conformational flexibility. The simplest approach is to generate and store multiple conformations of all ligands in the database. The software will then test rigidly all conformations of the ligand and return those that fit. Alignment methods require a quantitative measure to assess the degree of overlap between the ligands and the pharmacophore. Typically in point-based methods, the optimization algorithm attempts to reduce the root mean square deviation of the pharmacophoric features by least-squares fitting. Employing additional 2D substructure filters improves the efficiency of these approaches and reduces the computational time required.

Pharmacophore models can be used to quickly search databases of hundreds of thousands of compounds, returning compounds that will look very different from the initial set. As such, it is a very useful tool in lead finding.³⁵⁶

1.5.1.9. Virtual screening

High-throughput screening (HTS) is a well-established method for finding new lead compounds in drug discovery. HTS involves fully automated

assays, allowing fast biological evaluation of a large number of compounds for a given target. However, the costs associated to such screenings are high and the hit rates low. This problem might be avoided by not screening complete databases experimentally, but only a small subsets enriched in the most promising compounds.

Virtual screening describes any computational method to select compounds for experimental screening, predicted to have better probability of being active than random. Large electronic databases might be used, typically with hundreds to millions of structures, either in house available compounds, commercially available compounds or chemically feasible virtual compounds.

Virtual screening can follow a ligand-based strategy or a structure-based strategy. Ligand-based VS uses information from known active compounds to select other molecules. A training set of these structures is the starting point to build pharmacophore queries, as well as similarity or substructure searching procedures. Structure-based VS approaches use molecular docking to select compounds predicted to bind with strong affinity to the binding pocket of the target protein.³⁵⁷

Virtual screening can be applied to millions of molecules in a relatively short time scale, much quicker than HTS. However, the real value of VS is in its complementarity to HTS. Both ligand- and structure-based approaches are able to identify sets of compounds which must then be tested in a relevant *in vitro* assay.

The main disadvantage of virtual screening is that if tight constraints are used on the type of compounds selected, this will limit the possibility of finding novel and unexpected molecules due to serendipity.³⁵⁸

1.6. Objective of this thesis

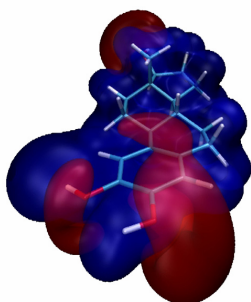
Recent clinical trials confirmed the important role of third generation aromatase inhibitors as first-line therapy for the treatment of breast cancer.^{14;15} However, even for the aromatase inhibitors most used in the clinic, there are still limitations arising from possible inhibition of other cytochrome P450 enzymes, from development of resistance in long-term treatments and from reduced efficacy in the treatment of more advanced stages of cancer.^{359;360} Therefore, the main motivation for this study was the development of new aromatase inhibitors with potentially better pharmacological and toxicological profiles.

Unlike early drug discovery methods based on trial and error, rational drug discovery uses structural information about drug targets and known ligands as a basis for the design of effective new drugs. With this in mind, we have combined state of the art computational drug discovery techniques with a biochemical evaluation assay for the rational discovery of new aromatase inhibitors.

The biochemical evaluation of compounds from emerging new classes of aromatase inhibitors, endogenous estrogens and natural polyphenols, provided new insights into the molecular basis of aromatase active site recognition and binding. This information was combined into a virtual screening strategy for the discovery of new aromatase inhibitors.



Biochemical and computational insights into the anti-aromatase activity of natural catechol estrogens



The main estrogen metabolites were tested on a biochemical assay with aromatase extracted from human term placenta. Catechol estrogens were identified as potent competitive inhibitors with IC_{50} in the low micromolar range. Their binding to the active site of the enzyme was characterized in terms of steric and electronic properties. The therapeutical and physiological relevance of this finding is discussed in this chapter.

Marco A. C. Neves, Teresa C. P. Dinis, Giorgio Colombo, M. Luisa Sá e Melo.
J. Steroid Biochem. Mol. Biol., **2008**, *110*, 10-17.

2.1. Abstract

High levels of endogenous estrogens are associated with increased propensity of developing breast cancer. Estrogen levels are mainly increased by the activity of the aromatase enzyme and reduced by oxidative/conjugative metabolic pathways. In this work, we demonstrate for the first time that catechol estrogen metabolites are potent aromatase inhibitors, thus establishing a link between aromatase activity and the processes involved in estrogen metabolism. In particular, the anti-aromatase activity of a set of natural hydroxyl and methoxyl estrogen metabolites was investigated using an *in vitro* assay with aromatase extracted from human term placenta and subsequently compared with the anti-aromatase potency of estradiol and two reference aromatase inhibitors. Catechol estrogens proved to be strong inhibitors with an anti-aromatase potency two orders of magnitude higher than estradiol. A competitive inhibition mechanism was found for the most potent molecule, 2-hydroxyestradiol and a rational model identifying the interaction determinants of the metabolites with the enzyme is proposed based on *ab initio* quantum mechanic calculations. A strong relationship between activity and electrostatic properties was found for catechol estrogens. Moreover, our results suggest that natural catechol estrogens may be involved in the control mechanisms of estrogen production.

2.2. Introduction

Estrogen metabolism is no longer seen as the simple transformation of hydrophobic hormones into more polar compounds, prone to urinary excretion. Instead it is considered a much more complex process with several estrogen metabolites playing important and unique biological functions in target cells, not directly associated to the parent hormones.⁷⁵ Recent advances in this area confirmed that estrogen metabolites are far

from being inactive compounds. They retain the potential to bind to the estrogen receptor with variable degree of estrogenic activity,^{89;104} and have potent pro and anticarcinogenic activities.^{77;96;111} The involvement of estrogens in breast cancer is therefore not limited to the proliferative effects of estradiol, but involves a complex balance between the actions of multiple compounds.³⁶¹

An additional link between estrogens and breast cancer was established with the work of Shimizu *et al.* demonstrating that natural estrogens, like estradiol and estrone, are able to block its own formation through aromatase active site binding as competitive inhibitors.¹⁴⁴ Since estrogens are produced endogenously, an *in situ* mechanism of aromatase activity regulation might occur. However, the preliminary study performed by those researchers was not further extended to the catechol estrogen metabolites and their methoxy derivatives.

In this chapter, we have focused on the biochemical evaluation of the anti-aromatase potential of a set of natural hydroxyl and methoxyl estradiol/estrone metabolites and a related synthetic derivative, the 2-methoxyestradiol-3-methylether, using an *in vitro* assay with aromatase extracted from human term placenta. The involvement of these compounds in breast cancer is discussed based on our results and findings from other reports in the literature. Furthermore, a rationale for the molecular interaction of this type of compounds with aromatase is proposed, based on *ab initio* quantum chemical methods, and their potential for lead optimization towards better therapeutical prospects is discussed.

2.3. Results and discussion

2.3.1. Concentration-response study

Inhibition of the human placental aromatase by estradiol (E_2 , **2.1**), estrone (E_1 , **2.2**), their physiological metabolites 16α -OHE₁ (**2.3**), E_3 (**2.4**), 2-OHE₁ (**2.5**), 2-OHE₂ (**2.6**), 4-OHE₁ (**2.7**), 4-OHE₂ (**2.8**) 2-MeOE₂ (**2.9**), 4-MeOE₂ (**2.10**), 2-OHE_{2,3Me} (**2.11**) (**Figure 2.1**), and the related synthetic derivative 2-MeOE_{2,3Me} (**2.12**, **Figure 2.2**), was evaluated using an *in vitro* radiometric assay.

Briefly, the use of a radiolabeled androgen as the substrate of the enzyme allowed a simple and rigorous quantification of the extent of the aromatization reaction which is proportional to the amount of tritiated water formed together with the corresponding estrogen. Full concentration-response curves were obtained by evaluation of the aromatase activity in the presence of the potential inhibitors with the maximal activity being given by control experiments (i.e. experiments without the compounds in study). A broad range of inhibitor concentrations to allow the determination of the half maximal inhibitory concentrations (IC_{50}) was used. In the case of less active compounds, incomplete dissolution at higher concentrations did not allow the establishment of a full concentration-response curve. The IC_{50} and the percentage of aromatase inhibition at 100 μ M for the complete set of estrogens tested are shown in **Table 2.1**. The most active estrogens, 2-OHE₁ (**2.5**), 2-OHE₂ (**2.6**), 4-OHE₁ (**2.7**) and 4-OHE₂ (**2.8**) inhibited the aromatase enzyme with remarkable potency, showing a clear sigmoidal concentration-response behavior, as represented for compound **2.7** in **Figure 2.3**. The observed potency is stronger than for the reference non-steroid first generation aromatase inhibitor tested, aminoglutethimide ($IC_{50}=10$ μ M, **Table 2.1**). In contrast, E_2 (**2.1**), E_1 (**2.2**) and their methoxy- and 16α -hydroxy derivatives showed lower anti-aromatase potency, as

evidenced in **Figure 2.3** for 2-OHE₂,3Me (**2.11**), 2-MeOE₂,3Me (**2.12**) and 16 α -OHE₁ (**2.3**). However, all the compounds in study presented lower anti-aromatase potency than formestane, a second generation steroid AI, also used as a reference inhibitor (**Table 2.1**).

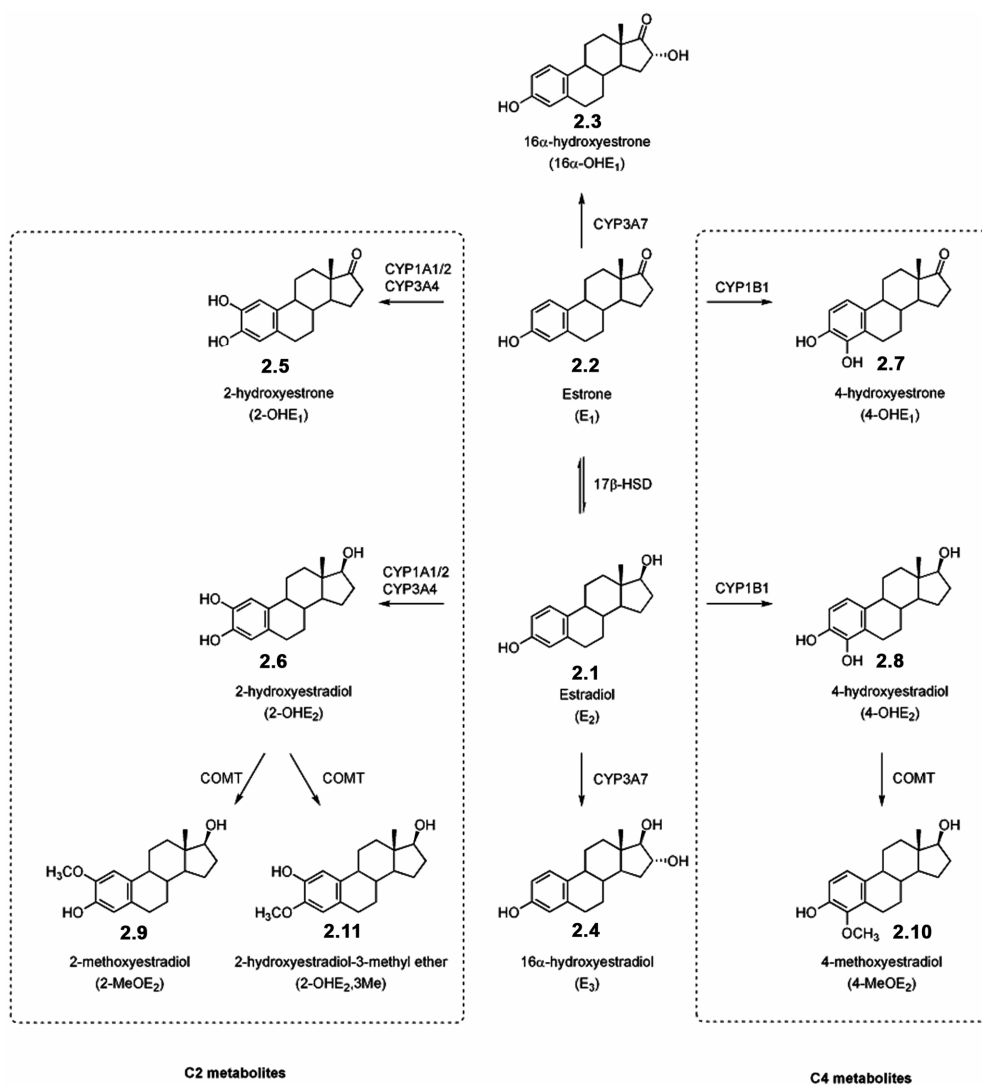
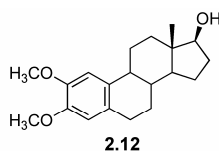


Figure 2.1. Schematic representation of estrogen conversion paths.



2-methoxyestradiol-3-methyl ether
(2-MeOE₂,3Me)

Figure 2.2. 2-Methoxyestradiol-3-methyl ether (**2.12**).

Table 2.1. *In vitro* aromatase inhibition by estradiol, estrone and derivatives. Aminoglutethimide and formestane were tested as reference compounds.

Compound	IC ₅₀ (μM) ^[a]	Inhibition at 100 μM
E ₂ (2.1)	227 ± 8	35%
E ₁ (2.2)	36 ± 1	47%
16α-OHE ₁ (2.3)	ND ^[b]	9%
E ₃ (2.4)	ND ^[b]	8%
2-OHE ₁ (2.5)	2.4 ± 0.06	94%
2-OHE ₂ (2.6)	1.1 ± 0.03	95%
4-OHE ₁ (2.7)	1.8 ± 0.05	96%
4-OHE ₂ (2.8)	2.6 ± 0.09	92%
2-MeOE ₂ (2.9)	296 ± 10	33%
4-MeOE ₂ (2.10)	ND ^[b]	14% ^[c]
2-OHE ₂ ,3Me (2.11)	134 ± 2	41%
2-MeOE ₂ ,3Me (2.12)	234 ± 3	21%
Aminoglutethimide	10 ± 0.09	ND ^[b]
Formestane	0.092 ± 0.004	ND ^[b]

[a] Results are shown as the mean ±SEM of three independent assays, each one in triplicate.
 [b] ND: not determined.
 [c] Percentage of inhibition at 31.62 μM.

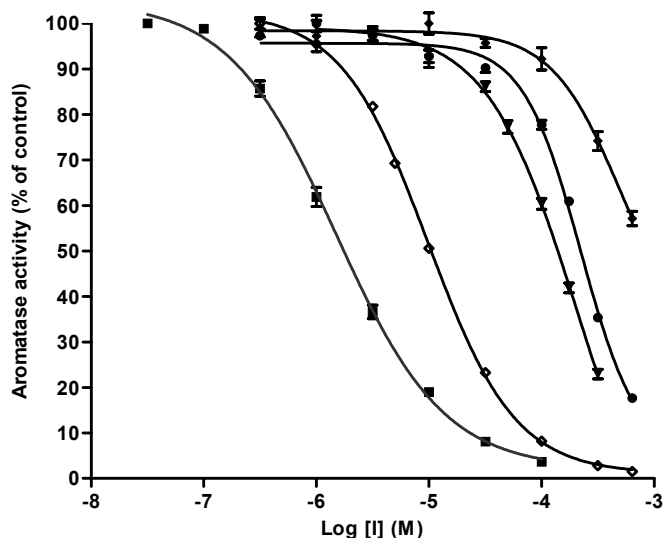


Figure 2.3. Concentration-response curves obtained with 4-OHE₁ (**2.7**, ■), 2-OHE₂,3Me (**2.11**, ▼), 2-MeOE₂,3Me (**2.12**, ●) and 16 α -OHE₁ (**2.3**, ◆) tested as AIs. Aminoglutethimide (◇) was tested as a reference AI. Each point represent the mean of three independent assays performed in triplicate and the vertical bars the standard error of the mean (SEM). The data were analyzed by nonlinear regression using a sigmoidal concentration-response curve with variable slope.

2.3.2. Kinetic analysis

A more detailed analysis on 2-OHE₂ (**2.6**), the most potent compound under study (lowest IC₅₀), showed a mechanism of competitive inhibition, as displayed in the Lineweaver-Burk plot (**Figure 2.4**). Experiments were performed with several concentrations of substrate in the absence and in the presence of three different concentrations of 2-OHE₂ (**2.6**). The data obtained were fitted by nonlinear regression to the Michaelis-Menten equation (**Figure 2.4**, inset) and the kinetic constants are shown in **Table 2.2**.

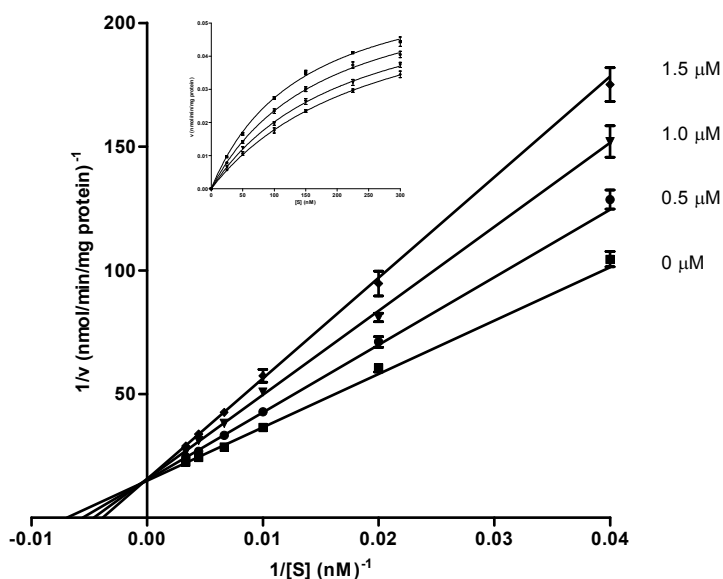


Figure 2.4. Lineweaver-Burk plot of the inhibition of human placental aromatase by 2-OHE₂ (**2.6**). A control (■) and three increasing inhibitor concentrations were used: 0.5 μM (●), 1.0 μM (▼) and 1.5 μM (◆). A Michaelis-Menten plot of the same data is shown in the inset. Each point represents the mean of three independent assays performed in duplicate and the vertical bars, the standard error of the mean.

Table 2.2. Kinetic constants (K_i , K_m and V_{max}), relative inhibitory potency (K_i / K_m) and type of aromatase inhibition by 2-OHE₂ (**2.6**).

K_i (μM) ^[a]	K_m (μM)	V_{max} (pmol/min/mg protein)	K_i / K_m	Type of inhibition
1.6 ± 0.03	0.14 ± 0.002	70 ± 0.5	11	Competitive

[a] Result is shown as the mean ±SEM of three independent assays, each one in duplicate.

2.3.3. Electrostatic surface potential calculation

Further understanding of the possible molecular recognition determinants leading to the binding of these catechol inhibitors to the active site of the aromatase, was pursued using *ab initio* quantum chemistry methods. Six representative compounds, including the best inhibitor found in this study (2-OHE₂, **2.6**), and five related compounds, the estradiol precursor E₂ (**2.1**), the 4-OHE₂ (**2.8**), a methoxy metabolite (2-MeOE₂, **2.9**), the 2-MeOE₂,3Me (**2.12**) and a 16 α -hydroxyl derivative (E₃, **2.4**), were represented in a three dimensional model with optimized geometry. The electrostatic potential derived from *ab initio* calculations at the Hartree-Fock theory level, along with the standard polarized ζ basis set (HF/6-31G*), mapped onto the electron density isosurface, is shown in **Figure 2.5**. As expected, catechol estrogens, i. e. 2-OHE₂ (**2.6**) and 4-OHE₂ (**2.8**) have a strong negative electrostatic potential centered at each catechol oxygen atom, and are partially stabilized through an intramolecular hydrogen bond. No steric hindrance limits the catechol access to a macromolecular target, therefore, intermolecular charge-transfer interactions might occur at the active site of the aromatase, either by hydrogen bonding or metal coordination, which might explain the strong anti-aromatase potency. Similar regions of negative electrostatic potential were found in 2-MeOE₂ (**2.9**), however, substitution of the C2 hydroxyl by a methoxyl group introduces sterical hindrance at the ring A and may limit the interaction with the enzyme, which might be responsible for the low anti-aromatase activity of 2-MeOE₂ (**2.9**). In a similar manner, 2-MeOE₂,3Me (**2.12**), a double methoxylated compound, will fail to establish strong electrostatic interactions with the aromatase active site. On the other hand, E₂ (**2.1**) and E₃ (**2.4**), show a different ESP, with a single negative potential area derived from the 3-hydroxyl at ring A.

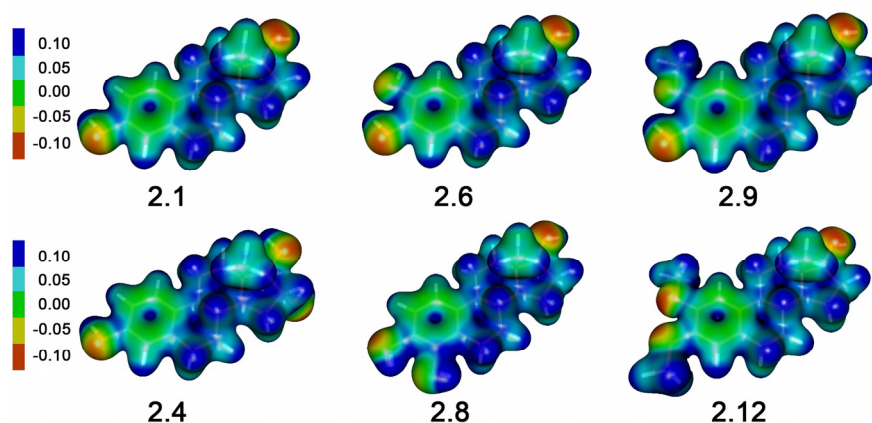


Figure 2.5. Electrostatic surface potential mapped on the $0.02 \text{ e}/\text{\AA}^3$ electron density isocontour derived from *ab initio* HF/6-31G* calculations. E_2 (**2.1**), E_3 (**2.4**), 2-OHE₂ (**2.6**), 4-OHE₂ (**2.8**), 2-MeOE₂ (**2.9**) and 2-MeOE₂,3Me (**2.12**) are displayed from the β -face as shown by the transparent capped-stick model on the inside of the electron density contour. ESP ranges from $V = 0.1 \text{ eV}$ (blue) to $V = -0.1 \text{ eV}$ (red). This figure was created using the program Molden.³⁶²

Electrostatic potential similarities between the two most active estrogens, 2-OHE₂ (**2.6**) and 4-OHE₂ (**2.8**), are clearly evident at the isosurface potential contour, represented in **Figure 2.6**. The negative potential at ring A of both catechols is remarkably superimposable, either considering its spatial location or intensity, suggesting a common binding mode, guided by strong electrostatic interactions.

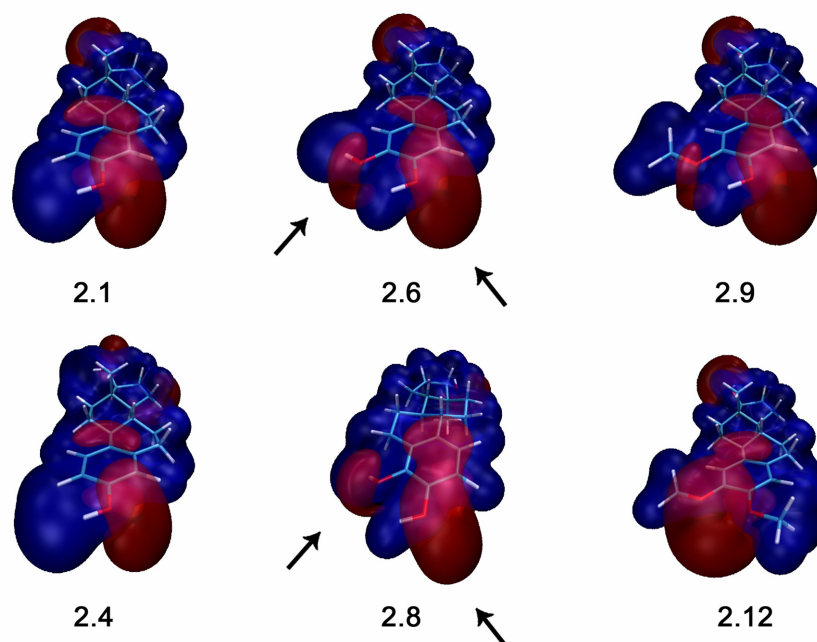


Figure 2.6. Electrostatic surface potential derived from *ab initio* HF/6-31G* calculations at isosurface values of $V = 0.025$ eV (blue) and $V = -0.025$ eV (red). E_2 (**2.1**), E_3 (**2.4**), 2-OHE₂ (**2.6**), 2-MeOE₂ (**2.9**) and 2-MeOE₂,3Me (**2.12**) are displayed from the β -face as shown by the transparent capped-stick model on the inside of the ESP contour. 4-OHE₂ (**2.8**) is displayed from the α -face. Arrows indicate similarities in the negative potential contour of the most active compounds. This figure was created using the program Molden.³⁶²

2.4. Conclusions

The biochemical evaluation of the main estradiol and estrone metabolites revealed that the catechol estrogens 2-OHE₁ (**2.5**), 2-OHE₂ (**2.6**), 4-OHE₁ (**2.7**) and 4-OHE₂ (**2.8**) are potent AIs with half maximal inhibitory concentrations in the range of 1.1 to 2.6 μ M (**Table 2.1**). In our assay conditions, E_2 (**2.1**) showed anti-aromatase activity, though only at higher concentrations ($IC_{50}=227$ μ M). The substitution of one hydroxyl group at the

catechol moiety by methoxy markedly decreased the anti-aromatase activity. In a similar manner, 2-MeOE₂,3Me (**2.12**), a 2,3-dimethoxy synthetic derivative, showed reduced anti-aromatase potency. Moreover, the 16 α -hydroxylation, leads to weak AIs with only 8 to 9% inhibition at a 100 μ M concentration, as seen for E₃ (**2.4**) and 16 α -OHE₁ (**2.3**).

In particular, the anti-aromatase activity of 2-OHE₂ (**2.6**), the most potent inhibitor tested, was found to be ca. 200 times stronger than E₂ (**2.1**). This molecule competed with androstenedione for the active site of the enzyme showing a typical competitive Lineweaver-Burk plot (**Figure 2.4**) and a good relative potency of aromatase inhibition ($K_i/K_m=11$). These results are in agreement with the type of inhibition found for estradiol and estrone¹⁴⁴ and demonstrate for the first time that estrogens metabolized to catechol derivatives have an increased anti-aromatase potential.

Steric and electronic effects are expected to control the recognition and binding affinity of these molecules to the aromatase active site. Catechol estrogens have in common a pair of hydroxyl groups prone to interact with the aromatase active site, either at C2 and C3, in compounds **2.5** and **2.6** or at C3 and C4 in compounds **2.7** and **2.8**. Large differences in anti-aromatase potency between catechols and the other estrogens in study suggest that catechol hydroxyls are involved in strong electrostatic interactions, like hydrogen bonds, either as donors or as acceptors, or in coordination with the heme iron at the aromatase active site. Methylation of one or both A-ring hydroxyl groups strongly blocks the accessibility to the enzyme and prevents the establishment of favorable interactions. No relationships between anti-aromatase activity and the oxidation state at C17, either hydroxyl or ketone, were found.

Human breast tissue is a major source of estrogen production in postmenopausal women. Breast cells contain steroidogenic enzymes essential to estrogen production, as well as estrogen metabolizing

enzymes.^{77;363;364} 2-OHE₂ (**2.6**) is produced mainly by CYP1A1, CYP1A2 and CYP3A4, whereas 4-OHE₂ (**2.8**) is produced mostly by the CYP1B1.⁹² Genetic polymorphisms of several estrogen metabolizing enzymes have been identified in human.³⁶⁵ Different variant alleles of CYP1A1 and CYP1B1 determine changes in the ratio of 2-/ 4-hydroxyestradiol formation and these differences have been correlated with postmenopausal breast cancer risk.⁷⁷ In particular, catechol estrogens seem to play a dual role on the initiation of breast tumors: while 2-hydroxy derivatives have preventive effect due to their anti-estrogenic and antiproliferative activities in hormone-dependent human breast cancer cells,^{91;366} 4-hydroxy derivatives may act as tumor initiators due to a significative estrogenic activity⁹⁰ and the formation of 3,4-quinones, electrophilic intermediates that covalently bind to DNA and form depurinating adducts.^{110;367}

Although plasma levels of estrogen metabolites are low, these concentrations do not reflect the local concentrations. Indeed, high levels of catechol estrogens were detected in both normal and breast cancer tissue samples. Castagnetta *et al.* reported a concentration of catechol estrogens 50 times higher than those of E₁ and E₂, suggesting that oxidative metabolism in the breast tissue is very effective.³⁶⁸ On the other hand, androstenedione concentration in tumor breast tissue was found to be approximately 10 times greater than the estradiol levels.^{369;370} Therefore, catechol estrogen concentrations might be greater than the levels of androgens, competing to the aromatase active site.

Catechol-O-methyltransferase is the major enzyme in catechol biotransformation. Kinetic analysis of this enzyme in the presence of catechol estrogens, has revealed higher catalytic efficiency for the formation of C4-methoxy estrogens than C2-methoxy estrogens and K_m values are the range of 24 to 108 μM .³⁷¹ Considering these data and the low K_i (1.6 μM) found by us for 2-OHE₂ (**2.6**), we can speculate that estrogens are stable

enough to inhibit the aromatase enzyme. Thus, the results of our study suggest that the oxidative metabolism of estrogens in the breast might be responsible for an intracrine control mechanism of the aromatase activity exerted by catechol estrogens. In particular the 2-OHE₂ (**2.6**), which is non carcinogenic *in vivo* and almost devoid of estrogenic activity,⁹⁰ might offer protection against excessive production of estrogens in postmenopausal women, and consequently against breast cancer. So, the effectiveness of this mechanism of competitive inhibition will depend on the *in situ* concentrations of estrogen catechols and androgens, and on the metabolic stability of the catechols.

Moreover, the strongest anti-aromatase activity found in the present work for the 2-OHE₂ (**2.6**), suggests that a shift towards the 2-hydroxylation pathway might determine some long term protection against breast cancer by a biochemical mechanism of competitive inhibition of the enzyme aromatase. Furthermore, 2-MeOE₂ (**2.9**), the product of 2-OHE₂ (**2.6**) methylation by COMT is a potent antiangiogenic and antiproliferative compound, already in clinical trials.⁹⁶

The reduced oral bioavailability of catechol estrogens due to methylation by COMT and the potential to undergo metabolic redox cycling with generation of free radicals and reactive semiquinone/quinone derivatives limits the use of catechol estrogens as therapeutical agents to the endocrine treatment of breast cancer. Further studies based on the chemical physical results obtained here should therefore be performed in order to find appropriate bioisosteric derivatives, devoid of estrogenic activity or having anti-estrogenic activity, with improved pharmacokinetics and reduced toxicity.

In summary, we have demonstrated that natural catechol estrogens have strong anti-aromatase activity and might be responsible for an intracrine control mechanism of estrogen production in postmenopausal women. With our study, important molecular recognition determinants have been

calculated and from this integrated approach, structure-activity rules have been rationalized which can be used for the lead optimization of new aromatase inhibitors.

2.5. Materials and methods

2.5.1. Materials and general methods

Estradiol, 2-hydroxyestradiol, 2-methoxyestradiol, 2-hydroxyestradiol-3-methyl ether, 2-methoxyestradiol-3-methyl ether, 4-hydroxyestradiol, 4-methoxyestradiol, 16 α -hydroxyestradiol, estrone, 2-hydroxyestrone, 4-hydroxyestrone and 16 α -hydroxyestrone were purchased from Steraloids, Inc. (London, UK). NADPH, dl-aminoglutethimide and formestane were purchased from Sigma-Aldrich (St. Louis, MO, U.S.A.). [1β - ^3H]-Androstenedione (specific activity: 25.3 Ci/mmol) and the liquid scintillation cocktail Optiphase Hisafe 2 were purchased from PerkinElmer (Boston, MA, USA), and the radioactive samples were counted on a Packard Tri-Carb 2000 CA liquid scintillation analyzer. All the other reagents were of adequate grade for biochemical analysis.

2.5.2. Enzymatic preparation

Human term placental microsomes were obtained according to the method described by Ryan and were used as a source of aromatase.³⁷² Briefly, the placenta was washed with saline solution, removed from large blood vessels and connective tissues, and homogenized in a buffer containing 0.05 M sodium phosphate, pH 7.0, 0.25 M sucrose and 0.04 M nicotinamide. Then, a microsomal preparation was isolated by a differential centrifugation procedure with the final centrifugation at 105000 \times g for one hour. The microsomes were resuspended in a medium containing 0.1 M sodium phosphate, pH 7.4, 0.25 M sucrose, 20% glycerol and 0.5 mM

dithiothreitol and stored in aliquots at $-80\text{ }^{\circ}\text{C}$ until needed. All procedures were carried out at $4\text{ }^{\circ}\text{C}$. No significant loss of activity occurred during the time required to complete the assays.

Microsomal protein content was determined by the biuret method using bovine serum albumin as standard.

2.5.3. Concentration-response study

Aromatase activity was measured by quantifying the amount of $^3\text{H}_2\text{O}$ released upon enzymatic conversion of the tritiated substrate, $[1\beta\text{-}^3\text{H}]$ -androstenedione, into the corresponding estrogen. This method was first described by Siiteri and Thompson.³⁷³ Incubations were performed at $37\text{ }^{\circ}\text{C}$ in a medium containing 67 mM sodium phosphate, pH 7.5, $[1\beta\text{-}^3\text{H}]$ -androstenedione (6.6×10^5 dpm / 24 nM), 15 μl methanol and 270 μM NADPH. The potential inhibitors were dissolved in DMSO and added to the assay in at least 8 concentrations ranging from 31.62 nM to 640 μM . The amount of DMSO in the assay was always equal to 2% and the final incubation volume was 500 μL . The reaction was started with the addition of 30 μg of microsomal protein and stopped after 20 minutes by adding 1 ml of chloroform and vortexing at 9000 rpm for 40 seconds. After centrifugation at 3000 rpm for 5 minutes, the organic phase was discarded and the extraction procedure was repeated. An aliquot (250 μl) of the aqueous layer was collected and mixed with 3 ml of liquid scintillation cocktail. The amount of tritiated water formed in each assay was determined in a Packard Tri-Carb 2000 CA Liquid Scintillation Analyzer. Appropriate controls without the compounds in study were performed in order to determine the maximum enzymatic activity to which the relative percentage of inhibition was determined. Results were expressed as mean \pm SEM of three independent assays, each one in triplicate. Data were treated by nonlinear regression

analysis, using a sigmoidal concentration-response curve with variable slope. GraphPad Prism software, version 4.00 was used for this purpose.

2.5.4. Kinetic analysis

For the kinetic study, similar conditions to the concentration-response study were used. The concentration of [1β - ^3H]-androstenedione was varied from 25 to 300 nM, the concentrations of 2-hydroxyestradiol tested were 0.5, 1.0 and 1.5 μM , and the reaction time was 5 minutes. An assay without inhibitor was also performed. Results were expressed as mean \pm SEM of three independent assays, each one in duplicate. Data were fitted by nonlinear regression to the Michaelis-Menten equation. The kinetic constants, V_{max} , K_{m} and K_{i} were estimated by nonlinear curve fitting, and the type of inhibition was determined from Lineweaver-Burk plots. GraphPad Prism software, version 4.00 was used for this purpose.

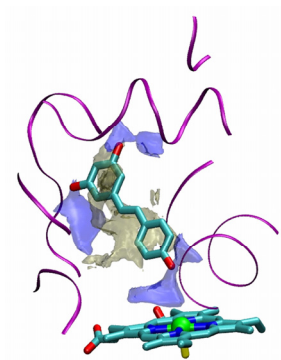
2.5.5. Electrostatic surface potential calculation details

Three-dimensional models of compounds **2.1**, **2.4**, **2.6**, **2.8**, **2.9** and **2.12** were constructed using building fragments from the standard libraries of MAESTRO v5.1.016.³⁷⁴ Flexibility was taken into account by conformational search using the systematic unbounded multiple minimum (SUMM)³⁷⁵ routine implemented in MACROMODEL³⁷⁶ v8.1 with the Merck molecular force field³¹⁴ and the Polak-Ribiere conjugate gradient minimization method, with an energy convergence criterion of 0.05 kJ/mol. The generalized Born equation/surface area (GB/SA) continuum solvation model was used with parameters for water, with a dielectric constant (ϵ) of 78.³¹⁹ A maximum of 2000 conformations were generated and saved if within an energy window of 50 kJ/mol over the global minimum. Similar structures were excluded based on heavy atom superimposition, i.e. hydrogens excluded. All other settings were used as default.

The molecular mechanics geometry was further optimized at the semi-empirical Austin Model 1 (AM1) level using the Gaussian 98 software³⁷⁷ and the electron density distribution for electrostatic surface potential mapping was calculated at the HF/6-31G* level.



Combining computational and biochemical studies for a rationale on the anti-aromatase activity of natural polyphenols



New potent polyphenol aromatase inhibitors were identified experimentally. The physicochemical determinants for their productive binding to the active site of the enzyme were characterized through a combination of molecular modelling techniques based on grid-independent descriptors, molecular interaction fields and docking into a 3D homology model of the enzyme. A rationale on the anti-aromatase activity of these compounds is presented in this chapter.

Marco A. C. Neves, Teresa C. P. Dinis, Giorgio Colombo, M. Luisa Sá e Melo.
ChemMedChem, **2007**, 2, 1750-1762.

3.1. Abstract

Aromatase, an enzyme of the cytochrome P450 family, is a very important pharmacological target, particularly for the treatment of breast cancer. The anti-aromatase activity of a set of natural polyphenolic compounds was evaluated *in vitro*. Strong aromatase inhibitors including flavones, flavanones, resveratrol, and oleuropein, with activities comparable to that of the reference anti-aromatase drug aminoglutethimide, were identified. Through the application of molecular modelling techniques based on grid-independent descriptors and molecular interaction fields, the major physicochemical features associated with inhibitory activity were disclosed, and a putative virtual active site of aromatase was proposed. Docking of the inhibitors into a 3D homology model structure of the enzyme defined a common binding mode for the small molecules under investigation. The good correlation between computational and biological results provides the first rationalization of the anti-aromatase activity of polyphenolic compounds. Moreover, the information generated in this approach should be further exploited for the design of new aromatase inhibitors.

3.2. Introduction

As discussed in the previous chapter, mimicking the products of the aromatase reaction might be an alternative strategy to the design of new aromatase inhibitors. Strong molecules were identified based on the estradiol and estrone scaffolds. Polyphenols, a large family of natural compounds is another example of aromatase inhibitors related to estrogens. Several compounds of this class are phytoestrogens with selective estrogen receptor modulator and anti-aromatase activities.^{237;378}

The use of natural compounds as starting leads represents an attractive approach for the discovery of new breast cancer drugs based on an

aromatase inhibition mechanism.^{258;259} However, to fully understand the pharmaceutical and therapeutic potential of these natural compounds, a deeper rational study of the physicochemical determinants of their aromatase binding is needed.

To this end, we used a combination of experimental and theoretical approaches to correlate concentration–response curves of *in vitro* aromatase inhibition with calculated alignment-independent three-dimensional structure descriptors. Based on these preliminary data, molecular interaction fields were translated into the main relevant non-bonded interactions expected to occur in the process of enzyme–inhibitor recognition and binding, allowing us to obtain a representation of the putative active site. Finally, this virtual receptor site was compared with the active site structure of a homology model of the enzyme. The good agreement between hydrophobic and hydrophilic portions of the 3D-QSAR virtual receptor site with the homology model prompted us to perform semi-flexible docking at the binding cavity.

With this strategy we were able to identify a common binding mode in all inhibitors tested and propose structure–activity rules that might be extrapolated to other types of compounds and used to optimize the activity of existing derivatives.

3.3. Results and discussion

3.3.1. Biochemical evaluation

Several natural compounds, with scaffolds ranging from low to high molecular weight and with various degrees of hydrophobicity, were considered in this study. In particular, we tested 12 flavones (**Table 3.1**), five flavanones (**Table 3.2**), one anthocyanin and one anthocyanidin (**Table 3.3**), four coumarins (**Table 3.4**), and *trans*-resveratrol and

oleuropein (Table 3.5). The first-generation AI, aminoglutethimide, was also tested and used as a reference compound (Table 2.1).

The compounds in study were tested for the ability to inhibit aromatase by using human placental microsomes as the source of aromatase. Full concentration-response curves were obtained, allowing the determination of the half-maximal inhibitory concentration. The concentration-response curves for the most active compound 5,7,3',4'-tetrahydroxyflavanone **3.14**, flavone **3.12**, and aminoglutethimide, the reference inhibitor, are shown in Figure 3.1. The IC₅₀ values obtained are shown in Tables 3.1-3.5.

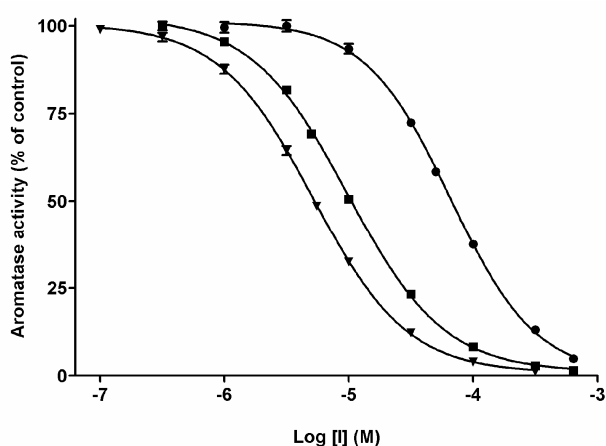
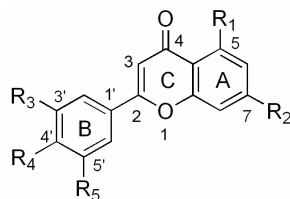


Figure 3.1. Concentration-response curves of compounds **3.14** (▼) and **3.12** (●). Aminoglutethimide (■) was tested as a reference AI. Each point represents the mean of three assays performed in triplicate (n=3), and the vertical bars indicate the standard error of the mean. The data were analyzed by nonlinear regression using a sigmoidal concentration-response curve with variable slope.

Flavones inhibited aromatase with a potency between 7.2 and 100 μ M (Table 3.1). Several structural variations such as hydroxylation and methoxylation at C5, C7, C3', C4', and C5' were considered in order to generate a high number of hypotheses about the spatial distribution of

hydrophilic, hydrogen bond donors and acceptors, and small cavities within the active site of the enzyme. Most of these molecules had stronger activity than the unsubstituted flavone **3.12**, confirming the potential of this type of compounds for lead optimization into potent aromatase inhibitors.

Table 3.1. Estimated binding energies (EBE) and aromatase inhibitory activities of flavones **3.1-3.12**.



Compd	R ₁	R ₂	R ₃	R ₄	R ₅	EBE (kcal/mol) ^[a]	IC ₅₀ (μM) ^[b]
3.1	OH	OH	H	H	H	-16.5	8.9 ± 0.1
3.2	OH	OH	H	OH	H	-16.2	15 ± 0.2
3.3	OH	OH	OH	OH	H	-16.1	8.6 ± 0.07
3.4	OH	OH	OH	OCH ₃	H	-15.6	27 ± 0.7
3.5	OH	OH	OCH ₃	OH	H	-15.8	7.2 ± 0.09
3.6	H	OH	H	H	H	-16.2	8.2 ± 0.1
3.7	H	OH	OH	OH	H	-15.4	38 ± 0.5
3.8	H	OH	OH	OH	OH	-16.1	45 ± 0.7
3.9	H	H	OH	OH	H	-15.1	100 ± 3
3.10	H	H	OCH ₃	OH	H	-16.0	73 ± 2
3.11	H	H	OCH ₃	OCH ₃	H	-15.8	42 ± 0.8
3.12	H	H	H	H	H	-16.2	67 ± 1

[a] Binding energies were estimated on a model of the aromatase active site using the GRID force field implemented in the GLUE docking software.

[b] Results shown are the mean ±SEM.

Hydroxylation at C7 markedly increased the anti-aromatase activity, as observed in flavones **3.1**, **3.3**, **3.5**, and **3.6**, which have stronger activity than aminoglutethimide (IC₅₀=10 μM), the reference AI tested. These molecules

inhibited aromatase with 8- to 9-fold greater activity than the unsubstituted flavone **3.12**. Compound **3.6**, with just a single hydroxyl group at C7, was the least functionalized flavone with potent aromatase inhibition activity. Furthermore, comparing the activities of flavone **3.7** and flavone **3.9**, hydroxylation at C7 provided a 3-fold increase in inhibitory potency.

Simultaneous hydroxylation at C5 and C7 was also important to the anti-aromatase activity, as observed with flavones **3.1**, **3.3**, and **3.5**. Comparison of the inhibitory potencies of compounds **3.3** and **3.5** (respectively 8.6 and 7.2 μM) with those of compounds **3.9** and **3.10** (respectively 100 and 73 μM), simultaneous hydroxylation at C5 and C7 appears to play an important role in aromatase inhibition. Hydroxylation at C4' is present in some of the most active flavones, compounds **3.2**, **3.3**, and **3.5**, and seems to contribute, at least partially, to the anti-aromatase activity of these molecules.

Flavanones lack the C2 unsaturation present in flavones, which decreases the planarity at ring C and introduces new stereocenters in the molecule, making it chiral. Conformational analysis (described in more detail below in **Section 3.5.4**) confirms, however, that both global minimum-energy conformations of flavone **3.12** and flavanone **3.17** are very well superimposed, particularly at the 4-oxo group and at C5, C7, and C4' (**Figure 3.2**).

As expected, substituted flavanones had greater activity than the nonfunctionalized flavanone **3.17**. The effect of substitutions is dependent on their positions (**Table 3.2**) and followed a similar pattern to that observed with flavones. However, compound **3.15** was less potent than flavone **3.5**, which might be the result of ring B rotation around the C2–C1' axis due to the transition from sp² to sp³ geometry at C2, imposing a different spatial disposition for the methoxyl group at C3' (**Figure 3.2**).

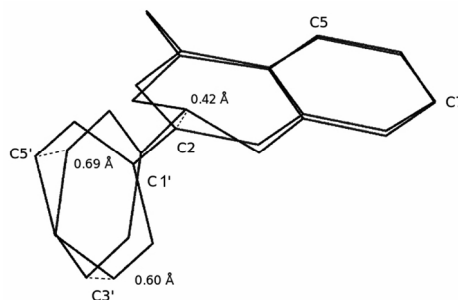
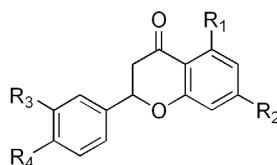


Figure 3.2. Superimposition of the global minimum-energy conformation found for flavone **3.12** and flavanone **3.17** using the Merck molecular force field³¹⁴ and a water GB/SA continuum solvation.³¹⁹ Distances separating equivalent C2, C3', and C5' are displayed. The RMSD of both structures is equal to 0.35 Å. This figure was created using the program MAESTRO.³⁷⁴

Table 3.2. Estimated binding energies (EBE) and aromatase inhibitory activities of flavanones **3.13-3.17**.



Compd	R ₁	R ₂	R ₃	R ₄	EBE (kcal/mol) ^[a]	IC ₅₀ (μM) ^[b]
3.13	OH	OH	H	H	-16.1	10 ± 0.1
3.14	OH	OH	OH	OH	-17.3	5.3 ± 0.06
3.15	OH	OH	OCH ₃	OH	-15.9	25 ± 0.4
3.16	H	OH	H	H	-16.9	10 ± 0.1
3.17	H	H	H	H	-16.5	32 ± 0.3

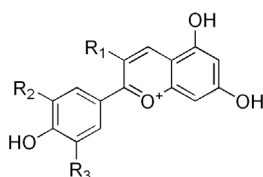
[a] Binding energies were estimated on a model of the aromatase active site using the GRID force field implemented in the GLUE docking software.

[b] Results shown are the mean ±SEM.

The anthocyanidin **3.18**, cyanidin (**Table 3.3**), shares some structural similarities with the most potent flavone and flavanone inhibitors tested, namely a similar scaffold and hydroxyl groups at C5, C7, C3' and C4'.

However, the anti-aromatase activity is much lower ($IC_{50}=72 \mu M$). Two structural differences may explain this: the extended hydroxylations at positions C3 and C5', which agree with the decreased activity of compound **3.8** compared to the less hydroxylated compound **3.7**, and the absence of a 4-oxo acceptor group.

Table 3.3. Estimated binding energies (EBE) and aromatase inhibitory activities of cyanidin **3.18** and malvidin-3-O-glucoside **3.19**.



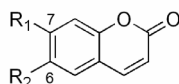
Compd	R ₁	R ₂	R ₃	EBE (kcal/mol) ^[a]	IC ₅₀ (μM) ^[b]
3.18	OH	OH	OH	-14.8	72 ± 0.7
3.19	OGLuc	OCH ₃	OCH ₃	-11.6	299 ± 3

[a] Binding energies were estimated on a model of the aromatase active site using the GRID force field implemented in the GLUE docking software.
 [b] Results shown are the mean ±SEM.

On the other hand, anthocyanin **3.19**, malvidin-3-O-glucoside, failed to show significant anti-aromatase activity in our assay conditions (**Table 3.3**). This compound shares the 5,7,4'-trihydroxy and 3'-methoxy groups found in the strongest flavone inhibitor tested, **3.5**, but a glucose moiety at C3 might impose a different alignment at the aromatase active site. In contrast, oleuropein **3.25**, a large glycosylated molecule, shows surprisingly strong anti-aromatase activity (**Table 3.5**). Unlike malvidin-3-O-glucoside **3.19**, oleuropein **3.25** is a highly flexible molecule and may therefore align several hydrogen bond donor and acceptor groups in favorable positions on the aromatase active site.

The coumarins studied showed greatly decreased anti-aromatase activity (**Table 3.4**). Low molecular volumes and simple scaffolds may be responsible for their poor interaction with the aromatase active site.

Table 3.4. Estimated binding energies (EBE) and aromatase inhibitory activities of coumarins **3.20-3.23**.



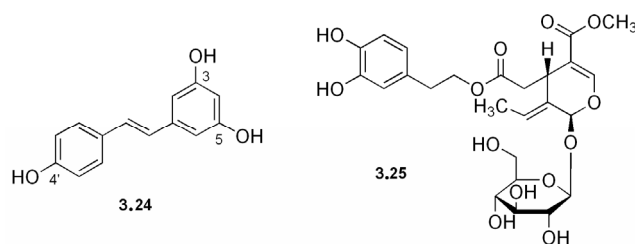
Compd	R ₁	R ₂	EBE (kcal/mol) ^[a]	IC ₅₀ (μM)
3.20	OH	OH	-11.4	NO ^[b]
3.21	OH	OCH ₃	-11.9	> 640
3.22	OCH ₃	OH	-12.7	> 640
3.23	OCH ₃	OCH ₃	-12.9	> 640

[a] Binding energies were estimated on a model of the aromatase active site using the GRID force field implemented in the GLUE docking software.

[b] Inhibition was not observed at concentrations ≤640 μM.

Although not equipped with the flavone phenylchromanone scaffold, *trans*-resveratrol **3.24** (**Table 3.5**) has a simple hydrophobic skeleton with two aromatic rings connected by an ethylene bridge, with hydroxyl groups at C3, C5, and C4', positions analogous to C5, C7, and C4' of the flavonoid inhibitors tested. Interestingly, *trans*-resveratrol is a good aromatase inhibitor (IC₅₀=13 μM) with potency similar to that of the related flavone **3.2**. This suggests that the lack of the 1-oxa and 4-oxo functionalities of the flavone scaffold is well balanced by the three hydrogen bond donor/acceptor groups with a good spatial disposition present in *trans*-resveratrol **3.24**.

Table 3.5. Estimated binding energies (EBE) and aromatase inhibitory activities of *trans*-resveratrol (**3.24**) and oleuropein (**3.25**).



Compd	EBE (kcal/mol) ^[a]	IC ₅₀ (μM) ^[b]
3.24	-13.0	13 ± 0.2
3.25	-16.5	27 ± 2

[a] Binding energies were estimated on a model of the aromatase active site using the GRID force field implemented in the GLUE docking software.
 [b] Results are shown as the mean ±SEM.

3.3.2. 3D-QSAR with GRIND descriptors

The three-dimensional quantitative structure-activity relationships between the anti-aromatase activity of the flavones in this study and their 3D properties were analyzed using grid-independent descriptors.³³⁴ The bioactive conformation of the flavones on the active site of aromatase is unknown. Therefore, the minimum-energy conformation, obtained by a conformational search described in detail in **Section 3.5.4**, was chosen as representative. Although the quality of the model is critically dependent on the 3D conformation chosen, the extended aromatic conjugation makes these molecules rigid and therefore less prone to conformational changes.

GRIND descriptors are alignment-independent descriptors that represent important non-bonding interactions in the recognition and binding to the active site of a macromolecular target. A two-step procedure, described in detail in **Section 3.5.5**, allowed the calculation of these descriptors from

MIFs³³² calculated with three chemical probes: DRY, O and N1. These probes report the interaction between the molecules under study and a hydrophobic group, a hydrogen bond acceptor and a hydrogen bond donor group, respectively. The MIFs chosen represent important types of interactions expected to guide the binding of flavones to the active site of aromatase. Besides chemical complementarity, good shape fit between the ligand and the protein is essential to binding. Therefore, the shape probe (TIP)³⁴⁰ was used to search for highly convex regions of the molecules. These regions interact most with the binding cavity. Therefore, 10 correlograms were obtained: four autocorrelograms (DRY-DRY, O-O, N1-N1 and TIP-TIP) and six cross-correlograms (DRY-O, DRY-N1, DRY-TIP, O-N1, O-TIP, and N1-TIP). Multivariate analysis with partial least squares regression was used to correlate the calculated descriptors with the activity, and the quality of the model was evaluated by the predictive correlation coefficient (q^2), obtained by LOO cross-validation or by a 3 random groups (3RG) procedure.

3D-QSAR studies usually require the calculation of hundreds of descriptors, most of them not correlated with the activity. Therefore, the fractional factorial design (FFD),³⁴¹ a variable selection procedure implemented in ALMOND³³³ v3.3, was performed, excluding variables that increase the standard deviation of errors of prediction (SDEP). Variables decreasing the SDEP or those with an unclear effect were retained.

Optimal predictive ability for the anti-aromatase 3D-QSAR model appears with a model dimensionality of three latent variables ($q^2_{\text{LOO}}=0.85$ and $q^2_{\text{3RG}}=0.53$) when it is able to explain 98% of the anti-aromatase activity variance ($r^2=0.98$). The residuals are shown in **Table 3.6**, and a plot of the predicted activity (LOO) versus the experimental activity is represented in **Figure 3.3**. All compounds were predicted with good confidence.

Table 3.6. LOO and 3RG cross-validation of the PLS 3D-QSAR regression model.

Compd	pIC ₅₀ exptl ^[a]	pIC ₅₀ pred (LOO) ^[b]	δ (LOO) ^[d]	pIC ₅₀ pred (3RG) ^[c]	δ (3RG) ^[e]
3.1	5.05	5.10	-0.05	4.91	0.14
3.2	4.83	5.01	-0.18	4.94	-0.11
3.3	5.07	4.84	0.23	4.77	0.30
3.4	4.56	4.50	0.06	4.53	0.03
3.5	5.14	4.93	0.21	4.84	0.30
3.6	5.09	4.85	0.24	4.70	0.39
3.7	4.42	4.57	-0.15	4.62	-0.20
3.8	4.35	4.50	-0.15	4.64	-0.29
3.9	4.00	4.12	-0.12	4.24	-0.24
3.10	4.14	4.32	-0.18	4.40	-0.26
3.11	4.38	4.44	-0.06	4.46	-0.08
3.12	4.17	4.19	-0.02	4.33	-0.16

[a] pIC₅₀ determined experimentally.
 [b] pIC₅₀ predicted by LOO cross-validation.
 [c] pIC₅₀ predicted by 3 random groups (3RG) cross-validation.
 [d] Residuals (pIC₅₀ exptl - pIC₅₀ pred) from LOO cross-validation.
 [e] Residuals (pIC₅₀ exptl - pIC₅₀ pred) from 3RG cross-validation.

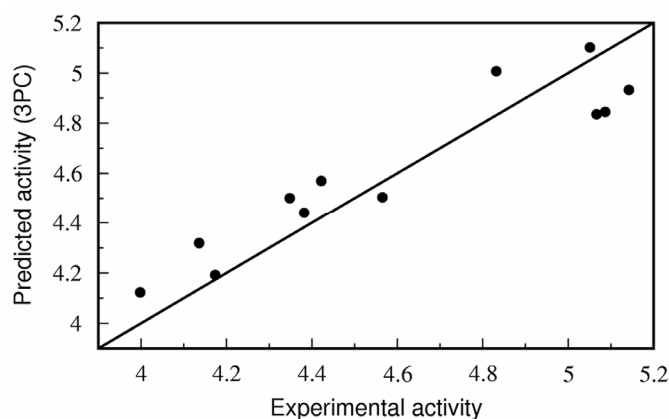


Figure 3.3. Plot of the predicted versus experimental pIC₅₀ from the optimal PLS model with three latent variables ($q^2_{\text{LOO}}=0.85$).

Further understanding of the PLS model was pursued using the PLS coefficients of the variables in study. Variables with large PLS coefficients are important for the biological activity fitting, whereas those with small coefficients are less important. Positive coefficients have a direct impact on the biological activity (that is, the greater the interaction energy, the stronger the inhibitor), whereas negative coefficients have an inverse impact. The PLS coefficients are plotted in **Figure 3.4** and the most influential variables are indicated with an arrow. Interestingly, only a few variables have coefficients of large absolute value and therefore have critical importance to the model fitting. These arise from the O-O, O-N1, and O-TIP correlograms (direct impact) and the N1-N1, DRY-O, O-N1, and N1-TIP correlograms (inverse impact), and are interpreted in **Table 3.7**.

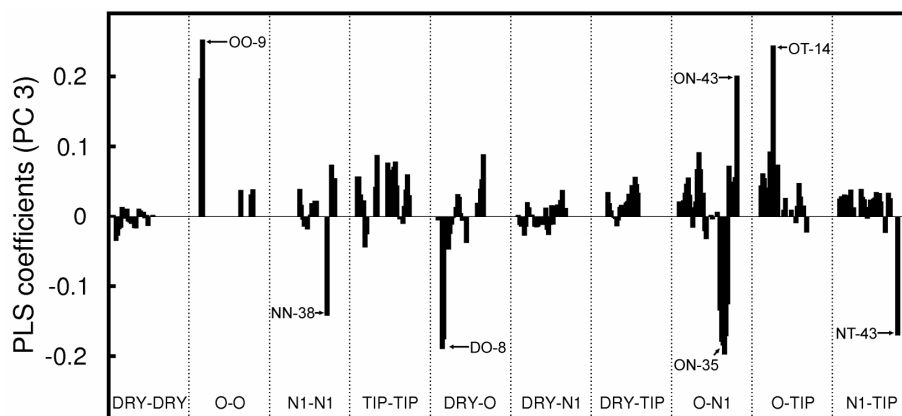


Figure 3.4. PLS coefficients plot of the GRIND variables used in the model. Correlograms are separated by dotted lines and the pairs of probes are defined at the bottom. The most relevant variables are indicated by the variable number with an arrow.

Table 3.7. Relevant variables with strong impact on the GRIND PLS model with three latent variables.

Probe pair	Variable number	Impact	Coeff.	Interpretation ^[a]
O-O	OO-9	Direct	0.25	Interaction of the groups at C5 and C7 (ring A) with the probe O
N1-N1	NN-38	Inverse	-0.14	Interaction of the 4-oxo group (ring C) and the group at C4' (ring B) with the probe N1
DRY-O	DO-8	Inverse	-0.19	Interaction of the group at C3' (ring B) with the probe O and hydrophobic properties of ring C
O-N1	ON-43	Direct	0.20	Interaction of the group at C7 (ring A) with the probe O and the group at C4' (ring B) with the probe N1
O-N1	ON-35	Inverse	-0.20	Interaction of the group at C3' and C4' (ring B) with the probe O and the 4-oxo group (ring C) with the probe N1
O-TIP	OT-14	Direct	0.24	Interaction of the group at C4' (ring B) with the probe O and shape of the group at C3' (ring B)
N1-TIP	NT-43	Inverse	-0.17	Interaction of the group at C4' (ring B) with the probe N1 and shape of the ring A

[a] Ring identification and numbering are defined in **Table 3.1**.

3.3.3. Virtual receptor site derivation

Because GRIND variables are the energy product of MIF pairs of grid points, tracing back the original grid nodes around the molecules under study gives information about essential pharmacophoric groups. Maximum auto and cross-covariance³³⁴ energy products and grid-filtered MIFs are shown in **Figure 3.5** for correlograms O-O, O-N1, and O-TIP obtained with the most active flavone **3.5** and flavone **3.12**, a weak inhibitor. The three most relevant variables with direct impact on biological activity (OO-9, ON-43 and OT-14) are indicated with an arrow in the MACC2 profile and the pairs of points connected by a line in the filtered MIFs. As expected, these most relevant variables have higher values for the potent inhibitor, the 5,7,4'-trihydroxy-3'-methoxyflavone **3.5**, and lower values or even none for flavone **3.12**. This is explained by the lack of hydrogen bond donors and protruding groups in compound **3.12**. Contrarily, appropriate substitutions in compound **3.5** optimally place chemical functions that are able to increase the interaction energy products and therefore these are recognized by the model as important structural features.

On the other hand, variables with a strong negative impact on the biological activity are increased for the weaker inhibitors found (for example, molecules **3.9** and **3.10**). These refer mostly to pairs of points between ring B (interaction of hydrogen bond donors/acceptors with groups at positions C3' and C4') and ring C (**Table 3.7**), which suggests that in the absence of hydroxylations on ring A (positions C5 and C7), the structure-activity relationships of ring B are different, favoring more hydrophobic groups (IC_{50} : **3.9**>**3.10**>**3.11**).

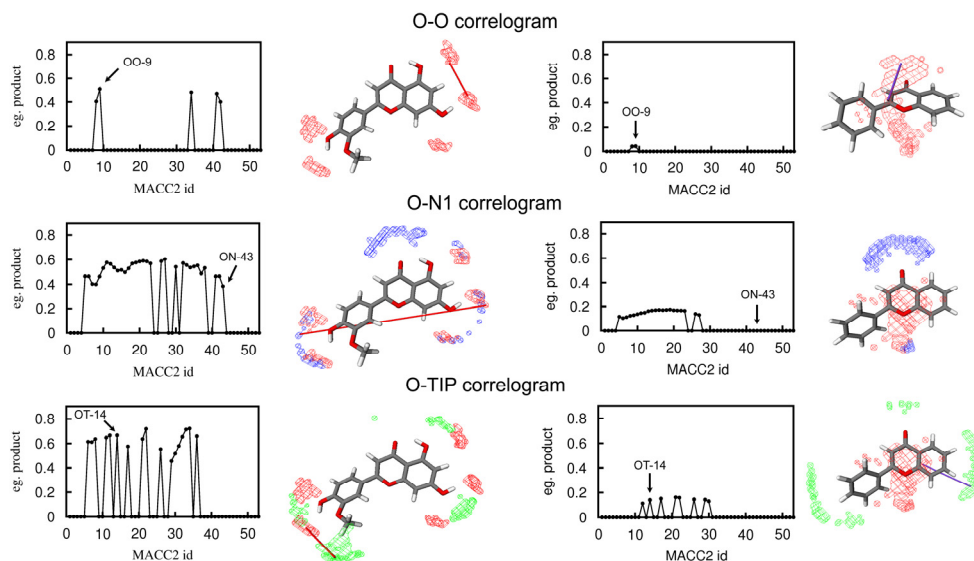


Figure 3.5. MACC2 interaction energy product and graphical representation of the three most relevant GRIND variables with direct impact obtained for the most active flavone, 5,7,4'-trihydroxy-3'-methoxyflavone (compound **3.5**, left), and flavone **3.12** (right), a moderate aromatase inhibitor. Arrows point to the most important variables OO-9, ON-43 and OT-14 in the MACC2 correlograms, and respectively correspond to the pairs of grid nodes O-O, O-N1 and O-TIP linked in the filtered MIFs shown. Molecules are shown (O, red; C, gray; H, white) at the minimum-energy conformation. The filtered MIFs are shown in colored contour (O probe, red; N1 probe, blue; shape probe, green). This figure was created using the program ALMOND.³³³

GRID probes use the GRID force field to calculate the interaction energy, which is the sum of several binding contributions, namely van der Waals interactions (E_{LJ}) given by the Lennard-Jones potential, electrostatic interactions (E_{EL}) given by the coulomb potential and hydrogen bond interactions given by a distance-, angle- and charge-dependent function (E_{HB}). The entropy decrease due to the freezing of degrees of freedom during the binding to the receptor is also considered with an entropic energy function ($E_{entropy}$).

$$E_{\text{GRID}} = E_{\text{LJ}} + E_{\text{EL}} + E_{\text{HB}} + E_{\text{entropy}}$$

Therefore, GRIND descriptors are based on the idea of a virtual receptor site with which the inhibitors interact. When the three selected variables with direct impact on the biological activity (OO-9, ON-43 and OT-14) were applied to the most active flavone **3.5**, a virtual receptor site was obtained (**Figure 3.6**). Two hydrogen bond acceptor regions are expected to be located in the vicinity of C5 and C7 of the flavone ring A. Hydrogen bonding with these hydroxyl groups explains the increased activities of flavones **3.1**, **3.3** and **3.5**. Position C4' on ring B is expected to lie close to a hydrogen bond donor/acceptor region. Furthermore, favorable steric and van der Waals interactions (good shape complementarity at the active site cavity) between the substitution at C3' (ring B) and the enzyme are also responsible for an increase in activity. In this virtual receptor model, hydrophobicity is important because of the apolar nature of the flavonoid scaffold and one hydrogen bond donor region was also considered, close to the 4-oxo group.

3.3.4. Comparison with an aromatase homology model

Knowledge of the 3D structure of a target protein is important to understand its mechanism of action and inhibition. Unique information can be extracted from the atomic detail of the binding site and used in the identification of key interactions between the protein and the ligand.

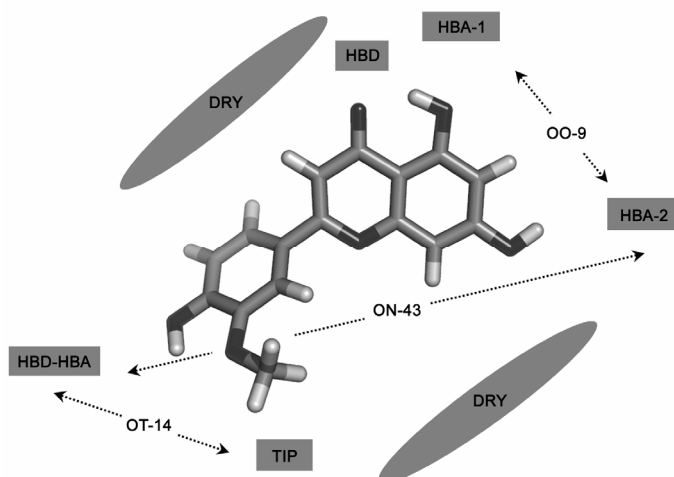


Figure 3.6. Virtual receptor site obtained when the most relevant descriptors with direct impact on the biological activity are coded into pharmacophoric regions around the strongest flavone tested, **3.5**. Two hydrogen bond acceptor regions (HBA-1 and HBA-2), a mixed hydrogen bond donor/acceptor region (HBD-HBA) and one cavity edge (TIP) were found. One additional large hydrophobic region (DRY) is responsible for the anchor of the flavone scaffold and one hydrogen bond donor (HBD) stabilizes the binding to the active site through hydrogen bonding with the 4-oxo group. The flavone is shown (O, black; C, gray; H, white) at the minimum-energy conformation. The pharmacophoric regions are linked by an arrow showing the GRIND variable number. This figure was created using the program ALMOND.³³³

Several cytochrome P450 enzymes have already been crystallized. Despite the low sequence identity (10-30%) between members of different P450 families, they all share the same overall topology and secondary structure elements.¹⁴¹ Furthermore, the internal heme binding pocket cavity shows a high percentage of sequence identity. Homology models have therefore been proposed for a variety of cytochrome P450 binding sites, including aromatase, based on the known structures. One of these models was proposed by Favia *et al.*¹⁴⁰ (PDB code 1TQA from the theoretical model

section) using the human cytochrome P450 2C9 as template.¹³⁷ This model was used in the current study to predict possible binding modes for the compounds under evaluation by using MIFs calculated within the active site with appropriate probes, and the results obtained were compared with the 3D-QSAR virtual receptor site. DRY (hydrophobic) and OH (aromatic hydroxyl group) probes were initially computed. As expected, the active site cavity of the aromatase model is extremely hydrophobic owing to a large number of residues with apolar side chains, such as Leu 120, Ile 133, Phe 134, Leu 227, Ile 305, Val 373, Met 374 and Leu 477, shown in **Figure 3.7**. The probe DRY interacts with these residues, defining a hydrophobic contour represented in **Figure 3.7** that is large enough to accommodate the inhibitors in study and place them close to the heme group, thus competing with the substrate for the active site of the enzyme. The OH probe accounts for hydrophilic portions of the active site that are prone to form hydrogen bonds with the ligands. This probe reveals several hydrophilic regions in the aromatase active site, three of which contour the hydrophobic plane obtained with the DRY probe with a spatial disposition similar to the virtual receptor model previously described (**Figure 3.7**). Contributions to these hydrophilic regions arise from backbone peptide bonds: the Ser 118 amide nitrogen atom and the Phe 116 and Met 374 carbonyl oxygen atoms (zone 1); the Tyr 244 hydroxyl group, the Asp 222 carboxylate and the Ala 226 carbonyl oxygen atom (zone 2); and finally, the Thr 310 hydroxyl group, the Ile 305 and the Ala 306 carbonyl oxygen atoms, and the heme iron (zone 3).

3.3.5. Docking calculations

The similarities between the 3D-QSAR virtual receptor site and the hydrophobic/hydrophilic regions inside the active site prompted us to search for possible binding modes for the aromatase inhibitors studied. GLUE³³³ is a docking software that uses the GRID MIFs to generate binding poses for the ligands, and the GRID force field to calculate the respective binding

energy. The aromatase binding cavity was initially explored with eight GRID probes that represent the most important non-bonded binding interactions (see **Section 3.5.8** for further details). The MIFs local energy minima calculated with the probes DRY, N1, O, O::, N+ and OH represent favorable interaction points between the probes and the protein and correspond to pharmacophoric locations where similar groups of a ligand might be placed.

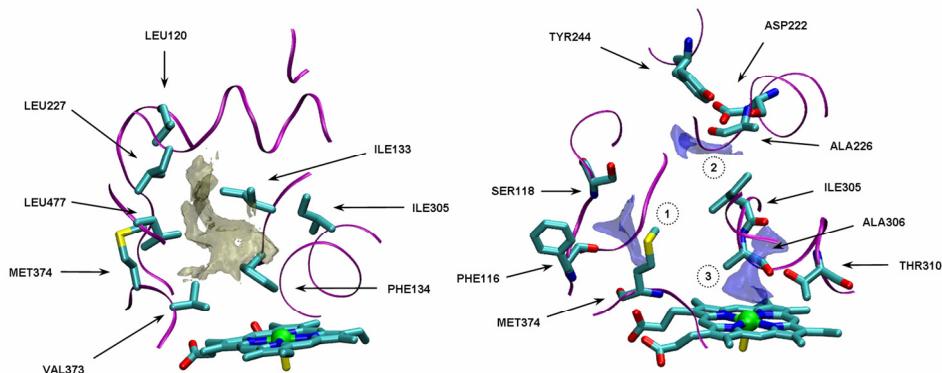


Figure 3.7. MIF isosurfaces obtained with the probe DRY (left) and OH (right) on the homology model of the aromatase active site.¹⁴⁰ The protein is shown in ribbons with the residues responsible for the interactions labeled with residue name and number; the heme group appears at the bottom (C, cyan; O, red; N, blue; S, yellow; Fe, green). The DRY (hydrophobic) MIF is represented in brown at an energy level of -0.4 kcal/mol and the OH (aromatic hydroxyl group) MIF is represented in blue at an energy level of -7.0 kcal/mol. The three hydrophilic zones are numbered from 1 to 3. This figure was created using the program VMD.¹¹⁷

A set of these active site points was recorded for each probe and together combined in a large number of pharmacophoric quadruplets. The large number of possible pharmacophoric alignments in the binding site was then confronted with the inhibitors under study, and only similar pharmacophoric quadruplets found in the molecules were accepted. The conformational flexibility of the ligands was taken into account as described in **Section 3.5.8**.

The estimated binding energy (EBE) of each best pose in the active site is shown in **Tables 3.1-3.5**. These results show that the docking program was able to discriminate between active and inactive compounds with good qualitative correlation between EBE and experimental activity, scoring coumarins **3.20**, **3.21**, **3.22**, **3.23**, and malvidin-3-O-glucoside **3.19**, weak AIs, with less-favorable binding energies.

Best-docked poses (that is, minimal EBE found) were further analyzed. Active site bound conformations found for flavone **3.5** (**Figure 3.8**), malvidin-3-O-glucoside **3.19** (**Figure 3.10**), oleuropein **3.25** (**Figure 3.11**), coumarin **3.20** (**Figure 3.13**) and *trans*-resveratrol **3.24** (**Figure 3.11**) are represented.

The most active flavone **3.5** fits the active site cavity with the apolar scaffold in the hydrophobic core (**Figure 3.8**, left side). This apolar region extends across the whole skeleton of the molecule and is relatively planar. A bulky residue (Phe 134) close to ring B of the flavone imposes planarity for this type of aromatase inhibitors (**Figure 3.8**, right side). In agreement with the virtual receptor site, the three hydrophilic zones are occupied by the 4-oxo and hydroxyl groups. The C4' hydroxyl group lies close to the hydrophilic zone 3 on the vicinity of the heme group, establishing a hydrogen bond with the hydroxyl group of Thr 310. The 4-oxo and the C5 hydroxy functions are located close to zone 1. The C5 hydroxy accepts a hydrogen bond from the amide N atom of Ser 118, and the C7 hydroxyl group lies close to zone 2, hydrogen bonding Ala 226. Also consistent with the 3D-QSAR model, the presence of a C3' methoxyl group allows better shape complementary between the flavonoid and Val 373, filling a small hydrophobic cavity. Other flavones and flavanones share similar docking conformations. Particularly interesting is the anti-aromatase activity of 7-hydroxyflavone **3.6** ($IC_{50}=8.2 \mu M$), the least functionalized strong inhibitor. Despite having only one hydroxyl group, this flavone places one hydrogen bond acceptor, the

4-oxo group, in one hydrophilic region and one hydrogen bond donor/acceptor, the C7 OH group, in another, and therefore retains most of the aromatase inhibitory potency.

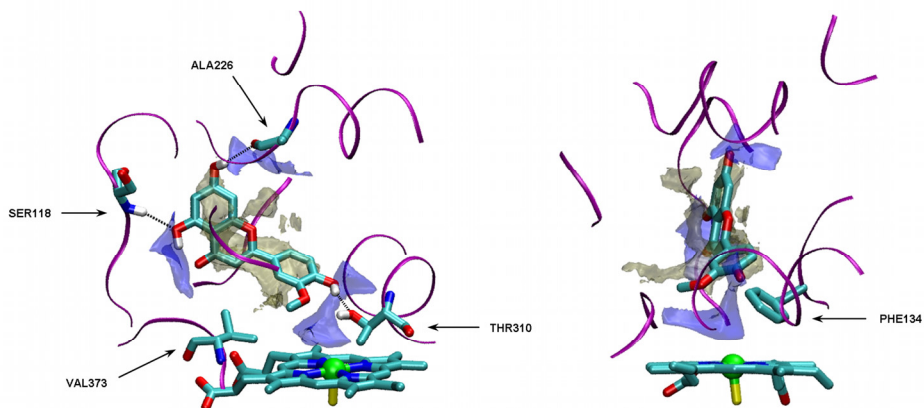


Figure 3.8. Docked pose of 5,7,4'-trihydroxy-3'-methoxyflavone **3.5**. MIF isosurfaces for the probes DRY (hydrophobic) and OH (aromatic hydroxyl group) are shown at an energy level of -0.4 kcal/mol (brown) and -7.0 kcal/mol (blue), respectively. Val 373 is displayed on the left, and dashed lines are drawn between the molecule and the residues involved in hydrogen bonding. Phe 134 is displayed on the right. This figure was created using the program VMD.¹¹⁷

Cyanidin **3.18** and malvidin-3-O-glucoside **3.19** form quinoidal bases at pH 7.5 due to double bond conjugation (**Figure 3.9**) and hydroxyl groups at positions C5, C7, and C4'.^{379;380} Therefore, the three different resonance forms were conformationally analyzed and docked. Docking results with malvidin-3-O-glucoside **3.19** agree with the experimental data, as the EBE obtained is higher than the most active compounds. Detailed analysis of the EBE contributions revealed a large steric penalty due to close contacts between the molecule and active site residues, namely Phe 134, Val 373, Met 374 and Leu 477 (**Figure 3.10**). These contacts are related to the low flexibility of this molecule and the presence of two bulky groups, a dimethoxy hydroxyphenyl group and a glucose moiety, linked at adjacent

positions. This Y-shaped rigid structure does not fit well in the active core of the enzyme.

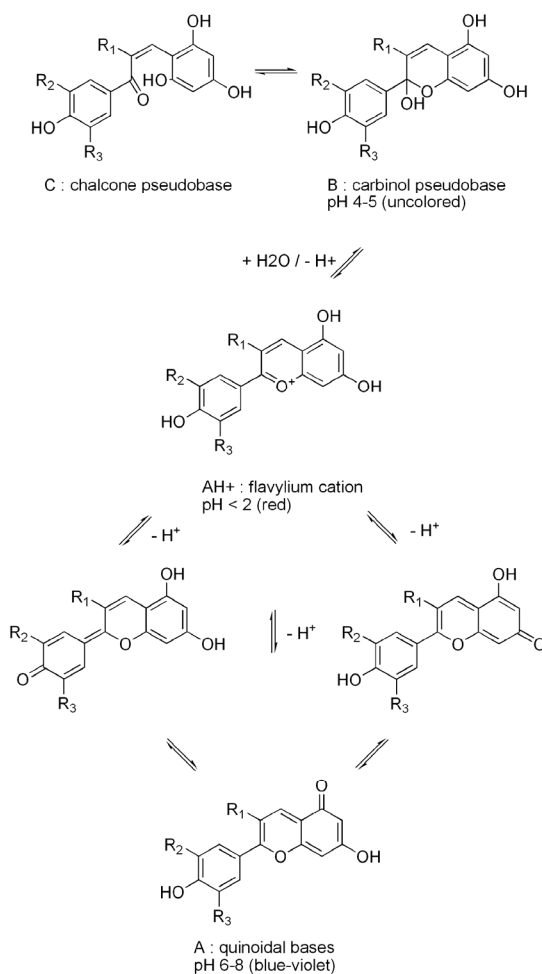


Figure 3.9. Structural transformations of anthocyanins in acidic aqueous solution. The flavylium cation (AH⁺; red) undergoes deprotonation to give the quinoidal bases (A; blue-violet) or hydration to give the carbinol pseudobase (B; uncolored). Tautomerism is responsible for the conversion of the latter in chalcone (C; uncolored). R₁= glycosyl and R₂ = R₃ = OCH₃ for malvidin-3-O-glucoside and R₁ = R₂ = R₃ = OH for cyanidin. This figure was adapted from literature.³⁸⁰

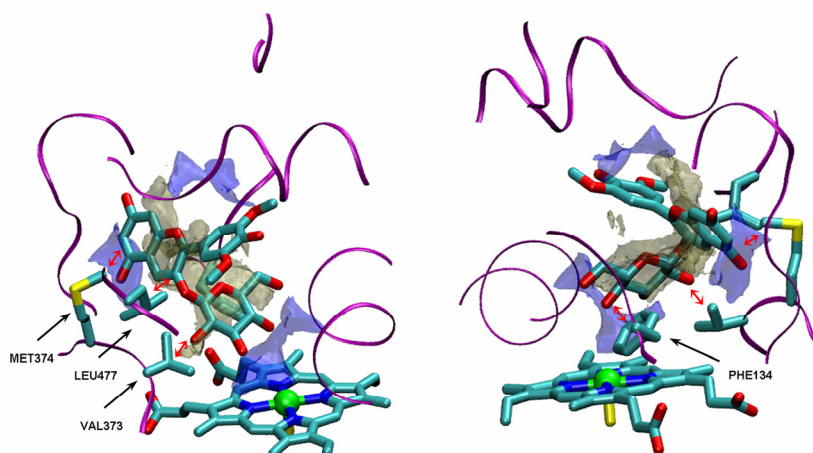


Figure 3.10. Docked pose of the malvidin-3-O-glucoside **3.19**. MIF isosurfaces for the probes DRY (hydrophobic) and OH (aromatic hydroxyl group) are shown at an energy level of -0.4 kcal/mol (brown) and -7.0 kcal/mol (blue), respectively. Red arrows sign steric clashes with active site residues. This figure was created using the program VMD.¹¹⁷

Despite the large molecular volume of oleuropein **3.25**, several rotatable bonds connecting the phenol moiety to the heterocyclic ring are determinant to a good fit within the aromatase active site. The docked molecule reveals that the glucose lies at the bottom of hydrophilic zone 3, close to the heme group, which allows anchoring of the phenol moiety at the top of the same area (**Figure 3.11**, left side). The two remaining hydrophilic areas are occupied by carboxyl groups. Therefore, superimposition of oleuropein **3.25** with 5,7,4'-trihydroxy-3'-methoxyflavone **3.5** in the active site conformation predicted with GLUE³³³ makes it clear that although apparently different, these two molecules share structural and pharmacophoric features (**Figure 3.12**). The heterocyclic carboxyl group lies in an intermediate position between the flavone 4-oxo and the C5 hydroxyl groups. The carboxyl group in the phenol heterocyclic linker lies close to the flavone C7 hydroxyl group, and both the sugar and the phenol point in the same direction of the flavone ring B. The length of both molecules is very similar

and the hydrophobic scaffolds are well overlapped. Different binding modes of the flexible molecule **3.25** could also be hypothesized in which a dynamic fitting of the substrate and the receptor lead to conformational changes that eventually determine a complex in which the sugar moiety is exposed to the solvent. P450 enzymes have actually been shown to undergo conformational changes upon substrate binding, characterized by the opening of solvent access channels.^{381;382} Moving the hydrophilic glucose moiety to a different orientation might determine a different energetically favorable binding configuration represented by an open conformation with a solvent-exposed sugar moiety. This hypothesis cannot be ruled out at this stage of calculations. It should be confirmed, however, with the use of molecular dynamics simulations allowing the full flexibility of the whole system, which were outside of the scopes of this work.

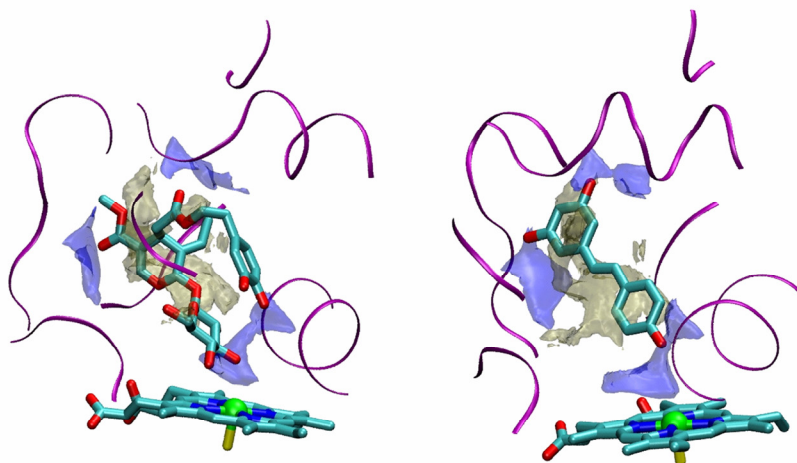


Figure 3.11. Docked pose of oleuropein (compound **3.25**, left) and *trans*-resveratrol (compound **3.24**, right). MIF isosurfaces for the probes DRY (hydrophobic) and OH (aromatic hydroxyl group) are shown at an energy level of -0.4 kcal/mol (brown) and -7.0 kcal/mol (blue), respectively. This figure was created using the program VMD.¹¹⁷

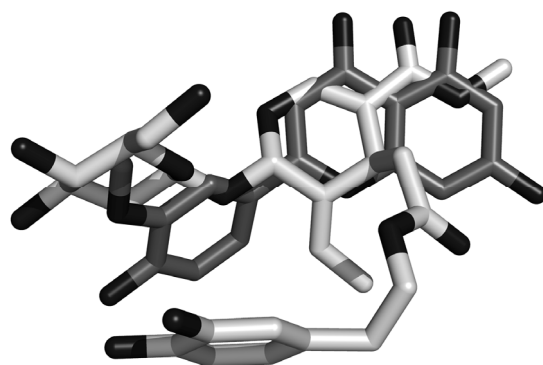


Figure 3.12. Predicted superimposition of 5,7,4'-trihydroxy-3'-methoxyflavone (compound **3.5**, dark-gray C atoms) and oleuropein (compound **3.25**, white C atoms) in the active site of the aromatase model. Oxygen atoms are represented in black. This figure was created using the program VMD.¹¹⁷

6,7-Dihydroxycoumarin **3.20** (**Figure 3.13**) aligns well in the same hydrophobic region as the other polyphenolic compounds. However, this short scaffold fails to put all hydroxyl groups in the vicinity of the hydrophilic areas. Together with the decreased hydrophobicity, this explains the experimentally observed low anti-aromatase potency and the higher EBE.

trans-Resveratrol **3.24**, a strong AI, had an unfavorable EBE compared to the other active molecules. Because this molecule docks within the active site, perfectly aligned with the hydrophobic region, with three hydroxyl groups oriented toward polar regions (**Figure 3.11**, right side), the EBE value is related to the lower hydrophobicity of the stilbene scaffold and the absence of the 4-oxo group. However, this is well balanced by a perfect planar conformation and a good disposition of the phenyl and hydroxyl groups, increasing the strength of the interaction. Superimposition of resveratrol **3.24** and the strongest flavone inhibitor **3.5** in the active site docked conformation shows a good pharmacophoric alignment between these two molecules (**Figure 3.14**). This simple molecule therefore gives

important information about the molecular determinants for the binding of polyphenolic inhibitors to the aromatase active site.

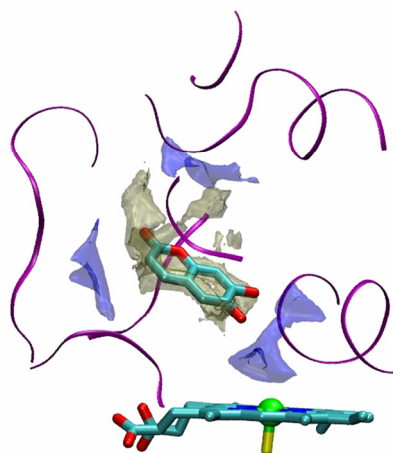


Figure 3.13. Docked pose of the 6,7-dihydroxycoumarin **3.20**. MIF isosurfaces for the probes DRY (hydrophobic) and OH (aromatic hydroxyl group) are shown at an energy level of -0.4 kcal/mol (brown) and -7.0 kcal/mol (blue), respectively. This figure was created using the program VMD.¹¹⁷

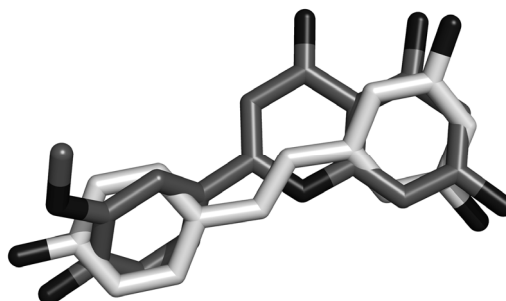


Figure 3.14. Predicted superimposition of 5,7,4'-trihydroxy-3'-methoxyflavone (compound **3.5**, dark-gray C atoms) and *trans*-resveratrol (compound **3.24**, white C atoms) in the active site of the aromatase model. Oxygen atoms are represented in black. This figure was created using the program VMD.¹¹⁷

In summary, the anti-aromatase activity of a set of natural polyphenolic compounds was rationalized through the combination of experimental data and molecular modelling. In the absence of an experimental 3D structure of the enzyme, a virtual receptor site was defined and validated. The binding site cavity of the enzyme is expected to be strongly hydrophobic. Three hydrophilic regions were predicted based on the models and linked to the presence of the hydroxyl functions at C5, C7 and C4' found in the strongest inhibitors tested. The C3' position was shown to be tolerant of bulky substituents, protruding towards a pocket near the active site. Docking of the compounds into a 3D structure of aromatase based on homology modelling is positively consistent with the results reported above. The docking experiments were able to distinguish between active and inactive molecules, and could define a common binding mode for all compounds in the study.

3.4. Conclusions

In the study reported herein, the anti-aromatase potency of a set of 25 polyphenols was tested. Strong inhibitors, compounds **3.1**, **3.3**, **3.5**, **3.6**, **3.13**, **3.14**, and **3.16**, with equal or better activity than the reference compound, aminoglutethimide ($IC_{50}=10\ \mu\text{M}$), were identified. All these molecules are flavone or flavanone derivatives, which confirms the potential of natural polyphenols for lead optimization into strong aromatase inhibitors. Flavone hydroxylation at position C7 of ring A proved to be determinant for good anti-aromatase potency, as well as the double hydroxylation at C5 and C7. Further improvement by C4' hydroxylation and either C3' hydroxylation or methoxylation on ring B, as with compounds **3.3** and **3.5**, was observed. Flavanones gave results in good agreement with the rules described above and led to the identification of compound **3.14**, the best aromatase inhibitor studied.

The 3D-QSAR study performed with the subset of flavones explained the variance of the data and showed a good predictive ability, even with the use of a less conservative cross-validation procedure with three random groups. The use of GRIND³³⁴ descriptors calculated with the GRID force field and extracted from relevant MIFs (hydrophobicity, hydrogen bonding and molecular shape) was a valid strategy to characterize a virtual receptor site and gain further insight into the molecular environment surrounding polyphenol inhibitors on the aromatase active site. Variables with a direct high impact on the inhibitory activity (**Figure 3.4**) defined a putative virtual receptor site (**Figure 3.6**): two hydrogen bond acceptor regions are expected to be close to C5 and C7 of flavone ring A, and a hydrogen bond donor/acceptor area close to C4' of ring B. C3' was found to be permissive to bulky substitutions, allowing good shape complementarity with the active site. A hydrophobic scaffold is common to all flavones and a 4-oxo group should also be important for binding.

Analysis of an aromatase homology model with molecular interaction probes that account for hydrophobicity and hydrogen bonding agreed with the virtual receptor site and showed a large hydrophobic region within the active site surrounded by three hydrogen bond donor/acceptor regions (**Figure 3.7**). Docking calculations with the GLUE³³³ software aligned the inhibitors under study on the hydrophobic plane, with polar groups correctly oriented to the hydrophilic areas (**Figure 3.8**). Therefore, hydroxylations at C5, C7 and C4' strengthens the affinity for the active site and increases the anti-aromatase potency. The binding cavity is large enough to accommodate most of the compounds studied without steric clashes, and it was found that Val 373 might be responsible for a better shape complementarity between bulky substitutions at flavone C3' and aromatase.

The higher EBE calculated for coumarins agreed with their weak anti-aromatase potency, and the docked poses confirmed that the benzopyrone

hydrophobic scaffold is too short for a strong interaction with the active site of the enzyme (**Figure 3.13**). Extension of this scaffold with apolar groups might increase the hydrophobicity and lead to strong AIs, as shown recently.²⁶⁵

The simple and conformationally restrained *trans*-resveratrol **3.24** was another strong AI tested ($IC_{50}=13\ \mu\text{M}$). Despite the absence of the 4-oxo group found in flavones and flavanones, the two aromatic rings and the three hydrogen bond donor/acceptor groups agreed with the virtual receptor site and the MIFs calculated on the active site model (**Figure 3.11**, right side), leading to an increase in binding strength to aromatase.

Herein we found that oleuropein **3.25**, the major polyphenolic constituent of olive oil is a good aromatase inhibitor,²²³ with an IC_{50} value of $27\ \mu\text{M}$. This strong inhibitory potency was rationalized based on a proper pharmacophoric superimposition with the best flavone inhibitor tested (compound **3.5**, **Figure 3.12**). A good fit was found within the hydrophilic/hydrophobic regions of the aromatase active site without steric clashes. The flexibility introduced by the ethyl acetate chain that connects the catechol to the glycosylated heterocyclic moiety is determinant for the adoption of an U-shaped conformation that fits well within the active site (**Figure 3.11**, left side). In contrast, the strong conformational barriers of malvidin-3-O-glucoside **3.19** do not allow a suitable conformation. Our docking protocol, with an extensive conformational search of flexible molecules and the use of adequate MIFs calculated with GLUE,³³³ is therefore a valid method to perform docking and molecular superimposition at the active site of a macromolecular target.

In conclusion, we have described a new methodology that combines biochemical evaluation, 3D-QSAR with alignment-independent descriptors and screening for energetically favorable binding sites for the rationalization of the anti-aromatase activity of a set of diverse natural polyphenolic

compounds. Starting from experimentally determined inhibitory profiles, our approach provided novel insights into the chemical and steric environment within the active site of aromatase and on the essential determinants for binding of polyphenolic inhibitors. Based on this information, a virtual receptor site was built, and a possible common binding mode was proposed. This was further corroborated by comparison with the results of docking experiments into a 3D homology model of aromatase. The good agreement between experimental and predicted activity, and between the properties of the virtual receptor model and the 3D homology model suggests that this approach could be extended to other cases for which the structure of the receptor is unknown. The virtual receptor site model might be used to perform 3D database searching and molecular design of new strong aromatase inhibitors.

3.5. Materials and methods

3.5.1. Materials and general methods.

See **Section 2.5.1.**

7-Hydroxyflavone, 5,7,4'-trihydroxy-3'-methoxyflavone, 5,7,4'-trihydroxyflavone, 3',4'-dihydroxyflavone, 5,7,3'-trihydroxy-4'-methoxyflavone, flavanone, 7-hydroxyflavanone, 5,7-dihydroxyflavanone, 5,7,3',4'-tetrahydroxyflavanone, 5,7,4'-trihydroxy-3'-methoxyflavanone, cyanidin chloride, resveratrol and oleuropein were purchased from Extrasynthese (Genay, France). Flavone, 5,7-dihydroxyflavone, 7,3',4'-trihydroxyflavone, 5,7,3',4'-tetrahydroxyflavone, 7,3',4',5'-tetrahydroxyflavone, 4'-hydroxy-3'-methoxyflavone, 3',4'-dimethoxyflavone, 6,7-dimethoxycoumarin, 6,7-dihydroxycoumarin, 7-hydroxy-6-methoxycoumarin and 6-hydroxy-7-methoxycoumarin were purchased from Indofine Chemical (Hillsborough, NJ, USA).

Malvidin-3-O-glucoside was obtained from Polyphenols (Hanaveien, Norway).

3.5.2. Enzymatic preparation

See **Section 2.5.2**.

3.5.3. Concentration-response study

See **Section 2.5.3**.

Incubations were performed at 37 °C in a medium containing 67 mM sodium phosphate, pH 7.5, [1β - ^3H]-androstenedione (6.6×10^5 dpm / 24 nM) and 270 μM NADPH. The potential inhibitors were dissolved in DMSO and added to the assay in at least 8 concentrations ranging from 316.2 nM to 640 μM .

3.5.4. Conformational search and geometry optimization

Three-dimensional models of the compounds in study were constructed and optimized as described in **Section 2.5.5**, using the MMFF³¹⁴ and a water-generalized Born equation/surface area continuum solvation.³¹⁹ 30000 conformations were generated during the conformational analysis of malvidin-3-O-glucoside **3.19** and oleuropein **3.25**. A maximum of 3000 conformations were generated for all other compounds.

3.5.5. 3D-QSAR using ALMOND

GRIND descriptors³³⁴ were calculated with ALMOND³³³ v3.3 using MIFs³³² computed with the chemical probes DRY (hydrophobic probe), O (hydrogen bond acceptor interactions) and N1 (hydrogen bond donor interactions), and the molecular shape probe TIP,³⁴⁰ with the grid spacing set to 0.5 Å. These descriptors encode geometrical relationships between pairs of non-bonded interactions, therefore, to represent only the highly favorable interactions,

one initial filtering step was performed, and 100 low-energy interaction points, separated from each other as much as possible, were extracted from each MIF. To this step, the relative importance of the field values was set to 50, and all other settings were set to default. Finally, the filtered MIFs were encoded into GRIND variables through a maximum auto and cross-covariance transformation performed with the width of the smoothing window set to 0.8. These variables represent the product of MIF energy node pairs separated by a certain distance around each molecule.

3.5.6. Statistical analysis

PLS was used to derive the 3D-QSAR model with the statistical tools included in ALMOND. No scaling was applied to the variables. The optimal dimensionality of the model was selected by cross-validation using either LOO or 3RG, recalculating the weights in both cases. The random groups validation was repeated 200 times to get a stable predictive correlation coefficient. The fractional factorial design,³⁴¹ a variable selection methodology implemented in ALMOND, allowed the removal of descriptors not correlated with activity, introducing only noise to the model. Uncertain variables were kept. The FFD was forced to “fold over”, and the combinations/variables ratio was set to 5 in order to better estimate the effect of each variable in the model predictive ability. The model noise level was evaluated by 20% of “dummy variables”.

3.5.7. Active site MIF calculations

GREATER, the graphical user interface for the GRID v22a package of programs,³³³ was used to calculate MIFs with the probes DRY (hydrophobic) and OH (aromatic hydroxyl group) on the active site of a homology model of aromatase (PDB entry 1TQA from the theoretical model section).¹⁴⁰ The protein was considered rigid and a grid box was built within the active site,

including the heme group and all interacting residues. This resulted in a cubic box of 8000 Å³ (20 Å × 20 Å × 20 Å) centered at the aromatase binding cavity and containing the heme group at the bottom. The MIFs were calculated with the grid spacing set to 0.25 Å and the directive ALMD set to 1.

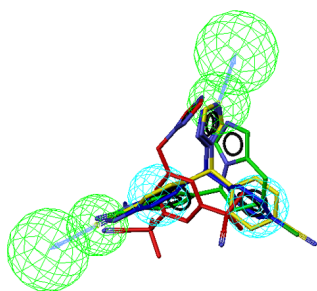
3.5.8. Binding mode prediction

GLUE³³³ v1.0 is a docking program that uses the GRID MIFs to generate ligand poses within the active site of a macromolecular target and the GRID force field to calculate binding energies. The aromatase binding cavity was initially explored with eight GRID probes that mimic most of the chemical groups present in the ligands: H2O (recognizes hydrophilic regions and evaluates competition with water molecules), DRY (recognizes hydrophobic regions), H (evaluates the protein shape), N1 (hydrogen bond donor to evaluate hydrogen bond acceptor groups), O (hydrogen bond acceptor to evaluate hydrogen bond donor groups), O:: (partially charged carboxylate to evaluate positively charged regions), N+ (positively charged nitrogen to evaluate negatively charged regions) and O1 (donor/acceptor probe to evaluate mixed groups). The MIFs obtained from the interaction of these probes with the active site were calculated in the same cubic box as described previously. Local energy minima extracted from the DRY, N1, O, O::, N+ and O1 MIFs were combined into a large number of pharmacophoric quadruplets. For this step the distance tolerance was set to 2.5 and the cavity expansion was set to 5 in order to maximize the number of combinations saved, available to the next steps. This large number of possible alignments was then filtered through comparison with the inhibitors in study, with the steric tolerance set to 1. When the number of rotatable bonds was three or fewer, several conformers were generated. When greater, a more refined conformational search was performed with MACROMODEL³⁷⁶ v8.1, and conformations found within an energy window

of 15 kJ/mol from the global minimum were submitted to GLUE.³³³ Both R and S flavanone stereoisomers were considered and all cyanidin **3.18** and malvidine-3-O-glucoside **3.19** equilibrium quinoidal bases were studied independently (**Figure 3.9**). The filtered pharmacophoric quadruplets were then docked within the active site of aromatase. Redundancy was avoided with a minimum RMSD set to 2 Å, and a maximum of 2000 minimization iterations were allowed in order to relax the ligands in the binding pocket. The GLUE scoring function was then applied to the binding poses, with contributions for steric repulsion, hydrogen bonding and hydrophobicity. Top-ranked orientations were extracted and further analyzed.

IV

Pharmacophore modelling, virtual screening and biochemical evaluation of new potent aromatase inhibitors



A fast and efficient ligand-based virtual screening strategy for potent aromatase inhibitors is proposed in this chapter. The procedure is based on pharmacophore models of three distinct classes of CYP19 inhibitors, namely azol non-steroid, steroid and polyphenol compounds. New potent aromatase inhibitors were found by biochemical evaluation of the most promising hits selected from the NCI database.

Marco A. C. Neves, Teresa C. P. Dinis, Giorgio Colombo, M. Luisa Sá e Melo. Fast 3D-pharmacophore virtual screening of new potent non-steroid aromatase inhibitors. *Journal of Medicinal Chemistry*, accepted (Nov 2008).

New potent non-steroid aromatase inhibitors, Provisional US Patent 39014/08.

Marco A. C. Neves, Teresa C. P. Dinis, Giorgio Colombo, M. Luisa Sá e Melo. A ligand-based strategy to identify new aromatase inhibitors. Submitted.

4.1. Abstract

Suppression of estrogen biosynthesis by aromatase inhibition is an effective approach for the treatment of hormone sensitive breast cancer. Third generation non-steroid aromatase inhibitors have shown important benefits in recent clinical trials with postmenopausal women. Furthermore, aromatase inhibition is also achieved with compounds structurally related to either the substrate or the product of the enzyme catalysis. C6-Substituted androstenedione derivatives and natural polyphenols, for example, are potent aromatase inhibitors. In this study we have developed a new ligand-based strategy combining important pharmacophoric, shape and structural features, according to the postulated aromatase binding mode, useful for the virtual screening of new potent aromatase inhibitors. Small subsets of promising drug candidates were identified from the large National Cancer Institute database and their anti-aromatase activities were assessed on an *in vitro* biochemical assay with aromatase extracted from human term placenta. New potent aromatase inhibitors were discovered, active in the low nanomolar range, and a common binding mode was proposed using a homology model of the enzyme. Considering the lack of a crystal structure for CYP19, this ligand-based method can be viewed as an important tool for the virtual screening of new aromatase inhibitors.

4.2. Introduction

The low sequence identity between members of different P450 families limits the use of the available aromatase homology models in structure-based virtual screening. An alternative strategy for the rational design of new aromatase inhibitors relies on ligand-based virtual screening that can be developed based on the vast information on strong aromatase inhibitors published in the literature. Pharmacophore-based approaches have been used for both steroid and non-steroid aromatase inhibitors, highlighting

important physicochemical features and guiding the design of new potent compounds.^{258;383-385} However, to date, only a few attempts to perform virtual screening based on such models have been performed. Langer and coworkers, for instance, have carried out a mixed qualitative and quantitative approach for non-steroid aromatase inhibitors, using the HipHop and HypoRefine algorithms of the Catalyst software.³⁸⁶ The final pharmacophore model proposed by this group consisted of one aromatic ring feature, one hydrophobic group, two hydrogen bond acceptors and one excluded volume sphere. Two possible anti-aromatase candidates were identified based on this approach, one of the compounds able to decrease in 68% the activity of the enzyme at 36 μM and the other in 15% at the same concentration.³⁸⁶

In the previous chapter we have underlined important pharmacophoric features to the anti-aromatase activity of natural polyphenols. 7-Hydroxyflavone proved to be a potent inhibitor and an interesting lead to the design of new anti-aromatase compounds. This information was summarized in the present work into a ligand-based strategy for fast *in silico* screening of new aromatase inhibitors. A similar approach was applied to compounds from structurally different classes of aromatase inhibitors, such as non-steroid nitrogen-containing heterocyclic compounds and C6-substituted androstenedione derivatives.

Starting from sets of potent anti-aromatase compounds, new pharmacophore models, recapitulating essential structural and functional features linked to activity, were built. The models combined information about the common pharmacophore features, binding to the aromatase active site, steric restrictions and “drug-likeness” filters.

The large National Cancer Institute (NCI) compound database was screened using this methodology and new potent aromatase inhibitors were identified. Several compounds have *in vitro* activity comparable to second

and third generation anti-aromatase agents. One of these was able to inactivate the enzyme in a mechanism-based manner. The most active molecules derived from the non-steroid set were docked on the active site of an aromatase homology model and these results were compared with the initial pharmacophore model. The similarities between one of the strong CYP19 inhibitors and androstenedione were explored based on quantum chemistry calculations.

4.3. Results and discussion

4.3.1. 3D-pharmacophore modelling

4.3.1.1. Pharmacophore model based on non-steroid inhibitors

Several non-steroid AIs have been used for the treatment of breast cancer in postmenopausal women with clinical efficacy.⁶ Having progressed through a pre-clinical development and clinical trials, these compounds are expected to include information about strong anti-aromatase potency and selectivity. In this model, we have built a training set with low energy conformations of second and third generation AIs, namely, anastrozole, letrozole, fadrozole and vorozole (**Figure 4.1A**) and used these molecules to generate a common-features pharmacophore model with the HipHop³⁸⁷ algorithm of the Catalyst software.³⁸⁸ Briefly, the program evaluates chemical features common to a set of active compounds and generates hypotheses for their activity. These hypotheses are spatial dispositions of pharmacophoric points, providing the compounds' relative alignment in the binding site of the enzyme. Each point accounts for an important chemical feature such as hydrogen bond donors/acceptors, hydrophobic groups, negative/positive ionizable groups and aromatic groups. Basic physicochemical features of known anti-aromatase compounds include a high degree of hydrophobicity and the potential to act as hydrogen bond

acceptors.²⁰¹ Therefore, hydrophobic (HYD) and hydrogen bond acceptor (HBA) pharmacophoric features were used in this model. The program found six possible alignment solutions displaying three or four pharmacophoric points. The first two top ranked solutions, NAI-HYP1 (rank=31.9) and NAI-HYP2 (rank=29.8), had four features, two hydrophobic groups and two hydrogen bond acceptors. Analysis of the training set molecules aligned to these hypotheses revealed overlapping imidazole and triazole groups in NAI-HYP2 but not in NAI-HYP1, with one nitrogen atom acting as hydrogen bond acceptor (HBA1, **Figure 4.1B**). This property of NAI-HYP2 reflects the binding mechanism found for this type of molecules, which entails binding through heterocyclic aromatic coordination to the heme iron of the P450 active site.¹⁹⁵ Therefore NAI-HYP2 was chosen for the subsequent steps. The second hydrogen bond acceptor feature (HBA2, **Figure 4.1B**) matches either a cyano group (anastrozole, letrozole and fadrozole) or the N2-atom of a methylbenzotriazole (vorozole), and the hydrophobic features superimpose with phenyl rings of all the molecules (HYD1, **Figure 4.1B**), a methyl group of anastrozole or the piperidine moiety of fadrozole (HYD2, **Figure 4.1B**).

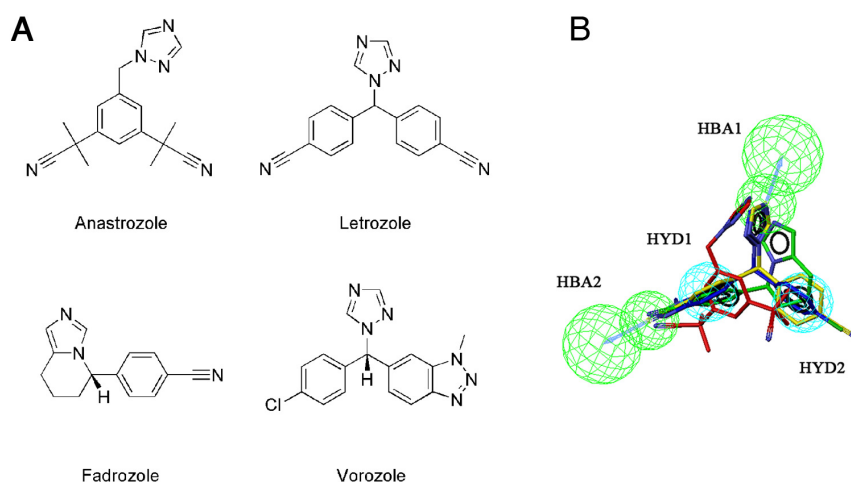


Figure 4.1. A) Training set of azole non-steroid AIs used for the common-features (HipHop) pharmacophore model generation. **B)** Common-features (Catalyst/HipHop) pharmacophore model of azole non-steroid AIs. The NAI-HYP2 pharmacophoric query had four features: two hydrogen bond acceptors (HBA1 and HBA2, green) and two hydrophobic groups (HYD1 and HYD2, cyan). The training set AIs (anastrozole, red C atoms; letrozole, yellow C atoms; fadrozole, green C atoms and vorozole, blue C atoms) are represented at the best fit alignment to the model. This figure was created using the program Catalyst.³⁸⁸

Pharmacophore models with a small number of points tend to be unspecific and return a large number of hits when used to screen large databases. In particular, hydrophobic and hydrogen bond acceptor features match a large number of chemical groups increasing the number of false positives. Therefore, in an attempt to increase the specificity of NAI-HYP2, the HBA1 feature was substituted with new fragment/function pharmacophoric features: the C5-N-HBA and the C6-N-HBA features (**Figure 4.2**). C5-N-HBA matches hydrogen bond acceptors only if present in certain types of five-membered nitrogen-containing heterocyclic rings (imidazole, 1,2,4-triazole, 1,2,3-triazole and tetrazole), whereas C6-N-HBA matches acceptors from six-membered nitrogen-containing heterocyclic rings

(pyridine, pyridazine, pyrimidine and pyrazine). The modified pharmacophore model was designated NAI-HYP2-HBA.

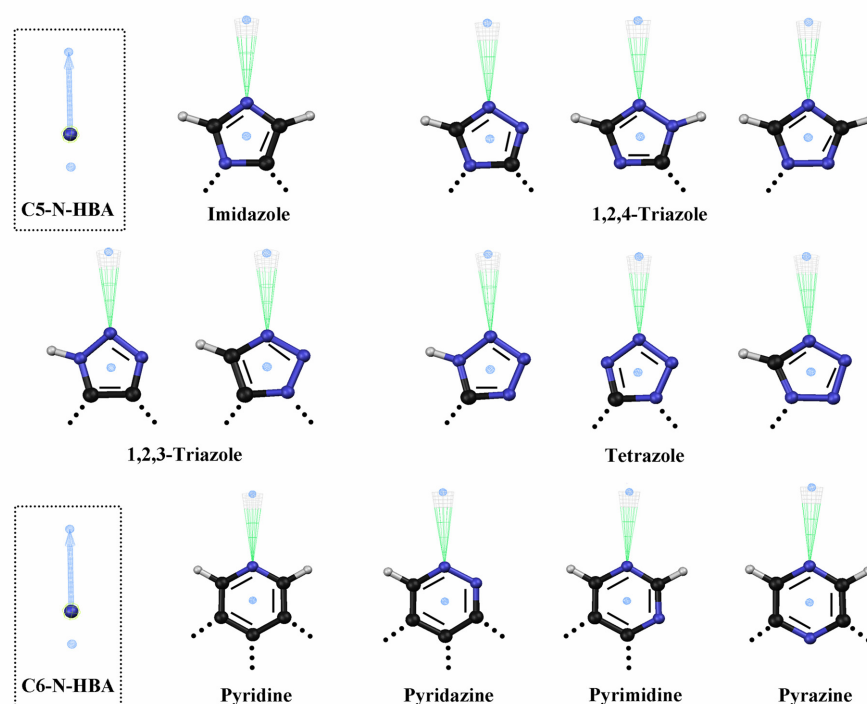


Figure 4.2. C5-N-HBA and C6-N-HBA fragment/function pharmacophore features. Imidazole, 1,2,4-triazole, 1,2,3-triazole and tetrazole rings were combined into a single fragment feature using the centroids of the five-membered ring moieties. Pyridine, pyridazine, pyrimidine and pyrazine rings were combined into another fragment feature using the centroids of the six-membered ring moieties. Possible anchoring points to the rest of the molecule are represented with dotted lines. The nitrogen atom distal to these points defined a hydrogen bond acceptor and the projected point, the position in space from which the participating hydrogen (or the heme iron) will extend. These positions are connected by a vector which indicates the direction from the heavy atom to the projected point of the hydrogen bond (C, black; N, blue; H, white). This figure was created using the program Catalyst.³⁸⁸

Cytochrome P450 enzymes have an inner binding pocket with well defined volume, accessible from the outside by several channels.³⁸⁹ Therefore, besides the physicochemical properties of the inhibitor, molecular shape is expected to be extremely important to the access and fit within the aromatase active site. Most aromatase inhibitors used to build the common-features model have a similar shape which is expected to be complementary to the volume of the aromatase active site. The shape of letrozole, a quite rigid third generation inhibitor with high degree of symmetry, was therefore converted into a set of inclusion volumes and combined with the pharmacophoric query.

Therefore, the final pharmacophore model (NAI-HYP2-HBA+Shape) combined pharmacophoric information (two hydrogen bond acceptors and two hydrophobic groups) with fragment information (nitrogen-containing aromatic heterocycles) and steric restrictions. All aromatase inhibitors used on the training set matched the final hypothesis with best fit values ranging from 2.98 to the maximum value of 4.00 (letrozole=4.00, vorozole=3.46, anastrozole=3.40 and fadrozole=2.98).

To validate the new pharmacophore model, a test set with 82 non-steroid AIs collected from the literature was built (**Appendix A**).^{202;203;219;258-260;390} Each molecule contained a five- or six-membered aromatic heterocyclic ring able to coordinate with the aromatase heme iron. The initial pharmacophore model (NAI-HYP2) returned 58 molecules (71% of the database, **Table 4.1**). The pharmacophore modified to match acceptors from five- or six-membered nitrogen-containing heterocyclic rings (NAI-HYP2-HBA) returned 40 molecules (49% of the database). Using the inclusion volumes (NAI-HYP2-HBA+Shape) 26 molecules were retrieved (35% of the database). The final sub-set was enriched with the most potent aromatase inhibitors. These results demonstrate that the NAI-HYP2-HBA+Shape pharmacophore

model is able to identify not only inhibitors from the training set, but also potent non-steroid AIs with different structures.

Table 4.1. Screening results on a literature database^{202;203;219;258-260;390} with non-steroid AIs (model validation).

Hypothesis	Literature database
NAI-HYP2	58
NAI-HYP2-HBA ^[a]	40
NAI-HYP2-HBA+Shape ^[b]	26
Post-processing filtering ^[c]	26

[a] Modified NAI-HYP2 to match acceptors from five- or six-membered nitrogen-containing heterocyclic rings.

[b] Letrozole was converted into a shape query and combined with the NAI-HYP2-HBA hypothesis.

[c] Filters applied: Lipinski Rule of Five, rotatable bonds ≤ 7 , PSA ≤ 150 .

4.3.1.2. Pharmacophore model based on C6-substituted steroids

Androstenedione derivatives are among the most potent AIs found to date. In particular, it has been postulated that *n*-alkyl and phenylaliphatic groups linked at the position C6 increase the anti-aromatase activity due to the presence of a hydrophobic cavity at the enzyme binding site. In this sense, we have used a training set of potent C6-substituted androstenedione derivatives reported in the literature¹⁶⁹⁻¹⁷² (**Figure 4.3A**), namely, 6 β -ethylandrosta-1,4-diene-3,17-dione (**4.1**), 6-ethylandrosta-1,4,6-triene-3,17-dione (**4.2**), 6-*n*-propylandrosta-1,4,6-triene-3,17-dione (**4.3**), 6-benzylandrosta-4,6-diene-3,17-dione (**4.4**), 6 α -phenethylandrosta-4-ene-3,17-dione (**4.5**) and 6-phenethylandrosta-1,4,6-triene-3,17-dione (**4.6**), to derive a common-features pharmacophore model using the HipHop³⁸⁷ algorithm of the Catalyst software.³⁸⁸ For this type of compounds, hydrogen bond acceptor groups and hydrophobic groups were used. Besides its strong

potency, this training set of molecules was chosen in order to account for the effect of different lengths, shapes and volumes of the hydrophobic moiety at C6, as well as its stereochemistry in relation to the steroid framework.

Ten different pharmacophore hypotheses were generated with 4 or 5 pharmacophore features and scores ranging from 54 to 66. The top ranked solutions had two hydrogen bond acceptor groups and three hydrophobic moieties, whereas less ranked solutions had only two acceptors and two hydrophobic groups. Visual inspection of the training set molecules aligned to the top ranked solution, SAI-HYP1 (**Figure 4.3B**), revealed that the hydrogen bond acceptor groups matched the 3-oxo (HBA1) and the 17-oxo (HBA2) groups. One of the hydrophobic features, HYD1, superimposes with the 19-methyl and the A-B ring junction, HYD2 matches ring C and the 18-methyl, and the third apolar feature, HYD3, is related to the hydrophobic moiety linked at C6. Due to the rigid nature of the steroid scaffold, most of the common-feature solutions were very similar to the top ranked pharmacophore model, with slight differences on the projection vectors of HBA1 and HBA2 (the location of a hypothetical hydrogen bond donor) and the location of HYD3. The top ranked solution was therefore selected for the following steps.

Inclusion volumes based on the shape compound **4.5** were applied to SAI-HYP1, and the steric tolerance was adjusted to allow good shape complementarity with the training set molecules.

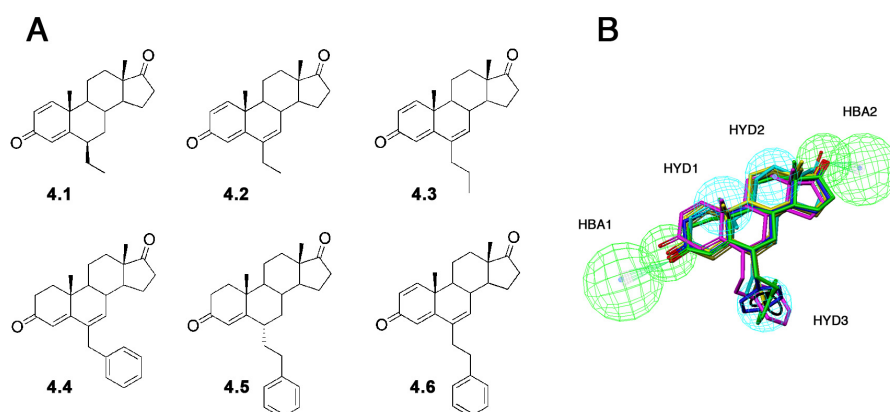


Figure 4.3. **A)** Training set of C6-substituted steroid AIs¹⁶⁹⁻¹⁷² used for the common-features pharmacophore model generation. **B)** Common-features pharmacophore model of C6-substituted steroid AIs.¹⁶⁹⁻¹⁷² The SAI-HYP1 pharmacophoric query had five features: two hydrogen bond acceptors (HBA1 and HBA2, green) and three hydrophobic groups (HYD1, HYD2 and HYD3, cyan). The training set inhibitors (**4.1**, cyan C atoms, **4.2**, brown C atoms, **4.3**, yellow C atoms, **4.4**, blue C atoms, **4.5**, green C atoms, **4.6**, purple C atoms) are represented at the best fit alignment to the model. This figure was created using the program Catalyst.³⁸⁸

4.3.1.3. Pharmacophore model based on polyphenols

As discussed in the previous chapter, 7-hydroxyflavone, **3.6**, (**Figure 4.4A**) is a simple polyphenol with strong anti-aromatase properties and potential for lead optimization. In this model we have used this molecule to build a new pharmacophore hypothesis (PAI-HYP) combining a set of pharmacophoric features expected to account for important binding determinants of this class of inhibitors. Two aromatic rings were included in the pharmacophore model (**Figure 4.4B**), matching the ring B (AR1) and the ring A (AR2), as well as one hydrogen bond acceptor to match the 4-oxo group (HBA), one hydrogen bond donor for the 7-hydroxyl (HBD) and one hydrophobic group located at the ring B (HYD). The model was validated

using a test set of polyphenol AIs (**Figure 4.4A**), namely the 5,7-dihydroxyflavone (**3.1**), 5,7,3',4'-tetrahydroxyflavone (**3.3**), 5,7,4'-trihydroxy-3'-methoxyflavone (**3.5**), and the *trans*-resveratrol (**3.24**). All molecules were identified as hits by the pharmacophore hypothesis (**Figure 4.4B**).

Inclusion volumes based on the shape of compound **3.6** were applied to PAI-HYP, and the steric tolerance was adjusted to allow good shape complementarity with the test set molecules.

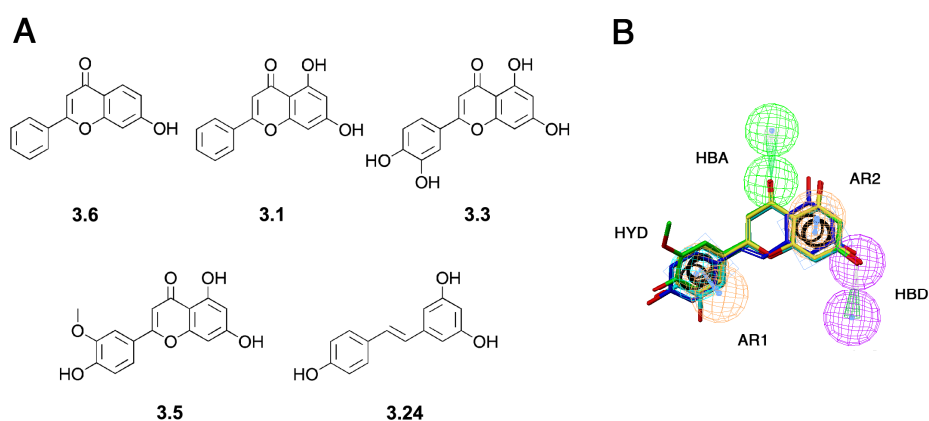


Figure 4.4. **A)** Polyphenol AIs used for the pharmacophore model generation and validation. **B)** Pharmacophore model of polyphenol AIs. The PAI-HYP pharmacophoric query had five features: one hydrogen bond acceptor (HBA, green), one hydrogen bond donor (HBD, purple), two aromatic rings (AR1 and AR2, orange) and one hydrophobic group (HYD, cyan). 7-Hydroxyflavone (**3.6**, red C atoms) and the training set inhibitors (**3.1**, yellow C atoms, **3.3**, cyan C atoms, **3.5**, green C atoms, **3.24**, blue C atoms) are represented at the best fit alignment to the model. This figure was created using the program Catalyst.³⁸⁸

4.3.2. Virtual screening

4.3.2.1. Pharmacophore model based on non-steroid inhibitors

The NCI open chemical repository collection is a large library of synthetic and natural compounds,³⁹¹ with more than 290000 different structures. This library has been used to screen, both *in vitro* and *in vivo*, for new anti-cancer and anti-viral agents, with the goal of identifying and evaluating novel chemical leads and their underlying biological mechanisms of action. The electronic version of the NCI repository (NCI database) was downloaded from the ZINC^{392,393} website and converted into a multiconformer database using the catDB utility program of the Catalyst software.³⁸⁸

One initial VS run performed on the NCI database, with NAI-HYP2 returned more than 90000 molecules (**Table 4.2**). As expected, the reduced number of pharmacophoric points failed to filter a large database for new aromatase inhibitors. The modified pharmacophoric query (NAI-HYP2-HBA) returned 676 hits, less than 0.3% of the total number of molecules, and with the final hypothesis (NAI-HYP2-HBA+Shape) 89 molecules were found, 0.03% of the total number of molecules. Therefore, three different levels of filtering were able to reduce a large database with thousands of molecules to a small subset of promising anti-aromatase candidates. Calculations took about 6 minutes (NAI-HYP2), 24 seconds (NAI-HYP2-HBA) and 50 seconds (NAI-HYP2-HBA+Shape) to be completed on an Intel Pentium D 3.4GHz processor.

Table 4.2. NCI database screening results.

Hypothesis	NAI hits ^[a]	SAI hits ^[a]	PAI hits ^[a]
Initial HYP	91050	16212	17481
Modified HBA ^[b]	676	-	-
HYP+Shape ^[c]	89	2189	2578
Post-processing filtering ^[d]	76	1462	1566
Visual inspection	29	19	24

[a] Hits derived from the pharmacophore model based on azol non-steroid AIs (NAI hits), steroid AIs (SAI hits) and polyphenols (PAI hits).

[b] Modified NAI-HYP2 to match acceptors from five- or six-membered nitrogen-containing heterocyclic rings.

[c] Letrozole, compound **4.5** and compound **3.6** were converted into shape queries and combined with the initial hypotheses, NAI-HYP2-HBA, SAI-HYP1 and PAI-HYP, respectively.

[d] Filters applied: Lipinski Rule of Five, PSA \leq 150, rotatable bonds \leq 7 (NAI-HYP2-HBA+Shape) or \leq 8 (SAI-HYP1+Shape and PAI-HYP+Shape)

The 89 hits derived from the NCI database were superimposed with the NAI-HYP2-HBA+Shape pharmacophore model and visually inspected. Furthermore, a Lipinski Rule of Five³⁹⁴ filter was applied using the Instant JChem software.³⁹⁵ The maximum number of rotatable bonds was set to seven per molecule and the maximum polar surface area (PSA) was set to 150. Furthermore, compounds with ester groups were avoided due to possible *in vivo* hydrolysis. 29 molecules were selected from the VS hits, 15 of these being available from the NCI open chemical repository collection to perform biological evaluation (**Figure 4.5**).

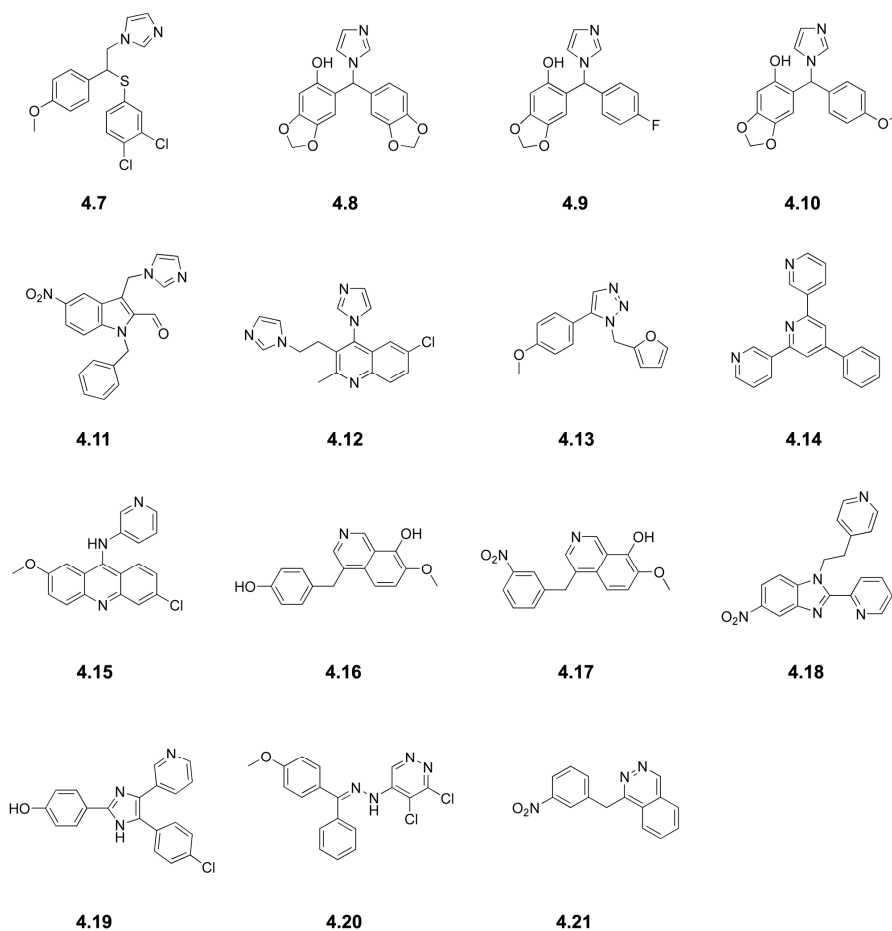


Figure 4.5. NCI database hits selected based on the NAI-HYP2-HBA+Shape pharmacophore model.

Four different types of nitrogen-containing aromatic heterocycles were retrieved as hits, namely imidazoles (compounds **4.7 - 4.12**), one triazole (compound **4.13**), pyridines (compounds **4.14 - 4.19**) and pyridazines (compounds **4.20** and **4.21**). The nitrogen-containing heterocycles are linked to several types of hydrophobic molecular scaffolds such as diphenylmethane (**4.8, 4.9, 4.10** and **4.20**), arylbenzylsulfane (**4.7**), diphenylimidazole (**4.19**), pyridinylbenzoimidazole (**4.18**), phenylpyridine (**4.14**), benzyl-1*H*-indol (**4.11**), acridine (**4.15**), phenyl/methylfuran (**4.13**)

and quinoline (**4.12**), or in other cases, appears extended with another phenyl ring, such as in two isoquinolines (**4.16** and **4.17**) and in one phthalazine (**4.21**). As hydrogen bond acceptors, methoxyl groups (**4.7**, **4.13**, **4.15** and **4.20**), nitro groups (**4.11**, **4.17**, **4.18** and **4.21**), dioxol groups (**4.8**, **4.9** and **4.10**), hydroxyl groups (**4.16** and **4.19**), imidazole (**4.12**) and pyridine (**4.14**) were found.

4.3.2.2. Pharmacophore model based on C6-substituted steroids

As expected, the initial VS run performed on the NCI database with SAI-HYP1 returned a large number of hits (16212 hits, **Table 4.2**). More efficient filtering was however possible with the introduction of inclusion volumes, SAI-HYP1+Shape, yielding 2189 hits, 0.8% of the total number of compounds in the database. Most of the molecules excluded are expected to be false positives due to the presence of protruding groups that may clash with aromatase binding site residues.

Furthermore, in order to increase the “drug-likeness” of the anti-aromatase candidates, several filters were applied, namely a Lipinski Rule of Five filter³⁹⁴ and filters based on the maximum number of rotatable bonds (not more than 8) and polar surface area (not more than 150). This procedure reduced the initial number of compounds to 1462 (0.5% of the NCI database). The molecules were then superimposed with the pharmacophore model and visually inspected, 19 of them being selected based on a good fit to the pharmacophoric features. Of these, 10 were available from the NCI database (**Figure 4.6**).

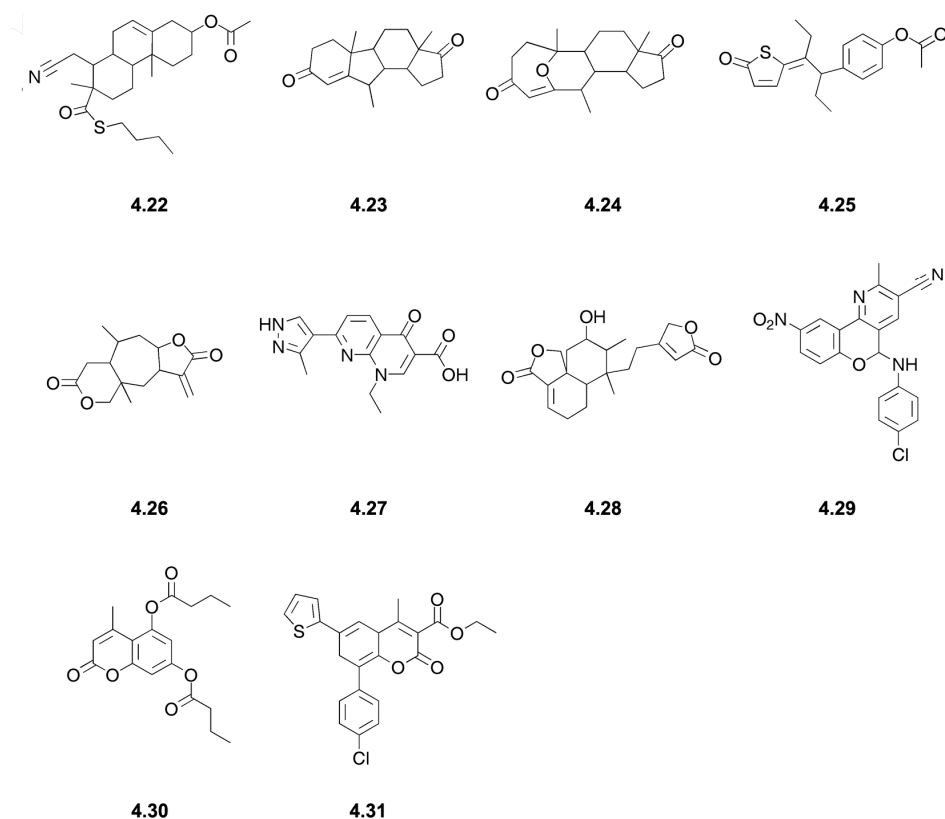


Figure 4.6. NCI database hits selected based on the SAI-HYP1+Shape pharmacophore model.

4.3.2.3. Pharmacophore model based on polyphenols

A virtual screening run performed on the NCI database with the pharmacophore model based on polyphenol inhibitors, PAI-HYP, returned 17481 hits (**Table 4.2**). Using inclusion volumes, PAI-HYP+Shape, yielded 2578 hits, 0.9% of the total number of compounds in the database, 1566 of these (0.5%) satisfying the “drug-likeness” rules (Lipinski Rule of Five, $PSA \leq 150$, rotatable bonds ≤ 8). The molecules were then superimposed with the pharmacophore model and visually inspected, 24 of them being selected based on a good fit to the model. Of these, 11 were available from the NCI database (**Figure 4.7**).

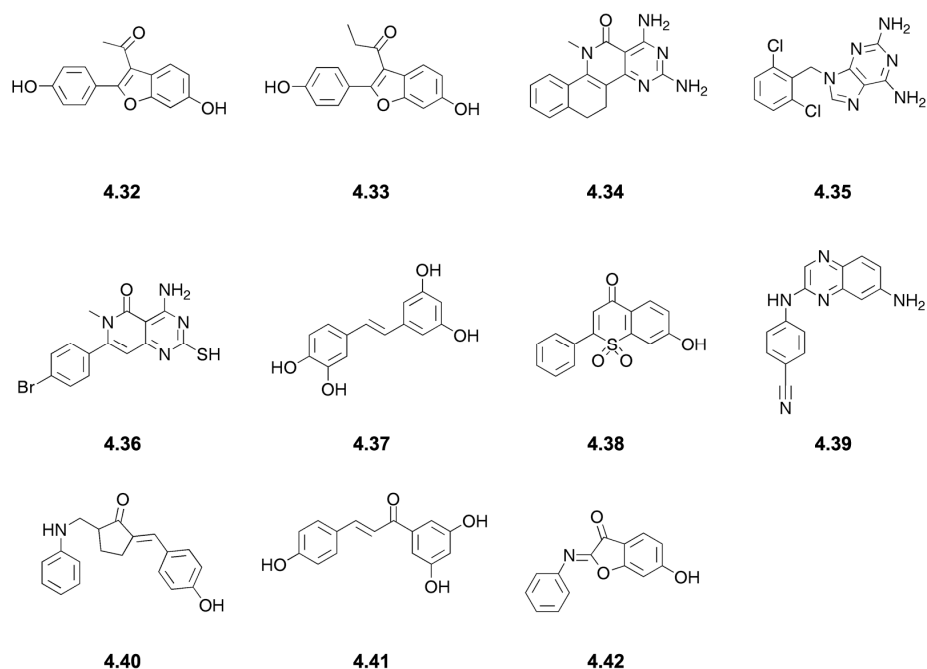


Figure 4.7. NCI database hits selected based on the PAI-HYP+Shape pharmacophore model.

4.3.3. Biochemical evaluation

Before performing the biochemical evaluation, the 36 hits derived from pharmacophoric hypotheses based on non-steroid, steroid and polyphenol inhibitors, were inspected on a large electronic collection of organic chemistry (CrossFire Beilstein) using the MDL CrossFire Commander.³⁹⁶ Additional searches were performed using the PubChem Compound database,³⁹⁷ a publicly available resource with chemical and biological information of small molecules, including results from NCI anticancer drug screenings. Literature database searches using ISI Web of Knowledge and b-on were also performed.^{398;399} Of utmost importance was the finding that none of them had been previously tested as aromatase inhibitor.

4.3.3.1. Pharmacophore model based on non-steroid inhibitors

Aromatase inhibition was studied *in vitro*, in an enzymatic assay according to Siiteri and Thompson³⁷³ using human placental microsomes as the source of aromatase.³⁷² The molecules were initially screened at 1 μM concentration, followed by a full concentration–response study, allowing the determination of the IC_{50} value (**Table 4.3**). Formestane (**Table 2.1**) and letrozole (**Table 4.3**), second and third generation aromatase inhibitors were used in the same assay conditions as a reference compounds.

Table 4.3. Aromatase inhibitory activity of the selected NCI hits based on the NAI-HYP2-HBA+Shape pharmacophore model and letrozole.

Compd	NCI code	IC_{50} (μM) ^[a]	K_i (μM) ^[a,b]
4.7	NSC289311	0.025 \pm 0.0002	0.0065 \pm 0.0001
4.8	NSC368272	0.025 \pm 0.0002	0.0056 \pm 0.0001
4.9	NSC368280	0.0053 \pm 0.00002	0.0019 \pm 0.00003
4.10	NSC369087	0.055 \pm 0.0007	0.013 \pm 0.0002
4.11	NSC625409	0.190 \pm 0.002	0.053 \pm 0.0008
4.12	NSC666292	0.096 \pm 0.001	0.033 \pm 0.004
4.13	NSC356483	3.1 \pm 0.03	-
4.14	NSC598	47 \pm 2	-
4.15	NSC12999	0.076 \pm 0.001	0.026 \pm 0.0003
4.16	NSC131735	30 \pm 0.7	-
4.17	NSC131736	1.4 \pm 0.01	-
4.18	NSC356781	2.1 \pm 0.02	-
4.19	NSC683634	0.048 \pm 0.0005	0.015 \pm 0.0003
4.20	NSC75308	5.6 \pm 0.1	-
4.21	NSC226644	38 \pm 0.8	-
Letrozole	-	0.0061 \pm 0.0001	0.0022 \pm 0.00003
[a] Results shown are the mean \pm SEM of three independent experiments.			
[b] All compounds with reported K_i values were competitive inhibitors.			

Interestingly, all molecules in study were able to inhibit the enzyme aromatase with IC_{50} potencies ranging from micromolar to low nanomolar

concentrations. Compound **4.9** ($IC_{50}=0.0053 \mu\text{M}$) presented a better activity than letrozole ($IC_{50}=0.0061 \mu\text{M}$), whereas compounds **4.7** ($IC_{50}=0.025 \mu\text{M}$), **4.8** ($IC_{50}=0.025 \mu\text{M}$), **4.10** ($IC_{50}=0.055 \mu\text{M}$), **4.15** ($IC_{50}=0.076 \mu\text{M}$) and **4.19** ($IC_{50}=0.048 \mu\text{M}$) had better potency than formestane ($IC_{50}=0.092 \mu\text{M}$).

Kinetic analysis of the enzyme in the presence of the most potent inhibitors was also performed (**Table 4.3**) and Lineweaver-Burk plots were recorded. For all of them a mechanism of competitive inhibition was found and the K_i values indicate that they have a greater affinity to the active site of the enzyme than the natural substrate, androstenedione. Control experiments, in the absence of the inhibitors in study allowed the determination of kinetic constants, Michaelis-Menten constant ($K_m=0.092 \mu\text{M}$) and maximum velocity of catalysis ($V_{max} = 161 \text{ pmol of substrate/min/mg of protein}$).

4.3.3.2. Pharmacophore model based on C6-substituted steroids

The compounds selected based on the steroid pharmacophore model were initially screened at $10 \mu\text{M}$ and $100 \mu\text{M}$ concentrations, followed by a full concentration–response study for the IC_{50} calculation (**Table 4.4**). Aminoglutethimide and formestane (**Table 2.1**), first and second generation aromatase inhibitors, were also tested, in the same assay conditions, as reference compounds.

Table 4.4. Aromatase inhibitory activity of the selected NCI hits based on the SAI-HYP1+Shape pharmacophore model.

Compd	NCI code	IC ₅₀ (μM) ^[a]	Inhibition at 100 μM
4.22	NSC76982	-	21% ^[b]
4.23	NSC93358	0.274 ± 0.004	-
4.24	NSC94891	9.8 ± 0.2	-
4.25	NSC122427	15 ± 0.1	-
4.26	NSC136718	-	N.O. ^[c]
4.27	NSC302379	-	N.O. ^[c]
4.28	NSC383467	126 ± 15	-
4.29	NSC613604	0.678 ± 0.007	-
4.30	NSC688803	176 ± 3	-
4.31	NSC692587	-	26%

[a] Results are shown as the mean ± SEM of three independent experiments.
[b] Inhibition at 30 μM.
[c] Inhibition was not observed at concentrations ≤ 100 μM.

Most of the selected compounds based on the SAI-HYP1+Shape pharmacophore model showed anti-aromatase activity in the assay conditions used (**Table 4.4**). Compounds **4.22**, **4.28**, **4.30** and **4.31** are weak aromatase inhibitors with IC₅₀ higher than 100 μM. Compounds **4.24** (IC₅₀=9.8 μM) and **4.25** (IC₅₀=15 μM), have anti-aromatase potencies comparable to the first generation AI tested, aminoglutethimide (IC₅₀=10 μM), and, more interestingly, compounds **4.23** and **4.29** have an IC₅₀ in the nanomolar range. Compound **4.23** (IC₅₀=0.274 μM) is 36 times more active than aminoglutethimide, and compound **4.29** (IC₅₀=0.678 μM) 15 times more potent. However, these two molecules are less active than formestane (IC₅₀=0.092 μM), the second generation AI tested.

Kinetic analysis of the enzyme activity was also performed. The kinetic constants, Michaelis-Menten constant ($K_m=0.094$ μM) and maximum velocity of catalysis ($V_{max}=164$ pmol of substrate/min/mg of protein) were

calculated under initial velocity conditions. The type of inhibition was characterized using a Lineweaver-Burk plot. As expected, the most potent AIs (compounds **4.23**, $K_i=0.266 \mu\text{M}$, and **4.29**, $K_i=0.385 \mu\text{M}$), inhibited the enzyme in a competitive manner (**Table 4.5**).

Table 4.5. Enzyme kinetic parameters for compounds **4.23** and **4.29**, based on a kinetic and time-dependent inactivation procedure.

Compd	K_i (μM) ^[a]	Type of inhibition ^[a]	K_i (μM) ^[b]	k_{inact} (min^{-1}) ^[b]
4.23	0.266 ± 0.002	Competitive	N.O. ^c	N.O. ^c
4.29	0.385 ± 0.008	Competitive	21 ± 1	0.608 ± 0.044

[a] Apparent inhibition constants (K_i) were calculated by a nonlinear regression analysis using the Michaelis-Menten equation, and the type of inhibition was determined by a Lineweaver-Burk plot.

[b] K_i and k_{inact} were obtained by a Kitz-Wilson plot.

[c] Inactivation was not observed at concentrations $\leq 2 \mu\text{M}$.

Compounds **4.23** and **4.29** were further tested for their ability to cause time-dependent inactivation of aromatase. Compound **4.29**, but not compound **4.23**, was able to inactivate the enzyme in the presence of NADPH, with a pseudo first order kinetics during the first 12 minutes of incubation (**Figure 4.8**). Kitz-Wilson analysis of the results obtained,⁴⁰⁰ gave a k_{inact} of 0.608 min^{-1} and K_i of $21 \mu\text{M}$. Since the K_i observed from the competition kinetics is lower than the K_i obtained from the inactivation experiments, this suggests that the covalent binding of the inhibitor to the active site of the enzyme is the rate-limiting step of the inactivation.

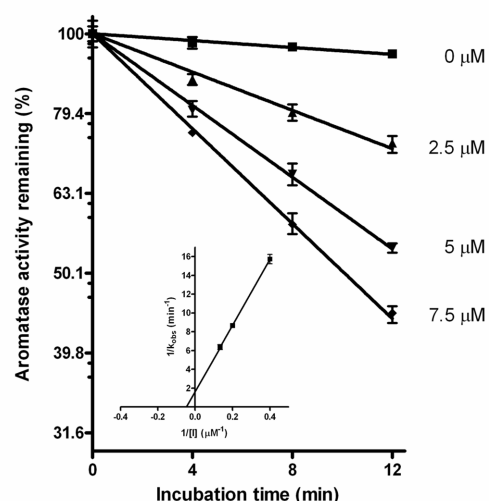


Figure 4.8. Time- and concentration-dependent inactivation of human placental aromatase by compound **4.29** in the presence of NADPH. The concentrations of inhibitor used were 0 μM (\blacksquare), 2.5 μM (\blacktriangle), 5 μM (\blacktriangledown) and 7.5 μM (\blacklozenge). A Kitz-Wilson plot of the same data is shown in the inset. Each point represents the mean of three independent assays and the vertical bars, the standard error of the mean.

On the other hand, substrate androstenedione in excess prevented inactivation (**Figure 4.9A**), as well as not including NADPH in the medium (**Figure 4.9B**). This suggests that the inhibitor acts at or near the active site of aromatase, and, since NADPH was essential for the time-dependent aromatase activity loss by compound **4.29**, that the inhibitor transformation into a reactive intermediate depends on enzyme catalysis. Furthermore, the nucleophilic trapping agent L-cysteine did not prevent enzyme inactivation to a significant extent (**Figure 4.9C**), suggesting a covalent bond formation at the active site, between aromatase and the reactive electrophilic intermediate, therefore preventing diffusion of the activated inhibitor to the surrounding media.

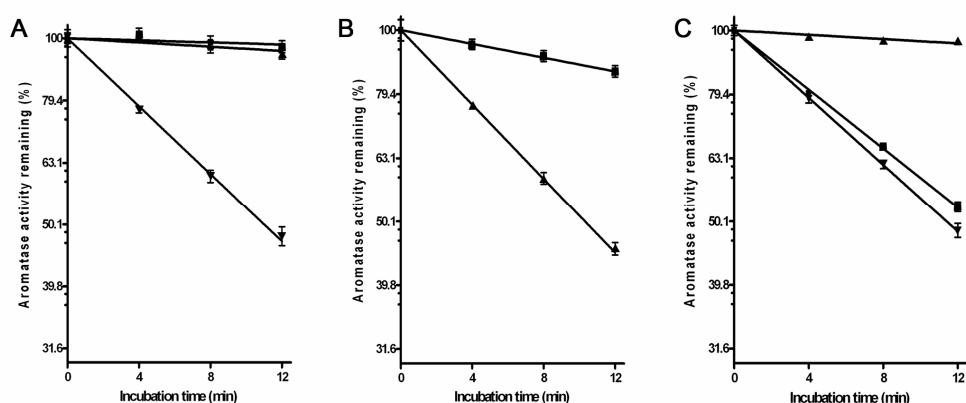


Figure 4.9. Effect of androstenedione (**A**), NADPH (**B**) and L-cysteine (**C**) on the time-dependent inactivation of human placental aromatase by compound **4.29**. (**A**) 7.5 μM of androstenedione were incubated with (\blacksquare) or without (\blacktriangle) 7.5 μM of inhibitor. Incubations of 7.5 μM of inhibitor without androstenedione (\blacktriangledown) were also performed. (**B**) 7.5 μM of inhibitor were incubated with (\blacktriangle) or without (\blacksquare) NADPH. (**C**) 0.5 mM of L-cysteine were incubated with (\blacksquare) or without (\blacktriangle) 7.5 μM of inhibitor. Incubations of 7.5 μM of inhibitor without L-cysteine (\blacktriangledown) were also performed. Each point represents the mean of three independent assays and the vertical bars, the standard error of the mean.

4.3.3.3. Pharmacophore model based on polyphenols

Although all selected compounds based on the PAI-HYP+Shape pharmacophore model had activity on the assay conditions used, most of them were weak aromatase inhibitors with IC_{50} greater than 100 μM . Compounds **4.32**, **4.33** and **4.37** were the most potent aromatase inhibitors identified, with IC_{50} ranging from 30 to 57 μM (**Table 4.6**). These results are related to the lower anti-aromatase potency of the natural polyphenol inhibitors used to build and validate the PAI-HYP+Shape model, when compared to the potencies of theazole non-steroid aromatase inhibitors used for the NAI-HYP2-HBA+Shape model and the androstenedione derivatives used for the SAI-HYP1+Shape pharmacophore model.

Polyphenols have an IC₅₀ in the low micromolar range, whereas azole non-steroid and steroids are active at nanomolar concentrations.

Table 4.6. Aromatase inhibitory activity of the selected NCI hits based on the PAI-HYP+Shape pharmacophore model.

Compnd	NCI code	IC ₅₀ (μM) ^[a]	Inhibition at 100 μM
4.32	NSC84036	57 ± 3	-
4.33	NSC97869	48 ± 3	-
4.34	NSC337764	-	7%
4.35	NSC339176	-	9%
4.36	NSC342739	-	22% ^[b]
4.37	NSC365798	30 ± 8	-
4.38	NSC375008	180 ± 31	-
4.39	NSC653250	-	18%
4.40	NSC661232	-	27%
4.41	NSC665696	-	23%
4.42	NSC666463	-	15%

[a] Results are shown as the mean ±SEM of three independent experiments.
[b] Inhibition at 80 μM.

4.3.4. Docking into the active site of an aromatase homology model

The most active compounds (**4.7**, **4.8**, **4.9**, **4.10**, **4.11**, **4.12**, **4.15** and **4.19**) were docked with the GOLD docking software⁴⁰¹ into the active site of an aromatase homology model built by Favia *et al.*¹⁴⁰ using the structure of CYP2C9 as template.¹³⁷ The distance between the coordinating nitrogen and the heme iron was constrained to a value between 1.9 and 2.5 Å in order to reproduce the binding mode found for non-steroid aromatase inhibitors.¹⁹⁹ This distance range was chosen based on the analysis of P450 enzymes found in the PDB database with imidazole and pyridine ligands complexed with the heme group.⁴⁰²⁻⁴⁰⁴ The GOLDScore fitness function was used to rank the binding modes to the enzyme. This scoring function is the

negative of the sum of five energy terms, i.e. protein-ligand hydrogen bond energy, protein-ligand van der Waals energy, ligand internal van der Waals energy, ligand torsional strain energy and an additional constraint scoring contribution.

Analysis of the docking results revealed that all the molecules in study fit well within the binding site cavity, with fitness scores ranging from 53 to 68. With exception of compounds **4.7** and **4.12**, the top ranked poses of all molecules have a hydrogen bond between an acceptor group and Ser 478. Slightly lower scored binding modes of compound **4.7** (62 versus 67, pose ranked number 12) and compound **4.12** (56 versus 57, pose ranked number 2) showed the same hydrogen bond interaction (**Figure 4.10**). These results are in agreement with previous mutagenesis and docking studies pointing out Ser 478 as a key residue to the catalysis mechanism of the enzyme and binding of non-steroid aromatase inhibitors.^{140;215;220} Compounds **4.8**, **4.9** and **4.10** share the same binding mode, with an additional hydrogen bond between the hydroxyl group and Thr 310. This extra anchoring point might explain the strongest anti-aromatase activity found for compound **4.9**. More detailed analysis of the docking mode of compounds **4.7**, **4.8** and **4.15** (**Figure 4.10**) revealed a very close superimposition of hydrophobic and hydrogen bond acceptor pharmacophoric points similar to the pharmacophore model used for virtual screening, NAI-HYP2 (**Figure 4.1B**). The HYD1 area is defined by three phenyl rings docked on a relatively apolar region of the aromatase binding cavity defined by hydrophobic residues Val 313 and Leu 477. The HYD2 area has either phenyl rings or a phenylsulfanyl group, fitting a small hydrophobic pocket due to Pro 368 and Val 370.

Letrozole, the third generation reference compound used in this study, fits into the binding pocket of the enzyme in a similar way to the other

compounds. Good superimposition is observed between the hydrophobic and nitrogen-containing moieties of these molecules.

Furthermore, the docking poses of compounds **4.7**, **4.8**, **4.9**, **4.10**, **4.11**, **4.12**, **4.15** and **4.19** were loaded into Catalyst and rigidly fitted to the pharmacophore model. With exception of compound **4.11**, all other docked conformations fitted into all features of the model with an average fit value of 2.45.

These results further validate the NAI-HYP2-HBA+Shape pharmacophore model as a screening methodology for potent non-steroid aromatase inhibitors.

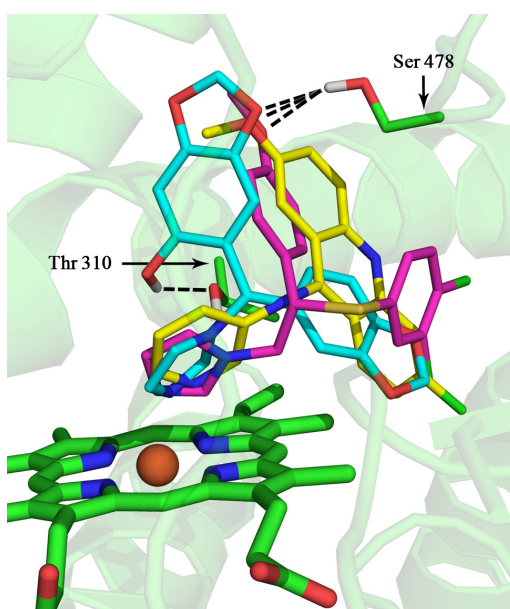


Figure 4.10. Docked poses of compounds **4.7** (magenta C carbons), **4.8** (cyan C carbons) and **4.15** (yellow C carbons) into the binding site of an aromatase homology model.¹⁴⁰ Dashed lines are drawn between Thr 310 and the hydroxyl group of compound **4.8** (distance=2.05 Å), and between Ser 478 and methoxyl groups of compounds **4.7** (distance=2.85 Å) and **4.15** (distance=2.61 Å), and a dioxol group of compound **4.8** (distance=2.42 Å). This figure was created using the program Pymol.³⁴⁶

4.3.5. Stereoelectronic characterization

The strong anti-aromatase activity of compound **4.23**, a B-nor steroid with similar hydrophobic core compared to the substrate androstenedione, prompted us to further evaluate the molecular geometry and electronic properties of these structures using high level *ab initio* quantum chemistry methods. It was found that the geometries of androstenedione and its B-nor derivative are very superimposable, with a root mean square deviation of 0.31 Å based on pair-wise alignment of the A, C and D ring carbons (**Figure 4.11A**). Furthermore, the distances between hydrogen bond acceptor groups, i.e. androstenedione 3- and 17-oxo groups and equivalent functions on the B-nor-derivative, which are important features of the SAI-HYP1 pharmacophore model, are very similar (10.44 Å and 10.38 Å, respectively). Slight differences were however identified, namely the shape and size of the B ring, and the location of the acceptor linked to the ring A. The B-ring of the nor-steroid, a cyclopentane, adopts an envelope conformation less bulky than the cyclohexane chair in androstenedione. The 3-oxo groups are located 0.63 Å apart based on this superimposition.

Electronic properties of these molecules were also calculated, namely the electrostatic surface potential and the valence orbitals, i.e. the HOMO and LUMO. These properties are similar in both compounds (**Figure 4.11B**). Negative potential was found in both carbonyls and along the O=C3–C4=C5 conjugation due to π electron delocalization. The HOMO and the LUMO are located at the A-ring, on the delocalized system. Therefore, these two compounds might have a similar aromatase recognition mechanism and reactivity.

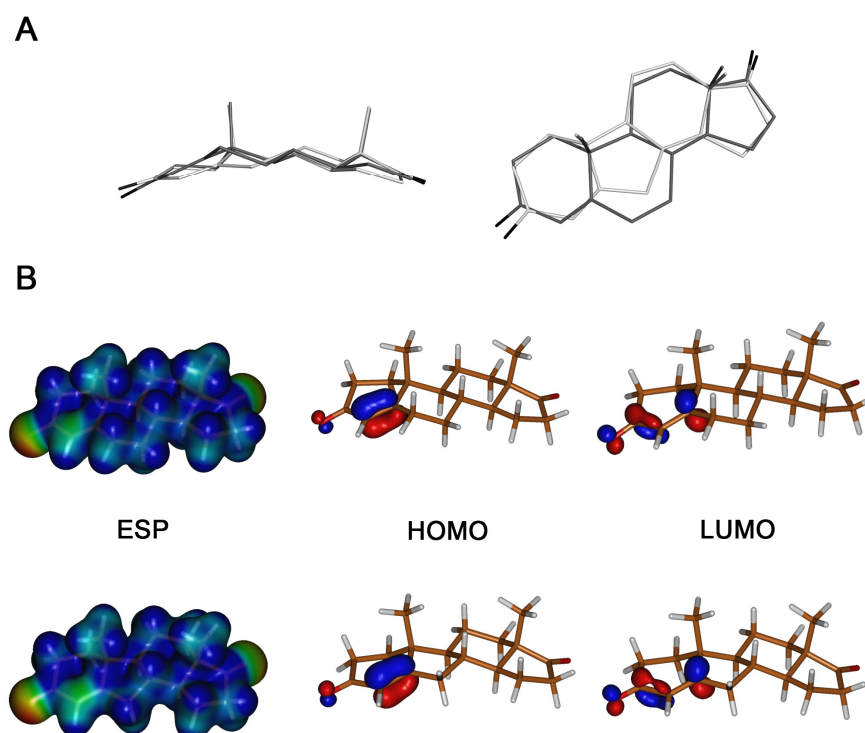


Figure 4.11. **A)** Superimposition of the minimized structures of androstenedione (grey carbons) and B-nor-androstenedione (white carbons) at the *ab initio* HF/6-31G** level. The molecules were superimposed based on RMSD of carbon atoms at A, C and D rings, and represented on a side (right) and top view (left). This figure was created using the program VMD.¹¹⁷ **B)** Electrostatic surface potential, HOMO and LUMO valence orbitals derived for androstenedione (top) and B-nor-androstenedione (bottom). The ESP was mapped on the 0.02 e/A³ electron density isocontour derived from *ab initio* HF/6-31G** calculations (V= 0.1 eV, blue; V= -0.1 eV, red). The HOMO and LUMO are represented at orbital amplitude of 0.1 (blue) and -0.1 (red). This figure was created using the program Molden.³⁶²

4.4. Conclusions

In this study, a new virtual screening strategy for potent aromatase inhibitors was proposed. The most successful screening was based on the common

features of a training set of second and third generation non-steroid aromatase inhibitors (fadrozole, anastrozole, letrozole and vorozole), combined with heme coordinating fragments (five- or six-membered nitrogen-containing aromatic heterocycles), inclusion volumes and several “drug-likeness” filters. The model was first validated theoretically on a literature database of known aromatase inhibitors, and used subsequently to screen the NCI database, a large library of molecules focused on research for new antitumor and AIDS antiviral agents. A small number of the NCI compounds (0.03%) were identified as interesting anti-aromatase candidates. Finally, the model was validated experimentally by testing the most promising virtual screening hits in an *in vitro* biochemical assay. New potent aromatase inhibitors with similar or better *in vitro* potency than the reference molecules were identified.

All compounds selected on the basis of NAI-HYP2-HBA+Shape, were able to inhibit the aromatase with IC₅₀ potencies ranging from micromolar to the low nanomolar range. These results demonstrate that the virtual screening strategy based on this pharmacophore model was very effective at filtering the large NCI compound database, with no false positives. Furthermore, several compounds had anti-aromatase activities between second and third generation aromatase inhibitors (**4.7**, **4.8**, **4.10**, **4.15** and **4.19**), and one of them (compound **4.9**) was stronger than the third generation reference AI. Kinetic studies confirmed a competitive inhibition mechanism. These molecules are therefore interesting targets for lead optimization and ADMET studies.

Although to the best of our knowledge these compounds had never been tested as aromatase inhibitors, molecules with the diphenylmethylimidazole or the 3-((1*H*-imidazol-1-yl)methyl)-1-benzyl-1*H*-indole motifs have already been reported as potent aromatase inhibitors with IC₅₀ values in the nanomolar range.^{200;405;406} Furthermore, compound **4.18** was tested for

antimicrobial and antifungal properties with no activity on the assay conditions,⁴⁰⁷ and derivatives of compound **4.11** had antifungal activity only when tested at micromolar concentrations.⁴⁰⁸ These results indicate that these compounds, used at very low nanomolar concentrations, might be selective for the aromatase enzyme. Additional studies should be performed in order to confirm this hypothesis. Other interesting biological activities have also been identified for some of these molecules and reported in the literature, for example, 9-anilinoacridines related to compound **4.15** have potential antitumor activity due to their DNA binding properties.⁴⁰⁹ Large scale screenings performed by the anticancer drug discovery program of the NCI identified potential new activities for compounds **4.7** and **4.12**. Compound **4.7** was active, *in vivo*, using a model for colon carcinoma in mice. Compound **4.12** was another interesting compound identified. It was found to inhibit the growth of a human leukemia cell line.

Docking of the most potent compounds into the active site of a homology model¹⁴⁰ of the aromatase led to a common binding mode that is in good agreement with the common features in the pharmacophore model. Besides the essential HBA1 feature involved in coordination with the heme iron, establishment of an additional hydrogen bond with Ser 478 appears to be important, therefore justifying the presence of the HBA2 feature. Several apolar active site residues explain the hydrophobic nature of the new aromatase inhibitors (HYD1 and HYD2) and Thr 310, involved in an additional hydrogen bond, might explain the strong anti-aromatase properties of compound **4.9**.

These results, supported by extensive experimental validation, represent a clear improvement over previous ligand-based virtual screening approaches for new non-steroid aromatase inhibitors,³⁸⁶ providing an effective new tool for the identification of novel molecular entities acting on important cytochrome P450 targets. Common to all members of this large superfamily,

is a heme cofactor which should be carefully addressed when designing new pharmacophore models for such targets, in order to achieve strong binding affinities. On the other hand, fine tuning of the ligand potency and selectivity among different P450 targets can be addressed exploring specific hydrophobic, hydrogen bonding and shape complementarity interactions. Therefore, starting with potent inhibitors of different cytochrome P450 enzymes such as CYP17 and aldosterone synthase, this methodology can be easily applied to the design of new drugs for other relevant diseases.

The NAI-HYP2-HBA+Shape pharmacophore model includes a broad range of nitrogen-containing heterocycles, comprising imidazole, triazole and pyridine, the most extensively used to design non-steroid aromatase inhibitors. However, it might be extended with other heterocycles such as rings containing both nitrogen and sulfur/oxygen heteroatoms (thiazole, oxazole).

Additional pharmacophore models for two different classes of aromatase inhibitors, steroid derivatives and polyphenols were proposed and used to perform virtual screening of new compounds. Previous knowledge on the binding determinants of these molecules to the aromatase active site was essential to this ligand-based methodology. A hydrophobic pocket close to the C6 position of steroid inhibitors has been widely studied, as well as the importance of a hydrogen bonding group at C7 in flavones. Therefore, the combination of essential pharmacophoric features with steric restrictions and “drug-likeness” filters allowed the isolation of small subsets, enriched in aromatase inhibitors, from the large NCI database.

The SAI-HYP1+Shape pharmacophore model identified compounds active in the nanomolar range whereas PAI-HYP+Shape identified less potent compounds, active in the micromolar range. This agrees with the strongest anti-aromatase activity found for androstenedione derivatives compared to polyphenols. 6-Methyl-B-nor-androstenedione (**4.23**) was one of the most

interesting compounds identified, with a low nanomolar IC₅₀ and a competitive mechanism of inhibition. The strong anti-aromatase potency was rationalized based on structural and physicochemical similarities between the B-nor-androstenedione scaffold and the endogenous substrate of the enzyme. To the best of our knowledge, this is the first report of B-nor-androgens as aromatase inhibitors. Therefore, these compounds might be an important new structural class of anti-aromatase agents for lead optimization.

Compound **4.29**, a potent mechanism-based aromatase inactivator was another interesting molecule identified based on the SAI-HYP1+Shape pharmacophore model.

The PAI-HYP+Shape pharmacophore model identified three interesting polyphenol aromatase inhibitors, **4.32**, **4.33** and **4.37**. Compound **4.37**, piceatannol, is a natural stilbene found in red wine⁴¹⁰ and one of the metabolites of resveratrol.⁴¹¹ This compound has been widely studied as an anti-cancer agent due to strong antileukaemic⁴¹² and tyrosine kinase inhibition properties.⁴¹³ It is also a known phytoestrogen with agonist activity at the ER α .⁴¹⁴ Therefore, the piceatannol might have more than one effect in breast cancer and should be further evaluated. Compounds **4.32** and **4.33** are arylbenzofurans, a class of natural polyphenols found in rice and other crops.⁴¹⁵ 2-Arylbenzofurans, in particular, have been studied for their anti-cancer and selective estrogenic activities. These compounds have a selective estrogen modulator profile, i.e. antiestrogenic effects in breast cancer cells and estrogenic effects in bone cells, acting by a classical estrogen receptor mechanism.^{416;417}

In conclusion, we have described and validated a new ligand-based virtual screening methodology for new aromatase inhibitors based on pharmacophore models of non-steroid, steroid and polyphenol inhibitors. The screening of a large compound database was very fast and new potent

aromatase inhibitors were identified. Moreover, this methodology will have a broader application for a large variety of compound databases.

4.5. Materials and methods

4.5.1. Materials and general methods

See **Section 2.5.1**.

The NCI selected compounds were obtained from the Drug Synthesis and Chemistry Branch, Developmental Therapeutics Program, Division of Cancer Treatment and Diagnosis of the National Cancer Institute. Letrozole was purchased from USP (Rockville, MD, USA). Androstenedione and L-cysteine were purchased from Sigma-Aldrich (St. Louis, MO, U.S.A.). The radioactive samples were counted on a Packard Tri-Carb 2900 TR Liquid Scintillation Analyzer.

4.5.2. Pharmacophore modelling

Pharmacophore design was performed using the Catalyst software.³⁸⁸ Potent aromatase inhibitors were collected from the literature, their three-dimensional structures constructed as described in **Section 2.5.5**, and submitted to a conformational search with internal energy minimization using the catDB utility program. A maximum of 250 conformers were saved within an energy window of 20 kcal/mol above the global minimum, using the best quality generation type.

For theazole non-steroid model, anastrozole, letrozole, S-vorozole and S-fadrozole¹⁹⁵ were included in a training set and used to build a common-features pharmacophore model using the HipHop³⁸⁷ algorithm of Catalyst. The remaining molecules^{202;203;219;258-260;390} were included in a test set and used for model validation (**Appendix A**). The most active enantiomers of

vorozole⁴¹⁸ and letrozole¹⁹⁹ were preferred. For the initial hypothesis generation methodology, hydrophobic and hydrogen bond acceptor functions were used. The “Principal” value was set to 2 for letrozole (all features in the molecule were considered to build the pharmacophore model) and 1 for the other compounds (at least one mapping for each generated hypothesis was found). The “Maximum Omitted Features” value was set to 1 for all molecules (all but one feature was forced to map) and default settings were used for the other options. The nitrogen-containing aromatic heterocyclic rings were built and 3D-minimized within Catalyst, converted into pharmacophore features using the “View Hypothesis” workbench and combined into a new fragment/function feature using the “Exclude/Or” tool. A similarity tolerance of 0.48 was used in the shape query. This value was chosen in order to match all molecules of the training set.

For the pharmacophore model based on C6-substituted steroids, hydrophobic and hydrogen bond acceptor functions were used. The “Principal” value was set to 2 for molecule **4.3** and 1 for the other compounds. The “Maximum Omitted Features” value was set to 1 for all molecules and default settings were used for the other options. A similarity tolerance of 0.5 was used in the shape query.

The function mapping tool of the “View Hypothesis Workbench” was used for building the pharmacophore model based on polyphenols, using compound **3.6** as template.

4.5.3. Virtual screening

The NCI database was downloaded from the 2007 release of the ZINC library^{392;393} and converted into a multiconformer Catalyst database. A maximum of 100 conformations were generated for each molecule using the “FAST” conformational analysis model of catDB utility program.

Pharmacophore searches were performed using the “Fast flexible database search” settings.

4.5.4. Post-processing filtering

Instant JChem³⁹⁵ was used for management, search and prediction of molecular descriptors for the NCI hits. A Lipinski Rule of Five³⁹⁴ filter was applied (not more than 5 hydrogen bond donors, not more than 10 hydrogen bond acceptors, molecular weight under 500 g/mol and calculated partition coefficient clogP less than 5), as well as a filter based on the maximum number of rotatable bonds (less than 8 for hits based on the azole non-steroid pharmacophore model, and less than 9 for hits based on the steroid and polyphenol pharmacophore models) and maximum polar surface area (not more than 150). Sub-structure searches were performed using the same software.

4.5.5. Enzymatic preparation

See **Section 2.5.2**.

4.5.6. Concentration-response study

See **Section 2.5.3**.

Incubations were performed at 37 °C in a medium containing 67 mM sodium phosphate, pH 7.5, [1β -³H]-androstenedione (6.6×10^5 dpm / 24 nM) and 270 μ M NADPH.

The molecules selected based on the azole non-steroid pharmacophore model were initially tested at 1 μ M concentration, followed by a full concentration-response study with at least 8 concentrations ranging from 3.162×10^{-4} μ M to 160 μ M.

The molecules selected based on the steroid and polyphenol pharmacophore models were initially tested at 10 μM and 100 μM concentrations, followed by a full concentration-response study with at least 8 concentrations ranging from 10 nM to 320 μM .

4.5.7. Kinetic analysis

See **Section 2.5.4**.

The concentration of [1β - ^3H]-androstenedione was varied from 7.5 to 100 nM and three different concentrations of each inhibitor were tested.

4.5.8. Time-dependent inactivation assay

Several concentrations of compounds **4.23** and **4.29** (up to ca. 10 times the IC_{50}) were incubated at 37°C in a medium containing 67 mM sodium phosphate buffer, pH 7.5, 300 μg microsomal protein and 900 μM NADPH, in a final volume of 500 μL . Aliquots (50 μL) were extracted in duplicate at several times (0, 4, 8 and 12 min), and immediately diluted in 67 mM sodium phosphate buffer, pH 7.5, [1β - ^3H]-androstenedione (6.6×10^5 dpm / 24 nM) and 270 μM NADPH in a final volume of 500 μL . The mixture was then incubated at 37°C for 20 min, and the extent of the aromatization reaction was determined by liquid scintillation counting as described previously. Each assay was performed three times. First order apparent inactivation rate constants (k_{obs}), at each inactivator concentration, were obtained from the slope of linear regressions of log aromatase activity remaining versus incubation time plots, multiplied by 2.303. The K_i and k_{inact} were determined from the slope and y intercept of a Kitz-Wilson plot,⁴⁰⁰ respectively. Inactivation studies in the absence of NADPH were performed in the same manner, but NADPH was omitted of the initial incubation. For the same studies in the presence of androstenedione or L-cysteine, the

substrate (7.5 μ M) or L-cysteine (0.5 mM) were included in the initial incubation.

4.5.9. Docking calculations

The GOLD⁴⁰¹ software was used to perform semi-flexible docking of the best compounds into the binding cavity of a aromatase homology model.¹⁴⁰ The binding site was defined as a 10 Å sphere centered approximately 5 Å above the heme iron and including all active site residues important to the binding. An octahedral coordinating geometry was assigned to the heme iron and the GOLDScore fitness function was used with metal parameters optimized for P450 enzymes, taking account of different hydrogen bond acceptor types.⁴¹⁹ Since it has been reported that in some cases the GOLD program fails to reproduce the known binding mode of non-steroid aromatase inhibitors, i.e. binding through coordination between the heme iron and an acceptor nitrogen from an aromatic heterocycle,²⁸⁰ substructure constraints were created for the pyridine and imidazole rings in order place the nitrogen within a distance between 1.9 and 2.5 Å from the heme iron. These upper and lower values were chosen based on the analysis of PDB entries of cytochrome P450 enzymes complexed with imidazole and pyridine derivatives.⁴⁰²⁻⁴⁰⁴ Twenty independent docking runs were performed with the default genetic algorithm search parameters.

For comparison, unrestrained docking was also performed, being able to identify docking modes in which the nitrogen-containing heterocycle interacted correctly with the heme iron, however, for most molecules, failing to score these poses in the top ranked solutions. As a consequence, the docking algorithm spent most of the computational time exploring unrealistic conformations.

4.5.10. *ab initio* calculation details

The minimum energy conformations and electronic properties of androstenedione and its B-nor derivative were determined by *ab initio* quantum chemistry calculations. Initial molecular mechanics geometries calculated as described in **Section 2.5.5** were further optimized with Gaussian 98³⁷⁷ using a split-valence basis set with polarization d-orbitals added to heavy atoms and polarization p-orbitals added to hydrogens (HF/6-31G**).

The optimized geometries were used to calculate electronic properties, namely the total density, ESP, HOMO and LUMO. Contour surfaces were represented using the software Molden v4.6.³⁶²

V

Concluding remarks

The work reported in this thesis highlights the importance of combining biochemical evaluation data with molecular modelling studies for a rational design of new drugs. Applied to the study of aromatase inhibitors, an important class of drugs for the treatment of breast cancer in postmenopausal women, this symbiotic approach allowed a deeper understanding of the physicochemical determinants for strong inhibition. These results encouraged the development of a virtual screening strategy for new potent aromatase inhibitors.

Aromatase inhibition is an intensively pursued field of research, and by now numerous potent inhibitor classes are known. In the initial part of this study we focused on two emerging types of compounds, estrogen derivatives and polyphenols.

The biochemical evaluation of the main estradiol and estrone metabolites revealed that catechol estrogens are potent aromatase inhibitors. Quantum chemistry calculations pointed to a common aromatase binding mode, driven by the catechol moiety which is expected to establish strong electrostatic interactions with the enzyme. While the interest of catechol estrogens as therapeutic agents might be limited due to reduced oral bioavailability and toxicological issues, these compounds have potential for improvement by molecular derivation. Furthermore, the interest of this study goes beyond the field of medicinal chemistry, and a link between estrogen metabolism and production was discussed. The strong anti-aromatase activity of endogenous catechol estrogens might be responsible for an intracrine control mechanism of estrogen production in postmenopausal women.

Plant natural compounds offer a tremendous pool of potent and highly diverse structures able to inspire the development of new drugs. Although not having the degree of potency found in other classes of aromatase inhibitors, natural polyphenols are interesting leads for the design of better compounds. Furthermore, these molecules might be interesting chemical

probes, used to achieve a deeper understanding of the aromatase binding pocket.

In this sense, we have evaluated the anti-aromatase potency of natural polyphenols from several plant sources and identified strong inhibitors, including flavones, flavanones, resveratrol and oleuropein, the major polyphenolic compound of olive oil. This information was combined into a molecular modelling study for a rational on the anti-aromatase activity of natural polyphenols. Good agreement was found between a putative virtual receptor site derived from the three-dimensional quantitative structure-activity relationships based on alignment independent descriptors, and molecular interaction fields calculated at the binding pocket of a homology model of the enzyme. Briefly, both ligand-based and structure-based models highlighted a very hydrophobic binding core surrounded by three polar regions prone to hydrogen bond formation. This was further corroborated by docking experiments using the model of the enzyme. A common binding mode was found for all compounds in study.

As a major conclusion from the initial biochemical and computational studies with estrogen derivatives and polyphenols, it was found that each class of compounds share common pharmacophoric and shape features, namely an hydrophobic scaffold and hydrogen bond donor/acceptor groups at specific locations. This finding encouraged the development of a virtual screening strategy based on pharmacophore models derived from structures of potent aromatase inhibitors. Nitrogen-containing heterocyclic non-steroid, steroid and polyphenol compounds, the most relevant classes of aromatase inhibitors, were used.

Virtual screening of the NCI database with these three different pharmacophore models led to thirty six new promising compounds which were then tested as aromatase inhibitors and their activities compared to those of reference aromatase inhibitors. Most compounds inhibited the

aromatase enzyme, one of these with stronger activity than letrozole, five compounds with activities between letrozole and formestane and nine compounds with potency between formestane and aminoglutethimide.

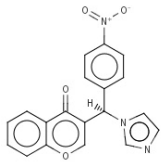
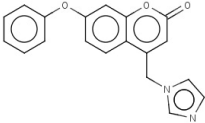
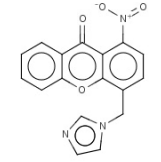
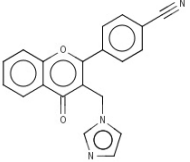
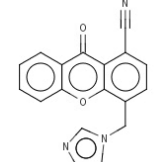
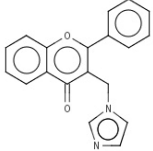
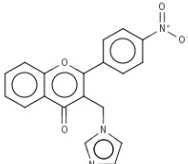
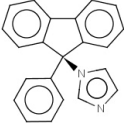
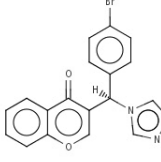
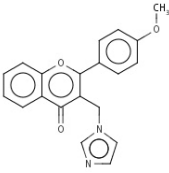
In summary, the results presented in this thesis emphasize the benefits of combining computer-aided drug design techniques with biochemical evaluation. New insights into the molecular basis of the anti-aromatase activity of endogenous estrogen metabolites and natural polyphenols were provided, and a fast *in silico* screening methodology for new potential candidates was described.

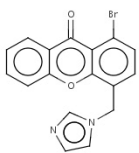
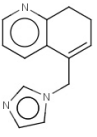
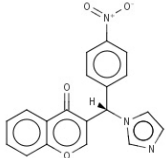
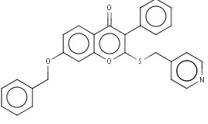
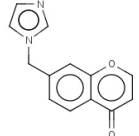
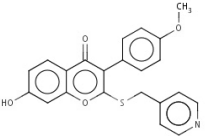
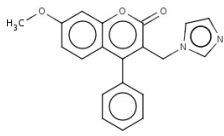
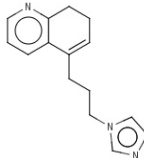
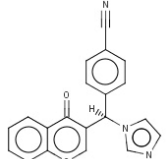
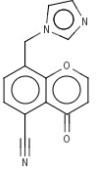
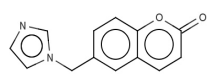
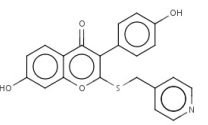
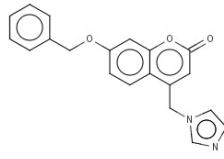
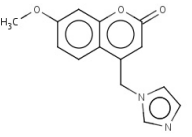
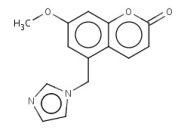
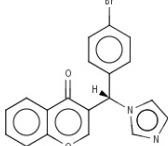
VI

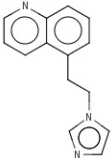
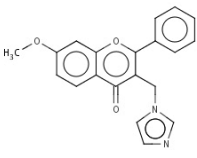
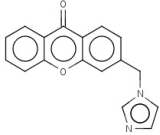
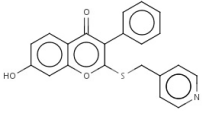
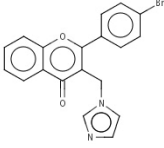
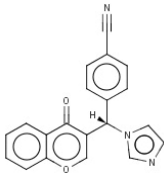
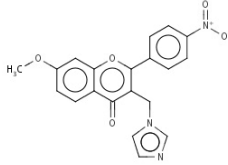
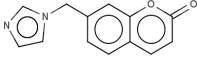
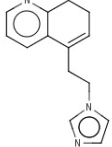
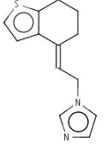
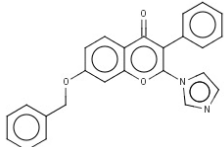
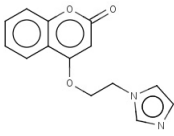
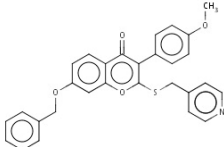
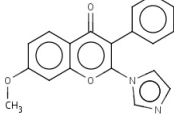
Appendix

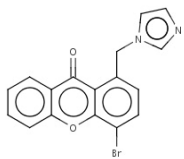
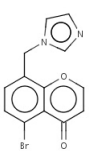
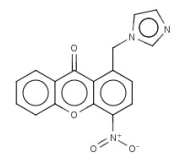
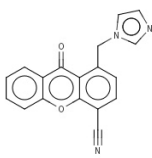
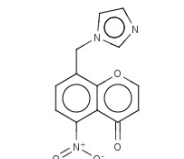
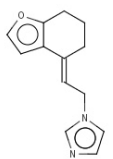
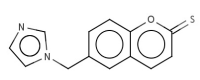
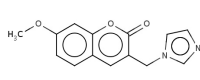
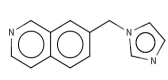
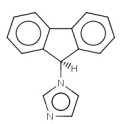
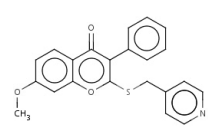
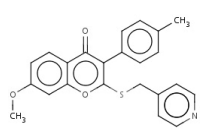
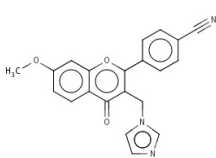
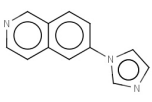
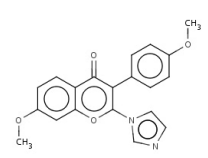
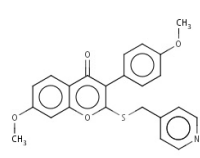
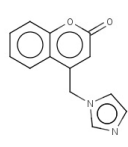
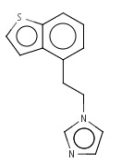
Appendix A. NAI-HYP2-HBA+Shape pharmacophore model validation results.

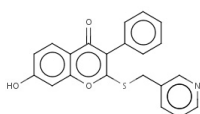
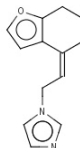
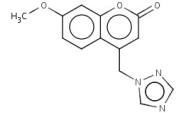
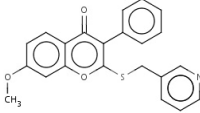
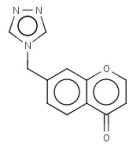
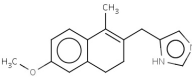
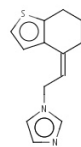
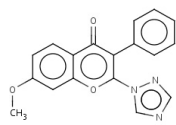
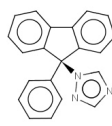
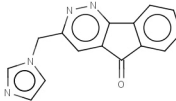
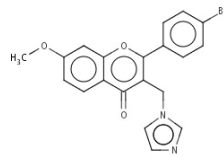
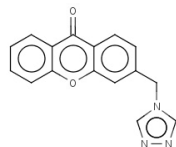
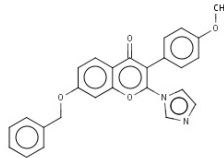
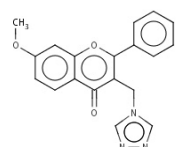
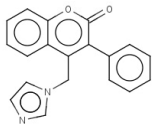
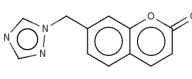
A test set of 82 non-steroid aromatase inhibitors was collected from the literature and used to evaluate the potential of NAI-HYP2-HBA+Shape to identify known aromatase inhibitors not included in the training set. Compounds fitting the model are marked with a (√) in the table above.

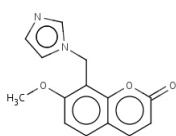
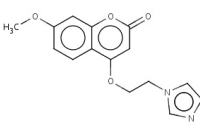
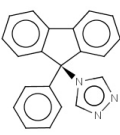
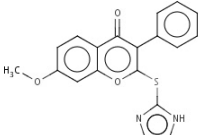
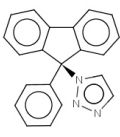
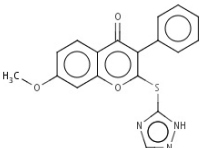
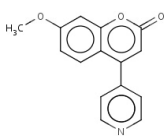
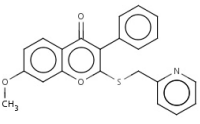
Structure	IC ₅₀ (μM)		Structure	IC ₅₀ (μM)	
	0.0023			0.051	√
	0.040	√		0.069	√
	0.043	√		0.071	
	0.045			0.074	
	0.049			0.080	√

	0.089	✓		0.170
	0.096			0.210
	0.100			0.220 ✓
	0.106	✓		0.220
	0.110	✓		0.240
	0.144			0.280 ✓
	0.150	✓		0.280 ✓
	0.168	✓		0.290

	0.350		0.550	✓
	0.390		0.610	✓
	0.440		0.630	✓
	0.470		0.680	
	0.500		0.680	
	0.520		0.760	
	0.530		0.770	✓

	0.940			2.10	
	0.970			2.30	√
	1.10			2.40	
	1.13			2.82	
	1.38			2.85	
	1.60	√		3.00	
	1.80	√		3.06	
	2.00	√		3.10	
	2.10			3.56	

	3.60	✓		6.00	
	3.60			9.20	✓
	3.70			17.0	
	3.90			18.0	✓
	4.00			26.6	
	4.10	✓		27% inhibition at 25 μM	
	4.70			21% inhibition at 25 μM	✓
	5.13			60% inhibition at 36 μM	

	59% inhibition at 36 μ M		12% inhibition at 36 μ M
	44% inhibition at 36 μ M		> 50 μ M
	30% inhibition at 36 μ M		> 50 μ M
	27% inhibition at 36 μ M		> 100 μ M

VII

References

- (1) Lacroix, M. Significance, detection and markers of disseminated breast cancer cells. *Endocr. -Relat. Cancer* **2006**, *13*, 1033-1067.
- (2) Ferlay, J.; Autier, P.; Boniol, M.; Heanue, M.; Colombet, M.; Boyle, P. Estimates of the cancer incidence and mortality in Europe in 2006. *Ann. Oncol.* **2007**, *18*, 581-592.
- (3) Jemal, A.; Siegel, R.; Ward, E.; Hao, Y. P.; Xu, J. Q.; Murray, T.; Thun, M. J. Cancer statistics, 2008. *CA Cancer J. Clin.* **2008**, *58*, 71-96.
- (4) McPherson, K.; Steel, C. M.; Dixon, J. M. ABC of breast disease: Breast cancer-epidemiology, risk factors, and genetics. *Br. Med. J.* **2000**, *321*, 624-628.
- (5) Breast cancer treatment [online], National Cancer Institute, [accessed on 20-07-2008]. Available at <http://www.cancer.gov>
- (6) Smith, I. E.; Dowsett, M. Aromatase inhibitors in breast cancer. *N. Engl. J. Med.* **2003**, *348*, 2431-2442.
- (7) Osborne, C. K. Drug therapy - Tamoxifen in the treatment of breast cancer. *N. Engl. J. Med.* **1998**, *339*, 1609-1618.
- (8) Eastell, R.; Adams, J. E.; Coleman, R. E.; Howell, A.; Hannon, R. A.; Cuzick, J.; Mackey, J. R.; Beckmann, M. W.; Clack, G. Effect of anastrozole on bone mineral density: 5-year results from the anastrozole, tamoxifen, alone or in combination trial 18233230. *J. Clin. Oncol.* **2008**, *26*, 1051-1058.
- (9) Powles, T.; Hickish, T.; Kanis, J. A.; Tidy, A.; Ashley, S. Effect of tamoxifen on bone mineral density measured by dual-energy X-ray absorptiometry in healthy premenopausal and postmenopausal women. *J. Clin. Oncol.* **1996**, *14*, 78-84.
- (10) Wickerham, D. L.; Fisher, B.; Wolmark, N.; Bryant, J.; Costantino, J.; Bernstein, L.; Runowicz, C. D. Association of tamoxifen and uterine sarcoma. *J. Clin. Oncol.* **2002**, *20*, 2758-2760.
- (11) Morales, L.; Timmerman, D.; Neven, P.; Konstantinovic, M. L.; Carbonez, A.; Van Huffel, S.; Ameye, L.; Weltens, C.; Christiaens, M. R.; Vergote, I.; Paridaens, R. Third generation aromatase inhibitors may prevent endometrial growth and reverse tamoxifen-induced uterine changes in postmenopausal breast cancer patients. *Ann. Oncol.* **2005**, *16*, 70-74.
- (12) Meier, C. R.; Jick, H. Tamoxifen and risk of idiopathic venous thromboembolism. *Br. J. Clin. Pharmacol.* **1998**, *45*, 608-612.
- (13) Riggins, R. B.; Schrecengost, R. S.; Guerrero, M. S.; Bouton, A. H. Pathways to tamoxifen resistance. *Cancer Lett.* **2007**, *256*, 1-24.

- (14) Baum, M.; Buzdar, A. U.; Cuzick, J.; Forbes, J.; Houghton, J.; Klijn, J. G. M.; Sahmoud, T. Anastrozole alone or in combination with tamoxifen versus tamoxifen alone for adjuvant treatment of postmenopausal women with early breast cancer: first results of the ATAC randomised trial. *Lancet* **2002**, *359*, 2131-2139.
- (15) Mouridsen, H.; Gershanovich, M.; Sun, Y.; Perez-Carrion, R.; Boni, C.; Monnier, A.; Apffelstaedt, J.; Smith, R.; Sleeboom, H. P.; Janicke, F.; Pluzanska, A.; Dank, M.; Becquart, D.; Bapsy, P. P.; Salminen, E.; Snyder, R.; Lassus, M.; Verbeek, J. A.; Staffler, B.; Chaudri-Ross, H. A.; Dugan, M. Superior efficacy of letrozole versus tamoxifen as first-line therapy for postmenopausal women with advanced breast cancer: Results of a phase III study of the international letrozole breast cancer group. *J. Clin. Oncol.* **2001**, *19*, 2596-2606.
- (16) Cuzick, J. Aromatase inhibitors for breast cancer prevention. *J. Clin. Oncol.* **2005**, *23*, 1636-1643.
- (17) Celio, L.; Martinetti, A.; Ferrari, L.; Buzzoni, R.; Mariani, L.; Miceli, R.; Seregini, E.; Procopio, G.; Cassata, A.; Bombardieri, E.; Bajetta, E. Premenopausal breast cancer patients treated with a gonadotropin-releasing hormone analog alone or in combination with an aromatase inhibitor: A comparative endocrine study. *Anticancer Res.* **1999**, *19*, 2261-2268.
- (18) de Ziegler, D.; Mattenberger, C.; Luyet, C.; Romoscanu, I.; Irion, N. F.; Bianchi-Demicheli, F. Clinical use of aromatase inhibitors (AI) in premenopausal women. *J. Steroid Biochem. Mol. Biol.* **2005**, *95*, 121-127.
- (19) Farhat, M. Y.; Lavigne, M. C.; Ramwell, P. W. The vascular protective effects of estrogen. *Faseb J.* **1996**, *10*, 615-624.
- (20) Riggs, B. L.; Khosla, S.; Melton, L. J. Sex steroids and the construction and conservation of the adult skeleton. *Endocr. Rev.* **2002**, *23*, 279-302.
- (21) Garcia-Segura, L. M.; Azcoitia, I.; DonCarlos, L. L. Neuroprotection by estradiol. *Prog. Neurobiol.* **2001**, *63*, 29-60.
- (22) Henderson, B. E.; Feigelson, H. S. Hormonal carcinogenesis. *Carcinogenesis* **2000**, *21*, 427-433.
- (23) Beatson, G. T. On the treatment of inoperable cases of carcinoma of the mamma: suggestions for a new method of treatment, with illustrative cases. *Lancet* **1896**, *2*, 104-107.
- (24) Harrell, J. C.; Dye, W. W.; Allred, D. C.; Jedlicka, P.; Spoelstra, N. S.; Sartorius, C. A.; Horwitz, K. B. Estrogen receptor positive breast cancer metastasis: Altered hormonal sensitivity and tumor aggressiveness in lymphatic vessels and lymph nodes. *Cancer Res.* **2006**, *66*, 9308-9315.

-
- (25) Keen, J. C.; Davidson, N. E. The biology of breast carcinoma. *Cancer* **2003**, *97*, 825-833.
- (26) Geisler, J. Breast cancer tissue estrogens and their manipulation with aromatase inhibitors and inactivators. *J. Steroid Biochem. Mol. Biol.* **2003**, *86*, 245-253.
- (27) Masamura, S.; Santner, S. J.; Gimotty, P.; George, J.; Santen, R. J. Mechanism for maintenance of high breast tumor estradiol concentrations in the absence of ovarian function: Role of very high affinity tissue uptake. *Breast Cancer Res. Treat.* **1997**, *42*, 215-226.
- (28) Reed, M. J.; Purohit, A.; Woo, L. W. L.; Newman, S. P.; Potter, B. V. L. Steroid sulfatase: Molecular biology, regulation, and inhibition. *Endocr. Rev.* **2005**, *26*, 171-202.
- (29) Simard, J.; Ricketts, M. L.; Gingras, B.; Soucy, P.; Feltus, F. A.; Melner, M. H. Molecular biology of the 3 β -hydroxysteroid dehydrogenase/ Δ^5 - Δ^4 isomerase gene family. *Endocr. Rev.* **2005**, *26*, 525-582.
- (30) Macedo, L. F.; Guo, Z. Y.; Tilghman, S. L.; Sabnis, G. J.; Qiu, Y.; Brodie, A. Role of androgens on MCF-7 breast cancer cell growth and on the inhibitory effect of letrozole. *Cancer Res.* **2006**, *66*, 7775-7782.
- (31) Adams, J.; Garcia, M.; Rochefort, H. Estrogenic effects of physiological concentrations of 5-androstene-3 β ,17 β -diol and its metabolism in MCF₇ human breast cancer cells. *Cancer Res.* **1981**, *41*, 4720-4726.
- (32) Kitawaki, J.; Inoue, S.; Tamura, T.; Yamamoto, T.; Noguchi, T.; Osawa, Y.; Okada, H. Increasing aromatase cytochrome P-450 level in human placenta during pregnancy: Studied by immunohistochemistry and enzyme-linked immunosorbent assay. *Endocrinology* **1992**, *130*, 2751-2757.
- (33) Szymczak, J.; Milewicz, A.; Thijssen, J. H. H.; Blankenstein, M. A.; Daroszewski, J. Concentration of sex steroids in adipose tissue after menopause. *Steroids* **1998**, *63*, 319-321.
- (34) Frost, P. G.; Reed, M. J.; James, V. H. T. The aromatization of androstenedione by human adipose and liver tissue. *J. Steroid Biochem.* **1980**, *13*, 1427-1431.
- (35) Larionov, A. A.; Vasyliov, D. A.; Mason, J. I.; Howie, A. F.; Berstein, L. M.; Miller, W. R. Aromatase in skeletal muscle. *J. Steroid Biochem. Mol. Biol.* **2003**, *84*, 485-492.
- (36) Roselli, C. F. Brain aromatase: Roles in reproduction and neuroprotection. *J. Steroid Biochem. Mol. Biol.* **2007**, *106*, 143-150.
- (37) Miller, W. R. Biological rationale for endocrine therapy in breast cancer. *Best Pract. Res. Clin. Endoc. Metab.* **2004**, *18*, 1-32.

- (38) Thijssen, J. H.; Blankenstein, M. A. Endogenous oestrogens and androgens in normal and malignant endometrial and mammary tissues. *Eur. J Cancer Clin. Oncol.* **1989**, *25*, 1953-1959.
- (39) Lukacik, P.; Kavanagh, K. L.; Oppermann, U. Structure and function of human 17 β -hydroxysteroid dehydrogenases. *Mol. Cell. Endocrinol.* **2006**, *248*, 61-71.
- (40) Puranen, T.; Poutanen, M.; Ghosh, D.; Vihko, P.; Vihko, R. Characterization of structural and functional properties of human 17 β -hydroxysteroid dehydrogenase type 1 using recombinant enzymes and site-directed mutagenesis. *Mol. Endocrinol.* **1997**, *11*, 77-86.
- (41) Puranen, T. J.; Kurkela, R. M.; Lakkakorpi, J. T.; Poutanen, M. H.; Itaranta, P. V.; Melis, J. P. J.; Ghosh, D.; Vihko, R. K.; Vihko, P. T. Characterization of molecular and catalytic properties of intact and truncated human 17 β -hydroxysteroid dehydrogenase type 2 enzymes: Intracellular localization of the wild-type enzyme in the endoplasmic reticulum. *Endocrinology* **1999**, *140*, 3334-3341.
- (42) Miettinen, M.; Mustonen, M.; Poutanen, M.; Isomaa, V.; Wickman, M.; Soderqvist, G.; Vihko, R.; Vihko, P. 17 β -hydroxysteroid dehydrogenases in normal human mammary epithelial cells and breast tissue. *Breast Cancer Res. Treat.* **1999**, *57*, 175-182.
- (43) Irahara, N.; Miyoshi, Y.; Taguchi, T.; Tamaki, Y.; Noguchi, S. Quantitative analysis of *aromatase*, *sulfatase* and *17 β -HSD1* mRNA expression in soft tissue metastases of breast cancer. *Cancer Lett.* **2006**, *243*, 23-31.
- (44) Oduwale, O. O.; Li, Y.; Isomaa, V. V.; Mantyniemi, A.; Pulkka, A. E.; Soini, Y.; Vihko, P. T. 17 β -hydroxysteroid dehydrogenase type 1 is an independent prognostic marker in breast cancer. *Cancer Res.* **2004**, *64*, 7604-7609.
- (45) Poirier, D. Inhibitors of 17 β -hydroxysteroid dehydrogenases. *Curr. Med. Chem.* **2003**, *10*, 453-477.
- (46) Miki, Y.; Nakata, T.; Suzuki, T.; Darnel, A. D.; Moriya, T.; Kaneko, C.; Hidaka, K.; Shiotsu, Y.; Kusaka, H.; Sasano, H. Systemic distribution of steroid sulfatase and estrogen sulfotransferase in human adult and fetal tissues. *J. Clin. Endocrinol. Metab.* **2002**, *87*, 5760-5768.
- (47) Suzuki, T.; Nakata, T.; Miki, Y.; Kaneko, C.; Moriya, T.; Ishida, T.; Akinaga, S.; Hirakawa, H.; Kimura, M.; Sasano, H. Estrogen sulfotransferase and steroid sulfatase in human breast carcinoma. *Cancer Res.* **2003**, *63*, 2762-2770.

- (48) Noel, C. T.; Reed, M. J.; Jacobs, H. S.; James, V. H. The plasma concentration of oestrone sulphate in postmenopausal women: lack of diurnal variation, effect of ovariectomy, age and weight. *J Steroid Biochem.* **1981**, *14*, 1101-1105.
- (49) Ruder, H. J.; Loriaux, L.; Lipsett, M. B. Estrone sulfate: Production rate and metabolism in man. *J. Clin. Invest.* **1972**, *51*, 1020-1033.
- (50) Koehler, K. F.; Helguero, L. A.; Haldosen, L. A.; Warner, M.; Gustafsson, J. A. Reflections on the discovery and significance of estrogen receptor β . *Endocr. Rev.* **2005**, *26*, 465-478.
- (51) Zhang, W. H.; Saji, S.; Makinen, S.; Cheng, G. J.; Jensen, E. V.; Warner, M.; Gustafsson, J. A. Estrogen receptor (ER) β , a modulator of ER α in the uterus. *Proc. Natl. Acad. Sci. U. S. A* **2000**, *97*, 5936-5941.
- (52) Palmieri, C.; Cheng, G. J.; Saji, S.; Zelada-Hedman, M.; Warri, A.; Weihua, Z.; Van Noorden, S.; Wahlstrom, T.; Coombes, R. C.; Warner, M.; Gustafsson, J. A. Estrogen receptor beta in breast cancer. *Endocr. -Relat. Cancer* **2002**, *9*, 1-13.
- (53) Weihua Z.; Makela, S.; Andersson, L. C.; Salmi, S.; Saji, S.; Webster, J. I.; Jensen, E. V.; Nilsson, S.; Warner, M.; Gustafsson, J. A. A role for estrogen receptor β in the regulation of growth of the ventral prostate. *Proc. Natl. Acad. Sci. U. S. A* **2001**, *98*, 6330-6335.
- (54) Makinen, S.; Makela, S.; Zhang, W. H.; Warner, M.; Rosenlund, B.; Salmi, S.; Hovatta, O.; Gustafsson, J. A. Localization of oestrogen receptors alpha and beta in human testis. *Mol. Hum. Reprod.* **2001**, *7*, 497-503.
- (55) Braidman, I. P.; Hainey, L.; Batra, G.; Selby, P. L.; Saunders, P. T. K.; Hoyland, J. A. Localization of estrogen receptor β protein expression in adult human bone. *J. Bone Miner. Res.* **2001**, *16*, 214-220.
- (56) Shim, G. J.; Wang, L.; Andersson, S.; Nagy, N.; Kis, L. L.; Zhang, Q. H.; Makela, S.; Warner, M.; Gustafsson, J. A. Disruption of the estrogen receptor β gene in mice causes myeloproliferative disease resembling chronic myeloid leukemia with lymphoid blast crisis. *Proc. Natl. Acad. Sci. U. S. A* **2003**, *100*, 6694-6699.
- (57) Zhu, Y.; Bian, Z.; Lu, P.; Karas, R. H.; Bao, L.; Cox, D.; Hodgkin, J.; Shaul, P. W.; Thoren, P.; Smithies, O.; Gustafsson, J. A.; Mendelsohn, M. E. Abnormal vascular function and hypertension in mice deficient in estrogen receptor β . *Science* **2002**, *295*, 505-508.
- (58) Mitra, S. W.; Hoskin, E.; Yudkovitz, J.; Pear, L.; Wilkinson, H. A.; Hayashi, S.; Pfaff, D. W.; Ogawa, S.; Rohrer, S. P.; Schaeffer, J. M.; Mcewen, B. S.; Alves, S. E. Immunolocalization of estrogen receptor β in the mouse brain: Comparison with estrogen receptor α . *Endocrinology* **2003**, *144*, 2055-2067.

- (59) Bardin, A.; Boulle, N.; Lazennec, G.; Vignon, F.; Pujol, P. Loss of ER β expression as a common step in estrogen-dependent tumor progression. *Endocr. -Relat. Cancer* **2004**, *11*, 537-551.
- (60) Roger, P.; Sahla, M. E.; Makela, S.; Gustafsson, J. A.; Baldet, P.; Rochefort, H. Decreased expression of estrogen receptor β protein in proliferative preinvasive mammary tumors. *Cancer Res.* **2001**, *61*, 2537-2541.
- (61) Hodges-Gallagher, L.; Valentine, C. D.; El Bader, S.; Kushner, P. J. Estrogen receptor beta increases the efficacy of antiestrogens by effects on apoptosis and cell cycling in breast cancer cells. *Breast Cancer Res. Treat.* **2008**, *109*, 241-250.
- (62) Paruthiyil, S.; Parmar, H.; Kerekatte, V.; Cunha, G. R.; Firestone, G. L.; Leitman, D. C. Estrogen receptor β inhibits human breast cancer cell proliferation and tumor formation by causing a G₂ cell cycle arrest. *Cancer Res.* **2004**, *64*, 423-428.
- (63) Strom, A.; Hartman, J.; Foster, J. S.; Kietz, S.; Wimalasena, J.; Gustafsson, J. A. Estrogen receptor β inhibits 17 β -estradiol-stimulated proliferation of the breast cancer cell line T47D. *Proc. Natl. Acad. Sci. U. S. A* **2004**, *101*, 1566-1571.
- (64) Hall, J. M.; Couse, J. F.; Korach, K. S. The multifaceted mechanisms of estradiol and estrogen receptor signaling. *J. Biol. Chem.* **2001**, *276*, 36869-36872.
- (65) Kato, S.; Endoh, H.; Masuhiro, Y.; Kitamoto, T.; Uchiyama, S.; Sasaki, H.; Masushige, S.; Gotoh, Y.; Nishida, E.; Kawashima, H.; Metzger, D.; Chambon, P. Activation of the estrogen receptor through phosphorylation by mitogen-activated protein kinase. *Science* **1995**, *270*, 1491-1494.
- (66) Powers, C. J.; McLeskey, S. W.; Wellstein, A. Fibroblast growth factors, their receptors and signaling. *Endocr. -Relat. Cancer* **2000**, *7*, 165-197.
- (67) Coutts, A. S.; Murphy, L. C. Elevated mitogen-activated protein kinase activity in estrogen-nonresponsive human breast cancer cells. *Cancer Res.* **1998**, *58*, 4071-4074.
- (68) Shim, W.-S.; Conaway, M.; Masamura, S.; Yue, W.; Wang, J. P.; Kumar, R.; Santen, R. J. Estradiol hypersensitivity and mitogen-activated protein kinase expression in long-term estrogen deprived human breast cancer cells *in vivo*. *Endocrinology* **2000**, *141*, 396-405.
- (69) Webb, P.; Nguyen, P.; Kushner, P. J. Differential SERM effects on corepressor binding dictate ER α activity *in vivo*. *J. Biol. Chem.* **2003**, *278*, 6912-6920.

-
- (70) Smith, C. L.; Nawaz, Z.; O'Malley, B. W. Coactivator and corepressor regulation of the agonist/antagonist activity of the mixed antiestrogen, 4-hydroxytamoxifen. *Mol. Endocrinol.* **1997**, *11*, 657-666.
- (71) Jordan, V. C. Antiestrogens and selective estrogen receptor modulators as multifunctional medicines. 1. Receptor interactions. *J. Med. Chem.* **2003**, *46*, 883-908.
- (72) Branham, W. S.; Dial, S. L.; Moland, C. L.; Hass, B. S.; Blair, R. M.; Fang, H.; Shi, L. M.; Tong, W. D.; Perkins, R. G.; Sheehan, D. M. Phytoestrogens and mycoestrogens bind to the rat uterine estrogen receptor. *J. Nutr.* **2002**, *132*, 658-664.
- (73) Shiau, A. K.; Barstad, D.; Loria, P. M.; Cheng, L.; Kushner, P. J.; Agard, D. A.; Greene, G. L. The structural basis of estrogen receptor/coactivator recognition and the antagonism of this interaction by tamoxifen. *Cell* **1998**, *95*, 927-937.
- (74) Osborne, C. K.; Fuqua, S. A. W. Selective estrogen receptor modulators: Structure, function, and clinical use. *J. Clin. Oncol.* **2000**, *18*, 3172-3186.
- (75) Zhu, B. T.; Conney, A. H. Functional role of estrogen metabolism in target cells: review and perspectives. *Carcinogenesis* **1998**, *19*, 1-27.
- (76) Lee, A. J.; Kosh, J. W.; Conney, A. H.; Zhu, B. T. Characterization of the NADPH-dependent metabolism of 17 β -estradiol to multiple metabolites by human liver microsomes and selectively expressed human cytochrome P450 3A4 and 3A5. *J. Pharmacol. Exp. Ther.* **2001**, *298*, 420-432.
- (77) Liehr, J. G.; Ricci, M. J. 4-Hydroxylation of estrogens as marker of human mammary tumors. *Proc. Natl. Acad. Sci. U. S. A* **1996**, *93*, 3294-3296.
- (78) Hoffman, A. R.; Paul, S. M.; Axelrod, J. Catecholesterogen synthesis and metabolism by human breast tumors *in vitro*. *Cancer Res.* **1979**, *39*, 4584-4587.
- (79) Bunyagidj, C.; Mclachlan, J. A. Catechol estrogen formation in mouse uterus. *J. Steroid Biochem.* **1988**, *31*, 795-801.
- (80) Liehr, J. G.; Ricci, M. J.; Jefcoate, C. R.; Hannigan, E. V.; Hokanson, J. A.; Zhu, B. T. 4-Hydroxylation of estradiol by human uterine myometrium and myoma microsomes: Implications for the mechanism of uterine tumorigenesis. *Proc. Natl. Acad. Sci. U. S. A* **1995**, *92*, 9220-9224.
- (81) Fishman, J.; Dixon, D. 2-Hydroxylation of estradiol by human placental microsomes. *Biochemistry* **1967**, *6*, 1683-1687.
- (82) Hammond, D. K.; Zhu, B. T.; Wang, M. Y.; Ricci, M. J.; Liehr, J. G. Cytochrome P450 metabolism of estradiol in hamster liver and kidney. *Toxicol. Appl. Pharmacol.* **1997**, *145*, 54-60.

- (83) Zhu, B. T.; Bui, Q. D.; Weisz, J.; Liehr, J. G. Conversion of estrone to 2- and 4-hydroxyestrone by hamster kidney and liver microsomes: Implications for the mechanism of estrogen-induced carcinogenesis. *Endocrinology* **1994**, *135*, 1772-1779.
- (84) Hersey, R. M.; Williams, K. I. H.; Weisz, J. Catechol estrogen formation by brain tissue: Characterization of a direct product isolation assay for estrogen-2- and 4-hydroxylase activity and its application to studies of 2- and 4-hydroxyestradiol formation by rabbit hypothalamus. *Endocrinology* **1981**, *109*, 1912-1920.
- (85) Karhunen, T.; Tilgmann, C.; Ulmanen, I.; Julkunen, I.; Panula, P. Distribution of catechol-O-methyltransferase enzyme in rat tissues. *J. Histochem. Cytochem.* **1994**, *42*, 1079-1090.
- (86) Tenhunen, J.; Heikkila, P.; Alanko, A.; Heinonen, E.; Akkila, J.; Ulmanen, I. Soluble and membrane-bound catechol-O-methyltransferase in normal and malignant mammary gland. *Cancer Lett.* **1999**, *144*, 75-84.
- (87) Mueck, A. O.; Seeger, H.; Lippert, T. H. Estradiol metabolism and malignant disease. *Maturitas* **2002**, *43*, 1-10.
- (88) Gupta, M.; McDougal, A.; Safe, S. Estrogenic and antiestrogenic activities of 16 α - and 2-hydroxy metabolites of 17 β -estradiol in MCF-7 and T47D human breast cancer cells. *J. Steroid Biochem. Mol. Biol.* **1998**, *67*, 413-419.
- (89) Martucci, C.; Fishman, J. Uterine estrogen receptor binding of catecholestrogens and of estetrol (1,3,5(10)-estratriene-3,15 α ,16 α ,17 β -tetrol). *Steroids* **1976**, *27*, 325-333.
- (90) Schutze, N.; Vollmer, G.; Tiemann, I.; Geiger, M.; Knuppen, R. Catecholestrogens are MCF-7 cell estrogen receptor agonists. *J. Steroid Biochem. Mol. Biol.* **1993**, *46*, 781-789.
- (91) Schneider, J.; Huh, M. M.; Bradlow, H. L.; Fishman, J. Antiestrogen action of 2-hydroxyestrone on MCF-7 human breast cancer cells. *J. Biol. Chem.* **1984**, *259*, 4840-4845.
- (92) Lee, A. J.; Cai, M. X. X.; Thomas, P. E.; Conney, A. H.; Zhu, B. T. Characterization of the oxidative metabolites of 17 β -estradiol and estrone formed by 15 selectively expressed human cytochrome P450 isoforms. *Endocrinology* **2003**, *144*, 3382-3398.
- (93) Modugno, F.; Knoll, C.; Kanbour-Shakir, A.; Romkes, M. A potential role for the estrogen-metabolizing cytochrome P450 enzymes in human breast carcinogenesis. *Breast Cancer Res. Treat.* **2003**, *82*, 191-197.

-
- (94) Spink, D. C.; Lincoln, D. W.; Dickerman, H. W.; Gierthy, J. F. 2,3,7,8-Tetrachlorodibenzo-*p*-dioxin causes an extensive alteration of 17 β -estradiol metabolism in MCF-7 breast tumor cells. *Proc. Natl. Acad. Sci. U. S. A* **1990**, *87*, 6917-6921.
- (95) D'Amato, R. J.; Lin, C. M.; Flynn, E.; Folkman, J.; Hamel, E. 2-Methoxyestradiol, an endogenous mammalian metabolite, inhibits tubulin polymerization by interacting at the colchicine site. *Proc. Natl. Acad. Sci. U. S. A* **1994**, *91*, 3964-3968.
- (96) Fotsis, T.; Zhang, Y.; Pepper, M. S.; Adlercreutz, H.; Montesano, R.; Nawroth, P. P.; Schweigener, L. The endogenous oestrogen metabolite 2-methoxyoestradiol inhibits angiogenesis and suppresses tumour growth. *Nature* **1994**, *368*, 237-239.
- (97) Dahut, W. L.; Lakhani, N. J.; Gulley, J. L.; Arlen, P. M.; Kohn, E. C.; Kotz, H.; McNally, D.; Parr, A.; Nguyen, D.; Yang, S. X.; Steinberg, S. M.; Venitz, J.; Sparreboom, A.; Figg, W. D. Phase I clinical trial of oral 2-methoxyestradiol, an antiangiogenic and apoptotic agent, in patients with solid tumors. *Cancer Biol. Ther.* **2006**, *5*, 22-27.
- (98) Sweeney, C.; Liu, G.; Yiannoutsos, C.; Kolesar, J.; Horvath, D.; Staab, M. J.; Fife, K.; Armstrong, V.; Treston, A.; Sidor, C.; Wilding, G. A phase II multicenter, randomized, double-blind, safety trial assessing the pharmacokinetics, pharmacodynamics, and efficacy of oral 2-methoxyestradiol capsules in hormone-refractory prostate cancer. *Clin. Cancer Res.* **2005**, *11*, 6625-6633.
- (99) Cushman, M.; Mohanakrishnan, A. K.; Hollingshead, M.; Hamel, E. The effect of exchanging various substituents at the 2-position of 2-methoxyestradiol on cytotoxicity in human cancer cell cultures and inhibition of tubulin polymerization. *J. Med. Chem.* **2002**, *45*, 4748-4754.
- (100) La Vallee, T. M.; Burke, P. A.; Swartz, G. M.; Hamel, E.; Agoston, G. E.; Shah, J.; Suwandi, L.; Hanson, A. D.; Fogler, W. E.; Sidor, C. F.; Treston, A. M. Significant antitumor activity *in vivo* following treatment with the microtubule agent ENMD-1198. *Mol. Cancer Ther.* **2008**, *7*, 1472-1482.
- (101) Tinley, T. L.; Leal, R. M.; Randall-Hlubek, D. A.; Cessac, J. W.; Wilkens, L. R.; Rao, P. N.; Mooberry, S. L. Novel 2-methoxyestradiol analogues with antitumor activity. *Cancer Res.* **2003**, *63*, 1538-1549.
- (102) Barnea, E. R.; Maclusky, N. J.; Naftolin, F. Kinetics of catechol estrogen-estrogen receptor dissociation: A possible factor underlying differences in catechol estrogen biological activity. *Steroids* **1983**, *41*, 643-656.
- (103) Hayes, C. L.; Spink, D. C.; Spink, B. C.; Cao, J. Q.; Walker, N. J.; Sutter, T. R. 17 β -estradiol hydroxylation catalyzed by human cytochrome P450 1B1. *Proc. Natl. Acad. Sci. U. S. A* **1996**, *93*, 9776-9781.

- (104) Swaneck, G. E.; Fishman, J. Covalent binding of the endogenous estrogen 16 α -hydroxyestrone to estradiol receptor in human breast cancer cells: characterization and intranuclear localization. *Proc. Natl. Acad. Sci. U. S. A* **1988**, *85*, 7831-7835.
- (105) Schneider, J.; Kinne, D.; Fracchia, A.; Pierce, V.; Anderson, K. E.; Bradlow, H. L.; Fishman, J. Abnormal oxidative metabolism of estradiol in women with breast cancer. *Proc. Natl. Acad. Sci. U. S. A* **1982**, *79*, 3047-3051.
- (106) Kabat, G. C.; Chang, C. J.; Sparano, J. A.; Sepkovic, D. W.; Hu, X. P.; Khalil, A.; Rosenblatt, R.; Bradlow, H. L. Urinary estrogen metabolites and breast cancer: A case-control study. *Cancer Epidemiol. Biomarkers Prev.* **1997**, *6*, 505-509.
- (107) Zacharia, L. C.; Piche, C. A.; Fielding, R. M.; Holland, K. M.; Allison, S. D.; Dubey, R. K.; Jackson, E. K. 2-Hydroxyestradiol is a prodrug of 2-methoxyestradiol. *J. Pharmacol. Exp. Ther.* **2004**, *309*, 1093-1097.
- (108) Spierto, F. W.; Gardner, F.; Smith, S. J. Evaluation of an EIA method for measuring serum levels of the estrogen metabolite 2-hydroxyestrone in adults. *Steroids* **2001**, *66*, 59-62.
- (109) Nutter, L. M.; Ngo, E. O.; Abulhadj, Y. J. Characterization of DNA damage induced by 3,4-estrone-*o*-quinone in human cells. *J. Biol. Chem.* **1991**, *266*, 16380-16386.
- (110) Cavaliere, E.; Chakravarti, D.; Guttenplan, J.; Hart, E.; Ingle, J.; Jankowiak, R.; Muti, P.; Rogan, E.; Russo, J.; Santen, R.; Sutter, T. Catechol estrogen quinones as initiators of breast and other human cancers: implications for biomarkers of susceptibility and cancer prevention. *Biochim. Biophys. Acta* **2006**, *1766*, 63-78.
- (111) Liehr, J. G.; Fang, W. F.; Sirbasku, D. A.; Ariulubelen, A. Carcinogenicity of catechol estrogens in Syrian hamsters. *J. Steroid Biochem.* **1986**, *24*, 353-356.
- (112) Mobley, J. A.; Bhat, A. S.; Brueggemeier, R. W. Measurement of oxidative DNA damage by catechol estrogens and analogues in vitro. *Chem. Res. Toxicol.* **1999**, *12*, 270-277.
- (113) Zahid, M.; Kohli, E.; Saeed, M.; Rogan, E.; Cavaliere, E. The greater reactivity of estradiol-3,4-quinone vs estradiol-2,3-quinone with DNA in the formation of depurinating adducts: Implications for tumor-initiating activity. *Chem. Res. Toxicol.* **2006**, *19*, 164-172.
- (114) Roy, D.; Liehr, J. G. Temporary decrease in renal quinone reductase activity induced by chronic administration of estradiol to male Syrian hamsters - Increased superoxide formation by redox cycling of estrogen. *J. Biol. Chem.* **1988**, *263*, 3646-3651.

-
- (115) Nelson, D. R. Cytochrome P450 homepage [online], [accessed on 25-07-2008]. Available at <http://dnelson.utm.edu/CytochromeP450.html>
- (116) Ding, X.; Kaminsky, L. S. Human extrahepatic cytochromes P450: Function in xenobiotic metabolism and tissue-selective chemical toxicity in the respiratory and gastrointestinal tracts. *Annu. Rev. Pharmacol. Toxicol.* **2003**, *43*, 149-173.
- (117) Humphrey, W.; Dalke, A.; Schulten, K. VMD: Visual molecular dynamics. *J. Mol. Graph.* **1996**, *14*, 33-38.
- (118) Filatov, M.; Reckien, W.; Peyerimhoff, S. D.; Shaik, S. What are the reasons for the kinetic stability of a mixture of H₂ and O₂? *J. Phys. Chem. A* **2000**, *104*, 12014-12020.
- (119) Rendic, S. Summary of information on human CYP enzymes: Human P450 metabolism data. *Drug Metab. Rev.* **2002**, *34*, 83-448.
- (120) Meunier, B.; de Visser, S. P.; Shaik, S. Mechanism of oxidation reactions catalyzed by cytochrome P450 enzymes. *Chem. Rev.* **2004**, *104*, 3947-3980.
- (121) Munro, A. W.; Noble, M. A.; Robledo, L.; Daff, S. N.; Chapman, S. K. Determination of the redox properties of human NADPH-cytochrome P450 reductase. *Biochemistry* **2001**, *40*, 1956-1963.
- (122) Centeno, F.; Gutierrez-Merino, C. Location of functional centers in the microsomal cytochrome P450 system. *Biochemistry* **1992**, *31*, 8473-8481.
- (123) Edwards, R. J.; Murray, B. P.; Singleton, A. M.; Boobis, A. R. Orientation of cytochromes P450 in the endoplasmic reticulum. *Biochemistry* **1991**, *30*, 71-76.
- (124) Nelson, D. R.; Strobel, H. W. On the membrane topology of vertebrate cytochrome P450 proteins. *J. Biol. Chem.* **1988**, *263*, 6038-6050.
- (125) Danielson, P. B. The cytochrome P450 superfamily: Biochemistry, evolution and drug metabolism in humans. *Curr. Drug Metab.* **2002**, *3*, 561-597.
- (126) Nelson, D. R.; Koymans, L.; Kamataki, T.; Stegeman, J. J.; Feyereisen, R.; Waxman, D. J.; Waterman, M. R.; Gotoh, O.; Coon, M. J.; Estabrook, R. W.; Gunsalus, I. C.; Nebert, D. W. P450 superfamily: Update on new sequences, gene mapping, accession numbers and nomenclature. *Pharmacogenetics* **1996**, *6*, 1-42.
- (127) Poulos, T. L.; Finzel, B. C.; Gunsalus, I. C.; Wagner, G. C.; Kraut, J. The 2.6 Å crystal structure of *Pseudomonas putida* cytochrome P-450. *J. Biol. Chem.* **1985**, *260*, 6122-6130.

- (128) Ravichandran, K. G.; Boddupalli, S. S.; Hasemann, C. A.; Peterson, J. A.; Deisenhofer, J. Crystal structure of hemoprotein domain of P450_{BM-3}, a prototype for microsomal P450's. *Science* **1993**, *261*, 731-736.
- (129) Hasemann, C. A.; Ravichandran, K. G.; Peterson, J. A.; Deisenhofer, J. Crystal structure and refinement of cytochrome P450_{terp} at 2.3 Å resolution. *J. Mol. Biol.* **1994**, *236*, 1169-1185.
- (130) Cupp-Vickery, J. R.; Poulos, T. L. Structure of cytochrome P450_{eryF} involved in erythromycin biosynthesis. *Nature Struct. Bio.* **1995**, *2*, 144-153.
- (131) Williams, P. A.; Cosme, J.; Sridhar, V.; Johnson, E. F.; Mcrec, D. E. Microsomal cytochrome P450_{2C5}: comparison to microbial P450s and unique features. *J. Inorg. Biochem.* **2000**, *81*, 183-190.
- (132) Scott, E. E.; He, Y. A.; Wester, M. R.; White, M. A.; Chin, C. C.; Halpert, J. R.; Johnson, E. F.; Stout, C. D. An open conformation of mammalian cytochrome P450_{2B4} at 1.6 Å resolution. *Proc. Natl. Acad. Sci. U. S. A* **2003**, *100*, 13196-13201.
- (133) Sansen, S.; Yano, J. K.; Reynald, R. L.; Schoch, G. A.; Griffin, K. J.; Stout, C. D.; Johnson, E. F. Adaptations for the oxidation of polycyclic aromatic hydrocarbons exhibited by the structure of human P450 1A2. *J. Biol. Chem.* **2007**, *282*, 14348-14355.
- (134) Yano, J. K.; Hsu, M. H.; Griffin, K. J.; Stout, C. D.; Johnson, E. F. Structures of human microsomal cytochrome P450 2A6 complexed with coumarin and methoxsalen. *Nat. Struct. Mol. Biol.* **2005**, *12*, 822-823.
- (135) Smith, B. D.; Sanders, J. L.; Porubsky, P. R.; Lushington, G. H.; Stout, C. D.; Scott, E. E. Structure of the human lung cytochrome P450 2A13. *J. Biol. Chem.* **2007**, *282*, 17306-17313.
- (136) Schoch, G. A.; Yano, J. K.; Wester, M. R.; Griffin, K. J.; Stout, C. D.; Johnson, E. F. Structure of human microsomal cytochrome P450_{2C8} - Evidence for a peripheral fatty acid binding site. *J. Biol. Chem.* **2004**, *279*, 9497-9503.
- (137) Williams, P. A.; Cosme, J.; Ward, A.; Angova, H. C.; Vinkovic, D. M.; Jhoti, H. Crystal structure of human cytochrome P450_{2C9} with bound warfarin. *Nature* **2003**, *424*, 464-468.
- (138) Rowland, P.; Blaney, F. E.; Smyth, M. G.; Jones, J. J.; Leydon, V. R.; Oxbrow, A. K.; Lewis, C. J.; Tennant, M. G.; Modi, S.; Eggleston, D. S.; Chenery, R. J.; Bridges, A. M. Crystal structure of human cytochrome P450 2D6. *J. Biol. Chem.* **2006**, *281*, 7614-7622.

-
- (139) Williams, P. A.; Cosme, J.; Vinkovic, D. M.; Ward, A.; Angove, H. C.; Day, P. J.; Vonrhein, C.; Tickle, I. J.; Jhoti, H. Crystal structures of human cytochrome P450 3A4 bound to metyrapone and progesterone. *Science* **2004**, *305*, 683-686.
- (140) Favia, A. D.; Cavalli, A.; Masetti, M.; Carotti, A.; Recanatini, M. Three-dimensional model of the human aromatase enzyme and density functional parameterization of the iron-containing protoporphyrin IX for a molecular dynamics study of heme-cysteinato cytochromes. *Proteins* **2006**, *62*, 1074-1087.
- (141) Hasemann, C. A.; Kurumbail, R. G.; Boddupalli, S. S.; Peterson, J. A.; Deisenhofer, J. Structure and function of cytochromes P450: A comparative analysis of 3 crystal structures. *Structure* **1995**, *3*, 41-62.
- (142) Scheidt, W. R.; Reed, C. A. Spin-state/stereochemical relationships in iron porphyrins: Implications for the hemoproteins. *Chem. Rev.* **1981**, *81*, 543-555.
- (143) Testa, B.; Kramer, S. D. The biochemistry of drug metabolism - An introduction - Part 2. Redox reactions and their enzymes. *Chem. Biodivers.* **2007**, *4*, 257-405.
- (144) Shimizu, Y.; Yarborough, C.; Osawa, Y. Competitive product inhibition of aromatase by natural estrogens. *J. Steroid Biochem. Mol. Biol.* **1993**, *44*, 651-656.
- (145) Hackett, J. C.; Brueggemeier, R. W.; Hadad, C. M. The final catalytic step of cytochrome P450 aromatase: A density functional theory study. *J. Am. Chem. Soc.* **2005**, *127*, 5224-5237.
- (146) Cole, P. A.; Bean, J. M.; Robinson, C. H. Conversion of a 3-desoxysteroid to 3-desoxyestrogen by human placental aromatase. *Proc. Natl. Acad. Sci. U. S. A* **1990**, *87*, 2999-3003.
- (147) Graham-Lorence, S.; Amarnah, B.; White, R. E.; Peterson, J. A.; Simpson, E. R. A 3-dimensional model of aromatase cytochrome P450. *Protein Sci.* **1995**, *4*, 1065-1080.
- (148) Akhtar, M.; Calder, M. R.; Corina, D. L.; Wright, J. N. Mechanistic studies on C-19 demethylation in estrogen biosynthesis. *Biochem. J.* **1982**, *201*, 569-580.
- (149) Cole, P. A.; Robinson, C. H. Mechanism and inhibition of cytochrome P-450 aromatase. *J. Med. Chem.* **1990**, *33*, 2933-2942.
- (150) Klingenberg, M. Pigments of rat liver microsomes. *Arch. Biochem. Biophys.* **1958**, *75*, 376-386.

- (151) Omura, T.; Sato, R. The carbon monoxide-binding pigment of liver microsomes. I. Evidence for its hemoprotein nature. *J. Biol. Chem.* **1964**, *239*, 2370-2378.
- (152) Santen, R. J.; Samojlik, E.; Lipton, A.; Harvey, H.; Ruby, E. B.; Wells, S. A.; Kendall, J. Kinetic, hormonal and clinical studies with aminoglutethimide in breast cancer. *Cancer* **1977**, *39*, 2948-2958.
- (153) Santen, R. J.; Santner, S.; Davis, B.; Veldhuis, J.; Samojlik, E.; Ruby, E. Aminoglutethimide inhibits extraglandular estrogen production in postmenopausal women with breast carcinoma. *J. Clin. Endocrinol. Metab.* **1978**, *47*, 1257-1265.
- (154) Goss, P. E.; Jarman, M.; Wilkinson, J. R.; Coombes, R. C. Metabolism of the aromatase inhibitor 4-hydroxyandrostenedione in vivo. Identification of the glucuronide as a major urinary metabolite in patients and biliary metabolite in the rat. *J. Steroid Biochem.* **1986**, *24*, 619-622.
- (155) Goss, P. E.; Powles, T. J.; Dowsett, M.; Hutchison, G.; Brodie, A. M. H.; Gazet, J. C.; Coombes, R. C. Treatment of advanced postmenopausal breast cancer with an aromatase inhibitor, 4-hydroxyandrostenedione: Phase-II report. *Cancer Res.* **1986**, *46*, 4823-4826.
- (156) Stein, R. C.; Dowsett, M.; Davenport, J.; Hedley, A.; Ford, H. T.; Gazet, J. C.; Coombes, R. C. Preliminary study of the treatment of advanced breast cancer in postmenopausal women with the aromatase inhibitor CGS 16949A. *Cancer Res.* **1990**, *50*, 1381-1384.
- (157) Miller, W. R.; Dixon, J. M. Antiaromatase agents: preclinical data and neoadjuvant therapy. *Clin. Breast Cancer* **2000**, *1 Suppl 1*, S9-14.
- (158) Bisagni, G.; Cocconi, G.; Scaglione, F.; Frascini, F.; Pfister, C.; Trunet, P. F. Letrozole, a new oral non-steroidal aromatase inhibitor in treating postmenopausal patients with advanced breast cancer. A pilot study. *Ann. Oncol.* **1996**, *7*, 99-102.
- (159) Plourde, P. V.; Dyroff, M.; Dowsett, M.; Demers, L.; Yates, R.; Webster, A. Arimidex: a new oral, once-a-day aromatase inhibitor. *J. Steroid Biochem. Mol. Biol.* **1995**, *53*, 175-179.
- (160) Brueggemeier, R. W.; Hackett, J. C.; Diaz-Cruz, E. S. Aromatase inhibitors in the treatment of breast cancer. *Endocr. Rev.* **2005**, *26*, 331-345.
- (161) Numazawa, M.; Mutsumi, A.; Nakakoshi, M.; Nagaoka, M. A radiometric assay method for aromatase activity using [1β - ^3H]16 α -hydroxyandrostenedione. *Chem. Pharm. Bull.* **1992**, *40*, 1839-1842.
- (162) Numazawa, M.; Yamada, K.; Nitta, S.; Sasaki, C.; Kidokoro, K. Role of hydrophilic interaction in binding of hydroxylated 3-deoxy C₁₉ steroids to the active site of aromatase. *J. Med. Chem.* **2001**, *44*, 4277-4283.

- (163) Nagaoka, M.; Watari, Y.; Yajima, H.; Tsukioka, K.; Muroi, Y.; Yamada, K.; Numazawa, M. Structure-activity relationships of 3-deoxy androgens as aromatase inhibitors. synthesis and biochemical studies of 4-substituted 4-ene and 5-ene steroids. *Steroids* **2003**, *68*, 533-542.
- (164) Cepa, M. M. D. S.; da Silva, E. J. T.; Correia-Da-Silva, G.; Roleira, F. M. F.; Teixeira, N. A. A. Structure-activity relationships of new A,D-ring modified steroids as aromatase inhibitors: Design, synthesis, and biological activity evaluation. *J. Med. Chem.* **2005**, *48*, 6379-6385.
- (165) Henderson, D.; Norbistrath, G.; Kerb, U. 1-Methyl-1,4-androstadiene-3,17-dione (SH 489): Characterization of an irreversible inhibitor of estrogen biosynthesis. *J. Steroid Biochem.* **1986**, *24*, 303-306.
- (166) Marsh, D. A.; Brodie, H. J.; Garrett, W.; Tsaimorris, C. H.; Brodie, A. M. H. Aromatase inhibitors. Synthesis and biological activity of androstenedione derivatives. *J. Med. Chem.* **1985**, *28*, 788-795.
- (167) Brueggemeier, R. W.; Floyd, E. E.; Counsell, R. E. Synthesis and biochemical evaluation of inhibitors of estrogen biosynthesis. *J. Med. Chem.* **1978**, *21*, 1007-1011.
- (168) Li, P.-K.; Brueggemeier, R. W. Synthesis and biochemical studies of 7-substituted 4,6-androstadiene-3,17-diones as aromatase inhibitors. *J. Med. Chem.* **1990**, *33*, 101-105.
- (169) Numazawa, M.; Oshibe, M.; Yamaguchi, S.; Tachibana, M. Time-dependent inactivation of aromatase by 6-alkylandrosta-1,4-diene-3,17-diones. Effects of length and configuration of 6-alkyl group. *J. Med. Chem.* **1996**, *39*, 1033-1038.
- (170) Numazawa, M.; Oshibe, M.; Yamaguchi, S. 6-Alkylandrosta-4,6-diene-3,17-diones and their 1,4,6-triene analogs as aromatase inhibitors. Structure-activity relationships. *Steroids* **1997**, *62*, 595-602.
- (171) Numazawa, M.; Yamaguchi, S. 6-Phenylaliphatic-substituted androst-4-ene-3,17-diones as aromatase inhibitors: structure-activity relationships. *J. Steroid Biochem. Mol. Biol.* **1998**, *67*, 41-48.
- (172) Numazawa, M.; Yamaguchi, S. Synthesis and structure-activity relationships of 6-phenylaliphatic-substituted C₁₉ steroids having a 1,4-diene, 4,6-diene, or 1,4,6-triene structure as aromatase inhibitors. *Steroids* **1999**, *64*, 187-196.
- (173) Numazawa, M.; Shelangouski, M.; Nagasaka, M. Probing the binding pocket of the active site of aromatase with 6-ether or 6-ester substituted androst-4-ene-3,17-diones and their diene and triene analogs. *Steroids* **2000**, *65*, 871-882.

- (174) Bednarski, P. J.; Porubek, D. J.; Nelson, S. D. Thiol-containing androgens as suicide substrates of aromatase. *J. Med. Chem.* **1985**, *28*, 775-779.
- (175) Kellis, J. T.; Childers, W. E.; Robinson, C. H.; Vickery, L. E. Inhibition of aromatase cytochrome P-450 by 10-oxirane and 10-thiirane substituted androgens. Implications for the structure of the active site. *J. Biol. Chem.* **1987**, *262*, 4421-4426.
- (176) Shih, M.-J.; Carrell, M. H.; Carrell, H. L.; Wright, C. L.; Johnston, J. O.; Robinson, C. H. Stereoselective inhibition of aromatase by novel epoxysteroids. *J. Chem. Soc. Chem. Commun.* **1987**, 213-214.
- (177) Wright, J. N.; Calder, M. R.; Akhtar, M. Steroidal C-19 sulfur and nitrogen derivatives designed as aromatase inhibitors. *J. Chem. Soc. Chem. Commun.* **1985**, 1733-1735.
- (178) Numazawa, M.; Ando, M.; Watari, Y.; Tominaga, T.; Hayata, Y.; Yoshimura, A. Structure-activity relationships of 2-, 4-, or 6-substituted estrogens as aromatase inhibitors. *J. Steroid Biochem. Mol. Biol.* **2005**, *96*, 51-58.
- (179) Hollenberg, P. F.; Kent, U. M.; Bumpus, N. N. Mechanism-based inactivation of human cytochromes P450s: Experimental characterization, reactive intermediates, and clinical implications. *Chem. Res. Toxicol.* **2008**, *21*, 189-205.
- (180) Correia, M. A.; Ortiz de Montellano, P. R. Inhibition of cytochrome P450 enzymes. In *Cytochrome P450: Structure, mechanism, and biochemistry*. 3rd ed.; Kluwer Academic/Plenum Press, New York, **2005**, pp 247-322.
- (181) Covey, D. F.; Hood, W. F.; Parikh, V. D. 10 β -Propynyl-substituted steroids. Mechanism-based enzyme-activated irreversible inhibitors of estrogen biosynthesis. *J. Biol. Chem.* **1981**, *256*, 1076-1079.
- (182) Metcalf, B. W.; Wright, C. L.; Burkhardt, J. P.; Johnston, J. O. Substrate-induced inactivation of aromatase by allenic and acetylenic steroids. *J. Am. Chem. Soc.* **1981**, *103*, 3221-3222.
- (183) Brodie, A. M. H.; Garrett, W. M.; Hendrickson, J. R.; Tsaimorris, C. H.; Marcotte, P. A.; Robinson, C. H. Inactivation of aromatase in vitro by 4-hydroxy-4-androstene-3,17-dione and 4-acetoxy-4-androstene-3,17-dione and sustained effects in vivo. *Steroids* **1981**, *38*, 693-702.
- (184) Brueggemeier, R. W.; Moh, P. P.; Ebrahimian, S.; Darby, M. V. Steroidal inhibitors as chemical probes of the active site of aromatase. *J. Steroid Biochem. Mol. Biol.* **1993**, *44*, 357-365.
- (185) Numazawa, M.; Mutsumi, A.; Hoshi, K.; Kigawa, H.; Oshibe, M. A time-dependent inactivation of aromatase by 19-oxygenated androst-4-ene-3,6,17-triones. *J. Steroid Biochem. Mol. Biol.* **1991**, *39*, 959-966.

- (186) Numazawa, M.; Mutsumi, A.; Tachibana, M. Mechanism for aromatase inactivation by a suicide substrate, androst-4-ene-3,6,17-trione - The 4 β ,5 β -epoxy-19-oxo derivative as a reactive electrophile irreversibly binding to the active site. *Biochem. Pharmacol.* **1996**, *52*, 1253-1259.
- (187) Covey, D. F.; Hood, W. F. Enzyme-generated intermediates derived from 4-androstene-3,6,17-trione and 1,4,6-androstatriene-3,17-dione cause a time-dependent decrease in human placental aromatase activity. *Endocrinology* **1981**, *108*, 1597-1599.
- (188) Giudici, D.; Ornati, G.; Briatico, G.; Buzzetti, F.; Lombardi, P.; Disalle, E. 6-Methylenandrosta-1,4-diene-3,17-dione (FCE 24304): a new irreversible aromatase inhibitor. *J. Steroid Biochem.* **1988**, *30*, 391-394.
- (189) Lombardi, P. Exemestane, a new steroidal aromatase inhibitor of clinical relevance. *Biochim. Biophys. Acta-Mol. Basis Dis.* **2002**, *1587*, 326-337.
- (190) Barone, R. M.; Shamonki, I. M.; Siiteri, P. K.; Judd, H. L. Inhibition of peripheral aromatization of androstenedione to estrone in postmenopausal women with breast cancer using Δ^1 -testololactone. *J. Clin. Endocrinol. Metab.* **1979**, *49*, 672-676.
- (191) Judd, H. L.; aromatization; Laufer, L. R.; Gambone, J. C.; Monfort, S. L.; Lasley, B. L. *In vivo* effects of Δ^1 -testololactone on peripheral aromatization. *Cancer Res.* **1982**, *42*, 3345-3348.
- (192) Li, P.-K.; Brueggemeier, R. W. 7-Substituted 1,4,6-androstatriene-3,17-diones as enzyme-activated irreversible inhibitors of aromatase. *J. Steroid Biochem.* **1990**, *36*, 533-539.
- (193) Snider, C. E.; Brueggemeier, R. W. Potent enzyme-activated inhibition of aromatase by a 7 α -substituted C₁₉ steroid. *J. Biol. Chem.* **1987**, *262*, 8685-8689.
- (194) Covey, D. F.; Hood, W. F. A new hypothesis based on suicide substrate inhibitor studies for the mechanism of action of aromatase. *Cancer Res.* **1982**, *42*, 3327-3333.
- (195) Recanatini, M.; Cavalli, A.; Valenti, P. Nonsteroidal aromatase inhibitors: recent advances. *Med. Res. Rev.* **2002**, *22*, 282-304.
- (196) Chung, B.; Matteson, K. J.; Voutilainen, R.; Mohandas, T. K.; Miller, W. L. Human cholesterol side-chain cleavage enzyme, P450scc: cDNA cloning, assignment of the gene to chromosome 15, and expression in the placenta. *Proc. Natl. Acad. Sci. U. S. A* **1986**, *83*, 8962-8966.
- (197) Hakki, T.; Bernhardt, R. CYP17- and CYP11B-dependent steroid hydroxylases as drug development targets. *Pharmacol. Ther.* **2006**, *111*, 27-52.

- (198) Kawamoto, T.; Mitsuuchi, Y.; Toda, K.; Yokoyama, Y.; Miyahara, K.; Miura, S.; Ohnishi, T.; Ichikawa, Y.; Nakao, K.; Imura, H.; Ulick, S.; Shizuta, Y. Role of steroid 11 β -hydroxylase and steroid 18-hydroxylase in the biosynthesis of glucocorticoids and mineralocorticoids in humans. *Proc. Natl. Acad. Sci. U. S. A* **1992**, *89*, 1458-1462.
- (199) Furet, P.; Batzl, C.; Bhatnagar, A.; Francotte, E.; Rihs, G.; Lang, M. Aromatase inhibitors: synthesis, biological activity, and binding mode ofazole-type compounds. *J. Med. Chem.* **1993**, *36*, 1393-1400.
- (200) Jones, C. D.; Winter, M. A.; Hirsch, K. S.; Stamm, N.; Taylor, H. M.; Holden, H. E.; Davenport, J. D.; Vonkumkalns, E.; Suhr, R. G. Estrogen synthetase inhibitors. 2. Comparison of the in vitro aromatase inhibitory activity for a variety of nitrogen heterocycles substituted with diarylmethane or diarylmethanol groups. *J. Med. Chem.* **1990**, *33*, 416-429.
- (201) Cavalli, A.; Recanatini, M. Looking for selectivity among cytochrome P450s inhibitors. *J. Med. Chem.* **2002**, *45*, 251-254.
- (202) Leonetti, F.; Favia, A.; Rao, A.; Aliano, R.; Paluszczak, A.; Hartmann, R. W.; Carotti, A. Design, synthesis, and 3D QSAR of novel potent and selective aromatase inhibitors. *J. Med. Chem.* **2004**, *47*, 6792-6803.
- (203) Jacobs, C.; Frotscher, M.; Dannhardt, G.; Hartmann, R. W. 1-Imidazolyl(alkyl)-substituted di- and tetrahydroquinolines and analogues: syntheses and evaluation of dual inhibitors of thromboxane A₂ synthase and aromatase. *J. Med. Chem.* **2000**, *43*, 1841-1851.
- (204) Hartmann, R. W.; Bayer, H.; Grun, G. Aromatase inhibitors. Syntheses and structure-activity studies of novel pyridyl-substituted indanones, indans, and tetralins. *J. Med. Chem.* **1994**, *37*, 1275-1281.
- (205) Sonnet, P.; Guillon, J.; Enguehard, C.; Dallemagne, P.; Bureau, R.; Rault, S.; Auvray, P.; Moslemi, S.; Sourdain, P.; Galopin, S.; Seralini, G. E. Design and synthesis of a new type of non steroidal human aromatase inhibitors. *Bioorg. Med. Chem. Lett.* **1998**, *8*, 1041-1044.
- (206) Auvray, P.; Sourdain, P.; Moslemi, S.; Seralini, G. E.; Sonnet, P.; Enguehard, C.; Guillon, J.; Dallemagne, P.; Bureau, R.; Rault, S. MR 20492 and MR 20494: two indolizinone derivatives that strongly inhibit human aromatase. *J. Steroid Biochem. Mol. Biol.* **1999**, *70*, 59-71.
- (207) Goss, P. E.; Oza, A.; Goel, R.; Nabholtz, J. M.; De Coster, R.; Bruynseels, J.; Reid, C.; Wadden, N.; Crump, M.; Tye, L. M. Liarozole fumarate (R85246): a novel imidazole in the treatment of receptor positive postmenopausal metastatic breast cancer. *Breast Cancer Res. Treat.* **2000**, *59*, 55-68.

- (208) Le Borgne, M.; Marchand, P.; Duflos, M.; DelevoyeSeiller, B.; PiessardRobert, S.; LeBaut, G.; Hartmann, R. W.; Palzer, M. Synthesis and *in vitro* evaluation of 3-(1-azolylmethyl)-1*H*-indoles and 3-(1-azolyl-1-phenylmethyl)-1*H*-indoles as inhibitors of P450 arom. *Arch. Pharm.* **1997**, *330*, 141-145.
- (209) Le Borgne, M.; Marchand, P.; Delevoye-Seiller, B.; Robert, J. M.; Le Baut, G.; Hartmann, R. W.; Palzer, M. New selective nonsteroidal aromatase inhibitors: Synthesis and inhibitory activity of 2, 3 or 5-(α -azolylbenzyl)-1*H*-indoles. *Bioorg. Med. Chem. Lett.* **1999**, *9*, 333-336.
- (210) Leze, M.-P.; Le Borgne, M.; Pinson, P.; Paluszczak, A.; Duflos, M.; Le Baut, G.; Hartmann, R. W. Synthesis and biological evaluation of 5-[(aryl)(1*H* imidazol-1-yl)methyl]-1*H*-indoles: Potent and selective aromatase inhibitors. *Bioorg. Med. Chem. Lett.* **2006**, *16*, 1134-1137.
- (211) Marchand, P.; Le Borgne, M.; Palzer, M.; Le Baut, G.; Hartmann, R. W. Preparation and pharmacological profile of 7-(α -azolylbenzyl)-1*H*-indoles and indolines as new aromatase inhibitors. *Bioorg. Med. Chem. Lett.* **2003**, *13*, 1553-1555.
- (212) Owen, C. P.; Nicholls, P. J.; Smith, H. J.; Whomsley, R. Inhibition of aromatase (P450_{Arom}) by some 1-(benzofuran-2-ylmethyl)imidazoles. *J. Pharm. Pharmacol.* **1999**, *51*, 427-433.
- (213) Saberi, M. R.; Vinh, T. K.; Yee, S. W.; Griffiths, B. J. N.; Evans, P. J.; Simons, C. Potent CYP19 (aromatase) 1-[(benzofuran-2-yl)(phenylmethyl)pyridine, -imidazole, and -triazole inhibitors: Synthesis and biological evaluation. *J. Med. Chem.* **2006**, *49*, 1016-1022.
- (214) Vinh, T. K.; Ahmadi, M.; Delgado, P. O. L.; Perez, S. F.; Walters, H. M.; Smith, H. J.; Nicholls, P. J.; Simons, C. 1-[(Benzofuran-2-yl)phenylmethyl]-triazoles and -tetrazoles - potent competitive inhibitors of aromatase. *Bioorg. Med. Chem. Lett.* **1999**, *9*, 2105-2108.
- (215) Jackson, T.; Woo, L. W. L.; Trusselle, M. N.; Purohit, A.; Reed, M. J.; Potter, B. V. L. Non-steroidal aromatase inhibitors based on a biphenyl scaffold: Synthesis, *in vitro* SAR, and molecular modelling. *Chemmedchem* **2008**, *3*, 603-618.
- (216) Karjalainen, A.; Kalapudas, A.; Sodervall, M.; Pelkonen, O.; Lammintausta, R. Synthesis of new potent and selective aromatase inhibitors based on long-chained diarylalkylimidazole and diarylalkyltriazole molecule skeletons. *Eur. J. Pharm. Sci.* **2000**, *11*, 109-131.
- (217) Okada, M.; Yoden, T.; Kawaminami, E.; Shimada, Y.; Kudoh, M.; Isomura, Y.; Shikama, H.; Fujikura, T. Studies on aromatase inhibitors. 1. Synthesis and biological evaluation of 4-amino-4*H*-1,2,4-triazole derivatives. *Chem. Pharm. Bull.* **1996**, *44*, 1871-1879.

- (218) Okada, M.; Yoden, T.; Kawaminami, E.; Shimada, Y.; Kudoh, M.; Isomura, Y. Studies on aromatase inhibitors. 4. Synthesis and biological evaluation of *N,N*-disubstituted-5-aminopyrimidine derivatives. *Chem. Pharm. Bull.* **1997**, *45*, 1293-1299.
- (219) Recanatini, M.; Bisi, A.; Cavalli, A.; Belluti, F.; Gobbi, S.; Rampa, A.; Valenti, P.; Palzer, M.; Paluszczak, A.; Hartmann, R. W. A new class of nonsteroidal aromatase inhibitors: design and synthesis of chromone and xanthone derivatives and inhibition of the P450 enzymes aromatase and 17 α -hydroxylase/C17,20-lyase. *J. Med. Chem.* **2001**, *44*, 672-680.
- (220) Kao, Y.-C.; Korzekwa, K. R.; Laughton, C. A.; Chen, S. Evaluation of the mechanism of aromatase cytochrome P450 - A site-directed mutagenesis study. *Eur. J. Biochem.* **2001**, *268*, 243-251.
- (221) Bravo, L. Polyphenols: Chemistry, dietary sources, metabolism, and nutritional significance. *Nutr. Rev.* **1998**, *56*, 317-333.
- (222) Hodek, P.; Trefil, P.; Stiborova, M. Flavonoids-potent and versatile biologically active compounds interacting with cytochromes P450. *Chem. - Biol. Interact.* **2002**, *139*, 1-21.
- (223) Tuck, K. L.; Hayball, P. J. Major phenolic compounds in olive oil: metabolism and health effects. *J. Nutr. Biochem.* **2002**, *13*, 636-644.
- (224) Rice-Evans, C. A.; Miller, N. J.; Paganga, G. Structure-antioxidant activity relationships of flavonoids and phenolic acids. *Free Radic. Biol. Med.* **1996**, *20*, 933-956.
- (225) Frei, B.; Higdon, J. V. Antioxidant activity of tea polyphenols in vivo: evidence from animal studies. *J. Nutr.* **2003**, *133*, 3275S-3284S.
- (226) Hamdi, H. K.; Castellon, R. Oleuropein, a non-toxic olive iridoid, is an anti-tumor agent and cytoskeleton disruptor. *Biochem. Biophys. Res. Commun.* **2005**, *334*, 769-778.
- (227) Aggarwal, B. B.; Shishodia, S. Molecular targets of dietary agents for prevention and therapy of cancer. *Biochem. Pharmacol.* **2006**, *71*, 1397-1421.
- (228) Micol, V.; Caturla, N.; Perez-Fons, L.; Mas, V.; Perez, L.; Estepa, A. The olive leaf extract exhibits antiviral activity against viral haemorrhagic septicaemia rhabdovirus (VHSV). *Antiviral Res.* **2005**, *66*, 129-136.
- (229) Aziz, N. H.; Farag, S. E.; Mousa, L. A.; Abo-Zaid, M. A. Comparative antibacterial and antifungal effects of some phenolic compounds. *Microbios* **1998**, *93*, 43-54.

- (230) Carluccio, M. A.; Siculella, L.; Ancora, M. A.; Massaro, M.; Scoditti, E.; Storelli, C.; Visioli, F.; Distante, A.; De Caterina, R. Olive oil and red wine antioxidant polyphenols inhibit endothelial activation: antiatherogenic properties of Mediterranean diet phytochemicals. *Arterioscler. Thromb. Vasc. Biol.* **2003**, *23*, 622-629.
- (231) Vita, J. A. Polyphenols and cardiovascular disease: effects on endothelial and platelet function. *Am. J. Clin. Nutr.* **2005**, *81*, 292S-297S.
- (232) Adlercreutz, H.; Goldin, B. R.; Gorbach, S. L.; Hockerstedt, K. A. V.; Watanabe, S.; Hamalainen, E. K.; Markkanen, M. H.; Makela, T. H.; Wahala, K. T.; Hase, T. A.; Fotsis, T. Soybean phytoestrogen intake and cancer risk. *J. Nutr.* **1995**, *125*, S757-S770.
- (233) Adlercreutz, H. Phytoestrogens: Epidemiology and a possible role in cancer protection. *Environ. Health Perspect.* **1995**, *103*, 103-112.
- (234) Kuiper, G. G. J. M.; Lemmen, J. G.; Carlsson, B.; Corton, J. C.; Safe, S. H.; van der Saag, P. T.; van der Burg, P.; Gustafsson, J. A. Interaction of estrogenic chemicals and phytoestrogens with estrogen receptor β . *Endocrinology* **1998**, *139*, 4252-4263.
- (235) An, J.; Tzagarakis-Foster, C.; Scharschmidt, T. C.; Lomri, N.; Leitman, D. C. Estrogen receptor β -selective transcriptional activity and recruitment of coregulators by phytoestrogens. *J. Biol. Chem.* **2001**, *276*, 17808-17814.
- (236) Ososki, A. L.; Kennelly, E. J. Phytoestrogens: A review of the present state of research. *Phytother. Res.* **2003**, *17*, 845-869.
- (237) Kellis, J. T. Jr.; Vickery, L. E. Inhibition of human estrogen synthetase (aromatase) by flavones. *Science* **1984**, *225*, 1032-1034.
- (238) Adlercreutz, H.; Bannwart, C.; Wahala, K.; Makela, T.; Brunow, G.; Hase, T.; Arosemena, P. J.; Kellis, J. T.; Vickery, L. E. Inhibition of human aromatase by mammalian lignans and isoflavonoid phytoestrogens. *J. Steroid Biochem. Mol. Biol.* **1993**, *44*, 147-153.
- (239) Ibrahim, A. R.; Abulhaji, Y. J. Aromatase inhibition by flavonoids. *J. Steroid Biochem. Mol. Biol.* **1990**, *37*, 257-260.
- (240) Le Bail, J. C.; Laroche, T.; Marre-Fournier, F.; Habrioux, G. Aromatase and 17β -hydroxysteroid dehydrogenase inhibition by flavonoids. *Cancer Lett.* **1998**, *133*, 101-106.
- (241) Le Bail, J. C.; Champavier, Y.; Chulia, A. J.; Habrioux, G. Effects of phytoestrogens on aromatase, 3β and 17β -hydroxysteroid dehydrogenase activities and human breast cancer cells. *Life Sci.* **2000**, *66*, 1281-1291.

- (242) Pelissero, C.; Lenczowski, M. J. P.; Chinzi, D.; DavailCuisset, B.; Sumpster, J. P.; Fostier, A. Effects of flavonoids on aromatase activity, an *in vitro* study. *J. Steroid Biochem. Mol. Biol.* **1996**, *57*, 215-223.
- (243) Ta, N.; Walle, T. Aromatase inhibition by bioavailable methylated flavones. *J. Steroid Biochem. Mol. Biol.* **2007**, *107*, 127-129.
- (244) Maiti, A.; Cuendet, M.; Croy, V. L.; Endringer, D. C.; Pezzuto, J. M.; Cushman, M. Synthesis and biological evaluation of (+/-)-abyssinone II and its analogues as aromatase inhibitors for chemoprevention of breast cancer. *J. Med. Chem.* **2007**, *50*, 2799-2806.
- (245) Monteiro, R.; Becker, H.; Azevedo, I.; Calhau, C. Effect of hop (*Humulus lupulus* L.) flavonoids on aromatase (estrogen synthase) activity. *J. Agric. Food Chem.* **2006**, *54*, 2938-2943.
- (246) Pouget, C.; Fagnere, C.; Basly, J. P.; Besson, A. E.; Champavier, Y.; Habrioux, G.; Chulia, A. J. Synthesis and aromatase inhibitory activity of flavanones. *Pharm. Res.* **2002**, *19*, 286-291.
- (247) Campbell, D. R.; Kurzer, M. S. Flavonoid inhibition of aromatase enzyme activity in human preadipocytes. *J. Steroid Biochem. Mol. Biol.* **1993**, *46*, 381-388.
- (248) Lee, D.; Bhat, K. P. L.; Fong, H. H. S.; Farnsworth, N. R.; Pezzuto, J. M.; Kinghorn, A. D. Aromatase inhibitors from *Broussonetia papyrifera*. *J. Nat. Prod.* **2001**, *64*, 1286-1293.
- (249) Monteiro, R.; Azevedo, I.; Calhau, C. Modulation of aromatase activity by diet polyphenolic compounds. *J. Agric. Food Chem.* **2006**, *54*, 3535-3540.
- (250) Le Bail, J. C.; Pouget, C.; Fagnere, C.; Basly, J. P.; Chulia, A. J.; Habrioux, G. Chalcones are potent inhibitors of aromatase and 17 β -hydroxysteroid dehydrogenase activities. *Life Sci.* **2001**, *68*, 751-761.
- (251) Way, T. D.; Lee, H. H.; Kao, M. C.; Lin, J. K. Black tea polyphenol theaflavins inhibit aromatase activity and attenuate tamoxifen resistance in HER2/*neu*-transfected human breast cancer cells through tyrosine kinase suppression. *Eur. J. Cancer* **2004**, *40*, 2165-2174.
- (252) Eng, E. T.; Ye, J. J.; Williams, D.; Phung, S.; Moore, R. E.; Young, M. K.; Gruntmanis, U.; Braunstein, G.; Chen, S. Suppression of estrogen biosynthesis by procyanidin dimers in red wine and grape seeds. *Cancer Res.* **2003**, *63*, 8516-8522.
- (253) Satoh, K.; Sakamoto, Y.; Ogata, A.; Nagai, F.; Mikuriya, H.; Numazawa, M.; Yamada, K.; Aoki, N. Inhibition of aromatase activity by green tea extract catechins and their endocrinological effects of oral administration in rats. *Food Chem. Toxicol.* **2002**, *40*, 925-933.

- (254) Wang, C.; Makela, T.; Hase, T.; Adlercreutz, H.; Kurzer, M. S. Lignans and flavonoids inhibit aromatase enzyme in human preadipocytes. *J. Steroid Biochem. Mol. Biol.* **1994**, *50*, 205-212.
- (255) Filleur, F.; Le Bail, J. C.; Duroux, J. L.; Simon, A.; Chulia, A. J. Antiproliferative, anti-aromatase, anti-17 β -HSD and antioxidant activities of lignans isolated from *Myristica argentea*. *Planta Med.* **2001**, *67*, 700-704.
- (256) Kao, Y.-C.; Zhou, C. B.; Sherman, M.; Laughton, C. A.; Chen, S. Molecular basis of the inhibition of human aromatase (estrogen synthetase) by flavone and isoflavone phytoestrogens: A site-directed mutagenesis study. *Environ. Health Perspect.* **1998**, *106*, 85-92.
- (257) Kellis, J. T.; Nesnow, S.; Vickery, L. E. Inhibition of aromatase cytochrome P-450 (estrogen synthetase) by derivatives of α -naphthoflavone. *Biochem. Pharmacol.* **1986**, *35*, 2887-2891.
- (258) Gobbi, S.; Cavalli, A.; Rampa, A.; Belluti, F.; Piazzini, L.; Paluszczak, A.; Hartmann, R. W.; Recanatini, M.; Bisi, A. Lead optimization providing a series of flavone derivatives as potent nonsteroidal inhibitors of the cytochrome P450 aromatase enzyme. *J. Med. Chem.* **2006**, *49*, 4777-4780.
- (259) Kim, Y. W.; Hackett, J. C.; Brueggemeier, R. W. Synthesis and aromatase inhibitory activity of novel pyridine-containing isoflavones. *J. Med. Chem.* **2004**, *47*, 4032-4040.
- (260) Hackett, J. C.; Kim, Y. W.; Su, B.; Brueggemeier, R. W. Synthesis and characterization of azole isoflavone inhibitors of aromatase. *Bioorg. Med. Chem* **2005**, *13*, 4063-4070.
- (261) Pouget, C.; Fagnere, C.; Basly, J. P.; Habrioux, G.; Chulia, A. J. New aromatase inhibitors. Synthesis and inhibitory activity of pyridinyl-substituted flavanone derivatives. *Bioorg. Med. Chem. Lett.* **2002**, *12*, 1059-1061.
- (262) Pouget, C.; Fagnere, C.; Basly, J. P.; Habrioux, G.; Chulia, A. J. Design, synthesis and evaluation of 4-imidazolylflavans as new leads for aromatase inhibition. *Bioorg. Med. Chem. Lett.* **2002**, *12*, 2859-2861.
- (263) Yahiaoui, S.; Pouget, C.; Fagnere, C.; Champavier, Y.; Habrioux, G.; Chulia, A. J. Synthesis and evaluation of 4-triazolylflavans as new aromatase inhibitors. *Bioorg. Med. Chem. Lett.* **2004**, *14*, 5215-5218.
- (264) Pouget, C.; Yahiaoui, S.; Fagnere, C.; Habrioux, G.; Chulia, A. J. Synthesis and biological evaluation of 4-imidazolylflavans as nonsteroidal aromatase inhibitors. *Bioorganic Chem.* **2004**, *32*, 494-503.
- (265) Chen, S.; Cho, M.; Karlsberg, K.; Zhou, D.; Yuan, Y. C. Biochemical and biological characterization of a novel anti-aromatase coumarin derivative. *J. Biol. Chem.* **2004**, *279*, 48071-48078.

- (266) Dessalew, N.; Mikre, W. On the paradigm shift towards multitarget selective drug design. *Curr. Comput. -Aided Drug. Des.* **2008**, *4*, 76-90.
- (267) Shen, R. F.; Tai, H. H. Thromboxanes: Synthase and receptors. *J. Biomed. Sci.* **1998**, *5*, 153-172.
- (268) Nie, D. T.; Che, M. X.; Zacharek, A.; Qiao, Y.; Li, L.; Li, X. L.; Lamberti, M.; Tang, K. Q.; Cai, Y. L.; Guo, Y. D.; Grignon, D.; Honn, K. V. Differential expression of thromboxane synthase in prostate carcinoma - Role in tumor cell motility. *Am. J. Pathol.* **2004**, *164*, 429-439.
- (269) Onguru, O.; Casey, M. B.; Kajita, S.; Nakamura, N.; Lloyd, R. V. Cyclooxygenase-2 and thromboxane synthase in non-endocrine and endocrine tumors: A review. *Endocr. Pathol.* **2005**, *16*, 253-277.
- (270) Sakai, H.; Suzuki, T.; Takahashi, Y.; Ukai, M.; Tauchi, K.; Fujii, T.; Horikawa, N.; Minamimura, T.; Tabuchi, Y.; Morii, M.; Tsukada, K.; Takeguchi, N. Upregulation of thromboxane synthase in human colorectal carcinoma and the cancer cell proliferation by thromboxane A₂. *FEBS Lett.* **2006**, *580*, 3368-3374.
- (271) Yokoyama, I.; Hayashi, S.; Kobayashi, T.; Negita, M.; Yasutomi, M.; Uchida, K.; Takagi, H. Prevention of experimental hepatic metastasis with thromboxane synthase inhibitor. *Res. Exp. Med.* **1995**, *195*, 209-215.
- (272) Moussa, O.; Riker, J.; Klein, J.; Fraig, M.; Halushka, P.; Watson, D. Inhibition of thromboxane synthase activity modulates bladder cancer cell responses to chemotherapeutic agents. *Oncogene* **2008**, *27*, 55-62.
- (273) Santner, S. J.; Feil, P. D.; Santen, R. J. In situ estrogen production via the estrone sulfatase pathway in breast tumors: relative importance versus the aromatase pathway. *J. Clin. Endocrinol. Metab.* **1984**, *59*, 29-33.
- (274) Howarth, N. M.; Purohit, A.; Reed, M. J.; Potter, B. V. L. Estrone sulfamates: Potent inhibitors of estrone sulfatase with therapeutic potential. *J. Med. Chem.* **1994**, *37*, 219-221.
- (275) Nussbaumer, P.; Billich, A. Steroid sulfatase inhibitors. *Med. Res. Rev.* **2004**, *24*, 529-576.
- (276) Woo, L. W. L.; Purohit, A.; Malini, B.; Reed, M. J.; Potter, B. V. L. Potent active site-directed inhibition of steroid sulphatase by tricyclic coumarin-based sulphamates. *Chem. Biol.* **2000**, *7*, 773-791.
- (277) Stanway, S. J.; Purohit, A.; Woo, L. W. L.; Sufi, S.; Vigushin, D.; Ward, R.; Wilson, R. H.; Stanczyk, F. Z.; Dobbs, N.; Kulinskaya, E.; Elliott, M.; Potter, B. V. L.; Reed, M. J.; Coombes, R. C. Phase I study of STX 64 (667 Coumate) in breast cancer patients: The first study of a steroid sulfatase inhibitor. *Clin. Cancer Res.* **2006**, *12*, 1585-1592.

- (278) Stanway, S. J.; Delavault, P.; Purohit, A.; Woo, L. W. L.; Thurieau, C.; Potter, B. V. L.; Reed, M. J. Steroid sulfatase: A new target for the endocrine therapy of breast cancer. *Oncologist* **2007**, *12*, 370-374.
- (279) Wood, P. M.; Woo, L. W. L.; Humphreys, A.; Chander, S. K.; Purohit, A.; Reed, M. J.; Potter, B. V. L. A letrozole-based dual aromatase-sulphatase inhibitor with in vivo activity. *J. Steroid Biochem. Mol. Biol.* **2005**, *94*, 123-130.
- (280) Woo, L. W. L.; Bubert, C.; Sutcliffe, O. B.; Smith, A.; Chander, S. K.; Mahon, M. F.; Purohit, A.; Reed, M. J.; Potter, B. V. L. Dual aromatase-steroid sulfatase inhibitors. *J. Med. Chem.* **2007**, *50*, 3540-3560.
- (281) Jackson, T.; Woo, L. W. L.; Trusselle, M. N.; Chander, S. K.; Purohit, A.; Reed, M. J.; Potter, B. V. L. Dual aromatase-sulfatase inhibitors based on the anastrozole template: synthesis, *in vitro* SAR, molecular modelling and *in vivo* activity. *Org. Biomol. Chem.* **2007**, *5*, 2940-2952.
- (282) Woo, L. W. L.; Sutcliffe, O. B.; Bubert, C.; Grasso, A.; Chander, S. K.; Purohit, A.; Reed, M. J.; Potter, B. V. L. First dual aromatase-steroid sulfatase inhibitors. *J. Med. Chem.* **2003**, *46*, 3193-3196.
- (283) Numazawa, M.; Tominaga, T.; Watari, Y.; Tada, Y. Inhibition of estrone sulfatase by aromatase inhibitor-based estrogen 3-sulfamates. *Steroids* **2006**, *71*, 371-379.
- (284) Brodie, A. Aromatase inhibitors and models for breast cancer. In *Aromatase inhibitors*. 2nd ed.; Birkhäuser, Basel, **2006**, pp 23-44.
- (285) Switzer, R. L.; Garrity, L. F. Expt. 3 Radioisotope techniques. In *Experimental biochemistry*. 3rd ed.; W.H. Freeman, New York, **1999**, pp 45-59.
- (286) Blomquist, C. H.; Lindemann, N. J.; Hakanson, E. Y. 17β -Hydroxysteroid and 20α -hydroxysteroid dehydrogenase activities of human placental microsomes: Kinetic evidence for two enzymes differing in substrate specificity. *Arch. Biochem. Biophys.* **1985**, *239*, 206-215.
- (287) Satoh, K.; Nonaka, R.; Ishikawa, F.; Ogata, A.; Nagai, F. *In vitro* screening assay for detecting aromatase activity using rat ovarian microsomes and estrone ELISA. *Biol. Pharm. Bull.* **2008**, *31*, 357-362.
- (288) Bhatnagar, A. S.; Brodie, A. M. H.; Long, B. J.; Evans, D. B.; Miller, W. R. Intracellular aromatase and its relevance to the pharmacological efficacy of aromatase inhibitors. *J. Steroid Biochem. Mol. Biol.* **2001**, *76*, 199-202.
- (289) Brueggemeier, R. W.; Gilbert, N. E.; Gu, X. Y.; O'Reilly, J. M.; Lovely, C. J. Aromatase inhibition in JAr choriocarcinoma cells by 7α -arylaliphatic androgens. *J. Steroid Biochem. Mol. Biol.* **1997**, *61*, 73-77.

- (290) Yue, W.; Brodie, A. M. H. Mechanisms of the actions of aromatase inhibitors 4-hydroxyandrostenedione, fadrozole, and aminoglutethimide on aromatase in JEG-3 cell culture. *J. Steroid Biochem. Mol. Biol.* **1997**, *63*, 317-328.
- (291) Prefontaine, M.; Shih, C.; Pan, C. C.; Bhavnani, B. R. Applicability of the product isolation and the radiometric aromatase assays for the measurement of low-levels of aromatase - Lack of aromatase-activity in the human endometrium. *J. Endocrinol.* **1990**, *127*, 539-551.
- (292) Santen, R. J.; Demers, L.; Ohorodnik, S.; Settlage, J.; Langecker, P.; Blanchett, D.; Goss, P. E.; Wang, S. Superiority of gas chromatography/tandem mass spectrometry assay (GC/MS/MS) for estradiol for monitoring of aromatase inhibitor therapy. *Steroids* **2007**, *72*, 666-671.
- (293) Miller, W. R. Biology of aromatase inhibitors: pharmacology endocrinology within the breast. *Endocr. -Relat. Cancer* **1999**, *6*, 187-195.
- (294) Ohno, K.; Araki, N.; Yanase, T.; Nawata, H.; Iida, M. A novel nonradioactive method for measuring aromatase activity using a human ovarian granulosa-like tumor cell line and an estrone ELISA. *Toxicol. Sci.* **2004**, *82*, 443-450.
- (295) Cooke, G. M. Effect of organotin on human aromatase activity in vitro. *Toxicol. Lett.* **2002**, *126*, 121-130.
- (296) Toma, Y.; Higashiyama, T.; Yarborough, C.; Osawa, Y. Diverse functions of aromatase: O-deethylation of 7-ethoxycoumarin. *Endocrinology* **1996**, *137*, 3791-3796.
- (297) Stresser, D. M.; Turner, S. D.; McNamara, J.; Stocker, P.; Miller, V. P.; Crespi, C. L.; Patten, C. J. A high-throughput screen to identify inhibitors of aromatase (CYP19). *Anal. Biochem.* **2000**, *284*, 427-430.
- (298) Hughes, B. 2007 FDA drug approvals: a year of flux. *Nat. Rev. Drug Discov.* **2008**, *7*, 107-109.
- (299) Dimasi, J. A.; Hansen, R. W.; Grabowski, H. G. The price of innovation: new estimates of drug development costs. *J. Health Econ.* **2003**, *22*, 151-185.
- (300) Rawlins, M. D. Cutting the cost of drug development? *Nat. Rev. Drug Discov.* **2004**, *3*, 360-364.
- (301) Kola, I.; Landis, J. Can the pharmaceutical industry reduce attrition rates? *Nat. Rev. Drug Discov.* **2004**, *3*, 711-715.
- (302) Bajorath, J. Integration of virtual and high-throughput screening. *Nat. Rev. Drug Discov.* **2002**, *1*, 882-894.

- (303) Bleicher, K. H.; Bohm, H. J.; Muller, K.; Alanine, A. I. Hit and lead generation: Beyond high-throughput screening. *Nat. Rev. Drug Discov.* **2003**, *2*, 369-378.
- (304) van de Waterbeemd, H.; Gifford, E. ADMET in silico modelling: Towards prediction paradise? *Nat. Rev. Drug Discov.* **2003**, *2*, 192-204.
- (305) Greer, J.; Erickson, J. W.; Baldwin, J. J.; Varney, M. D. Application of the three-dimensional structures of protein target molecules in structure-based drug design. *J. Med. Chem.* **1994**, *37*, 1035-1054.
- (306) Vonitzstein, M.; Wu, W. Y.; Kok, G. B.; Pegg, M. S.; Dyason, J. C.; Jin, B.; Phan, T. V.; Smythe, M. L.; White, H. F.; Oliver, S. W.; Colman, P. M.; Varghese, J. N.; Ryan, D. M.; Woods, J. M.; Bethell, R. C.; Hotham, V. J.; Cameron, J. M.; Penn, C. R. Rational design of potent sialidase-based inhibitors of influenza-virus replication. *Nature* **1993**, *363*, 418-423.
- (307) Wlodawer, A.; Vondrasek, J. Inhibitors of HIV-1 protease: A major success of structure-assisted drug design. *Annu. Rev. Biophys. Biomolec. Struct.* **1998**, *27*, 249-284.
- (308) Williams, D. H.; Mitchell, T. Latest developments in crystallography and structure-based design of protein kinase inhibitors as drug candidates. *Curr. Opin. Pharmacol.* **2002**, *2*, 567-573.
- (309) Höltje, H.-D.; Sippl, W.; Rognan, D.; Folkers, G. Small molecules. In *Molecular modeling: basic principles and applications*. 2nd ed.; Wiley-VCH, **2003**, pp 9-72.
- (310) Leach, A. R. Empirical force field methods: molecular mechanics. In *Molecular modelling: principles and applications*. 2nd ed.; Pearson Education, Dorchester, **2001**, pp 165-252.
- (311) Case, D. A.; Cheatham, T. E.; Darden, T.; Gohlke, H.; Luo, R.; Merz, K. M.; Onufriev, A.; Simmerling, C.; Wang, B.; Woods, R. J. The Amber biomolecular simulation programs. *J. Comput. Chem.* **2005**, *26*, 1668-1688.
- (312) Van der Spoel, D.; Lindahl, E.; Hess, B.; Groenhof, G.; Mark, A. E.; Berendsen, H. J. C. GROMACS: Fast, flexible, and free. *J. Comput. Chem.* **2005**, *26*, 1701-1718.
- (313) MacKerell, A. D.; Bashford, D.; Bellott, M.; Dunbrack, R. L.; Evanseck, J. D.; Field, M. J.; Fischer, S.; Gao, J.; Guo, H.; Ha, S.; Joseph-McCarthy, D.; Kuchnir, L.; Kuczera, K.; Lau, F. T. K.; Mattos, C.; Michnick, S.; Ngo, T.; Nguyen, D. T.; Prodhom, B.; Reiher, W. E.; Roux, B.; Schlenkrich, M.; Smith, J. C.; Stote, R.; Straub, J.; Watanabe, M.; Wiorkiewicz-Kuczera, J.; Yin, D.; Karplus, M. All-atom empirical potential for molecular modeling and dynamics studies of proteins. *J. Phys. Chem. B* **1998**, *102*, 3586-3616.

- (314) Halgren, T. A. Merck molecular force field. I. Basis, form, scope, parametrization, and performance of MMFF94*. *J. Comput. Chem.* **1996**, *17*, 490-519.
- (315) Leach, A. R. Energy minimisation and related methods for exploring the energy surface. In *Molecular modelling: principles and applications*. 2nd ed.; Pearson Education, Dorchester, **2001**, pp 253-302.
- (316) Hansson, T.; Oostenbrink, C.; van Gunsteren, W. F. Molecular dynamics simulations. *Curr. Opin. Struct. Biol.* **2002**, *12*, 190-196.
- (317) Karplus, M.; McCammon, J. A. Molecular dynamics simulations of biomolecules. *Nature Struc. Bio.* **2002**, *9*, 646-652.
- (318) Leach, A. R. Monte Carlo simulation methods. In *Molecular modelling: principles and applications*. 2nd ed.; Pearson Education, Dorchester, **2001**, pp 410-456.
- (319) Still, W. C.; Tempczyk, A.; Hawley, R. C.; Hendrickson, T. Semianalytical treatment of solvation for molecular mechanics and dynamics. *J. Am. Chem. Soc.* **1990**, *112*, 6127-6129.
- (320) Kubli-Garfias, C. Ab initio comparative study of the electronic structure of testosterone, epitestosterone and androstenedione. *Theochem-J. Mol. Struct.* **1998**, *422*, 167-177.
- (321) Leach, A. R. An introduction to computational quantum mechanics. In *Molecular modelling: principles and applications*. 2nd ed.; Pearson Education, Dorchester, **2001**, pp 26-107.
- (322) Huo, S. H.; Wang, J. M.; Cieplak, P.; Kollman, P. A.; Kuntz, I. D. Molecular dynamics and free energy analyses of cathepsin D-inhibitor interactions: Insight into structure-based ligand design. *J. Med. Chem.* **2002**, *45*, 1412-1419.
- (323) Rizzo, R. C.; Toba, S.; Kuntz, I. D. A molecular basis for the selectivity of thiadiazole urea inhibitors with stromelysin-1 and gelatinase-A from generalized born molecular dynamics simulations. *J. Med. Chem.* **2004**, *47*, 3065-3074.
- (324) Totrov, M.; Abagyan, R. Flexible ligand docking to multiple receptor conformations: a practical alternative. *Curr. Opin. Struct. Biol.* **2008**, *18*, 178-184.
- (325) Meli, M.; Pennati, M.; Curto, M.; Daidone, M. G.; Plescia, J.; Toba, S.; Altieri, D. C.; Zaffaroni, N.; Colombo, G. Small-molecule targeting of heat shock protein 90 chaperone function: Rational identification of a new anticancer lead. *J. Med. Chem.* **2006**, *49*, 7721-7730.

- (326) Kuhn, B.; Jacobsen, W.; Christians, U.; Benet, L. Z.; Kollman, P. A. Metabolism of sirolimus and its derivative everolimus by cytochrome P450 3A4: Insights from docking, molecular dynamics, and quantum chemical calculations. *J. Med. Chem.* **2001**, *44*, 2027-2034.
- (327) Marhefka, C. A.; Moore, B. M.; Bishop, T. C.; Kirkovsky, L.; Mukherjee, A.; Dalton, J. T.; Miller, D. D. Homology modeling using multiple molecular dynamics simulations and docking studies of the human androgen receptor ligand binding domain bound to testosterone and nonsteroidal ligands. *J. Med. Chem.* **2001**, *44*, 1729-1740.
- (328) Huang, X. Q.; Liu, T.; Gu, J. D.; Luo, X. M.; Ji, R. Y.; Cao, Y.; Xue, H.; Wong, J. T. F.; Wong, B. L.; Pei, G.; Jiang, H. L.; Chen, K. X. 3D-QSAR model of flavonoids binding at benzodiazepine site in GABA_A receptors. *J. Med. Chem.* **2001**, *44*, 1883-1891.
- (329) Sukalovic, V.; Andric, D.; Roglic, G.; Kostic-Rajacic, S.; Soskic, V. Electrostatic surface potential calculation on several new halogenated benzimidazole-like dopaminergic ligands. *Arch. Pharm.* **2004**, *337*, 376-382.
- (330) Edsall, A. B.; Mohanakrishnan, A. K.; Yang, D. L.; Fanwick, P. E.; Hamel, E.; Hanson, A. D.; Agoston, G. E.; Cushman, M. Effects of altering the electronics of 2-methoxyestradiol on cell proliferation, on cytotoxicity in human cancer cell cultures, and on tubulin polymerization. *J. Med. Chem.* **2004**, *47*, 5126-5139.
- (331) Höltje, H.-D.; Höltje, M. Applications of quantum chemical methods in drug design. In *Quantum medicinal chemistry*. Wiley-VCH, **2003**, pp 255-274.
- (332) Goodford, P. J. A computational procedure for determining energetically favorable binding sites on biologically important macromolecules. *J. Med. Chem.* **1985**, *28*, 849-857.
- (333) Molecular Discovery Ltd software. Available at <http://www.moldiscovery.com>
- (334) Pastor, M.; Cruciani, G.; McLay, I.; Pickett, S.; Clementi, S. GRIND-INdependent descriptors (GRIND): a novel class of alignment-independent three-dimensional molecular descriptors. *J. Med. Chem.* **2000**, *43*, 3233-3243.
- (335) Sciabola, S.; Carosati, E.; Baroni, M.; Mannhold, R. Comparison of ligand-based and structure-based 3D-QSAR approaches: A case study on (aryl-) bridged 2-aminobenzonitriles inhibiting HIV-1 reverse transcriptase. *J. Med. Chem.* **2005**, *48*, 3756-3767.
- (336) Kastenholz, M. A.; Pastor, M.; Cruciani, G.; Haaksma, E. E. J.; Fox, T. GRID/CPCA: A new computational tool to design selective ligands. *J. Med. Chem.* **2000**, *43*, 3033-3044.

- (337) Kubinyi, H. QSAR and 3D QSAR in drug design. Part 1: methodology. *Drug Discov. Today* **1997**, *2*, 457-467.
- (338) Gasteiger, J. 2006 American Chemical Society Award for Computers in Chemical and Pharmaceutical Research - Of molecules and humans. *J. Med. Chem.* **2006**, *49*, 6429-6434.
- (339) Lemmen, C.; Lengauer, T. Computational methods for the structural alignment of molecules. *J. Comput. -Aided Mol. Des.* **2000**, *14*, 215-232.
- (340) Fontaine, F.; Pastor, M.; Sanz, F. Incorporating molecular shape into the alignment-free GRid-INdependent Descriptors. *J. Med. Chem.* **2004**, *47*, 2805-2815.
- (341) Baroni, M.; Costantino, G.; Cruciani, G.; Riganelli, D.; Valigi, R.; Clementi, S. Generating optimal linear PLS estimations (Golpe) - An advanced chemometric tool for handling 3D-QSAR problems. *Quant. Struct. -Act. Relat.* **1993**, *12*, 9-20.
- (342) Todeschini, R. Modelli, bias e validazione. In *Introduzione alla chemiometria*. Edises, Napoli, **1998**, pp 81-89.
- (343) Laskowski, R. A. Structural quality assurance. In *Structural bioinformatics*. John Wiley & Sons, Hoboken, NJ, **2003**, pp 273-303.
- (344) Chothia, C.; Lesk, A. M. The relation between the divergence of sequence and structure in proteins. *Embo J.* **1986**, *5*, 823-826.
- (345) Krieger, E.; Nabuurs, S. B.; Vriend, G. Homology modeling. In *Structural bioinformatics*. John Wiley & Sons, Hoboken, NJ, **2003**, pp 509-523.
- (346) DeLano, W. L. The PyMOL Molecular Graphics System v0.99, DeLano Scientific, Palo Alto, CA, USA. Available at <http://www.pymol.org>
- (347) Karkola, S.; Holtje, H. D.; Wahala, K. A three-dimensional model of CYP19 aromatase for structure-based drug design. *J. Steroid Biochem. Mol. Biol.* **2007**, *105*, 63-70.
- (348) Loge, C.; Le Borgne, M.; Marchand, P.; Robert, J. M.; Le Baut, G.; Palzer, M.; Hartmann, R. W. Three-dimensional model of cytochrome P450 human aromatase. *J. Enzym. Inhib. Med. Chem.* **2005**, *20*, 581-585.
- (349) Reddy, M. R.; Erion, M. D. Calculation of relative binding free energy differences for fructose 1,6-bisphosphatase inhibitors using the thermodynamic cycle perturbation approach. *J. Am. Chem. Soc.* **2001**, *123*, 6246-6252.

- (350) Verdonk, M. L.; Cole, J. C.; Hartshorn, M. J.; Murray, C. W.; Taylor, R. D. Improved protein-ligand docking using GOLD. *Proteins Struct. Funct. Genet.* **2003**, *52*, 609-623.
- (351) Velec, H. F. G.; Gohlke, H.; Klebe, G. DrugScore^{CSD}-knowledge-based scoring function derived from small molecule crystal data with superior recognition rate of near-native ligand poses and better affinity prediction. *J. Med. Chem.* **2005**, *48*, 6296-6303.
- (352) Taylor, R. D.; Jewsbury, P. J.; Essex, J. W. A review of protein-small molecule docking methods. *J. Comput. -Aided Mol. Des.* **2002**, *16*, 151-166.
- (353) Wermuth, G.; Ganellin, C. R.; Lindberg, P.; Mitscher, L. A. Glossary of terms used in medicinal chemistry (IUPAC Recommendations 1998). *Pure Appl. Chem.* **1998**, *70*, 1129-1143.
- (354) Van Drie, J. H. Strategies for the determination of pharmacophoric 3D database queries. *J. Comput. -Aided Mol. Des.* **1997**, *11*, 39-52.
- (355) Bostrom, J. Reproducing the conformations of protein-bound ligands: A critical evaluation of several popular conformational searching tools. *J. Comput. -Aided Mol. Des.* **2001**, *15*, 1137-1152.
- (356) Clement, O. O.; Freeman, C. M.; Hartmann, R. W.; Handratta, V. D.; Vasaitis, T. S.; Brodie, A. M. H.; Njar, V. C. O. Three dimensional pharmacophore modeling of human CYP17 inhibitors. Potential agents for prostate cancer therapy. *J. Med. Chem.* **2003**, *46*, 2345-2351.
- (357) Höltje, H.-D.; Sippl, W.; Rognan, D.; Folkers, G. Protein-based virtual screening. In *Molecular modeling: Basic principles and applications*. 2nd ed.; Wiley-VCH, **2003**, pp 145-168.
- (358) Kubinyi, H. Chance favors the prepared mind - From serendipity to rational drug design. *J. Recept. Signal Transduct. Res.* **1999**, *19*, 15-39.
- (359) Johnston, S. R. D.; Dowsett, M. Aromatase inhibitors for breast cancer: Lessons from the laboratory. *Nat. Rev. Cancer* **2003**, *3*, 821-831.
- (360) Buzdar, A. U.; Robertson, J. F. R.; Eiermann, W.; Nabholz, J. M. An overview of the pharmacology and pharmacokinetics of the newer generation aromatase inhibitors anastrozole, letrozole, and exemestane. *Cancer* **2002**, *95*, 2006-2016.
- (361) Jefcoate, C. R.; Liehr, J. G.; Santen, R. J.; Sutter, T. R.; Yager, J. D.; Yue, W.; Santner, S. J.; Tekmal, R.; Demers, L.; Pauley, R.; Naftolin, F.; Mor, G.; Berstein, L. Tissue-specific synthesis and oxidative metabolism of estrogens. *J. Natl. Cancer Inst. Monogr.* **2000**, 95-112.

- (362) Schaftenaar, G.; Noordik, J. H. Molden: a pre- and post-processing program for molecular and electronic structures. *J. Comput. -Aided Mol. Des.* **2000**, *14*, 123-134.
- (363) Berstein, L. M.; Larionov, A. A.; Kyshtobaeva, A. S.; Pozharisski, K. M.; Semiglazov, V. F.; Ivanova, O. A. Aromatase in breast cancer tissue: localization and relationship with reproductive status of patients. *J. Cancer Res. Clin. Oncol.* **1996**, *122*, 495-498.
- (364) Labrie, F.; Luu-The, V.; Labrie, C.; Belanger, A.; Simard, J.; Lin, S. X.; Pelletier, G. Endocrine and intracrine sources of androgens in women: inhibition of breast cancer and other roles of androgens and their precursor dehydroepiandrosterone. *Endocr. Rev.* **2003**, *24*, 152-182.
- (365) Tsuchiya, Y.; Nakajima, M.; Yokoi, T. Cytochrome P450-mediated metabolism of estrogens and its regulation in human. *Cancer Lett.* **2005**, *227*, 115-124.
- (366) Seeger, H.; Huober, J.; Wallwiener, D.; Mueck, A. O. Inhibition of human breast cancer cell proliferation with estradiol metabolites is as effective as with tamoxifen. *Horm. Metab. Res.* **2004**, *36*, 277-280.
- (367) Devanesan, P.; Santen, R. J.; Bocchinfuso, W. P.; Korach, K. S.; Rogan, E. G.; Cavaliere, E. Catechol estrogen metabolites and conjugates in mammary tumors and hyperplastic tissue from estrogen receptor- α knock-out (ERKO)/Wnt-1 mice: implications for initiation of mammary tumors. *Carcinogenesis* **2001**, *22*, 1573-1576.
- (368) Castagnetta, L. A.; Granata, O. M.; Traina, A.; Ravazzolo, B.; Amoroso, M.; Miele, M.; Bellavia, V.; Agostara, B.; Carruba, G. Tissue content of hydroxyestrogens in relation to survival of breast cancer patients. *Clin. Cancer Res.* **2002**, *8*, 3146-3155.
- (369) Blankenstein, M. A.; Maitimu-Smeele, I.; Donker, G. H.; Daroszewski, J.; Milewicz, A.; Thijssen, J. H. Tissue androgens and the endocrine autonomy of breast cancer. *J. Steroid Biochem. Mol. Biol.* **1992**, *43*, 167-171.
- (370) Blankenstein, M. A.; Maitimu-Smeele, I.; Donker, G. H.; Daroszewski, J.; Milewicz, A.; Thijssen, J. H. On the significance of *in situ* production of oestrogens in human breast cancer tissue. *J. Steroid Biochem. Mol. Biol.* **1992**, *41*, 891-896.
- (371) Dawling, S.; Roodi, N.; Mernaugh, R. L.; Wang, X.; Parl, F. F. Catechol-O-methyltransferase (COMT)-mediated metabolism of catechol estrogens: comparison of wild-type and variant COMT isoforms. *Cancer Res.* **2001**, *61*, 6716-6722.
- (372) Ryan, K. J. Biological aromatization of steroids. *J. Biol. Chem.* **1959**, *234*, 268-272.

- (373) Siiteri, P. K.; Thompson, E. A. Studies of human placental aromatase. *J. Steroid Biochem.* **1975**, *6*, 317-322.
- (374) Schrödinger software. Available at <http://www.schrodinger.com>
- (375) Goodman, J. M.; Still, W. C. An unbounded systematic search of conformational space. *J. Comput. Chem.* **1991**, *12*, 1110-1117.
- (376) Mohamadi, F.; Richards, N. G. J.; Guida, W. C.; Liskamp, R.; Lipton, M.; Caufield, C.; Chang, G.; Hendrickson, T.; Still, W. C. Macromodel - An integrated software system for modeling organic and bioorganic molecules using molecular mechanics. *J. Comput. Chem.* **1990**, *11*, 440-467.
- (377) Gaussian 98 (Revision A.7), Gaussian, Inc., Pittsburgh, PA, USA. Available at <http://www.gaussian.com>
- (378) So, F. V.; Guthrie, N.; Chambers, A. F.; Carroll, K. K. Inhibition of proliferation of estrogen receptor-positive MCF-7 human breast cancer cells by flavonoids in the presence and absence of excess estrogen. *Cancer Lett.* **1997**, *112*, 127-133.
- (379) Brouillard, R.; Delaporte, B. Chemistry of anthocyanin pigments. 2. Kinetic and thermodynamic study of proton transfer, hydration, and tautomeric reactions of malvidin 3-glucoside. *J. Am. Chem. Soc.* **1977**, *99*, 8461-8468.
- (380) Lapidot, T.; Harel, S.; Akiri, B.; Granit, R.; Kanner, J. pH-dependent forms of red wine anthocyanins as antioxidants. *J. Agric. Food Chem.* **1999**, *47*, 67-70.
- (381) Li, H.; Poulos, T. L. Conformational dynamics in cytochrome P450-substrate interactions. *Biochimie* **1996**, *78*, 695-699.
- (382) Dunn, A. R.; Dmochowski, I. J.; Bilwes, A. M.; Gray, H. B.; Crane, B. R. Probing the open state of cytochrome P450cam with ruthenium-linker substrates. *Proc. Natl. Acad. Sci. U. S. A* **2001**, *98*, 12420-12425.
- (383) Bak, A.; Polanski, J. Modeling robust QSAR 3: SOM-4D-QSAR with iterative variable elimination IVE-PLS: Application to steroid, azo dye, and benzoic acid series. *J. Chem Inf. Model.* **2007**, *47*, 1469-1480.
- (384) Su, B.; Tian, R.; Darby, M. V.; Brueggemeier, R. W. Novel sulfonanilide analogs decrease aromatase activity in breast cancer cells: Synthesis, biological evaluation, and ligand-based pharmacophore identification. *J. Med. Chem.* **2008**, *51*, 1126-1135.
- (385) Oprea, T. I.; Garcia, A. E. Three-dimensional quantitative structure-activity relationships of steroid aromatase inhibitors. *J. Comput. -Aided Mol. Des.* **1996**, *10*, 186-200.

- (386) Schuster, D.; Laggner, C.; Steindl, T. M.; Paluszczak, A.; Hartmann, R. W.; Langer, T. Pharmacophore modeling and in silico screening for new P450 19 (aromatase) inhibitors. *J. Chem Inf. Model.* **2006**, *46*, 1301-1311.
- (387) Clement, O. O.; Mehl, A. T. HipHop: Pharmacophores based on multiple common-feature alignments. In *Pharmacophore perception, development, and use in drug design*. International University Line, La Jolla, CA, **2000**, pp 69-84.
- (388) Catalyst, v4.11, Accelrys Software Inc. Available at www.accelrys.com
- (389) Schleinkofer, K.; Sudarko; Winn, P. J.; Ludemann, S. K.; Wade, R. C. Do mammalian cytochrome P450s show multiple ligand access pathways and ligand channelling? *EMBO Rep.* **2005**, *6*, 584-589.
- (390) Cavalli, A.; Bisi, A.; Bertucci, C.; Rosini, C.; Paluszczak, A.; Gobbi, S.; Giorgio, E.; Rampa, A.; Belluti, F.; Piazzzi, L.; Valenti, P.; Hartmann, R. W.; Recanatini, M. Enantioselective nonsteroidal aromatase inhibitors identified through a multidisciplinary medicinal chemistry approach. *J. Med. Chem.* **2005**, *48*, 7282-7289.
- (391) Developmental Therapeutics Program NCI/NIH, National Cancer Institute. Available at <http://dtp.nci.nih.gov>
- (392) Irwin, J. J.; Shoichet, B. K. ZINC: a free database of commercially available compounds for virtual screening. *J. Chem. Inf. Model.* **2005**, *45*, 177-182.
- (393) ZINC - A free database for virtual screening. Available at <http://zinc.docking.org>
- (394) Lipinski, C. A.; Lombardo, F.; Dominy, B. W.; Feeney, P. J. Experimental and computational approaches to estimate solubility and permeability in drug discovery and development settings. *Adv. Drug Deliv. Rev.* **1997**, *23*, 3-25.
- (395) Instant JChem v2.0.0, ChemAxon software. Available at <http://www.chemaxon.com>
- (396) MDL CrossFire Commander v7.0SP2, Elsevier MDL. Available at <http://www.mdli.com>
- (397) PubChem Compound database, National Center for Biotechnology Information. Available at <http://www.ncbi.nlm.nih.gov/sites/entrez/>
- (398) ISI Web of Knowledge v4.3. Available at <http://isiknowledge.com>
- (399) Biblioteca do conhecimento online. Available at <http://www.b-on.pt>

- (400) Kitz, R.; Wilson, I. B. Esters of methanesulfonic acid as irreversible inhibitors of acetylcholinesterase. *J. Biol. Chem.* **1962**, *237*, 3245-3249.
- (401) GOLD v3.2, The Cambridge Crystallographic Data Centre. Available at <http://www.ccdc.cam.ac.uk>
- (402) Cupp-Vickery, J. R.; Garcia, C.; Hofacre, A.; McGee-Estrada, K. Ketoconazole-induced conformational changes in the active site of cytochrome P450eryF. *J. Mol. Biol.* **2001**, *311*, 101-110.
- (403) Podust, L. M.; von Kries, J. P.; Eddine, A. N.; Kim, Y.; Yermalitskaya, L. V.; Kuehne, R.; Ouellet, H.; Warriar, T.; Altekoster, M.; Lee, J. S.; Rademann, J.; Oschkinat, H.; Kaufmann, S. H. E.; Waterman, M. R. Small-molecule scaffolds for CYP51 inhibitors identified by high-throughput screening and defined by X-ray crystallography. *Antimicrob. Agents Chemother.* **2007**, *51*, 3915-3923.
- (404) Raag, R.; Li, H. Y.; Jones, B. C.; Poulos, T. L. Inhibitor-induced conformational change in cytochrome P-450_{CAM}. *Biochemistry* **1993**, *32*, 4571-4578.
- (405) Bhatnagar, A. S.; Hausler, A.; Schieweck, K.; Browne, L. J.; Bowman, R.; Steele, R. E. Novel aromatase inhibitors. *J. Steroid Biochem. Mol. Biol.* **1990**, *37*, 363-367.
- (406) LeBorgne, M.; Marchand, P.; Duflos, M.; DelevoyeSeiller, B.; PiessardRobert, S.; LeBaut, G.; Hartmann, R. W.; Palzer, M. Synthesis and in vitro evaluation of 3-(1-azolylmethyl)-1*H*-indoles and 3-(1-azolyl-1-phenylmethyl)-1*H*-indoles as inhibitors of P450 arom. *Arch. Pharm.* **1997**, *330*, 141-145.
- (407) Hisano, T.; Ichikawa, M.; Tsumoto, K.; Tasaki, M. Synthesis of benzoxazoles, benzothiazoles and benzimidazoles and evaluation of their antifungal, insecticidal and herbicidal activities. *Chem. Pharm. Bull.* **1982**, *30*, 2996-3004.
- (408) Na, Y. M.; Le Borgne, M.; Pagniez, F.; Le Baut, G.; Le Pape, P. Synthesis and antifungal activity of new 1-halogenobenzyl-3-imidazolymethylindole derivatives. *Eur. J. Med. Chem.* **2003**, *38*, 75-87.
- (409) Baguley, B. C.; Denny, W. A.; Atwell, G. J.; Cain, B. F. Potential antitumor agents. 34. Quantitative relationships between DNA-binding and molecular structure for 9-anilinoacridines substituted in the anilino ring. *J. Med. Chem.* **1981**, *24*, 170-177.
- (410) Teguo, P. W.; Fauconneau, B.; Deffieux, G.; Huguet, F.; Vercauteren, J.; Merillon, J. M. Isolation, identification, and antioxidant activity of three stilbene glucosides newly extracted from *Vitis vinifera* cell cultures. *J. Nat. Prod.* **1998**, *61*, 655-657.

- (411) Potter, G. A.; Patterson, L. H.; Wanogho, E.; Perry, P. J.; Butler, P. C.; Ijaz, T.; Ruparelia, K. C.; Lamb, J. H.; Farmer, P. B.; Stanley, L. A.; Burke, M. D. The cancer preventative agent resveratrol is converted to the anticancer agent piceatannol by the cytochrome P450 enzyme CYP1B1. *Br. J. Cancer* **2002**, *86*, 774-778.
- (412) Wieder, T.; Prokop, A.; Bagci, B.; Essmann, F.; Bernicke, D.; Schulze-Osthoff, K.; Dorken, B.; Schmalz, H. G.; Daniel, P. T.; Henze, G. Piceatannol, a hydroxylated analog of the chemopreventive agent resveratrol, is a potent inducer of apoptosis in the lymphoma cell line BJAB and in primary, leukemic lymphoblasts. *Leukemia* **2001**, *15*, 1735-1742.
- (413) Geahlen, R. L.; Mclaughlin, J. L. Piceatannol (3,4,3',5'-tetrahydroxy-trans-stilbene) is a naturally occurring protein-tyrosine kinase inhibitor. *Biochem. Biophys. Res. Commun.* **1989**, *165*, 241-245.
- (414) Maggiolini, M.; Recchia, A. G.; Bonofiglio, D.; Catalano, S.; Vivacqua, A.; Carpino, A.; Rago, V.; Rossi, R.; Ando, S. The red wine phenolics piceatannol and myricetin act as agonists for estrogen receptor α in human breast cancer cells. *J. Mol. Endocrinol.* **2005**, *35*, 269-281.
- (415) Han, S. J.; Ryu, S. N.; Kang, S. S. A new 2-arylbenzofuran with antioxidant activity from the black colored rice (*Oryza sativa* L.) bran. *Chem. Pharm. Bull.* **2004**, *52*, 1365-1366.
- (416) Halabalaki, M.; Aligiannis, N.; Papoutsis, Z.; Mitakou, S.; Moutsatsou, P.; Sekeris, C.; Skaltsounis, A. L. Three new arylobenzofurans from *Onobrychis ebenoides* and evaluation of their binding affinity for the estrogen receptor. *J. Nat. Prod.* **2000**, *63*, 1672-1674.
- (417) Papoutsis, Z.; Kassi, E.; Papaevangelidou, D.; Pratsinis, H.; Zoumpourlis, V.; Halabalaki, M.; Mitakou, S.; Kalofoutis, A.; Moutsatsou, P. Plant 2-arylobenzofurans demonstrate a selective estrogen receptor modulator profile. *Steroids* **2004**, *69*, 727-734.
- (418) Vanden Bossche, H.; Willemsens, G.; Roels, I.; Bellens, D.; Moereels, H.; Coene, M. C.; Le Jeune, L.; Lauwers, W.; Janssen, P. A. R 76713 and enantiomers: selective, nonsteroidal inhibitors of the cytochrome P450-dependent oestrogen synthesis. *Biochem. Pharmacol.* **1990**, *40*, 1707-1718.
- (419) Kirton, S. B.; Murray, C. W.; Verdonk, M. L.; Taylor, R. D. Prediction of binding modes for ligands in the cytochromes P450 and other heme-containing proteins. *Proteins* **2005**, *58*, 836-844.

